9950-342

(NASA-CR-163208) ANALYSIS AND EVALUATION IN THE PRODUCTION PROCESS AND EQUIPMENT AREA OF THE LOW-COST SOLAR ARRAY PROJECT Annual Report, Oct. 1978 - Oct. 1979 (Pennsylvania Univ.) 203 p HC A10/MF A01 CSCL 10A G3/44

N80-25782

Unclas 22379

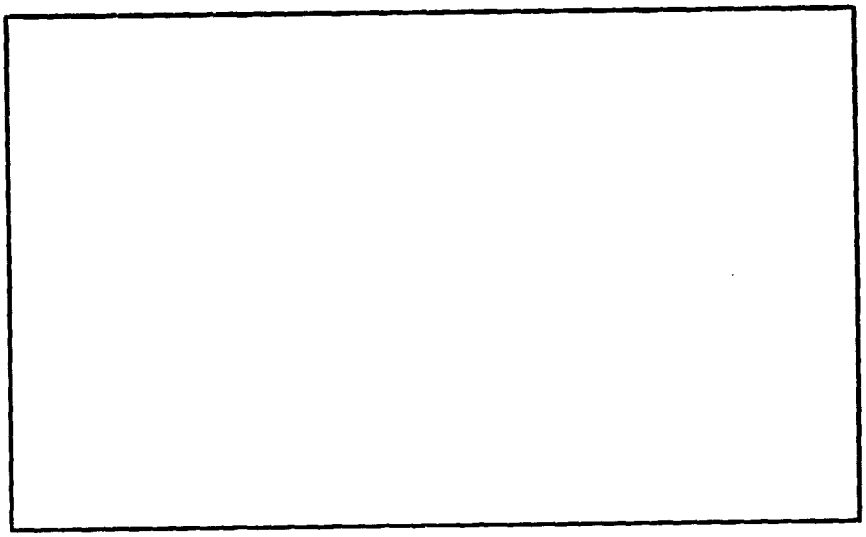

Contract JPL-954796
Annual Report Oct. 1973 to Oct. 1979
(DRD Line Item 7)

October 1979

H. Goldman and M. Wolf

UNIVERSITY of PENNSYLVANIA

The Moore School of Electrical Engineering

PHILADELPHIA, PENNSYLVANIA 19104

The JPL Low-Cost Silicon Solar Array Project is sponsored by the U.S. Department of Energy and forms part of the Solar Photovoltaic Conversion Program to initiate a major effort toward the development of low-cost solar arrays. This work was performed for the Jet Propulsion Laboratory, California Institute of Technology by agreement between NASA and DoE.

DoE/JPL-954796-79/7
Distribution Category UC-63

ANALYSIS AND EVALUATION IN THE PRODUCTION PROCESS AND EQUIPMENT AREA of the LOW-COST SOLAR ARRAY PROJECT

Contract JPL-954796

Annual Report Oct. 1978 to Oct. 1979

(DRD Line Item 7)

October 1979

H. Goldman and M. Wolf

The JPL Low-Cost Silicon Solar Array Project is sponsored by the U.S. Department of Energy and forms part of the Solar Photovoltaic Conversion Program to initiate a major effort toward the development of low-cost solar arrays. This work was performed for the Jet Propulsion Laboratory, California Institute of Technology by agreement between NASA and DoE.

Summary

This Annual Report summarizes the analyses performed and conclusions reached during the year from October 1978 to October 1979. This work was largely contained in three topical reports which were issued as Quarterly Reports. In addition, material is presented in this report which was covered in Monthly Reports, but which was not included in the Quarterly Reports. Much of this material makes up chapter V, "Energy Analysis."

The report is arranged by topics, with the analysis of slicing processes covered in chapter II and of junction formation processes in chapter III, with chapter IV containing the description of a simple method for evaluation of the relative economic merits of competing process options with respect to the cost of energy produced by the system, and chapter V the energy consumption analysis.

Subsequent to the analysis of the Czochralski crystal pulling process performed in the preceding year, the important companion to all ingot processes, slicing, was examined. Progress is being made or projected towards reduced kerf and decreased wafer thickness, together with higher throughput rates, on all approaches to slicing, including the generic types of fixed abrasive (diamond ID saw, wire saw) and slurry sawing (reciprocating multi-blade or multi-wire). From their current position of comparable add-on price, the projected improvements, if successfully carried out, could also yield comparable price reductions. However, all these advancements cannot eliminate the kerf losses, with the waste of valuable material.

The analysis of the junction function process contains an accumulation of the pertinent technical and economic data on current processes, such as the Spectrolab gaseous diffusion process for front junction formation, and ion implantation using the Varian-Extrion 200-1000 machine. These recent experience data were used to assay the projections to future improved process methods, such as diffusion processes proposed by Motorola and RCA, and ion implantation advances proposed by Lockheed, Motorola, RCA and Spire.

The analysis of the energy consumption in the solar module fabrication process sequence, from the mining of the SiO_2 to shipping, shows, in the current technology practice, inordinate energy use in the purification step, and large wastage of the invested energy through losses, particularly poor conversion in slicing, as well as inadequate yields throughout. The cell process energy expenditures already show a downward trend based on increased throughput rates. The large improvement, however, depends on the introduction of a more efficient purification process and of acceptable ribbon growing techniques.

TABLE OF CONTENTS

LIST OF TABLES

LIST OF FIGURES

I. INTRODUCTION

The manufacturing methods for photovoltaic solar energy utilization systems consist, in complete generality, of a sequence of individual processes. This process sequence has been, for convenience, logically segmented into five major "work areas": Reduction and purification of the semiconductor material, sheet or film generation, device generation, module assembly and encapsulation, and system completion, including installation of the array and the other subsystems. For silicon solar arrays, each work area has been divided into 10 generalized "processes" in which certain required modifications of the work-in-process are performed. In general, more than one method is known by which such modifications can be carried out. The various methods for each individual process are identified as process "options". This system of processes and options forms a two-dimensional array, which is here called the "process matrix".

In the search to achieve improved process sequences for producing silicon solar cell modules, numerous options have been proposed and/or developed, and will still be proposed and developed in the future. It is a near necessity to be able to evaluate such proposals for their technical merits relative to other known approaches, for their economic benefits, and for other techno-economic attributes such as energy consumption, and generation and disposal of waste by-products, etc. Such evaluations have to be as objective as possible in light of the available information, or the lack thereof, and have to be periodically updated as development progresses and new information becomes available. Since each individual

process option has to fit into a process sequence, technical interfaces between consecutive processes must be compatible. This places emphasis on the specifications for the work-in-process entering into and emanating from a particular process option.

The objective of this project is to accumulate the necessary information as input for such evaluations, to develop appropriate methodologies for the performance of such techno-economic analyses, and to perform such evaluations at various levels.

In evaluating even current processes substantial gaps or uncertainties were found in important information required for both technical and economical evaluation of the currently practiced processes. In proceeding to the evaluation of processes which are still in the developmental or even conceptual stage, the gaps in needed information become very large. In these cases, it is necessary to fill the gaps more extensively with estimates based on extrapolations or analogies. Such estimates always leave some doubt on the accuracy of the evaluations, and it will be necessary to also make "probable error" estimates to reduce decision mistakes based on early evaluations. Nevertheless, collecting the information and carrying out evaluations at the earliest possible time provides not only a planning tool, but also aids in uncovering the deciding attributes about which information ought to be obtained at an early stage of the development process.

This annual report describes the work completed during the last 12 months, and summarizes the work in progress. In the preceeding 12 month period, the basic methodologies for performing the comparative analyses of competing process options were developed, as well as the formats for accumulating the needed information. Also, the processes for the reduction of quartzite to silicon and

for Czochralski crystal growth were studied. The reduction process was investigated primarily from the energy consumption viewpoint, as the process is already carried out cost-effectively on a large industrial scale (~ 350,000 t /y worldwide, > 140,000 t /y in the U.S.A.). During the current 12 month period, the analysis of the slicing and junction formation processes was completed and is described in detail in this report. The processes for metallization (contact formation) and anti-reflection coating are at the state where the information which is available in contract reports and published literature has essentially been accumulated, and the analysis has been started, with considerable gaps in the information available in the reports becoming apparent. Finally, the methodology for the comparative evaluations has been refined and completed, based on the cost of the energy produced by the system rather than independent cost per unit peak power output value.

This report is arranged in chapters according to the subject items investigated. The detailed process-data formats to the individual process options which were included in the quarterly reports, have been omitted since they would have added greatly to the volume of paper used. It should also be noted that the subject items were studied during a certain time period and the conclusion reached then, with the subsequent effort devoted to a different subject area. In this approach, the analyses are not continuously updated by inclusion and reevaluation of new developments. It may also be noted that throughout this report, costs or prices are quoted in 1975 dollars, unless, in rare special cases, it is stated otherwise.

II. Slicing

1. Introduction

The fabrication process sequences for solar modules involves many steps, the principal ones of which up to crystal growth have been analyzed previously. The next major process following Czochralski crystal pulling, or any other process that results in bulk ingots, such as the casting of semicrystalline ingots or the Heat Exchanger Method of crystal growth, has to be the division of these ingots into wafers, commonly referred to as "slicing". The first application of this developing methodology was made to the Czochralski's crystal pulling process.

Previously, we had examined the reduction of quartzite to metallurgical grade silicon and did a comparative evaluation of competing Czochralski techniques for growing single crystal, cylindrical ingots. The next major process step in the sequence for producing single crystal silicon wafers, today and in the near future (up to 1982), is the slicing technique. The evaluations were started with the current methods of multiblade slurry slicing, and inner diameter slicing using a diamond coated blade for which a large amount of the needed information is available.

We have tabulated production experience data obtained from Spectrolab[1] for slicing 2-cm rectangular, 5.4-cm and 7.6-cm diameter wafers using the Varian multi-blade slicing system, and similar data obtained from HAMCO[2], for ID slicing of 10.16-cm diameter ingots using their equipment. Experimental data from OCLI[3], Varian[4] and TI[5] for multiblade wafering, from OCLI[6] and STC[7] for ID slicing, and from

JPL[8] for the Yasunaga multi-wire slurry slicing system, were also tabulated. To complete the analysis, projections made by Varian[9] for multi-blade slicing, by STC for ID slicing[7] by Crystal Systems[10] for their fixed abrasive multi-wire system, and by Solarex[11] for the Yasunaga multi-wire slurry system were examined.

Brief Descriptions of the Slicing Technique

2. Brief Descriptions of the Slicing Techniques

2.1 Multiblade Slicing

The multiblade slurry sawing method is one of the two techniques used in current production slicing. In its present configuration 230-250 blades of 38-cm length of hardened 1095 steel are mounted and evenly spaced on a blade head that is, for slicing, reciprocated, at frequencies below 2 Hz (normally about 1.6 Hz), across the workpiece using approximately a 20-cm stroke. The abrasive slurry is pulsed sprayed or, at times, dripped onto the top surface of the workpiece and recirculated by a pump. The slurry is a SiC abrasive suspended in PC oil. It is normally used for one load before it is discarded. There are no practical ways, at present, to re-use the abrasive slurry for more than one load.

The current multiblade slicing machines can accept blade heads up to 18.5-cm wide. However, the number of blades in a blade head, and consequently, the number of slices that could be produced per load, is not limited by the blade head width per se, but rather by the maximum tension force the blade head can exert on the blades. This is about 401,800 N for current production blade heads[4]. An adequate saw force commonly called "blade load", is necessary to achieve economically acceptable cutting rates in the slicing process. A blade load of about 1-2 N/blade[5], is usually applied. Excessive blade loading, and even normal loading after some blade wear, can cause deflection of the blades, often called "buckling", which results in inaccurately sliced wafers or even broken

wafers. To minimize buckling, the blades need to be stressed as much as possible, which, in current practice, is 80% of the yield strength of 1095 steel, or 1.37 GPa[5]. Therefore, the maximum number of blades permitted per blade head is 401.8/1.37*A, where A is the cross-sectional blade area in mm^2. For a 6.35 mm high blade, 0.20 mm thick, a size that is normally used in production[4], the maximum number of blades thus is 230. Reducing the blade thickness to 0.15 mm will increase the maximum number of 6.35 mm high blades to 307. At present, the thicker 0.20 mm blades are used in production because of their better wafer yield, as they are less susceptible to buckling which can be caused by vertical misalignment at the beginning of the slicing process and by increased blade tension, resulting from a reduced crossection because of blade wear near the end of slicing[5].

There are two types of blade packages available: the drill-pin package and the epoxy package. In the former, the alternately arranged blades and spacers which determine the thicknesses of the kerf and wafers are held together by four threaded rods. It is the cheaper of the two types of package ($50 compared to $175),but often requires additional alignment before mounting on the slicing machine[3]. In the epoxy package, an adhesive is applied between the spacers and the blade ends to hold the package together[4].

The production procedure for multi-blade slicing involves first mounting the workpiece, or silicon crystal, with wax, epoxy, or other suitable cement on a graphite or ceramic base plate. The workpiece is then clamped by the baseplate to the slicing machine. To help increase the

yield, ceramic bars are often similarly cemented longitudinally onto the cylindrical crystal near its top and bottom horizontal tangents. The bars "smooth-out" the slicing by decreasing the variation in kerf length and blade load as the blades travel downward through the cylindrical crystal. In addition, ceramic bars near the top tangent minimize the effect of vertical misalignment by reducing blade buckling by the time they enter the silicon crystal. Those bars near the bottom, help to smooth the transition of the blades cutting into the base material by equalizing the slicing properties above and below the crystal to base transition. Some of these benefits are also obtained, in some places, without the use of ceramic bars by varying the blade load according to the changing kerf length during the slicing process. After the slicing is finished, the wafers, still attached to the base, are removed from the slicing machine and the wafers are then detached from the base.

The effective linear cutting rate of the multiblade process is presently about 550 times smaller than the ID diamond saw. The linear cutting rate cannot be increased significantly because of the limit on the blade load and because of the blade head mass which limits the reciprocating frequency. The blade load cannot be increased much beyond its present value without significantly increasing blade buckling since the tensile strength of the blades is fixed. Varian found that a blade load of 2.77 N/blade caused severe enough buckling to separate the crystal from its mount[4]. In another experiment, a reciprocating frequency increase to 2 Hz resulted in sufficient vibration to break all wafers[4]. Therefore, in order to increase the throughput rate, or the wafer area produced in the multi-blade slicing process per unit time, either the number of slices

in the load, or the area yield per load, has to be increased without significantly increasing the time of the run. The area output per load can be increased in a combination of several ways: by increasing the number of blades per unit blade head width, as can be achieved by decreasing the blade and/or spacer thickness; by increasing the width of the blade head without changing blade and spacer thicknesses; or by increasing the width of the workpiece.

The blade thickness has a lower bound set by its strength. If the blade is too thin, it will buckle under the blade load, or break from the blade tension, resulting in broken wafers and low yields. Reduction of the spacer thickness is limited by the wafer strength. Slicing wafers too thin increases their chance of breakage due to pressure from the lateral blade movement, blade vibration, blade buckling, etc. As the blade and spacer thicknesses are decreased, the increased fragility of the blades and the wafers ultimately leads to significantly lowered yields. Experimentally, Varian[9] has found that using 0.15 mm thick blades with 0.30 mm spacers still results in good yields. Under these conditions 0.25 mm thick wafers with 0.20 mm kerf are produced. This gives, assuming a wafer yield of 95%, which has been demonstrated by Varian, an area conversion ratio of 0.9 m^2/kg-Si which is a 50% improvement over Spectrolab's recently experienced area conversion ratio in slicing 5.4-cm and 7.5-cm diameter wafers.

Varian is also currently experimenting with a larger blade head width that can accept 900 to 1000 blades. This blade head weighs approximately one ton. Therefore, the workpiece will be reciprocated against the stationary blades. The workpiece size is projected to be 12-cm in diameter and 40.5-cm long yielding a wafer area of 9.67 m^2/load using the 900-blade machine with the aforementioned blade and spacer thicknesses. This area yield is over four times higher than obtained in present commercial practice.

A third method to potentially increase the area yield per load without increasing the slicing time would be to increase the width of the workpiece, or the kerf length, by slicing two or more ingots, placed side-by-side, simultaneously. TI[5] has found that the machine slicing time, and, correspondingly, the linear cutting rate, is essentially independent of the kerf length. TI has therefore proposed slicing two 12-cm diameter ingots at one time to increase the multi-blade slicing productivity. The area yield per load, with details of this projection given in Tables I to III, can thus be doubled without significantly changing the slicing time.

2.2 Inner Diameter Slicing

In the process of inner diameter, or ID, slicing, one wafer is sliced at a time with a rotating, diamond impregnated blade. The rotation speed depends upon the blade size, and is 2,100 rpm for a bla with a

15.25-cm diameter hole, and 1650 rpm for a 20.32-cm diameter, inner diameter blade. The blade consists of a stainless steel core which is 0.10 and 0.15 mm thick for 15.24 and 20.32-cm blades, respectively, with diamond plated edges. The total thickness of the 15.24-cm blade is approximately 0.30 mm, and the 20.32-cm blade is about 10% thicker. The blade is mounted around its rim in a vise-like holder where hydraulic pressure is applied to tension it radially.

The linear cutting rate, or the rate that the inner diameter blade traverses the silicon can be up to 305 cm/h, or almost three orders of magnitude higher than for the slurry, multi-blade process. There are several reasons for this. First, the inner diameter blade speed is approximately 1,600 cm/sec as opposed to less than 80 cm/sec for multiblade slicing. Therefore, the contact length per unit time between the blade and the silicon for ID slicing is twenty times higher than for multiblade slicing. Also, fixed abrasive slicing removes more kerf in a unit contact length because there are two surfaces moving relative to each other instead of three as in slurry slicing. In slurry slicing, the abrasive is pushed into the workpiece and is "rolled out". Whereas for fixed abrasive slicing, the abrasive cuts into the workpiece to remove the kerf. Finally, the diamond plated layer on the ID blade increases the blade's rigidity and thickness and allows the application of more force, by the blade, on the workpiece than in multiblade slicing. The total thickness of the ID blade is 300-330 μm thick while the multiblade is 150-200 μm thick. It should be noted that the effective ID cutting rate is about 10-20% lower than indicated by the blade's linear cutting rate because of the 18 to 24 seconds between two consecutive slices, when the blade is returning to its

original vertical position and the silicon crystal is being indexed.

In mounting the ingot, one end is attached to a graphite base with epoxy and the ingot is then placed in a box with rubber supports along it's length to keep it rigid. The stiffness of the mount will affect the vibration level between the blade and workpiece, influencing the wafer thickness and yield[3]. At present, ID machines can accommodate ingots up to 50-cm long[2,3]. The current practice of slicing 10.16-cm diameter wafers, 0.50 mm thick with a 0.33 mm kerf, yields a area of 4.8 m^2/load or 0.50 m^2/kg, at a practical wafer yield of 98%. During slicing, either water or water mixed with a small percent of Rust-Lick is sprayed on the cutting edge, at a rate of about 2 mℓ/sec, to cool the blade. The blade must be dressed, every 50 slices for the 15.24-cm blade and every 25 slices for the 20.32-cm blades for proper slicing, in order to remove dirt and expose a fresh cutting surface. The dressing is done with 5 cuts of an alumina stick. The lifetime of the blade is dependent on the rate of diamond "pull-out" and the degree of metal fatigue and varies quite extensively from blade-to-blade. The lifetime median is about 3,000 7.52-cm diameter slices for the 15.24-cm blade and 5,000 10.16-cm diameter slices for the 20.32-cm blade.

A method being investigated, to increase the ID saw's productivity by a factor of two, is crystal rotation[7]. The cutting speed is doubled using a rotating crystal since the blade has to traverse only half-way through the crystal diameter. The half penetration in rotating crystal slicing permits the use of a cheaper, smaller diameter, and thinner inner diameter blade. For slicing 10-cm diameter wafers with this technique the wafer thickness and kerf are expected to be 225 μm and 210 μm respectively[7].

This process is expected to be in commercial use by 1982.

2.3 The Yasunaga YQ-100 Multiwire Saw System

The Yasunaga multiwire saw is a slurry slicing system which uses a single wire (600 to 30,000 m in length) routed around a rocker arm tensioning device, a wire guide catridge, and a take-up reel. The continuous wire forms up to 250 multiple loops around the three grooved wire guides, arranged in an equilateral triangle, that are the key parts of the wire guide catridge. During slicing, the wire guide catridge oscillates, while the workpiece is raised against the wires with a preset force. An abrasive slurry is sprayed on the cutting surface. The procedure for mounting the silicon crystal for multiblade slicing is similar to that described for multiblade slicing.

The chief potential benefit of the Yasunaga saw is its high area-mass conversion ratio by employing closely-spaced, small diameter wires. The current YQ-100 model has a workpiece capacity of 10×10×10 cm and as demonstrated by experiments,[8] it can slice 215, 212 ± 7 μm thick wafers with less than 200 μm kerf using 0.4 mm pitch guides, 0.16 mm diameter wire and 13 μm SiC abrasive. Under those conditions an area to unit mass ratio of 1.04 m^2/kg is obtained, which is about 50% higher than what any other current production or experimental slicing system achieves. This higher area to mass ratio effectively reduces the consumption of

single crystal silicon, to produce a given wafer area, by a third. It is projected that the Yasunaga saw can achieve an area-mass ratio of 1.42 m^2/kg by employing closer spaced pitch guides (0.3 mm), smaller diameter wire (0.08 mm) and a finer abrasive (5 μm). This would yield a 200 μm thick wafer with 100 μm kerf[11].

It is believed that the narrow lapping band of the wires of the Yasunaga saw results in wafers with less subsurface damage than with other commercial slicing techniques[11], and this is being investigated[8].

Currently, the Yasunaga saw is not used for the production of silicon wafers, at least not in the USA, although Solarex has recently obtained a machine for pilot line operation. However, Motorola is using, in its semiconductor device production an in-house developed, proprietory wire saw with capabilities which seem to be comparable to that of the Yasunaga saw.

2.4 The Multiwire Fixed Abrasive Slicing Technique ("FAST")

This method is similar to multiblade slicing, except that the silicon is sliced with diamond-impregnated wires instead of steel blades and an abrasive slurry. In FAST, the diamond impregnated wires are mounted and evenly spaced, at a linear density expected to be up to 25 cm^{-1}, on a light weight frame that is reciprocated across a rocking workpiece[10]. The wires are coated with 22 to 45 μm diamonds imbedded in a metal matrix, and can be coated on their bottom halves only to reduce abrasive costs. Development is still proceeding towards finding an optimum wire composition, but it has been found that heat-hardened, tungsten core wire, diamond-impregnated, and nickel-plated, has a good lifetime, which means it could be used for about 10 loads before significantly losing its cutting ability[10].

Crystal Systems has conducted most of their experiments, pertaining to FAST, on a modified Varian 686 wafering machine. Consequently, the slicing potential of multiwire, fixed abrasive slicing has not been fully demonstrated. For example, workpiece size has been, for most of the experiments only 4 x 4 cm, and the reciprocating rate lower than required for optimum fixed-abrasive slicing. A slicing machine, built to Crystal Systems' specifications, have just been delivered to them and slicing with this machine has just been initiated. The new slicing machine has been designed to provide higher cutting rates and lower wafer and kerf thicknesses and operate with a much lighter blade carriage, at higher reciprocating frequencies, and reduced vibration than the Varian machine. It is expected that this multiwire, fixed abrasive slicing technique could have a cutting rate of 0.6 cm/h (twice the value previously achieved with good yields), with an area to mass ratio of 1.1 m^2/kg by producing wafers 200 μm thick with a 200 μm kerf.

The add-on prices for "FAST" have been projected for 1986 since the state of development of the system and the comparatively small base of experimental data available, making it unlikely that this slicing technique could be in significant commercial operation by 1982.

3. TABULATION OF OPERATION, LABOR, MATERIAL AND COST DATA

Tables II-1 to II-3 summarize the data provided by various organizations for the slicing techniques that are being used or developed. Included in these tables are production experience data from Spectrolab[1] for multi-

TABLE II-1A

SLICING OPERATION DATA FOR MULTIBLADE WAFERING

	Organization	Spectrolab (Production Experience)			OCLI (Experimental)	Varian (Experiment no. P-005)	Varian (Projection)	Varian (900 blade projection)	TI (Experimental incl. Projection)
		2 cm Rectanqular	5.4 cm Diameter	7.5 cm Diameter	10.16 cm Diameter	10cm Diameter	10cm Diameter	12cm Diameter	12cm Diameter
1.	Workpiece size	8 x 17 cm	16 cm long	16 cm long	15 cm long	11.7 cm long	13.5 cm long	40.5 cm long	2,13 cm long ingots
2.	No. of workpieces/load	not applicable	3	2	1	1	1	1	2
3.	Slices/load	1750 (2x2 cm)	750	500	230	234	300	900	460
4.	Wafer thickness (mm)	0.35/0.45 cut 0.2/0.3 etched	0.4 cut 0.3 etched	0.4 cut 0.3 etched	0.33 ± 0.03	0.29 ± 0.04	0.25 ± 0.015	0.25	0.32
5.	Kerf thickness (mm)	0.275	0.275	0.275	0.33	0.22	0.2	0.2	0.24
6.	Practical Wafer Yield	0.95	0.95	0.95	0.84	0.83	0.95	0.95	1.00
7.	Fraction Silicon incorporated in wafer	0.53/0.59	0.56	0.56	0.42	0.47	0.53	0.53	0.57
8.	Depth of Subsurface damage (µm)	75	75	75	n a.	10-15	10-15	n.a.	10 severe 30 slight
9.	Abrasive	600 grit SiC	600 grit SiC	600 grit SiC	400 grit SiC	600 grit SiC	600 grit SiC	600 grit SiC	600 grit SiC
10.	Vehicle	PC oil	PC oil	PC oil	PC oil	PC oil	PC oil	PC oil	PC oil
11.	Concentration (kg/ℓ)	0.24	0.24	0.24	0.8	0.36	0.36	0.36	0.24
12.	Flow rate (ℓ/h)	low	low	low	n.a.	n.a.	n.a.	n.a.	18
13.	Type of Blade	1095 steel 0.2 mm thick	1095 steel 0.2 mm thick	1095 steel 0.2 mm thick	1095 steel 0.2 mm thick	1095 steel 0.15 mm thick	1095 steel 0.15 mm thick	1095 steel 0.15 mm thick	1095 steel 0.20 mm thick
14.	Blade dimensions	n.a.	n.a.	n.a.	6.35 mm high 0.46 mm spacers	6.35 mm high 0.35 mm spacers	6.35 mm high 0.30 mm spacers	6.35 mm high 0.30 mm spacers	6.35 mm high 0.36 mm spacers
15.	Amount on machine	250 blade drill pin pack	250 blade drill pin pack	250 blade drill pin pack	230 blade epoxy package	300 blade package	300 blade package	900 blade package	230 blade package
16.	No. of runs before blade change	7	2	1	1.5	1	1	2	1
17.	Wafer area/load (m^2)	0.69	1.63	2.10	1.57	1.53	2.24	9.67	5.20
18.	Area yield (m^2/kg)	0.65/0.56	0.60	0.60	0.54	0.71	0.90	0.90	0.76
19.	Effective cutting rate (cm/h)	0.36	0.25	0.34	0.5	0.31	0.34	0.41	0.66
20.	Slicing time segment/load (h)	5.5	22	22	20.5	32.0	29.5	29.5	18.2
21.	Load/Unload time (h/load)	0.25	0.25	0.25	0.45	0.5(p)	0.5	0.5	0.5
22.	Cutting tool change, machine service (h/load)	0.2	0.5	1.0	0.67	0.5(p)	0.5	0.5	0.6
23.	Machine segment time (h/load)	5.95	22.75	23.25	21.6	33.0	30.5	30.5	20.0
24.	Machine productivity (m^2/h)	0.115	0.071	0.090	0.07	0.046	0.074	0.317	0.24

TABLE II-1B

SLICING OPERATION DATA FOR MULTIWIRE AND INNER DIAMETER WAFERING

		Multiwire Wafering			Inner Diameter Slicing		
	Organization	Crystal Systems Fixed Abrasive Method (projection)	Yasunaga YQ-100 (Experimental) 7.6 cm diameter	Yasunaga YQ-100 (Projection) 10 cm diameter	OCLI (Experimental) 7.6 cm diameter	OCLI (Experimental) 10.16 cm diameter	HAMEO (Production exp.) 10.16 cm diameter
1.	Workpiece size	30x10x10 cm	10 cm long	10 cm long	50 cm long	25 mm long	46 cm long
2.	No. of workpieces/load	1	1	1	1	1	1
3.	Slices/load	250	215	333	725	350	555
4.	Wafer thickness (mm)	0.1	0.21 ± 0.01	0.2	0.36 ± 0.02	0.36 ± 0.02	0.50
5.	Kerf thickness (mm)	0.3	0.2	0.1	0.33	0.35	0.33
6.	Practical Wafer Yield	1.00	1.00	1.00	0.95	1.00	0.98
7.	Fraction Silicon Incorporated in Wafer	0.25	0.51	0.67	0.50	0.51	0.59
8.	Depth of Surface damage (μm)	Fissures extend 3 μm	~15	~6.5	n.a.	n.a.	n.a.
9.	Abrasive	none	GC 1200 (13 μm)	5 μm SiC	none	none	none
10.	Vehicle or coolant	1:1 water: ethylene glycol	lapping oil	n.a.	80:1 water: rust lick	80:1 water: rust lick	water
11.	Concentration (kg/ℓ)	-	~1.5	n.a.	-	-	-
12.	Flow rate (ℓ/h)	n.a.	3600	3600	7.2	8.4	n.a.
13.	Type of blade or wire	Ni plated, tungsten wire, diamond impregnated	Steel wire	Steel wire	Model STC-16 ID blade, diamond plated	Model STC-22, ID blade, diamond plated	ID blade diamond plated
14.	Blade or wire dimensions	0.125 mm core 0.25 mm total diameter 45 μm diamonds	0.16 mm diameter 0.4 mm pitch guides	0.08 mm diameter, 0.3 mm pitch guides	42.23 cm OD 15.24 cm ID 0.10 mm thick core, 0.28-0.30 total thickness	55.88 cm OD, 20.32 cm ID, 0.15 mm thick core, 0.33-0.36 total thickness	n.a.
15.	Amount on machine	250 wire blade package	~17,000 m	~35,000 m	1	1	1
16.	No. of loads before blade change	9	3	3	4.1	14.3	1
17.	Wafer area/load (m^2)	7.50	0.98	2.62	3.14	2.84	4.41
18.	Area yield (m^2/kg)	1.1	1.04	1.42	0.59	0.60	0.505
19.	Effective cutting rate (cm/h)	0.6	0.84	0.3	305	305	305
20.	Slicing time segment/load (h)	16.67	9.0	30.0	23.9	14.7	23.12
21.	Load/Unload time (h/load)	1.33	n.a.	n.a.	1.23	0.735	0.083
22.	Cutting tool change, machine service (h/load)	n.a.	n.a.	n.a.	1.02	0.84	0.33
23.	Machine segment time (h/load)	18.0	10.0(e)	3.1(e)	26.2	16.3	23.5
24.	Machine productivity (m^2/h)	0.42	0.098	0.085	0.126	0.176	0.19

blade slicing and from HAMCO [2] for ID slicing, and experimental results for multiblade slicing, from OCLI[6], Varian[4] and TI[5], for multiwire slicing from JPL[8] and ID slicing from OCLI[6]. In addition, projections made by Varian for multiblade slicing[9], by Crystal Systems[10] for their "FAST" method, and by Solarex[11] for the Yasunaga saw are included.

The operation data for multiblade slicing are listed in Table II-1A, while Table II-1B contains the corresponding data for the fixed abrasive and slurry multiwire and the inner diameter slicing processes. These tables contain the process attribute of slicing which are summarized on Figure II.1 The first two lines of Table II-1 are the dimensions of the workpiece and the number of workpieces per load, the product of which is the slicing machine's capacity. The wafer area produced in a load is related to the workpiece capacity through the wafer and kerf thicknesses and practical wafer yield. This wafer area per load (Table II-1, line 17) can also be calculated as the product of the theoretical number of slices cut per load (Table II-1, line 3), the "practical wafer yield" (Table II-1, line 5) and the area of the single wafers. The "practical wafer yield" fraction is the number of acceptable wafers divided by the theoretical number sliced per load. The wafer area per unit mass (Table II-1, line 18) is calculated by dividing the practical wafer yield by the product of the sum of the wafer and kerf thicknesses (Table II-1, lines 4 and 5) and the density of silicon, or

$$II\text{-}1.18 = \frac{10 * II\text{-}1.6}{(II\text{-}1.4+II\text{-}1.5)*2.34} \ m^2/kg \ ,$$

where II-1·n represents the value from Table II-1 , line n.

The wafer thickness, kerf and practical wafer yield are necessary for finding the division of the input silicon crystal or workpiece into the silicon incorporated in the work-in-process wafer (Table II-1, line 7) and that silicon lost in kerf and broken wafers.

The procedures for determining the subsurface damage depths, listed in line 8 of Table I, were not consistent between organizations. The most accurate method for determining subsurface damage depth is to remove wafer surface material until the cell efficiency becomes independent of any further removal. Spectrolab's values reflect this procedure[1]. The other subsurface damage depths were determined by chemical etching to remove surface material followed by Wright etching to reveal defects[4], by etching and x-ray topography[5], and by angle lapping and Sirtl etching[8].

Indirect material requirements, briefly summarized on Figure II.2, in terms of the abrasive and vehicle, or coolant type, the slurry concentration and its flow rate or that of the coolant, are listed in lines 9-12 of Table I. Lines 13-16 describe the expendible tooling requirements such as the type of blade or wire, its dimensions, the size of the blade pack and its life expectancy. These data are necessary for determining the expendible tooling and material costs.

The effective cutting rate (Table II-1, line 19) is defined here as the workpiece diameter divided by the slicing time segment, which is the

time the machine is actually sawing (Table II-1, line 20). The time periods when the machine is not actually slicing and cannot be used for slicing because of preparatory or service operations, are listed in lines 21 and 22. The sum of these lines and the slicing time segment is the machine segment time (Table II-1, line 23), or the average time needed for slicing a load, including loading, unloading and servicing. The machine segment time is needed for calculating the number of loads processed annually, and the machine productivity (Table II-1, line 24) which is the wafer area sliced in a load divided by the machine segment time.

The requirements per machine load for labor, included that needed for service and repair, for indirect material needs, including electricity consumption, for capital expenses, which consists of machine and facility components, are included in Tables II-2A and II-2B. These data form the basis for calculating of the manufacturing cost components of labor, expendable tooling, indirect materials, and capital. Also listed in these tables are values necessary for calculating direct material or silicon costs: the proportion of silicon lost in grinding the cylindrical ingots to a uniform diameter, the unit mass of silicon incorporated in the wafer and that lost in kerf and broken wafers.

The labor times required for each part of the crystal slicing operation (see Fig. 2), that is crystal mounting, machine loading and machine monitoring are listed in lines 1-3 of Table II-2, with their total on line 4. The service labor time, which includes changing the blades or wires, is listed in line 5.

TABLE II-2A

SLICING LABOR AND MATERIAL ANALYSIS FOR MULTIBLADE SLICING

	Organization	Spectrolab (Production Experience)			OCLI (Experimental)	Varian			TI
		2 cm Rectangular	5.4 cm Diameter	7.5 cm Diameter	10.16 cm Diameter	(Experiment no. P-605) 10cm Diameter	(Projection) 10cm Diameter	(900 blade projection) 12cm Diameter	(Experimental incl. Projection) 12cm Diameter
1.	Crystal Mount time (h/load)	0.5	0.25	0.25	0.25	0.27	n.a.	n.a.	1.0
2.	Machine load-unload labor (h/load)	0.25	0.25	0.25	0.45	0.4	0.67	0.67	n.a.
3.	Machine supervision during slicing (h/load)	0.58	5.1	5.2	0.45	0.67	0.67	1.60	0.07
4.	Total direct labor time (h/load) (excluding maintenance)	1.33	5.6	5.7	1.15	1.33	1.33	2.27	1.07
5.	Cutting tool change, machine service labor (h/load)	0.4	1.4	1.4	0.87	0.67	0.67	0.67	0.6
6.	Blade or wire set cost ($)	~50	~50	~50	175	~50	23.50	39.45	6.90
7.	Vehicle or coolant consumption (ℓ/load)	7.6	7.6	7.6	6.8	7.6	7.6	15.0	n.a.
8.	Amount of abrasive consumed (kg/load)	1.8	1.8	1.8	5.45	2.74	2.74	5.4	n.a.
9.	Power requirements (kW/machine)	1	1	1	1	1	0.75	1.67	1
10.	Energy consumption (kWh/load)	5.5	22	22	20.5	32	22	49.3	18.2
11.	Machine availability (%)	90	90	90	90	90	90	90	90
12.	Potential no. of runs in a year (8280 h work year)	1250	325	320	345	225	245	245	370
13.	Machine cost ($)	20,000	20,000	20,000	20,000	20,000	20,000	30,000	30,000
14.	Annual machine cost ($/year)	4,280	4,280	4,280	4,280	4,280	4,280	6,420	6,420
15.	Allocatable building area (m^2/machine)	11.2	11.2	11.2	11.2	11.2	11.2	11.2	11.2
16.	Allocatable building cost ($/machine)	8,400	8,400	8,400	8,400	8,400	8,400	8,400	8,400
17.	Annual building cost ($/y)	980	980	980	980	980	70	980	980
18.	Fraction of silicon lost in grinding ingots (%) (100 x(0.6/d))	-	11.1	8.0	5.9	6.0	6.0	5.0	5.0
19.	Silicon incorporated into wafer (kg/m^2-wafer)	0.81/1.05	0.94	0.94	0.77	0.58	0.59	0.59	0.75
20.	Kerf and broken wafer loss (kg/m^2-wafer)	0.68/0.73	0.73	0.73	1.07	0.76	0.52	0.52	0.56

TABLE II-2B

SLICING LABOR AND MATERIAL ANALYSIS FOR MULTIWIRE AND INNER DIAMETER WAFERING

	Organization	Multiwire Wafering			Inner Diameter Slicing		
		Crystal Systems Fixed Abrasive Method (Projection)	Yamunaka YC-100 (Experimental) 7.6 cm diameter	Yamunaka YC-100 (Projection) 10 cm diameter	OCLI (Experimental) 7.6 cm diameter	OCLI (Experimental) 10.16 cm diameter	HAMCO (Production exp.) 10.16 cm diameter
1.	Crystal Mount time (h/load)	n.a.	n.a.	n.a.	0.41	0.23	0.25
2.	Machine load-unload labor (h/load)	n.a.	n.a.	n.a.	1.015	0.525	0.083
3.	Machine supervision during slicing (h/load)	0.92	0.33(e)	1(e)	0.298	0.23	4.3
4.	Total direct labor time (h/load) (excluding maintence)	1.75(e)	0.83(e)	1.5(e)	1.72	0.985	4.63
5.	Cutting tool change, machine service labor (h/load)	0.5(e)	0.5(e)	0.5(e)	1.015	0.875	0.8
6.	Blade or wire set cost ($)	82	~97	143.50	60	150	55
7.	Vehicle or coolant consumption (ℓ/load)	n.a.	3 kg (~3.25ℓ)	n.a.	5.1	1.75	0
8.	Amount of abrasive consumed (kg/load)	0	5	n.a.	0	0	0
9.	Power requirements (kW/machine)	1.5	0.6	0.6	2(e)	2(e)	2(e)
10.	Energy consumption (kWh/load)	25	5.4	18	47.8	29.4	46.2
11.	Machine availability (%)	90(e)	90(e)	90(e)	95	95	95
12.	Potential no. of runs in a year (8280 h work year)	415	745	240	300	480	325
13.	Machine cost ($)	30,000	30,000	30,000	40,000	40,000	40,000
14.	Annual machine cost ($/y)	6,420	6,420	6,420	8,560	8,560	8,560
15.	Allocatable building area (m^2/machine)	11.2	8	8	18	18	18
16.	Allocatable building cost ($/machine)	8,400	6,000	6,000	13,500	13,500	13,500
17.	Annual building cost ($/y)	980	700	700	1,580	1,580	1,580
18.	Fraction of silicon lost in grinding ingots (%) (100 x(0.6/d))	6.0(e)	8.0	6.0	8.0	6.0	6.0
19.	Silicon incorporated into wafer (kg/m^2-wafer)	0.23	0.49	0.46	0.84	0.84	1.17
20.	Kerf and broken wafer loss (kg/m^2-wafer)	0.70	0.47	0.23	0.86	0.82	0.81

Expendable tooling and indirect material requirements, in terms of the blade or wire set costs and the quantities of vehicle or coolant and abrasive consumed during a run, are listed in lines 6-8 of Table II-2. The electrical consumption for a run (Table II-2, line 10) is considered as an indirect material and is obtained by multiplying the slicer's power requirements by the slicing time segment (Table II-1, line 20).

In order to calculate the potential number of loads that can be sliced annually, shown in line 12, the machine segment time (Table II-1, line 23) is divided into 8280. This last value, 8280, is taken from SAMICS[12] and is the number of annual hours the wafer slicing plant operates. The plant operation schedule is continuous except for one 1-week vacation, two 4-day weekends, and one 3-day weekend, and was chosen to maximize annual production by minimizing slicer shutdowns during a run due to plant closings.

After dealing with expenses, the sum of the machine and facility costs, or the capital cost portion of the manufacturing costs needs to be considered. The capital costs are dependent on the factors listed on Figure II.3. The annual machine cost (Table II-2, line 14) is the product of the initial cost of the slicing machine, including installation, taken from the data sources, and the standardized charge rate of 0.2135 y^{-1}. This charge rate was taken from SAMICS[12], using a depreciation schedule of 7 years, a state tax of 2% on one-half the capital, a 4% insurance premium, and a 12% interest-on-debt rate on one-twelfth the initial capital cost. The low ratio of dept to capital, or the low financial leverage, is due to the postulate that the photovoltaic industry would be

LABOR AND INDIRECT MATERIAL SLICING REQUIREMENTS

LABOR TIMES:

- ATTACH SUPPORT BLOCK TO INGOT
- MACHINE LOAD/UNLOAD
- MACHINE MONITORING
- TOOL CHANGE/MACHINE SERVICING

INDIRECT MATERIAL COSTS:

- SLURRY (COOLANT) TYPE
  - UNIT COST
  - USAGE
- TOOL (BLADE) TYPE
  - COST
  - LIFE
- MACHINE REPLACEMENT PARTS
- PURCHASED MACHINE SERVICING
- MISC. (MOUNTING BLOCKS, ADHESIVE)
- ENERGY

Figure II.2.

CAPITAL COSTS

MACHINE COST

(MACHINE LIFE)

ALLOCATABLE BUILDING AREA

(SPECIAL SERVICES)

Figure II.3.

unable to raise large amounts of debt capital, without large interest rates, because it will be a rapidly evolving industry with appreciable risks[12].

The second capital cost contribution comes from the building. The allocatible building area, shown in line 15 of Table II-2, was taken, according to SAMICS[12], as twice the machine's operating area. The doubling accounts for indirect and overhead space needed e.g., for functions such as maintenance, administration and receiving/inventorying, as well as for aisles, washrooms, etc. The initial building cost (Table II-2, line 16) is taken as $\$1506.95/m^2$, according to SAMICS[12] , and is based on the machine operating area only. This cost figure includes appropriate cost allocations for the additional building space needed as outlined above. The facilities charge rate used to calculate the annual building cost (Table II-2, line 17). from the initial cost, is $0.117\ y^{-1}$. This value was obtained in the same fashion as the equipment charge rate, except that a 40-year life expectancy is employed for determining the depreciation rate of the building. Also a 31% surcharge on the annual cost of capital is included, in the $0.117\ y^{-1}$ factor, to account for special services which are the "indirect" utility consumption, that is for heating, air-conditioning, lighting,etc. for the building.

To properly calculate the direct material cost, that is the cost of the cylindrical slicing ingot, the amount of the silicon crystal lost in grinding is necessary. The grinding of the cylindrical ingots to a uniform outside diameter, previous to slicing, facilitates the slicing operation, as well as tooling and handling of the sliced wafers in subsequent device fabrication procedures. In calculating the mass fraction of silicon lost in grinding, shown in line 18 of Table II-2, the average diameter

loss is assumed to be 0.6 cm. With this diameter loss, and the consequent loss of mass, the price per unit mass of silicon entering into the slicing operation can be determined. Since the grinding diameter loss stays constant with crystal diameter, the fraction of lost silicon is inversely proportional to the diameter of the crystal.

The difference between the add-on processing cost and the work-in-process cost is the cost of the direct material contained in the wafers. The latter value for a unit area can be obtained by multiplying line 19 of Table II-2 by the unit mass silicon cost. To obtain the amount of silicon contained in a unit wafer area, the incorporated silicon fraction is divided by the wafer area per unit mass (Table II-1, line 18). The incorporated wafer fraction is the product of the yield fraction (taken from Table II-1, line 6) and wafer thickness (Table II-1, line 4) divided by the sum of the wafer and kerf thicknesses. In equation form, the fraction of silicon contained in the wafer is,

$$\text{II-2.19} = \frac{\text{II-1.6}*\text{II-1.4}}{(\text{II-1.4}+\text{II-1.5})*\text{II-1.18}} \frac{kg}{m^2} ,$$

with the roman numerials dash arabic numbers representing the table numbers and the final arabic numbers, the line numbers for that table. The kerf and broken wafer loss, necessary for differentiating the operating add-on cost from the specific add-on cost, is calculated in a similar fashion to line 19 of Table II, except that the kerf loss is represented by the kerf thickness and the broken wafer loss by the broken wafer fraction multiplied by the wafer thickness. Therefore

$$\text{II-2.20} = \frac{(\text{II-1.5}+(1-\text{II-1.6})*\text{II-1.4})}{(\text{II-1.4}+\text{II-1.5})*\text{II-1.18}} \frac{kg}{m^2} ,$$

From the operation data and expenses, listed in the first two tables, the add-on components of the slicing manufacturing slicing cost can be calculated. For the most part, the add-on cost components, shown in Table II-3, on a per unit area basis, are derived from the data of the proceeding tables using the relationships given in that table. The exceptions include the unit costs of the indirect materials which were taken from the sources footnoted in Table II-3. In addition, the purchased service cost for multi-blade slicing (Table II-3, line 4), which includes the cost of machine maintenance and overhaul performed on the outside or under contract, used was \$1529.3 y^{-1} and was obtained from Spectrolab[1]. HAMCO[2] supplied the purchased service cost for an inner diameter slicing as \$285.7 y^{-1}. The total material cost which is the sum of the first four lines of Table II-3 was increased by 5.26%, in accordance to SAMICS charge factors[12], to account for handling and other miscellaneous expenses.

The labor costs were calculated using the labor times, listed in Table II-2 and the labor rates shown in the Cost Account Catalog of the SAMICS Support Study[13]. For calculating the direct labor costs which involve crystal mounting, machine loading and supervision the wages paid an electronics semiconductor assembler, whose duties are described under SAMICS' occupation classification no. 726884 and wages under catalog no. B3096D[13] were employed. The maintenance labor rate of a maintenance mechanic II (occupation classification no. 726884, catalog no. B3736D) was used to find the labor cost of internal machine service and cutting tool charges. The listed labor rates were multiplied by 1.432 to take into consideration fringe benefits, such as vacations, medical health plans, social security benefits, etc, and miscellaneous expenses. A surcharge of 25% was added to the direct

TABLE II-3A

ADD-ON COST COMPONENTS FOR MULTIBLADE SLICING ($/m²)

	Organization	2 cm Rectangular	Spectrolab (Production Experience) 5.4 cm Diameter	Spectrolab (Production Experience) 7.5 cm Diameter	OCLI (Experimental) 10.16 cm Diameter	Varian (Experiment no. P-005) 10cm Diameter	Varian (Projection) 10cm Diameter	TI (900 blade projection) 12cm Diameter	TI (Experimental) incl. Projection) 12cm Diameter
1.	Expendible tooling (IIA.6 ÷ IA.16* IA.17)	10.35	15.34	23.81	74.31	32.68	10.49	2.04	1.33
2.	Materials	21.15 (a)	8.95 (a)	6.95 (a)	16.35 (b)	7.50 (c)	3.40 (c)	3.85 (c)	0.30 (d)
3.	Electrical energy cost ($0.032 *IIA.10 ÷ IA.17)	0.25	0.43	0.33	0.42	0.67	0.32	0.16	0.11
4.	Replacement parts & purchased service	1.85	3.01	2.37	2.94	4.62	2.90	0.67	0.83
5.	Total material costs (1.0526* (1.+2.+3.+4.))	35.37	29.19	35.22	98.96	47.86	18.01	7.37	2.70
6.	Direct Labor ($5.58*IIA.4 ÷ IA.17)	10.[illegible]	19.16	15.14	4.08	4.85	3.31	1.31	1.15
7.	Maintenance labor ($ 8.12* IIA.4 ÷ IA.17)	4.71	6.98	5.42	4.50	3.55	2.43	0.96	0.94
8.	Other indirect labor (25% of 6. + 7.)	3.86	6.53	5.14	2.15	2.10	1.44	0.46	0.52
9.	Total labor (6. + 7. + 8.)	19.32	32.67	25.70	10.73	10.50	7.18	2.33	2.61
10.	Equipment cost (IIA.14 ÷ IIA.12 * IA.17)	4.96	8.08	6.37	7.90	12.43	7.80	2.71	2.22
11.	Facilities cost (IIA.17 ÷ IIA.12 *IA.17)	1.14	1.85	1.46	1.81	2.85	1.79	0.41	0.34
12.	Capital Cost (10. + 11.)	6.10	9.93	7.83	0.71	15.28	9.59	4.50	2.56
13.	Overhead (0.059 * (12.) + 0.1[illegible] * (11.))	0.42	0.68	0.53	0.66	1.04	0.65	0.20	0.17
14.	Return on equity (0.192*(5.) + 0.192*(9.)+ 1.22 * (10.) + 4.73*(11.))	21.94	30.49	25.37	39.26	39.85	22.82	7.05	5.34
15.	Add-on price ($1 price assumed zero) (5.+9.+12.+13. +14.)	83.15	102.70	95.53	199.25	114.29	58.10	21.15	13.34
		Silicon Ingot Price (Unground) @ $139.15/kg (1978 estimation)							
16.	Add-on cost of grinding ($/kg)	-	20.97	13.99	9.77	9.96	9.96	8.07	8.07
17.	Cost of ground Si ($/kg)	-	160.12	153.14	148.92	149.11	149.11	147.22	147.22
18.	Lost Silicon	-	116.89	111.79	158.80	113.21	78.05	77.05	82.68
19.	Add-on price	-	219.59	207.31	318.14	227.50	136.15	98.20	96.02
20.	Price	-	368.50	349.73	433.15	328.68	223.61	184.32	206.93
		Silicon Ingot Price (Unground) @ $65.98/kg (1982 projection)							
21.	Add-on cost of grinding ($/kg)	-	12.84	8.13	5.45	5.56	5.56	4.41	4.41
22.	Cost of ground Si ($/kg)	-	78.82	74.11	71.43	71.55	71.55	70.39	70.39
23.	Lost Si	-	57.84	54.10	76.61	54.66	37.31	36.84	40.43
24.	Add-on price	-	160.24	149.43	235.60	167.95	99.31	87.76	92.87
25.	Price ($/m²)		233.83	219.00	290.83	216.50	137.17	98.94	105.58
		Silicon Ingot Price (Unground) @ $26.44/kg (1986 projection)							
26.	Add-on cost of grinding ($/kg)	-	8.23	4.81	3.00	3.07	3.07	2.34	2.34
27.	Cost of ground Si ($/kg)		55.00	50.29	47.46	47.61	47.61	46.80	46.80
28.	Lost Silicon	-	33.00	31.37	49.18	40.65	14.32	13.84	15.06
29.	Add-on Price	-	116.58	110.90	180.83	134.94	71.42	35.09	38.39
30.	Price	-	157.16	144.30	209.83	161.62	98.41	60.77	60.44

(a) Calculated using $7/gallon for the slurry mixture and including $0.80/loaf for the ceramic base and bars.

(b) H.I. Yoo, "Assessment of Present State of the Art Sawing Technology," OCLI, DOE/JPL 954830-77/12, p. 34 (12/77).

(c) S.C. Holden and J.R. Fleming, "Slicing of Silicon into Sheet Material" Varian Associates, ERDA/JPL 954374-77/2, p. 22 (7/77).

(d) Samuel N. Rea and Paul S. Glein, "Large Area Czochralski Silicon," Texas Instruments, ERDA/JPL-954475-76/2, p. 17, (9/76).

TABLE II-3B

ADD-ON COST COMPONENTS FOR MULTIWIRE AND INNER DIAMETER SLICING ($/m²)

	Organization	Multiwire Wafering			Inner Diameter Slicing		
		Crystal Systems	Yasunaga V-100		OCLI		HAMCO
		Fixed Abrasive Method (projection)	(Experimental) 7.6 cm diameter	(Projection) 10 cm diameter	(Experimental) 7.6 cm diameter	(Experimental) 10.16 cm diameter	(Production exp.) 10.16 cm diameter
1.	Expendible tooling (IIB.6 ÷ 15.16 *IB17)	1.25	33	18.25	4.65	3.70	12.45
2.	Materials	0.30 (a)	32.95 (b)	41.05 (d)	2.65 (e)	2.05 (e)	1.85 (f)
3.	Electrical energy cost ($0.0319* IB.10 ÷ 6.17)	0.11	0.18	0.22	0.49	0.33	0.33
4.	Replacement parts and purchased service	n.a.	n.a.	n.a.	0.30 (g)	0.21 (g)	0.20 (g)
5.	Total materials (1.0526*(1. + 2. + 3. +4.))	1.74	69.61	62.65	8.52	4.52	13.51
6.	Direct labor ($5.58*IIB.4 ÷ IB.17)	1.30	4.72	1.19	3.05	1.93	5.85
7.	Maintenance labor ($8.12*IIB.5 ÷ IB.17)	0.56	4.14	1.55	2.63	2.50	1.47
8.	Other indirect labor (25% of (6. + 7.))	0.45	2.22	1.19	1.42	1.11	1.83
9.	Total labor (6. + 7. + 8.)	2.30	11.08	5.93	7.10	6.54	9.15
10.	Equipment cost (IIB.14 ÷ IIB.12 IB.17)	2.06	8.79	10.21	9.09	6.28	5.97
11.	Facilities cost (IIB.17 ÷ IIB.12 IB.17)	0.32	0.96	1.12	1.67	1.15	1.10
12.	Capital Cost (10. + 11.)	2.38	9.75	11.33	10.76	7.43	7.07
13.	Overhead (0.059* (10.) + 0.108.*(11.))	0.16	0.57	0.66	0.72	0.49	0.471
14.	Return on equity (0.192* (5.) 40.192*(9.) + 1.22* (10.) + 4.73*(11.))	4.80	30.57	30.92	21.99	15.22	16.84
15.	Add-on price (Si price assumed zero) (5. +9. +12. +13. +14.)	11.38	121.57	111.62	49.06	36.29	47.04
		Silicon Ingot Price (Unground) @ $139.15/kg (1978 estimation)					
16.	Add-on cost of grinding ($/kg)	9.94	13.77	9.96	13.77	9.77	9.77
17.	Cost of ground silicon ($/kg)	149.09	152.92	149.11	152.92	148.92	148.92
18.	Lost Silicon ($/m²)	104.66	71.57	34.30	131.09	122.17	120.96
19.	Add on price ($/m²)	116.04	193.14	145.92	180.15	158.46	168.00
20.	Price ($/m²)	150.93	268.45	215.70	309.02	280.48	342.31
		Silicon Ingot Price (Unground) @ $65.98/kg (1982 projection)					
21.	Add on cost of grinding ($/kg)	5.55	7.99	5.56	7.99	5.45	5.45
22.	Cost of ground Si ($/kg)	71.53	73.97	71.55	73.97	71.43	71.43
23.	Lost Si	50.21	34.03	16.46	62.87	58.57	57.99
24.	Add-on price	61.59	155.60	128.08	111.93	94.86	104.83
25.	Price ($/m²)	78.33	192.03	161.57	174.24	155.03	188.40
		Silicon Ingot Price (Unground) @ $24.46/kg (1986 projection)					
26.	Add-on cost of grinding ($/kg)	1.08	4.71	1.07	4.71	1.00	1.00
27.	Cost of ground Si ($/kg)	27.52	29.17	27.53	29.17	27.46	27.46
28.	Lost Si	19.33	13.43	6.33	24.79	22.52	22.29
29.	Add-on price	30.70	134.33	111.35	73.85	58.80	69.33
30.	Price	37.14	149.16	130.83	94.65	79.80	101.48

(a) F. Schmid and C.P. Khattack, "Heat Exchanger-Ingot Casting/Slicing Process" Crystal Systems, ERDA/JPL 954377-77/3, pp. 78-79 (10/77).

(b) Calculated using $12.10/kg[c] for the abrasive and $1.25/ℓ[c] for the PC oil and assuming the slurry is used twice.

(c) LSSA Project Report, "Multiwire Slurry Wafering Demonstrations," Jet Propulsion Laboratory, DOE/JPL-1012-7817, (2/78).

(d) Estimated from materials cost of Yasunaga's 7.6 cm diameter ingot.

(e) M.I. Yoo, "Assessment of Present State-of-the-Art Sawing Technology," OCLI, DOE/JPL 954830-77/12, p. 18 (12/77).

(f) Estimated from OCLI's material cost data.

(g) Assuming total purchased service is $2,000 for the machine's lifetime.

labor and maintenance labor costs to account for the cost of supervisory, management, and other support personnel.

The unit area equipment and facility costs, which constitute the capital cost, were obtained by dividing the respective annual costs by the annual area factory output. The overhead, listed in line 13 of Table II-3, is defined as the insurance, state taxes, and interest-on-debt payments on the working capital. As suggested by SAMICS[12], the working capital was taken as 15% of the equipment plus facility cost, or 15% of the capital cost.

The profit and the amortization of one-time costs is represented by the return-on-equity (ROE), shown in line 14 of Table II-3. This value is equal to the SAMICS' return-on-equity (EQR), which is 20% of the equity portion of the book value[12], plus the amortization of the start-up costs (AOC), minus the income tax investment credit (ITC) on 10% of the annual equipment depreciation divided by the product of one minus the federal income tax credit ($1 - \tau$) and one minus the miscellaneous expense fraction, $(1 - x)$, or

$$\text{ROE (II-3.14)} = \frac{\text{EQR} + \text{AOC} - \text{ITC}}{(1-x) * (1-\tau)} \quad \$/m^2.$$

The add-on cost components described above can be used to calculate a unit area wafer price that ignores the cost of the silicon ingots. This add-on price shown in line 15 of Table II-3, is the sum of the material, labor, capital, overhead and return-on-equity. To convert this value into a wafer price, the unit mass cylindrical crystal price, and the add-on

grinding cost must be added to it. The unground silicon crystal or ingot prices shown for 1978, 1982 and 1986 are taken from our previous evaluations.[14] For 1978, the ingot price is based on pulling 7.8-cm diameter ingots with a Leybold-Heraeus single charge puller. The silicon ingot prices employed for the years 1982 and 1986 are projections for multi-pulling Cz-grown 10.2-cm and 15.2-cm diameter ingots, respectively.

Previous to slicing, the silicon ingots must be ground to a uniform diameter and this cost has to be included in the cost of the direct material. The add-on cost of grinding, listed in line 16 of Table II-3, consists of two parts: a) the cost of the grinding operation which is projected to be \$0.20/cm-crystal length, based on industry data[1]; and b) the cost of the silicon lost from grinding, which is equal to $\frac{\text{II-2.18}}{(100 - \text{II-2.18})}$* (Si ingot price (\$/kg)), where II-2.18 is the percentage of material lost in grinding Summing the add-on grinding cost to the Si ingot price yields the cost of ground silicon prices (Table II-2, lines 17, 22, 27) which are used to calculate silicon wafer prices.

Also of interest in our analysis is the cost of the silicon lost in kerf and broken wafers. These values, shown in line 18, 23, 28 of Table II-3, are the product of the unit area kerf and wafer loss mass (Table II-2, line 20) and the ground silicon prices. The add-on wafer prices, shown in lines 19, 24 and 29 of Table II-3 are defined, here, as the sum of add-on wafer price assuming a zero silicon price (Table II-3, line 15) and the cost of the lost silicon.

To arrive at a unit area wafer price listed in lines 20, 25, and 30 of Table III, the add-on price and the cost of silicon incorporated in the

wafer are summed. The latter value is the cost of the ground silicon ingot multiplied by unit area silicon mass contained in the wafers (Table II-2, line 19).

4. Cost Structures of the Slicing Processes

The more important unit area manufacturing cost components for selected current production or experimental slicing capabilities, using 1978 silicon prices, and projected future capabilities, using 1982 and 1986 projected silicon prices are summarized in Table II-4. These silicon prices apply to single crystal ingots ground to a uniform diameter. The diameter tolerance for the ground ingots has been given as $\pm$ 0.125mm standard by Siltec, and as $\pm$ 0.075mm by Spectrolab. Also included in this table are the costs of the lost silicon and that contained in the wafer. In Table II-4, one can observe the decreases in expendible tooling, indirect materials, labor and capital costs that are expected for 1982 in ID multiblade and slurry multiwire slicing. Illustrated in Figure II-4 are the more relevant data of Tables II-3 and II-4, in a bar graph format. In Figure II-4, the relative impacts of the material, labor and capital costs can be readily compared to each other for the current multiblade and ID slicing processes and for the near future (1982) projected multiblade, ID, and slurry multiwire processes.

As evidenced in Table II-4, the indirect material costs (primarily slurry) and the costs for expendible tooling (the steel blades or wires) are much higher for the slurry sawing processes (multiblade and Yasunaga multiwire) than those for the fixed abrasive approaches (ID saw and FAST wire saw). This is a consequence of the more effective utilization of the abrasive in the fixed abrasive system, coupled with longer tool life. Reductions of these expendible tooling costs for the multiblade and slurry multiwire slicing processes are expected in the future through lower cost tool fabrication techniques[9,11] and through improved lifetimes[9]. The lower tool cost fabrication techniques are expected to result from larger

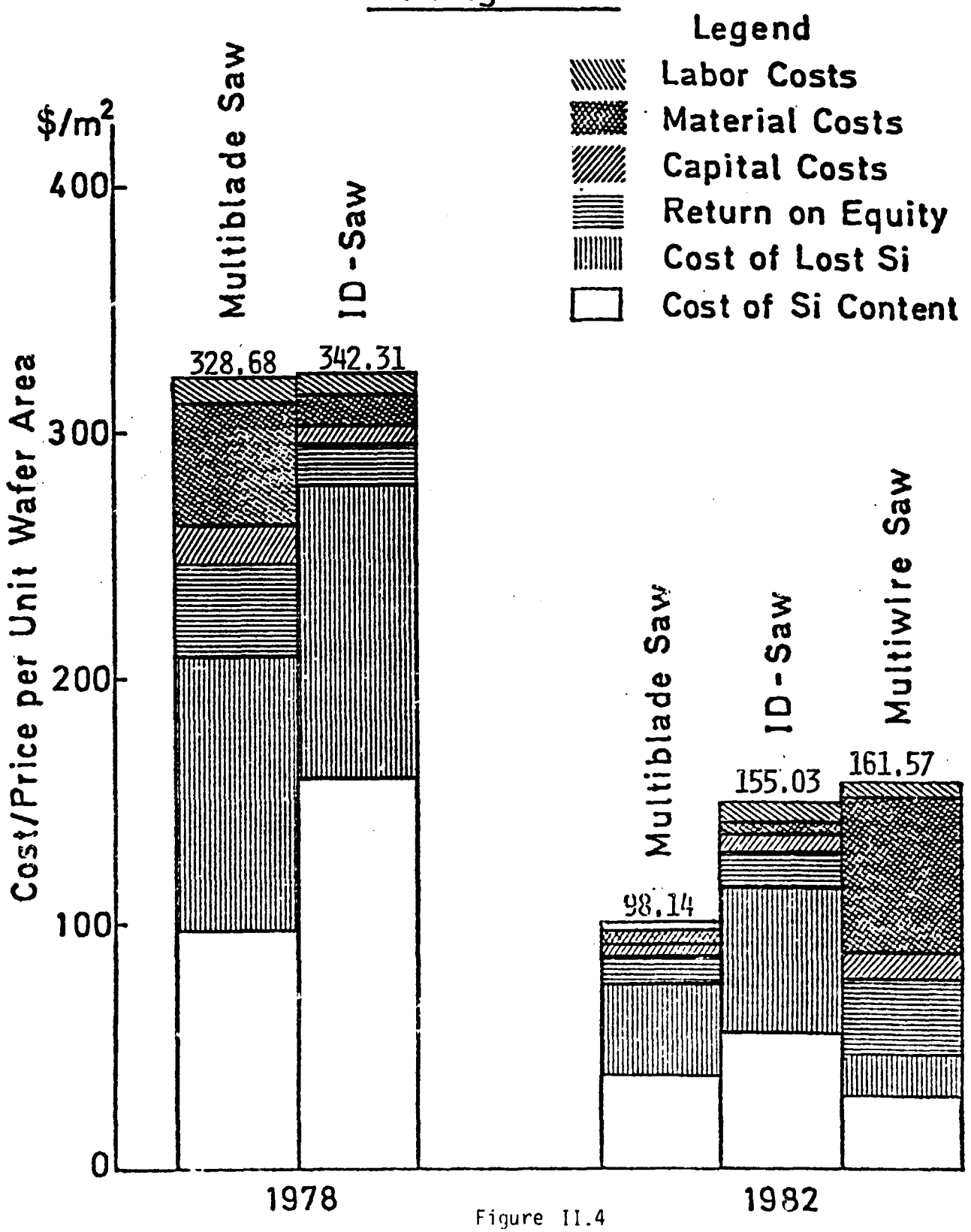

Figure II.4

Costs of silicon wafer production in the years 1978 and 1982 by the slicing cost components, including the cost of the single crystal silicon content.

TABLE II-4

KEY COST COMPONENTS OF SLICING

Type	ID Saw		Multiblade			Multiwire		
Source	OCLI	STC	Spectrolab	Varian		Yasunaga		Cryst. Systems*
X-tal Dia (cm)	7.6	10	7.5	10	12	7.6	10	10 x 10 rect.
Data Type	Exper. 1978	Projected 1982	Product.	Exper.	Projected 1982	Exper.	Projected 1982	Projected 1986
Tooling	4.65	1.46	23.81	32.68	2.04	33.00	18.25	0.33
Ind. Materials	2.65	-	6.95	7.50	3.85	32.95	41.05	0.35
Dir. Labor	3.05	1.48	15.14	4.85	0.77	4.72	3.19	1.67
Maint. Labor	2.63	0.15	5.42	3.55	0.56	4.14	1.55	0.54
Equip't Cost	9.09	3.66	6.37	12.43	2.71	8.79	10.21	2.55
Facil. Cost	1.67	0.50	1.46	2.85	0.41	0.96	1.12	0.47
Add-On Cost	27.07	7.25	69.16	74.44	13.43	91.00	80.70	7.61
Ret. on Equity	21.99	7.68	28.37	39.85	6.92	30.57	30.92	6.18
Lost Si	131.09	38.97	111.79	113.21	36.61	71.57	16.46	12.88
Add-On Price	180.15	53.90	207.32	227.50	56.96	193.14	128.08	26.67
Si Content	128.87	37.65	142.41	101.18	41.18	75.14	33.49	12.88
Price	309.02	91.55	349.73	328.68	98.14	268.14	161.57	39.55
Si ground X-tal ($/kg)	152.92	71.55	153.14	149.11	70.39	152.92	71.55	27.52

*Calculated using an effective cutting rate of 0.4 cm/h.

scale, automated assembly[9] and a simplification of the assembly process[11]. Investigations are currently being conducted into possibilities for lowering the slurry costs, for instance by reclycling the slurry or substituting a cheaper vehicle (e.g. mineral oil) for the PC oil. In spite of these projected reductions, the indirect material and expendible tooling costs for the multiblade and the Yasunaga multiwire techniques remain sizable components of the total add-on costs for those processes. In the near-term projections, these components are 44% and 73% of the add-on cost for the multiblade and slurry multiwire processes, respectively. This compares to 20% and 9% of the 1982 projections for the add-on costs in the ID and fixed abrasive multiwire saws, respectively.

The current prices are essentially equal for production wafers cut by either the Varian multiblade or the ID sawing processes, although the ID saw has twice the productivity (Table II-1, line 24) and experiences lower indirect material and tooling costs. The higher productivity directly results in lower labor, capital, and return-on-equity costs, as shown in Figure II.4. These lower processing costs for the ID slicing are counter-balanced, however, by a higher silicon consumption resulting from the practice to cut the wafers to greater thickness with higher kerf than achieved with the slurry saws. At the current silicon prices, this has a considerable cost impact.

The 1978 wafer prices shown here are somewhat lower than the contemporary commerical wafer and the 1978 values of the LSA Interim Price Allocation Guidelines[14]. This difference results from two facts: a) the data of this report do not include the cleaning, etching, or polishing process steps usually included in commercially sold wafers; and b) the standardized indirect cost model (SAMICS-IPEG) purposely omits several

indirect charges on partially processed items such as wafers. Since the indirect cost structure models a vertically integrated industry, marketing costs for wafers, e.g. are not incurred.

5. CONCLUSIONS

The cost-analysis data, and particularly the projections, which include reduced expendible tooling and indirect material cost components, show that the dominant influence on the add-on price of sliced wafers is the productivity of the slicing machine. The machine productivity (the time rate of output unit expressed in wafer area) has a direct inversely proportional impact on the capital cost allocation to the wafer area produced of the cost components for equipment and facility, and on that part of the labor expenditures which are devoted to machine monitoring and maintenance, as shown in Figure II.5. Figure II.5 shows that the effective linear cutting rate (the workpiece diameter divided by the slicing time-segment) is 0.55 $\pm$ 0.3 cm/h for the multiblade and multiwire processes. The inner diameter diamond-coated blade process has an effective linear cutting rate of approximately 300 cm/h, a nearly 550 times larger value than that for the other processes. To achieve comparable machine productivities, the low linear cutting rates have to be compensated by simultaneous multiple slicing. The current efforts of Crystal Systems, Solarex, and Varian are therefore directed at increasing the number of wafers sliced during a run. Current multiblade packages contain about 250 blades. Varian has built an experimental slicer incorporating a blade pack of over 900 blades. Similarly, the wire package proposed by Crystal Systems[10] is projected to have 750 cutting wires. Solarex hopes to slice[11] 333 wafers at a time with the Yasunaga YQ-100 slicing machine.

The slicing technology improvements projected for the 1982 production lines are based on the results of recent experimental runs and on

CUTTING RATES:

ID SAW ~300 cm/h

ALL OTHER SAWS ~0.55 ± 0.3 cm/h

↓

IMPACTS:

PRODUCTIVITY

↓

CAPITAL COST: EQUIPMENT
FACILITY
LABOR (?)

REMEDY: MULTIPLE CUTTING

Figure II.5

developments in progress (Table II-4, Fig. II.5). For the multiblade saw, the primary advancement will be a nearly four-fold productivity increase via Varian's development of a machine using a 900-blade-pack. Simultaneously, a 25% blade thickness reduction in combination with a 37.5% wafer thickness decrease, while maintaining a wafer yield of 95%, is projected to result in an area yield of 0.9 m^2/kg-Si crystal, a 50% increase from Spectrolab's mass to area conversion ratio in slicing round wafers.

Slice and kerf thickness reductions to values similar to those projected for the multiblade slurry process, are also expected for the ID-sawing method. Recently acquired data from STC are reflected in a 1982 projection for 10-cm diameter crystals using ID slicing with ingot rotation, as shown in Table II-4.
The wafers from this process are expected to be 225 μm thick with 210 μm kerf. In addition, crystal rotation is expected to double the effective cutting rate of the ID process. This essentially doubles the productivity of the ID saw, and results in comparable projected productivities for the 900-blade multiblade and the ID sawing processes. Remaining differences in the costs of these two processes are, however, overshadowed by the cost of the silicon incorporated into the wafer or lost. At the projected 1982 price for ground single crystal ingots, the cost of this silicon still amounts to nearly 80% of the wafer price.

One slicing method has been projected to 1986, primarily, because only a comparatively small base of experimental data is available, so that this method cannot be expected to be in significant commercial operation by 1982. This method is Crystal Systems' fixed abrasive

multiwire sawing. The current projections are contained in Table II-4, while Table II-3B is based on earlier inputs. The difference results primarily from a recently communicated reduction in tooling costs based on wirehead fabrication improvements, and from the use in Table IV of a more conservative effective cutting rate corresponding to the experimentally found rates averaged over the life of the bladehead. The process add-on costs are comparable to those of the two previously discussed processes. If the silicon price of 1982 would have been used, an approximately $\$11/m^2$ lower wafer price would have resulted in comparison to the ID process. While the fixed abrasive multiwire process currently projects the lowest wafer price, it is also the one with the least experience data. It is therefore of great importance to gain a significant data base through pilot line operation.

Considering the uncertainties in the projections, the data indicate no considerable differences in the competitiveness of the three approaches, and a reasonable potential for all three to meet the 1986 guideline goal.

6. REFERENCES

1. R. Oliver, Spectrolab Inc., Sylmar, CA., private communications (3/78).
2. C. McGinnis, HAMCO, Rochester, N.Y., private communications (4/78).
3. H.I. Yoo, OCLI, Report DOE/JPL 954830-77/12 (12/77).
4. S.C. Holden and J.R. Fleming, Varian Associates,Report ERDA/JPL 954374-77/2 (7/77).
5. S.N. Rea and P.S. Gleim, Texas Instruments, Report ERDA/JPL 954775-77/4 (4/77).
6. H.I. Yoo, ibid.
7. P. Alaronyan, Silicon Technology Corp., Oakland, N.Y., private communications (8/78).
8. C.P. Chen, JPL-LSA Project Report DoE/JPL-1012-78/7 (2/78).
9. S.C. Holden and J.R. Fleming, ibid.
10. F. Schmid and C.P. Khattack, Crystal Systems, Report ERDA/JPL 954373-77/3 and 77/4 (10/77 and 12/77).
11. J. Lindmayer et. al., Solarex, Report ERDA/JPL-77/2 (8/77).
12. R.W. Aster and R.G. Chamberlain, JPL-LSSA Project Report 5101-33 (9/77).
13. Theodore Barry and Associates, Report ERDA/JPL-954800-77/2.1 (9/77).
14. W. Callaghan, presented at the Ninth PIM; Pasadena, CA, (4/78).

III. Junction Formation

1. Introduction

In general, the first major step in the process sequence from quartzite to complete solar modules, following the generation of the silicon wafers, ribbons, or sheet, is that of pn junction formation. Of the primary present junction forming processes, gaseous diffusion was examined in great detail as the base case. Then, other diffusion processes and ion implantation, proposed as methods for lower cost junction formation, were analyzed.

As with our crystal growing and slicing studies, the evaluations were started with the current methods of diffusion and ion implantation for which a large amount of the needed information is available.

For the diffusion process, we have tabulated production experience data from Spectrolab[1] and projections made by Motorola[2] and RCA.[3] In our studies of ion implantation of pn junctions, experimental data from Spire[4] using a modified Varian-Extrion machine, along with material, labor, and capital projections made by Lockheed[5], Motorola,[6] and Spire[4] for their proposed machines were examined.

2. Diffusion Processes

The principles of the diffusion processes are extensively described in the literature and will not be repeated here. These processes are the ones most widely used in the semiconductor industry for the formation of pn junctions. There are two basic variations: the infinite dopant source method, which results in a complementary error function distribution of the dopant with depth below the surface, and the finite source method, which results in a Gaussian distribution. The infinite source method represents principally a one step process in which the dopant is transferred from an impurity carrier material into a surface layer of the silicon wafer which becomes dopant-rich up to the solid solubility of the respective impurity in silicon (source layer), and from which the diffusion into the wafer takes place, simultaneous with the formation of this source layer. In this case, the dopant carrier material (the "infinite source") remains present throughout the diffusion process. In the finite source method, the dopant carrier material is removed after a "back-on" cycle for source layer formation, and diffusion continues subsequently for a longer time period in the "drive-in" cycle, redistributing the dopant originally contained in the source layer deeper into the wafer.

In solar cell production, the infinite source method is used exclusively, and the processes vary only in the dopant carrier material used and the form of its application. Very commonly used is phosphine gas in an "open tube" system, generating a phosphorus glass layer on the silicon wafer.

This glass layer is formed during the first part of the diffusion step, but in the same furnace and at the same temperature as the rest of the process. This phosphorus glass is then the dopant carrier material from which the source layer is formed. The phosphorus glass is removed only after completion of the diffusion process. In an alternate approach, the dopant carrier material is supplied in semi-liquid form and applied to the wafer in a spray-on or spin-on step, with subsequent glass formation and diffusion occuring in a belt furnace potentially as a continuous flow process. While, in the "gaseous" diffusion process, the gas cycling and flow control is performed fully automatically, it is still at batch process with usual furnace loading and unloading.

As diffusion is currently the major competitive process, we have examined the attributes and costs of present and projected future diffusion processes. In the current production operation, Spectrolab uses open-tube diffusion with phosphine diluted heavily in hydrogen to form a pn junction. Thanks to the data supplied generously by R. Oliver and E.L. Ralph of Spectrolab,[1] we have been able to make a detailed analysis of the present diffusion process as a baseline case. The detail data of this process are presented in Tables III-4A through 4C and the cost summary in Table III-3. The diffusion process takes approximately 35 minutes for a run containing 75 wafers of 7.62-cm diameter. We have observed that the process as performed by Spectrolab is very labor intensive. The reason is that only two diffusion furnaces are needed to handle the entire production, but one operator is needed

to attend the process. Thus, this operator devotes most of his/her time to manually loading and unloading wafers onto and from the quartz diffusion boat, which could be done mechanically. If one assumes automatic wafer feeding, the operator's time could easily be reduced to 10 minutes per run, and the processing add-on price would be reduced to approximately $\$9.50/m^2$ from the present value of $\$12.74/m^2$ (SAMICS methodology).

Another significant cost contributor, and one that has been ignored in most projections for future diffusion processes, is that for cleaning the quartz furnace tubes and boats, which is usually done with a $HF-HNO_3-H_2O$ solution, as often as twice a day. Frequent quartzware cleaning has been found instrumental to maintaining high cell efficiency, but it contributes $\$2.23/m^2$ to the diffusion add-on price in the Spectrolab process. This price contribution was calculated assuming that the quartz cleaning operation requires 1 h/work day of labor, and a tube cleaning tower which costs $15,000 including installation, and which is shared between the two furnaces. About half of this cleaning cost contribution is due to equipment costs, with the remainder, listed in decreasing magnitude, shared between labor, facility, and material costs.

Future diffusion price projections, such as for Motorola's phosphine (PH_3) process,[2] also detailed in Table III-4A to 4C, are about a factor of four lower than present calculated prices ($\$3.10/m^2$ compared to

$12.74/m^2$). The Motorola process which has approximately the same wafer throughput rate as Spectrolab's current process, is applied to 12-cm diameter wafers, rather than 7.62-cm wafers in the Spectrolab process.

The 12-cm wafers have an area that is nearly 2.5 times larger than that of the 7.62-cm wafer, accounting for most of the cost difference between Motorola's and Spectrolab's diffusion processes. The rest of the cost difference can be attributed to the more automated nature of the Motorola process, requiring half-as-much labor as Spectrolab requires, and the lack of inclusion, by Motorola, of costs for cleaning the quartzware. On the other hand, notable are Motorola's projected use of significantly more energy and direct material (phosphine) than Spectrolab is consuming now.

Currently, the PN junction formation process by diffusion is not a large cost-contributing factor in cell processing. In application of the diffusion process, a separate annealing step is not required, at least not beyond a somewhat slowed cooling rate from diffusion temperature. A separate post-annealing step is, however, required after the ion implantation process to reduce the crystal damage resulting from implantation, and to activate the impurity species. Therefore, the annealing cost must be included in any cost analysis of ion implantation. Using a Thermco eight-tube diffusion furnace, which has an output rate of 1,000 12-cm diameter wafers/h, an add-on price of $\$1.18/m^2$

was calculated for the annealing process step.

If ion implantation is to replace diffusion, it may be able to become cost competitive only as part of a more extended sequence of vacuum processes, or by producing cells of significantly higher performance than achievable by the diffusion process.

3. Principals and Application of Ion Implantation

Ion implantation is a method for introducing dopant material below the semiconductor surface to form PN or high/low junctions. In the common type of ion implantation machine, the source material, usually a chemical compound containing the dopant, is broken down and ionized under electron bombardment in the ionization chamber, the ions are extracted from this chamber by an electric field and further accelerated and collimated, purified using a mass spectrometer, and then scanned either electrically, magnetically, or mechanically while impinging on the semiconductor wafer to be implanted. The top portion of Figure III.1 shows a schematic presentation of such an ion implanter with a magnetic analyzer. In simpler machines, as shown in the bottom part of Figure III.1, functions such as beam collimation, mass analysis, or scanning may be omitted.

In the machine shown in the top part of Figure III.1, the source material can be ionized in a number of ways, the principal ones of which are: heating and electron bombardment of the source material from a high temperature emitter, called the"hot cathode source"; electron discharge from a low work function emitter, such as barium, under the influence of a strong electric field, into the vaporized source material to form a plasma (cold cathode source); or by microwave discharge. In any of the mentioned sources, a magnetic field can be applied to concentrate the plasma density and increase the

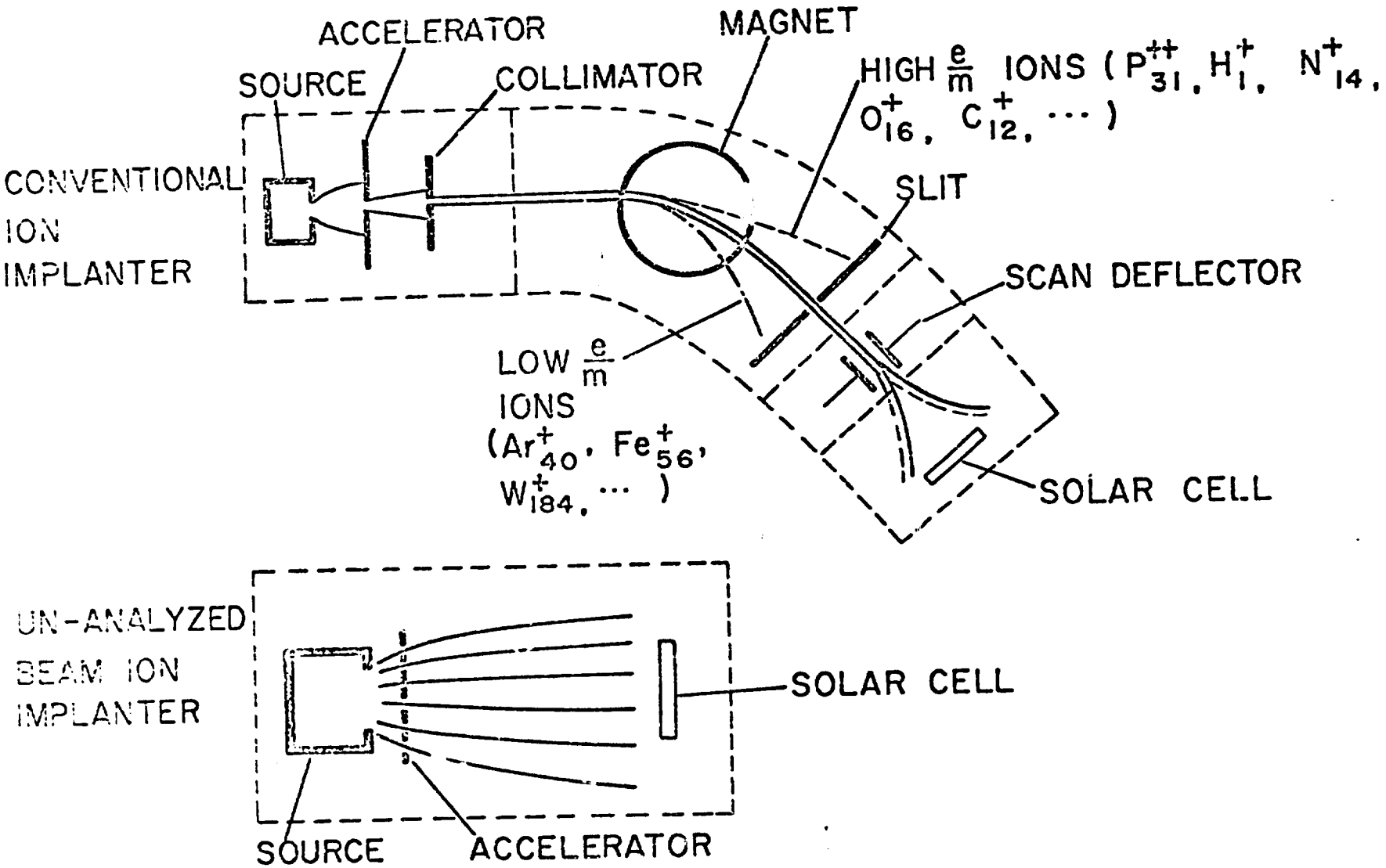

PRINCIPLES OF ION IMPLANTER DESIGN

FIGURE III.1

efficiency of ionization. This will also result, though, in lower source lifetime and a larger energy spread of the ions.

Three principal types of hot cathode ion sources are used in the implanters mentioned in this report. In all, the current density from a metal surface at temperature T with a work function of Φ is principally described by:

$$j_e = AT^2 e^{-e\Phi/kT} \qquad \text{III-2.1}$$

However, at adequately high emission rates, the current density j_e is usually reduced below the value given by Eq. III-2.1 because of space-charge effects, in which the mutual repulsion of the electrons crowding the space near the filament inhibits further emission. The electron density then becomes:

$$j_e = \frac{V^{2/3}}{9\pi d^2 \, (m/2e)^{1/2}} \qquad \text{III-2.2}$$

where V is the voltage between the cathode and anode, d is the thickness of the electron sheath and m/e is the electron's mass to charge ratio. The production of positive ions in the source chamber tends to neutralize this "electron cloud" and reduce the space charge effects. The cathode current thus increases in the presence of positive ions.

In the "Freeman source", the heated wire cathode has its terminals on opposite sides of the "extraction gap" through which the ions leave. In the "Chavet source", the filament wire is looped so that its electrodes are on the same side of

the extraction gap. The Chavet filament configuration was designed to increase the filament's lifetime by decreasing its exposure to the back-streaming ions and thus reduce the sputtering caused by them. Another thermionic source is the hollow cathode in which the interior of a cylindrical cavity is coated with a low work function material, such as barium oxide. Upon introduction of the vaporized source material, an arc discharge takes place between the cathode and anode so that the source material is ionized. As a result of applied high voltage, the ions are extracted through a hole in the cathode. Vaporized atoms also pass through this aperture. They are subsequently ionized by the accelerated electrons. One configuration of a cold cathode source known as the "Penning source", has an anode that is also cylindrical in shape with the end plates forming the cathode. In addition, a magnetic field is applied parallel to the cylindrical axis of the "Penning source" to force electrons from the cathode to form helical trajectories, thus increasing their path length and enhancing the ionization efficiency.

After the ion beam is extracted from the source chamber, it is accelerated through a potential drop. For small acceleration energies (<30 keV), a single gap electrode could be used. The accelerated ion beam is then subjected to a magnetic field for mass separation. A singly charged ion of atomic mass M (AMU's) moving through a magnetic field with strength B (in gauss) will be deflected into a circular

path with the radius of curvature equal to

$$R = \frac{143.95}{B} (MV)^{1/2} \text{ cm}, \qquad \text{III-2.3}$$

where V is the acceleration voltage. The dispersion between ions of two different masses is

$$D_M = \frac{\Delta M}{M} R \text{ cm} . \qquad \text{III-2.4}$$

In order to achieve good mass resolution, power supplies to the acceleration and magnet regions must have stabilities of 1 part in 10,000.

To form the junction, the analyzed beam is then scanned, with one of the techniques mentioned previously, on the silicon substrate. Overscanning is necessary because of the tails in the Gaussion distribution of the ion concentration in the beam.

Junction formation using ion implantation offers several potential advantages over the diffusion process. It is a dry, vacuum process, thus avoiding potential contamination from impurities contained in spin-on or gaseous vehicles for the dopants used in some varieties of the diffusion process. Where selective introduction of the dopant is wanted, this may be accomplished without application of masking and subsequent stripping, and without back-surface etching because of double-sided impurity penetrations. Thus, ion implantation can involve fewer handling or transferring operations than the diffusion process, and consequently can result in labor savings and increased

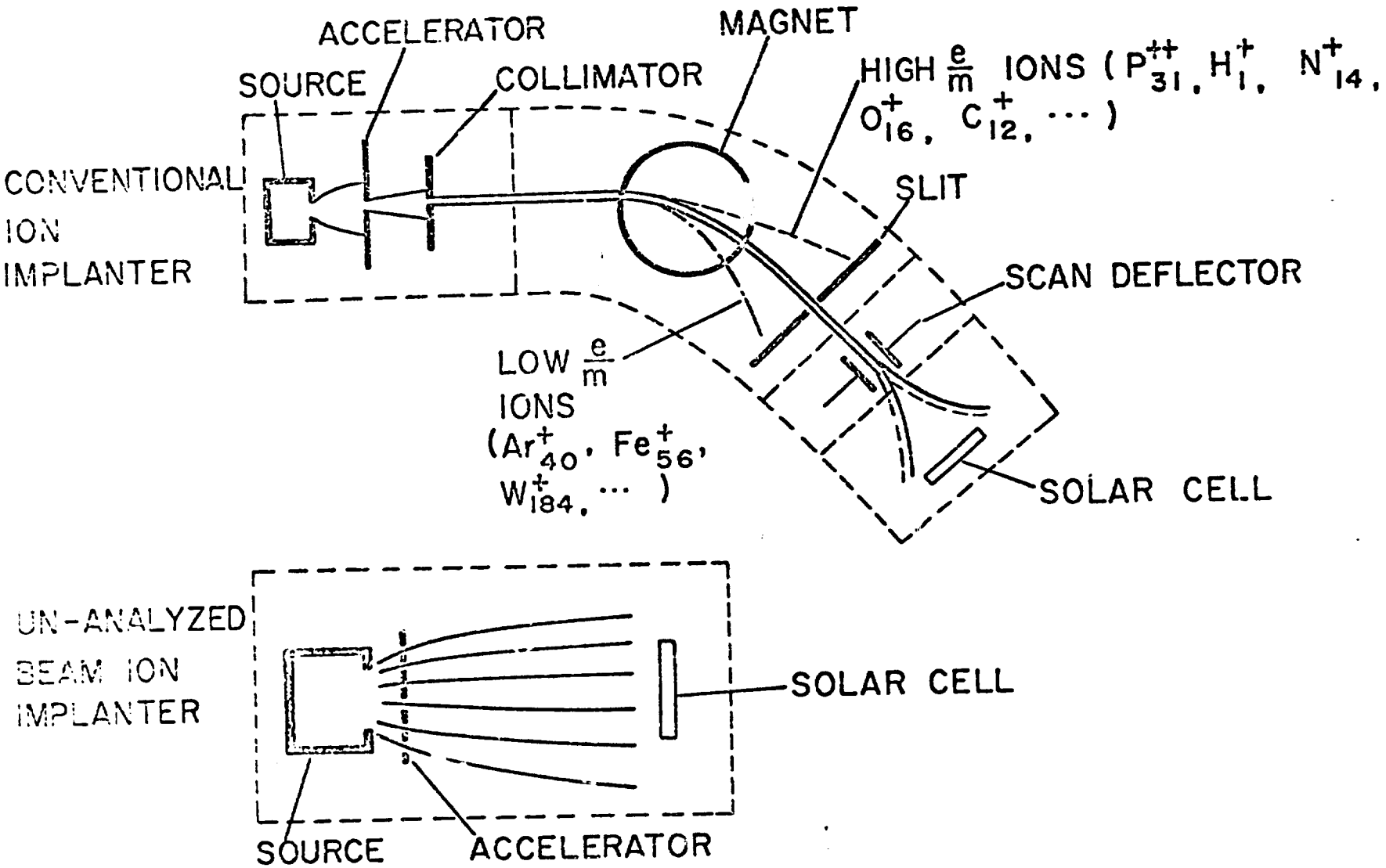

PRINCIPLES OF ION IMPLANTER DESIGN

FIGURE III.1

efficiency of ionization. This will also result, though, in lower source lifetime and a larger energy spread of the ions.

Three principal types of hot cathode ion sources are used in the implanters mentioned in this report. In all, the current density from a metal surface at temperature T with a work function of Φ is principally described by:

$$j_e = AT^2 e^{-e\Phi/kT} \qquad \text{III-2.1}$$

However, at adequately high emission rates, the current density j_e is usually reduced below the value given by Eq. III-2.1 because of space-charge effects, in which the mutual repulsion of the electrons crowding the space near the filament inhibits further emission. The electron density then becomes:

$$j_e = \frac{V^{2/3}}{9\pi d^2 \, (m/2e)^{1/2}} \qquad \text{III-2.2}$$

where V is the voltage between the cathode and anode, d is the thickness of the electron sheath and m/e is the electron's mass to charge ratio. The production of positive ions in the source chamber tends to neutralize this "electron cloud" and reduce the space charge effects. The cathode current thus increases in the presence of positive ions.

In the "Freeman source", the heated wire cathode has its terminals on opposite sides of the "extraction gap" through which the ions leave. In the "Chavet source", the filament wire is looped so that its electrodes are on the same side of

the extraction gap. The Chavet filament configuration was designed to increase the filament's lifetime by decreasing its exposure to the back-streaming ions and thus reduce the sputtering caused by them. Another thermionic source is the hollow cathode in which the interior of a cylindrical cavity is coated with a low work function material, such as barium oxide. Upon introduction of the vaporized source material, an arc discharge takes place between the cathode and anode so that the source material is ionized. As a result of applied high voltage, the ions are extracted through a hole in the cathode. Vaporized atoms also pass through this aperture. They are subsequently ionized by the accelerated electrons. One configuration of a cold cathode source known as the "Penning source", has an anode that is also cylindrical in shape with the end plates forming the cathode. In addition, a magnetic field is applied parallel to the cylindrical axis of the "Penning source" to force electrons from the cathode to form helical trajectories, thus increasing their path length and enhancing the ionization efficiency.

After the ion beam is extracted from the source chamber, it is accelerated through a potential drop. For small acceleration energies (<30 keV), a single gap electrode could be used. The accelerated ion beam is then subjected to a magnetic field for mass separation. A singly charged ion of atomic mass M (AMU's) moving through a magnetic field with strength B (in gauss) will be deflected into a circular

path with the radius of curvature equal to

$$R = \frac{143.95}{B} (MV)^{1/2} \text{ cm}, \qquad \text{III-2.3}$$

where V is the acceleration voltage. The dispersion between ions of two different masses is

$$D_M = \frac{\Delta M}{M} R \text{ cm} . \qquad \text{III-2.4}$$

In order to achieve good mass resolution, power supplies to the acceleration and magnet regions must have stabilities of 1 part in 10,000.

To form the junction, the analyzed beam is then scanned, with one of the techniques mentioned previously, on the silicon substrate. Overscanning is necessary because of the tails in the Gaussion distribution of the ion concentration in the beam.

Junction formation using ion implantation offers several potential advantages over the diffusion process. It is a dry, vacuum process, thus avoiding potential contamination from impurities contained in spin-on or gaseous vehicles for the dopants used in some varieties of the diffusion process. Where selective introduction of the dopant is wanted, this may be accomplished without application of masking and subsequent stripping, and without back-surface etching because of double-sided impurity penetrations. Thus, ion implantation can involve fewer handling or transferring operations than the diffusion process, and consequently can result in labor savings and increased

yields. However, ion implantation requires an annealing step, which will be further discussed later on. It has been suggested[8] to use ion implantation as an integral part of a total vacuum process sequence for fabricating solar cells after wafer or sheet generation. Such a sequence, although high in capital costs, could result in labor savings and high yields.

The charge on the dopant ions allows for mass-spectroscopic separation using magnetic fields, and for accurate measurement of the ion flux entering the deposition region, as long as neutral and doubly charged particles are handled correctly. The ion beam currents can be readily measured by placing a Faraday cup in the beam's path, but this requires a preceding calibration to determine the fraction of uncharged and doubly charged ions. The mass analysis and ion current measurement features of the ion implantation process can provide better control over the quantity and quality of the dopant than other processes, and can therefore be applied to obtain better process uniformity and repeatability. Dose uniformities of $\pm$ 5% (2σ) are achievable[9].

Since ion implantation can be performed at or near room temperature, low energy implantations can result in original dopant penetration of less than 100Å. This is shallower than can be achieved in most high temperature source deposition steps in the diffusion process.

Upon entering the substrate, the dominant interactions of the ion are with the electrons of the lattice, which slow the ion down through kinetic energy transfer. After

yields. However, ion implantation requires an annealing step, which will be further discussed later on. It has been suggested[8] to use ion implantation as an integral part of a total vacuum process sequence for fabricating solar cells after wafer or sheet generation. Such a sequence, although high in capital costs, could result in labor savings and high yields.

The charge on the dopant ions allows for mass-spectroscopic separation using magnetic fields, and for accurate measurement of the ion flux entering the deposition region, as long as neutral and doubly charged particles are handled correctly. The ion beam currents can be readily measured by placing a Faraday cup in the beam's path, but this requires a preceding calibration to determine the fraction of uncharged and doubly charged ions. The mass analysis and ion current measurement features of the ion implantation process can provide better control over the quantity and quality of the dopant than other processes, and can therefore be applied to obtain better process uniformity and repeatability. Dose uniformities of $\pm$ 5% (2σ) are achievable[9].

Since ion implantation can be performed at or near room temperature, low energy implantations can result in original dopant penetration of less than 100Å. This is shallower than can be achieved in most high temperature source deposition steps in the diffusion process.

Upon entering the substrate, the dominant interactions of the ion are with the electrons of the lattice, which slow the ion down through kinetic energy transfer. After

this initial slow-down to sufficiently low energies, i.e., ion velocity less than $Z_i e^2/\hbar$, collisions of the ion take place with the nuclei which completely stop the ion. In most cases, the stopped ion rests interstially in the crystal lattice. The largest impurity concentration is thus found at a penetration distance, "x_p", from the surface. As a first approximation in the region where nuclear collisions dominate, the penetration depth is proportional to the square root of the ion beam energy. This penetration depth is described by:

$$x_p = \frac{0.7\ (Z_I^{2/3} + Z_{Si}^{2/3})}{Z_I Z_{Si}} \cdot \frac{M_I + M_{Si}}{M_I} E_I\,(\text{Å}). \quad \text{III-2.5}$$

E_I is the energy of the ion beam in eV, Z and M refer to the atomic number and atomic weight, respectively, while the subscripts I and Si refer to the ion and to Si, respectively. The concentration varies from the penetration distance approximately according to a Gaussian distribution and the impurity distribution can be described by the empirical relationship,

$$C(x) = C_p \exp\ (-(x-x_p)^2/2\ \sigma_R^2). \quad \text{III-2.6}$$

C_p is the concentration at the penetration distance, and σ_R is called the standard deviation of the concentration

function, or the distance from x_p at which the concentration is equal to $C_p/\sqrt{e}$. The peak concentration depends upon the ion beam current (i) and the implantation time (t) or

$$C_p = \frac{10^{16} i \cdot t}{4 \sigma_R} \quad cm^{-2}. \qquad \text{III-2.7}$$

The unit of i is mA, that of t is seconds, and σ_R is is given in μm.

The penetration distance can be calculated from electron and nuclear ionic collisions only if "channeling" does not occur. Channeling is the name given to the considerably enhanced penetration distance of ions which are aligned with low index crystallographic directions, and therefore travel parallel to and in between high atomic density crystal planes. Since ions travelling this path experience relatively fewer collisions with silicon atoms, they can travel further into the silicon. To avoid channeling, the beam must be oriented at a slight angle (~7°) from the orientation of the low index crystallographic axes. This increases the apparent distribution of atoms in the crystal plane normal to the ion beam's path, and thus increases the probability of ion-nuclei collisions.

The implantation process results in the displacement of the silicon atoms from their normal lattice sites by the ion collisions, thus creating "vacancies" and "interstitials". The implanted impurity atoms, predominately located at intersti-

tial sites, are not electrically active. Thus few impurity atoms which take up substitutional positions, tend to compensate the originally present impurity atoms of opposite dopant type, and to shift the Fermi level of the silicon towards the center of the energy gap. Annealing of the ion implanted wafers is required both to reduce the mentioned crystal structure damage resulting from the implantation process, some of which is electrically active (recombination and trapping centers), and to electrically "activate" the dopant impurity by moving its implanted atoms from interstitial to substitutional sites. This annealing is usually accomplished by a high temperature soak, called thermal annealing.

Thermal annealing broadens the impurity profile, usually to a junction depth as great or greater than obtained by use of relatively low temperature, short time diffusions as they are normally used for solar cell production. Nevertheless, ion implantation followed by thermal annealing is capable of producing solar cells with efficiencies equivalent to those prepared using diffusion. A thermal annealing cycle of 1h at 450°C and 0.5h at 859°C has been repeatedly found to yield performance-wise competitive silicon solar cells. [10] This, in part negates the potential advantage of being able to control the dopant profile at will by varying the implantation energy and dosage. Such "designed profiles" might lead to higher efficiency solar cells than obtained so far. Electron and laser beam

annealing, as short transient annealing methods, have therefore been and are being investigated because of the potential profile maintenance as well as several other anticipated advantages. These advantages have, however, so far not been realized, and cells with efficiencies comparable to those obtained by the oven annealing process have so far not been reported. However, electron beam annealing, followed by a low temperature soak, at approximately 500°C, is now said to produce cells with efficiencies comparable to those using the "thermal annealing" process. The necessity of the low temperature soak seems to indicate that the electron beam annealing process does not reduce crystal damage or permit gettering as well as thermal annealing. Although the electron beam pulse anneal, followed by a low temperature soak, will be a more costly process than a higher temperature activation/annealing soak one, it appears attractive because of the greater freedom in selection and control of the impurity profile. If this pulse anneal/soak process, or some other, simpler process for activation/annealing could be developed, so that ion implanted solar cells might attain higher efficiencies than cells prepared by diffusion processes, then ion implantation would become a most interesting process option, even at a possibly somewhat higher process cost than diffusion.

With the attainability of a potential efficiency advantage of the ion implanted solar cells over the diffusion produced cells not demonstrated, the usefulness of ion implantation, as part of an LSA solar cell sequence will be determined by

the potentially achievable cost reduction. Currently, the high capital costs, the low reliability, and the low throughput rate of ion implantation machines, make junction formation with them too costly to be used for large scale solar cell production. Large cost reductions are, however, expected to be accomplished in the future (1986) by several approaches. Approaches to this end include the introduction of large throughput machines with high current, hot cathode ion beam sources incorporating an analyzer and more automated operation through computer control[7], and the development of ion implanters with unanalyzed or roughly analyzed ion beams[6,11] using hollow cathode sources. Some current and future applications of ion implantation are listed in Table I along with the conditions contingent to the two potential advantages of lower cost and higher efficiency.

In consequence of this discussion, it has to be observed, particularly in reading the following sections, that ion implantation and activation/annealing are inseparably connected, and that, even though only one of the process steps may be mentioned, it cannot be usefully carried out without the other. But there are several ways of carrying out ion implantation as well as annealing, with various combinations of the two, so that one really deals with an ion implantation/annealing submatrix of options. Consequently, both the process cost and the performance of the finished solar cells depend on the option selection within this submatrix.

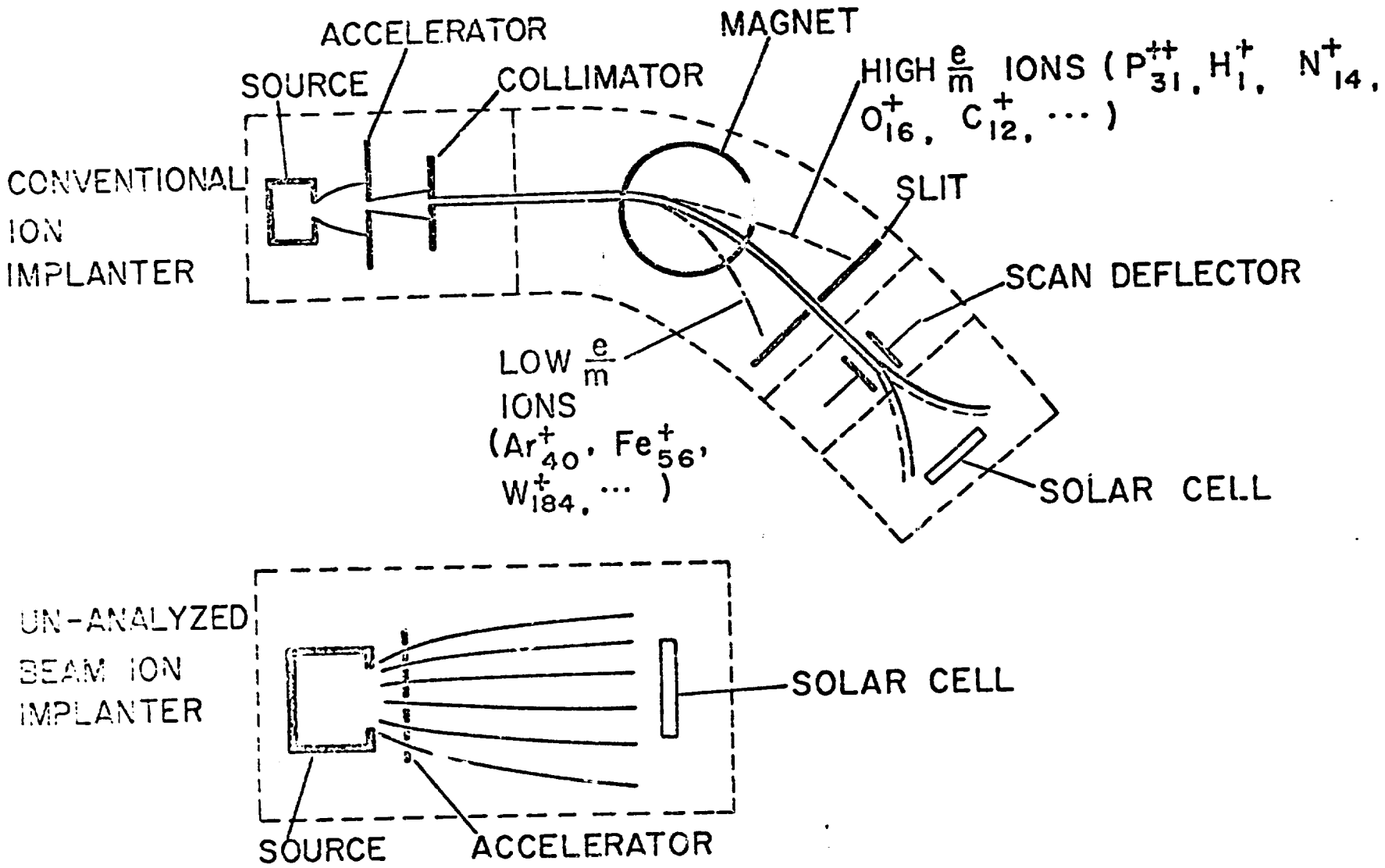

PRINCIPLES OF ION IMPLANTER DESIGN

FIGURE III.1

efficiency of ionization. This will also result, though, in lower source lifetime and a larger energy spread of the ions.

Three principal types of hot cathode ion sources are used in the implanters mentioned in this report. In all, the current density from a metal surface at temperature T with a work function of Φ is principally described by:

$$j_e = AT^2 e^{-e\Phi/kT} \qquad \text{III-2.1}$$

However, at adequately high emission rates, the current density j_e is usually reduced below the value given by Eq. III-2.1 because of space-charge effects, in which the mutual repulsion of the electrons crowding the space near the filament inhibits further emission. The electron density then becomes:

$$j_e = \frac{V^{2/3}}{9\pi d^2 (m/2e)^{1/2}} \qquad \text{III-2.2}$$

where V is the voltage between the cathode and anode, d is the thickness of the electron sheath and m/e is the electron's mass to charge ratio. The production of positive ions in the source chamber tends to neutralize this "electron cloud" and reduce the space charge effects. The cathode current thus increases in the presence of positive ions.

In the "Freeman source", the heated wire cathode has its terminals on opposite sides of the "extraction gap" through which the ions leave. In the "Chavet source", the filament wire is looped so that its electrodes are on the same side of

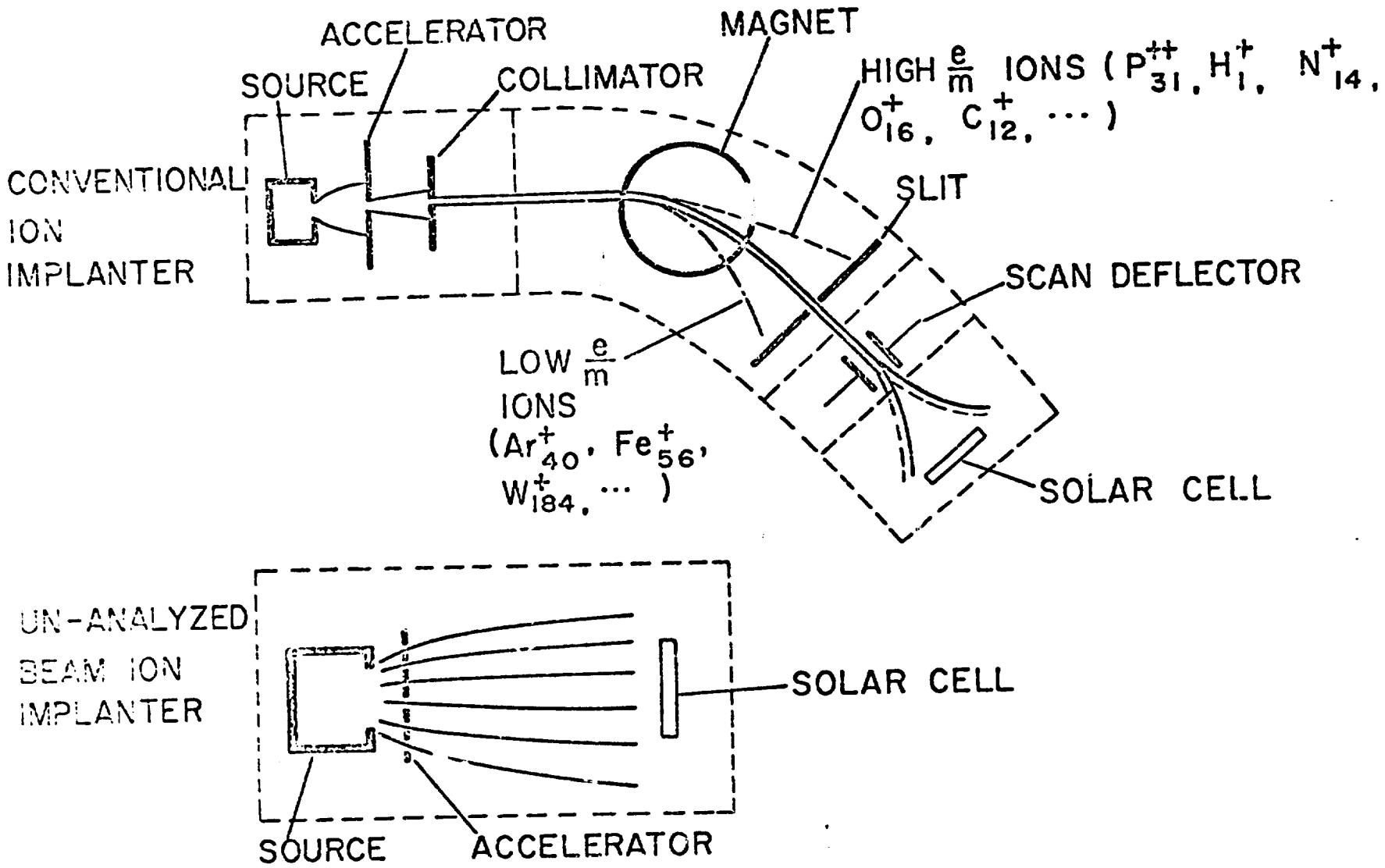

PRINCIPLES OF ION IMPLANTER DESIGN

FIGURE III.1

efficiency of ionization. This will also result, though, in lower source lifetime and a larger energy spread of the ions.

Three principal types of hot cathode ion sources are used in the implanters mentioned in this report. In all, the current density from a metal surface at temperature T with a work function of Φ is principally described by:

$$j_e = AT^2 e^{-e\Phi/kT} \qquad \text{III-2.1}$$

However, at adequately high emission rates, the current density j_e is usually reduced below the value given by Eq. III-2.1 because of space-charge effects, in which the mutual repulsion of the electrons crowding the space near the filament inhibits further emission. The electron density then becomes:

$$j_e = \frac{V^{2/3}}{9\pi d^2 (m/2e)^{1/2}} \qquad \text{III-2.2}$$

where V is the voltage between the cathode and anode, d is the thickness of the electron sheath and m/e is the electron's mass to charge ratio. The production of positive ions in the source chamber tends to neutralize this "electron cloud" and reduce the space charge effects. The cathode current thus increases in the presence of positive ions.

In the "Freeman source", the heated wire cathode has its terminals on opposite sides of the "extraction gap" through which the ions leave. In the "Chavet source", the filament wire is looped so that its electrodes are on the same side of

the extraction gap. The Chavet filament configuration was designed to increase the filament's lifetime by decreasing its exposure to the back-streaming ions and thus reduce the sputtering caused by them. Another thermionic source is the hollow cathode in which the interior of a cylindrical cavity is coated with a low work function material, such as barium oxide. Upon introduction of the vaporized source material, an arc discharge takes place between the cathode and anode so that the source material is ionized. As a result of applied high voltage, the ions are extracted through a hole in the cathode. Vaporized atoms also pass through this aperture. They are subsequently ionized by the accelerated electrons. One configuration of a cold cathode source known as the "Penning source", has an anode that is also cylindrical in shape with the end plates forming the cathode. In addition, a magnetic field is applied parallel to the cylindrical axis of the "Penning source" to force electrons from the cathode to form helical trajectories, thus increasing their path length and enhancing the ionization efficiency.

After the ion beam is extracted from the source chamber, it is accelerated through a potential drop. For small acceleration energies ($\lesssim$30 keV), a single gap electrode could be used. The accelerated ion beam is then subjected to a magnetic field for mass separation. A singly charged ion of atomic mass M (AMU's) moving through a magnetic field with strength B (in gauss) will be deflected into a circular

path with the radius of curvature equal to

$$R = \frac{143.95}{B} (MV)^{1/2} \text{ cm}, \qquad \text{III-2.3}$$

where V is the acceleration voltage. The dispersion between ions of two different masses is

$$D_M = \frac{\Delta M}{M} R \text{ cm} . \qquad \text{III-2.4}$$

In order to achieve good mass resolution, power supplies to the acceleration and magnet regions must have stabilities of 1 part in 10,000.

To form the junction, the analyzed beam is then scanned, with one of the techniques mentioned previously, on the silicon substrate. Overscanning is necessary because of the tails in the Gaussion distribution of the ion concentration in the beam.

Junction formation using ion implantation offers several potential advantages over the diffusion process. It is a dry, vacuum process, thus avoiding potential contamination from impurities contained in spin-on or gaseous vehicles for the dopants used in some varieties of the diffusion process. Where selective introduction of the dopant is wanted, this may be accomplished without application of masking and subsequent stripping, and without back-surface etching because of double-sided impurity penetrations. Thus, ion implantation can involve fewer handling or transferring operations than the diffusion process, and consequently can result in labor savings and increased

yields. However, ion implantation requires an annealing step, which will be further discussed later on. It has been suggested[8] to use ion implantation as an integral part of a total vacuum process sequence for fabricating solar cells after wafer or sheet generation. Such a sequence, although high in capital costs, could result in labor savings and high yields.

The charge on the dopant ions allows for mass-spectroscopic separation using magnetic fields, and for accurate measurement of the ion flux entering the deposition region, as long as neutral and doubly charged particles are handled correctly. The ion beam currents can be readily measured by placing a Faraday cup in the beam's path, but this requires a preceding calibration to determine the fraction of uncharged and doubly charged ions. The mass analysis and ion current measurement features of the ion implantation process can provide better control over the quantity and quality of the dopant than other processes, and can therefore be applied to obtain better process uniformity and repeatability. Dose uniformities of $\pm$ 5% (2σ) are achievable[9].

Since ion implantation can be performed at or near room temperature, low energy implantations can result in original dopant penetration of less than 100Å. This is shallower than can be achieved in most high temperature source deposition steps in the diffusion process.

Upon entering the substrate, the dominant interactions of the ion are with the electrons of the lattice, which slow the ion down through kinetic energy transfer. After

this initial slow-down to sufficiently low energies, i.e., ion velocity less than $Z_i e^2/\hbar$, collisions of the ion take place with the nuclei which completely stop the ion. In most cases, the stopped ion rests interstially in the crystal lattice. The largest impurity concentration is thus found at a penetration distance, "x_p", from the surface. As a first approximation in the region where nuclear collisions dominate, the penetration depth is proportional to the square root of the ion beam energy. This penetration depth is described by:

$$x_p = \frac{0.7\ (Z_I^{2/3} + Z_{Si}^{2/3})}{Z_I Z_{Si}} \cdot \frac{M_I + M_{Si}}{M_I} E_I(\text{Å}). \quad \text{III-2.5}$$

E_I is the energy of the ion beam in eV, Z and M refer to the atomic number and atomic weight, respectively, while the subscripts I and Si refer to the ion and to Si, respectively. The concentration varies from the penetration distance approximately according to a Gaussian distribution and the impurity distribution can be described by the empirical relationship,

$$C(x) = C_p \exp\ (-(x-x_p)^2/2\ \sigma_R^2). \quad \text{III-2.6}$$

C_p is the concentration at the penetration distance, and σ_R is called the standard deviation of the concentration

function, or the distance from x_p at which the concentration is equal to $C_p/\sqrt{e}$. The peak concentration depends upon the ion beam current (i) and the implantation time (t) or

$$C_p = \frac{10^{16} i \cdot t}{4 \sigma_R} \quad cm^{-2}. \qquad \text{III-2.7}$$

The unit of i is mA, that of t is seconds, and σ_R is is given in μm.

The penetration distance can be calculated from electron and nuclear ionic collisions only if "channeling" does not occur. Channeling is the name given to the considerably enhanced penetration distance of ions which are aligned with low index crystallographic directions, and therefore travel parallel to and in between high atomic density crystal planes. Since ions travelling this path experience relatively fewer collisions with silicon atoms, they can travel further into the silicon. To avoid channeling, the beam must be oriented at a slight angle (~7°) from the orientation of the low index crystallographic axes. This increases the apparent distribution of atoms in the crystal plane normal to the ion beam's path, and thus increases the probability of ion-nuclei collisions.

The implantation process results in the displacement of the silicon atoms from their normal lattice sites by the ion collisions, thus creating "vacancies" and "interstitials". The implanted impurity atoms, predominately located at intersti-

tial sites, are not electrically active. Thus few impurity atoms which take up substitutional positions, tend to compensate the originally present impurity atoms of opposite dopant type, and to shift the Fermi level of the silicon towards the center of the energy gap. Annealing of the ion implanted wafers is required both to reduce the mentioned crystal structure damage resulting from the implantation process, some of which is electrically active (recombination and trapping centers), and to electrically "activate" the dopant impurity by moving its implanted atoms from interstitial to substitutional sites. This annealing is usually accomplished by a high temperature soak, called thermal annealing.

Thermal annealing broadens the impurity profile, usually to a junction depth as great or greater than obtained by use of relatively low temperature, short time diffusions as they are normally used for solar cell production. Nevertheless, ion implantation followed by thermal annealing is capable of producing solar cells with efficiencies equivalent to those prepared using diffusion. A thermal annealing cycle of 1h at 450°C and 0.5h at 859°C has been repeatedly found to yield performance-wise competitive silicon solar cells. [10] This, in part negates the potential advantage of being able to control the dopant profile at will by varying the implantation energy and dosage. Such "designed profiles" might lead to higher efficiency solar cells than obtained so far. Electron and laser beam

annealing, as short transient annealing methods, have therefore been and are being investigated because of the potential profile maintenance as well as several other anticipated advantages. These advantages have, however, so far not been realized, and cells with efficiencies comparable to those obtained by the oven annealing process have so far not been reported. However, electron beam annealing, followed by a low temperature soak, at approximately 500°C, is now said to produce cells with efficiencies comparable to those using the "thermal annealing" process. The necessity of the low temperature soak seems to indicate that the electron beam annealing process does not reduce crystal damage or permit gettering as well as thermal annealing. Although the electron beam pulse anneal, followed by a low temperature soak, will be a more costly process than a higher temperature activation/annealing soak one, it appears attractive because of the greater freedom in selection and control of the impurity profile. If this pulse anneal/soak process, or some other, simpler process for activation/annealing could be developed, so that ion implanted solar cells might attain higher efficiencies than cells prepared by diffusion processes, then ion implantation would become a most interesting process option, even at a possibly somewhat higher process cost than diffusion.

With the attainability of a potential efficiency advantage of the ion implanted solar cells over the diffusion produced cells not demonstrated, the usefulness of ion implantation, as part of an LSA solar cell sequence will be determined by

the potentially achievable cost reduction. Currently, the high capital costs, the low reliability, and the low throughput rate of ion implantation machines, make junction formation with them too costly to be used for large scale solar cell production. Large cost reductions are, however, expected to be accomplished in the future (1986) by several approaches. Approaches to this end include the introduction of large throughput machines with high current, hot cathode ion beam sources incorporating an analyzer and more automated operation through computer control[7], and the development of ion implanters with unanalyzed or roughly analyzed ion beams[6,11] using hollow cathode sources. Some current and future applications of ion implantation are listed in Table I along with the conditions contingent to the two potential advantages of lower cost and higher efficiency.

In consequence of this discussion, it has to be observed, particularly in reading the following sections, that ion implantation and activation/annealing are inseparably connected, and that, even though only one of the process steps may be mentioned, it cannot be usefully carried out without the other. But there are several ways of carrying out ion implantation as well as annealing, with various combinations of the two, so that one really deals with an ion implantation/annealing submatrix of options. Consequently, both the process cost and the performance of the finished solar cells depend on the option selection within this submatrix.

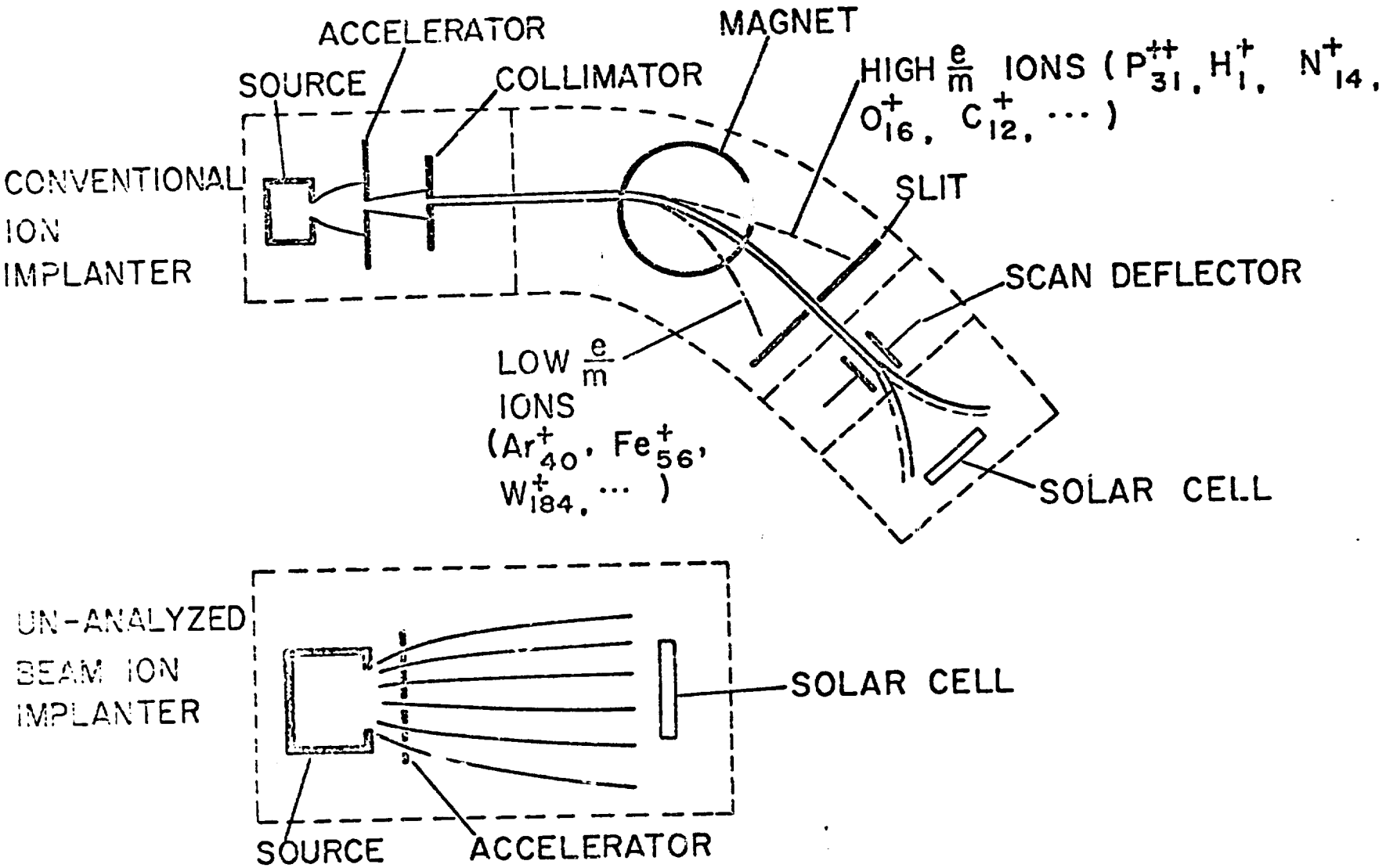

PRINCIPLES OF ION IMPLANTER DESIGN

FIGURE III.1

efficiency of ionization. This will also result, though, in lower source lifetime and a larger energy spread of the ions.

Three principal types of hot cathode ion sources are used in the implanters mentioned in this report. In all, the current density from a metal surface at temperature T with a work function of Φ is principally described by:

$$j_e = AT^2 e^{-e\Phi/kT} \qquad \text{III-2.1}$$

However, at adequately high emission rates, the current density j_e is usually reduced below the value given by Eq. III-2.1 because of space-charge effects, in which the mutual repulsion of the electrons crowding the space near the filament inhibits further emission. The electron density then becomes:

$$j_e = \frac{V^{2/3}}{9\pi d^2 \, (m/2e)^{1/2}} \qquad \text{III-2.2}$$

where V is the voltage between the cathode and anode, d is the thickness of the electron sheath and m/e is the electron's mass to charge ratio. The production of positive ions in the source chamber tends to neutralize this "electron cloud" and reduce the space charge effects. The cathode current thus increases in the presence of positive ions.

In the "Freeman source", the heated wire cathode has its terminals on opposite sides of the "extraction gap" through which the ions leave. In the "Chavet source", the filament wire is looped so that its electrodes are on the same side of

the extraction gap. The Chavet filament configuration was designed to increase the filament's lifetime by decreasing its exposure to the back-streaming ions and thus reduce the sputtering caused by them. Another thermionic source is the hollow cathode in which the interior of a cylindrical cavity is coated with a low work function material, such as barium oxide. Upon introduction of the vaporized source material, an arc discharge takes place between the cathode and anode so that the source material is ionized. As a result of applied high voltage, the ions are extracted through a hole in the cathode. Vaporized atoms also pass through this aperture. They are subsequently ionized by the accelerated electrons. One configuration of a cold cathode source known as the "Penning source", has an anode that is also cylindrical in shape with the end plates forming the cathode. In addition, a magnetic field is applied parallel to the cylindrical axis of the "Penning source" to force electrons from the cathode to form helical trajectories, thus increasing their path length and enhancing the ionization efficiency.

After the ion beam is extracted from the source chamber, it is accelerated through a potential drop. For small acceleration energies (<30 keV), a single gap electrode could be used. The accelerated ion beam is then subjected to a magnetic field for mass separation. A singly charged ion of atomic mass M (AMU's) moving through a magnetic field with strength B (in gauss) will be deflected into a circular

path with the radius of curvature equal to

$$R = \frac{143.95}{B} (MV)^{1/2} \text{ cm}, \qquad \text{III-2.3}$$

where V is the acceleration voltage. The dispersion between ions of two different masses is

$$D_M = \frac{\Delta M}{M} R \text{ cm} . \qquad \text{III-2.4}$$

In order to achieve good mass resolution, power supplies to the acceleration and magnet regions must have stabilities of 1 part in 10,000.

To form the junction, the analyzed beam is then scanned, with one of the techniques mentioned previously, on the silicon substrate. Overscanning is necessary because of the tails in the Gaussion distribution of the ion concentration in the beam.

Junction formation using ion implantation offers several potential advantages over the diffusion process. It is a dry, vacuum process, thus avoiding potential contamination from impurities contained in spin-on or gaseous vehicles for the dopants used in some varieties of the diffusion process. Where selective introduction of the dopant is wanted, this may be accomplished without application of masking and subsequent stripping, and without back-surface etching because of double-sided impurity penetrations. Thus, ion implantation can involve fewer handling or transferring operations than the diffusion process, and consequently can result in labor savings and increased

yields. However, ion implantation requires an annealing step, which will be further discussed later on. It has been suggested[8] to use ion implantation as an integral part of a total vacuum process sequence for fabricating solar cells after wafer or sheet generation. Such a sequence, although high in capital costs, could result in labor savings and high yields.

The charge on the dopant ions allows for mass-spectroscopic separation using magnetic fields, and for accurate measurement of the ion flux entering the deposition region, as long as neutral and doubly charged particles are handled correctly. The ion beam currents can be readily measured by placing a Faraday cup in the beam's path, but this requires a preceding calibration to determine the fraction of uncharged and doubly charged ions. The mass analysis and ion current measurement features of the ion implantation process can provide better control over the quantity and quality of the dopant than other processes, and can therefore be applied to obtain better process uniformity and repeatability. Dose uniformities of $\pm$ 5% (2σ) are achievable[9].

Since ion implantation can be performed at or near room temperature, low energy implantations can result in original dopant penetration of less than 100Å. This is shallower than can be achieved in most high temperature source deposition steps in the diffusion process.

Upon entering the substrate, the dominant interactions of the ion are with the electrons of the lattice, which slow the ion down through kinetic energy transfer. After

this initial slow-down to sufficiently low energies, i.e., ion velocity less than $Z_i e^2/\hbar$, collisions of the ion take place with the nuclei which completely stop the ion. In most cases, the stopped ion rests interstially in the crystal lattice. The largest impurity concentration is thus found at a penetration distance, "x_p", from the surface. As a first approximation in the region where nuclear collisions dominate, the penetration depth is proportional to the square root of the ion beam energy. This penetration depth is described by:

$$x_p = \frac{0.7\ (Z_I^{2/3} + Z_{Si}^{2/3})}{Z_I Z_{Si}} \cdot \frac{M_I + M_{Si}}{M_I} E_I\,(\text{Å}). \quad \text{III-2.5}$$

E_I is the energy of the ion beam in eV, Z and M refer to the atomic number and atomic weight, respectively, while the subscripts I and Si refer to the ion and to Si, respectively. The concentration varies from the penetration distance approximately according to a Gaussian distribution and the impurity distribution can be described by the empirical relationship,

$$C(x) = C_p \exp\ (-(x-x_p)^2/2\ \sigma_R^2). \quad \text{III-2.6}$$

C_p is the concentration at the penetration distance, and σ_R is called the standard deviation of the concentration

function, or the distance from x_p at which the concentration is equal to $C_p/\sqrt{e}$. The peak concentration depends upon the ion beam current (i) and the implantation time (t) or

$$C_p = \frac{10^{16} i \cdot t}{4 \sigma_R} \quad cm^{-2}. \qquad \text{III-2.7}$$

The unit of i is mA, that of t is seconds, and σ_R is is given in μm.

The penetration distance can be calculated from electron and nuclear ionic collisions only if "channeling" does not occur. Channeling is the name given to the considerably enhanced penetration distance of ions which are aligned with low index crystallographic directions, and therefore travel parallel to and in between high atomic density crystal planes. Since ions travelling this path experience relatively fewer collisions with silicon atoms, they can travel further into the silicon. To avoid channeling, the beam must be oriented at a slight angle (~7°) from the orientation of the low index crystallographic axes. This increases the apparent distribution of atoms in the crystal plane normal to the ion beam's path, and thus increases the probability of ion-nuclei collisions.

The implantation process results in the displacement of the silicon atoms from their normal lattice sites by the ion collisions, thus creating "vacancies" and "interstitials". The implanted impurity atoms, predominately located at intersti-

tial sites, are not electrically active. Thus few impurity atoms which take up substitutional positions, tend to compensate the originally present impurity atoms of opposite dopant type, and to shift the Fermi level of the silicon towards the center of the energy gap. Annealing of the ion implanted wafers is required both to reduce the mentioned crystal structure damage resulting from the implantation process, some of which is electrically active (recombination and trapping centers), and to electrically "activate" the dopant impurity by moving its implanted atoms from interstitial to substitutional sites. This annealing is usually accomplished by a high temperature soak, called thermal annealing.

Thermal annealing broadens the impurity profile, usually to a junction depth as great or greater than obtained by use of relatively low temperature, short time diffusions as they are normally used for solar cell production. Nevertheless, ion implantation followed by thermal annealing is capable of producing solar cells with efficiencies equivalent to those prepared using diffusion. A thermal annealing cycle of 1h at 450°C and 0.5h at 859°C has been repeatedly found to yield performance-wise competitive silicon solar cells. [10] This, in part negates the potential advantage of being able to control the dopant profile at will by varying the implantation energy and dosage. Such "designed profiles" might lead to higher efficiency solar cells than obtained so far. Electron and laser beam

annealing, as short transient annealing methods, have therefore been and are being investigated because of the potential profile maintenance as well as several other anticipated advantages. These advantages have, however, so far not been realized, and cells with efficiencies comparable to those obtained by the oven annealing process have so far not been reported. However, electron beam annealing, followed by a low temperature soak, at approximately 500°C, is now said to produce cells with efficiencies comparable to those using the "thermal annealing" process. The necessity of the low temperature soak seems to indicate that the electron beam annealing process does not reduce crystal damage or permit gettering as well as thermal annealing. Although the electron beam pulse anneal, followed by a low temperature soak, will be a more costly process than a higher temperature activation/annealing soak one, it appears attractive because of the greater freedom in selection and control of the impurity profile. If this pulse anneal/soak process, or some other, simpler process for activation/annealing could be developed, so that ion implanted solar cells might attain higher efficiencies than cells prepared by diffusion processes, then ion implantation would become a most interesting process option, even at a possibly somewhat higher process cost than diffusion.

With the attainability of a potential efficiency advantage of the ion implanted solar cells over the diffusion produced cells not demonstrated, the usefulness of ion implantation, as part of an LSA solar cell sequence will be determined by

the potentially achievable cost reduction. Currently, the high capital costs, the low reliability, and the low throughput rate of ion implantation machines, make junction formation with them too costly to be used for large scale solar cell production. Large cost reductions are, however, expected to be accomplished in the future (1986) by several approaches. Approaches to this end include the introduction of large throughput machines with high current, hot cathode ion beam sources incorporating an analyzer and more automated operation through computer control[7], and the development of ion implanters with unanalyzed or roughly analyzed ion beams[6,11] using hollow cathode sources. Some current and future applications of ion implantation are listed in Table I along with the conditions contingent to the two potential advantages of lower cost and higher efficiency.

In consequence of this discussion, it has to be observed, particularly in reading the following sections, that ion implantation and activation/annealing are inseparably connected, and that, even though only one of the process steps may be mentioned, it cannot be usefully carried out without the other. But there are several ways of carrying out ion implantation as well as annealing, with various combinations of the two, so that one really deals with an ion implantation/annealing submatrix of options. Consequently, both the process cost and the performance of the finished solar cells depend on the option selection within this submatrix.

EVALUATION OF ION IMPLANTATION FOR LSA PRODUCTION

APPLICATION	STATUS	PRINCIPAL ALTERNATE PROCESSES
PN JUNCTION FORMATION	PROVEN: PERFORMANCE EQUAL DIFF'D JCTN.	DIFFUSION CVD/ EPI
BSF OR BACK HI/LO JCTN.	CONCEPTUAL	THICK FILM/ALLOYING ; DIFFUSION; CVD/ EPI
FSF OR FRONT HI/LO JCTN.	EFFECTIVENESS NOT YET PROVEN	DIFUSSION CVD/EPI
CONTACT METALLIZATION	CONCEPTUAL	THICK FILM ELECTROLESS PLATING VACUUM EVAPOR'N SPUTTERING

ION IMPLANTATION FOR PN-JUNCTION FORMATION

CONCEIVED ADVANTAGES	CONDITIONS	STATUS
LOWER COST	LIKELY ONLY IN SEQUENCE WITH OTHER VACUUM PROCESSES	TECHNOLOGY ADVANCEMENTS REQUIRED.
HIGHER CELL PERFORMANCE THAN ACHIEVABLE BY ALTERNATE PROCESSES	DEPENDS ON SUPERIOR IMPURITY PROFILE, FEWER CRYSTAL DEFECTS	STILL TO BE DEMONSTRATED

Table III.1

4. Appraisal of Present-day Ion Implanters

The application of ion implantation for pn or high/low junction formation in process sequences for future large scale LSA manufacture depends on the fulfillment of either of two conditions: 1.) its costs are equal to or lower than those for pn junction formation using diffusion or high/low junction formation using alloying or diffusion, possibly in combination with each other or with other process steps; or 2.) the performance of the solar cells fabricated by use of ion implantation is adequately higher than that of cells prepared by other processes so as to justify a higher price.

Ion implantation is currently used in semi-conductor industry production activities for implanting, in solid state devices, impurities of low dosage and relatively deep penetration (high energy). In order to gather information on the current state of production line ion implantation, we visited, among others, RCA-Somerville, where a Varian-Extrion 200-1000 ion implanter is used for integrated circuit manufacture, as well as for solar cell[12] fabrication in pilot operations. Implantations are routinely performed at beam currents ranging from 0.1 μA to 1.5 mA, at voltages up to 100 kV, alternatingly with P^+, B^+ and As^+ ions, in a 24 hour-a-day schedule of 5 to 7 days-a-week.

The Varian-Extrion 200-1000 ion implanter is available with a semi-automatic cassette wafer feeding mechanism that allows continuous processing, increasing its output rate to 300, 7.62-cm

round wafers per hour. In order to achieve this output rate, the ion implanter also has to be modified to operate in a high current (4 mA), low voltage (<25 keV) mode. These options are included in a Varian-Extrion 200-1000 implanter in operation at Spire.[2] Additional options provide an off-axis beam tilt to minimize channeling. To achieve dose uniformity and avoid shadowing from a tilted beam on a texture-etched surface, the wafer is rotated about its axis at 1 rev/sec.

The cost of such a machine is approximately $315,000 and it requires one full-time operator. To achieve acceptable machine operation, the RCA personnel have found it necessary to have a skilled technician stationed within the immediate vicinity of their ion implanter at all times, and to make adjustments in the machine operating parameters quasi-continuously. They believe that computer controlled functions, similar to those proposed by Spire[7] in their ion implanter design, could considerably reduce the need for continuous skilled attendance. They mentioned, however, that designing adequate computer controls might be difficult since, so far, adequate sensing of the status of all parts of the machine and of the parameters affecting its operation does not exist. Thus, correctly operating the ion implanter is still more of an art than a science and requires the adjustment of many functionally interrelated controls. Similar statements were variously heard, summarized by Varian-Extrion personnel, in the remark that successful machine operation depends very heavily on the operator, and that wide variations are experienced among the various users. RCA personnel has found that leakage from the high voltage

machine elements, in part due to condensed source material, tends to interfere with the sensitive dose rate measurements and the machine control. Other problems resulted from persistent leakage of cooling fluid which could be reduced by the use of freon in lieu of the more common deionized water, albeit at significantly higher costs for the make-up fluid.

One of the major problems mentioned at RCA and elsewhere, is the deposition on many parts of the machine of atoms of the implanted species as well as of material sputtered off the various parts of the source. Arsenic is especially troublesome in this respect because of its relatively low vapor pressure compared to other implanted species. This deposition occasionally results in electrical malfunctions, such as shorting of insulators and arcing, which occasionally has led to power supply or logic board damage. The machine, therefore, requires frequent thorough cleaning of the affected regions. Phosphorus also condenses on the machine's interior, and we have heard of short phosphorous fires upon opening the machine.

Much of the unscheduled maintenance is performed under service contracts. RCA personnel mentioned that such a service contract with Varian-Extrion has an annual cost of $13,000. This contract provides the so-far extensive on-location servicing by Varian-Extrion personnel and replacement of failed parts, frequently circuit boards. RCA personnel estimates that about two-thirds of this money covers time and expenses of the service personnel, and the remainder replacement parts. RCA has recently introduced regular scheduled maintenance of their Varian-Extrion 200-1000 "high current" implanter for which 4 hours per week are allocated. During these maintenance periods, the

machine interior is cleaned, filaments, if needed, are replaced, vacuum pump oils are changed, the machine inspected, and potentially unreliable parts identified and replaced. Since this institution of preventive maintenance, the previously frequent machine breakdowns have decreased to a tolerable level. At RCA, the experienced filament lifetime, as plotted on Figure III.2, is in the 60 to 120 h range for an average ion beam current of around 0.75 mA, although much implantating is done with a 1 mA beam current. [12]

Because of the relatively frequent machine breakdowns of ion implanters, RCA's personnel have found it necessary to keep an extensive spare parts inventory, so that bad or suspicious parts can be replaced with minimal machine down time, in order to maintain production schedules and to reduce the impact on operating costs which are heavily influenced by the high cost of the equipment.

An ion implanter has been in operation at Western Electric since 1974 in a production line, high throughput mode. This implanter, called the PR-30, has an output rate of 450, 7.62-cm diameter wafers/h at a dosage of 1×10^{15} ions/cm^2.[13] The machine can accomodate either a hot cathode, Freeman-type source, or a cold cathode (Penning) source. It operates in a low voltage (30keV) mode. In the case of the cold cathode source, a phosphorus current of 5 mA is obtained, with a source lifetime of 40 h.[14] The wafers (7.62-cm diameter) are placed on a disk, 30 at a time. The

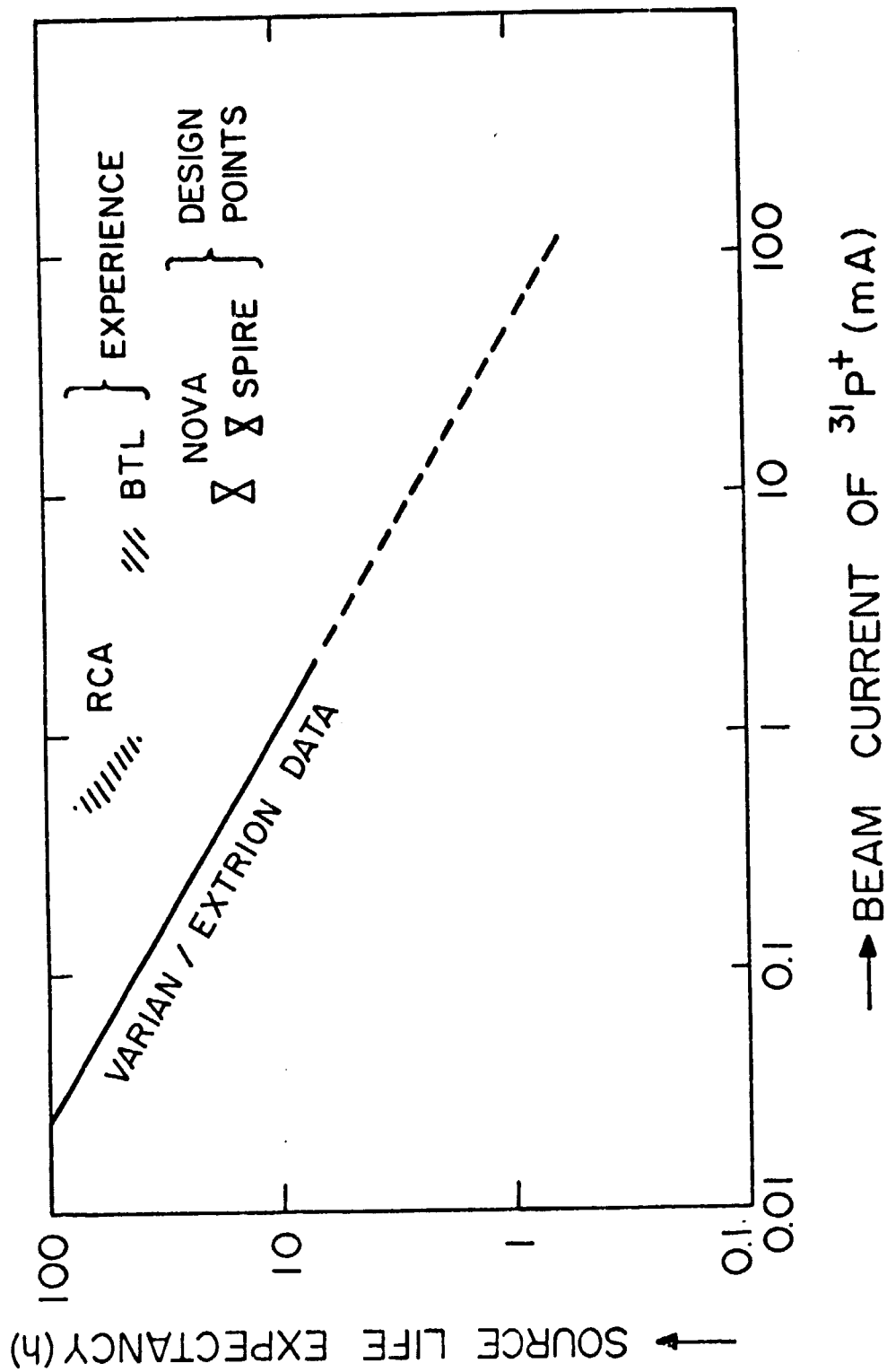
SOURCE LIFE EXPECTANCY (h)
100
10
1
0.1
0.01
BEAM CURRENT OF $^{31}P^+$ (mA)
0.1
1
10
100
VARIAN / EXTRION DATA
RCA
BTL
EXPERIENCE
NOVA
SPIRE
DESIGN POINTS

FIGURE III.2

disk is mounted horizontally in the ion implanter. After pump down to 10^{-5} torr, which takes approximately 3 minutes, the disk is rotated at 900 rpm while the underside of the wafers is exposed to the fixed ion beam. The total time of each run is approximately 4 min.

The PR-30 is physically, a relatively small machine. The implantation unit, without controls, occupies a floor area of 1.8m x 2.1m. Two standard instrument racks house the control units. The PR-30 is used only in Western Electric factories, and it is not sold on the open market. We have been given an estimated price for this machine, if it could be marketed, of less than $300,000.[15]

A high current (10 mA) and low voltage (10-50 keV) ion implanter, designated NV-10, is currently being readied by Nova Associates for introduction into the marketplace. The machine uses a Freeman, hot cathode source, with an expected lifetime of 16 h at 10 mA. The machine costs approximately $410,000.[16] Its output rate for a 2×10^{15} ions/cm^2 dosage of 270 wafers per hour of 7.62-cm diameter is limited by the wafer feed mechanism. If a faster feed mechanism could be installed, the output could be increased to 3-4 times the present one, to take better advantage of the machine's high beam current. The wafers are mounted, 18 at a time, in a disk that is rotated in a near vertical plane during implantation. The stationary beam is approximately 1cm x 2-3cm. As with the Western Electric implanter, wafer rotation eliminates the need for magnetic or electrical beam scanning.

An add-on process price of $38.96/m^2$ for implanting phosphorus with a $1-2 \times 10^{15}$ ions/cm^2 dose was calculated for the modified Varian-Extrion 200-1000 machine. This price includes the cost of the silicon sheet lost-in-process. The sheet price used applies to silicon wafers which have been texture etched on one side. The slicing cost was taken from our previous study[17] of current production slicing costs (HAMCO ID data).

The add-on process price for ion-implantation using the modified Varion-Extrion 200-1000 is low compared to other prices calculated for currently used ion implanters. For instance, the calculated add-on process price for the Varian-Extrion 200-20 A machine is $303.42/m^2$ [4] This high price is due to the machines's low throughput rate as it was designed for high voltage, low current (under 0.2 mA) operation. Its hourly output rate therefore is only 10, 12-cm diameter cells.

It should be noted that the given add-on price calculation for the modified Varian-Extrion 200-1000 implanter is based on experimental, not production line data. Therefore, this value does not reflect the breakdown or maintenance problems experienced by ion implanters in production operations. However, reliable detail data are not yet available for the cost components of regular production ion implantation, since this process was only rather recently introduced as a production process. Still, if such data would be available, they would not represent the ultimately achievable costs, after machine

and process maturity have been attained. While efforts are in progress to adapt the ion implanters better to production line operation by increasing their throughput rate, mechanizing their operation and improving their reliability, it will be some time before the process will be a mature production operation with similar costs experienced by the various users.

5. Technology Development for Future Ion Implantation Machines

The realization of the 1986 cost projections for ion implantation is contingent on several improvements in the technology of ion implantation machines. For one, the ion beam current has to be increased significantly to achieve economically acceptable throughput rates. Also needed to be increased is the lifetime of the source, in terms of mAh's, to avoid excessive costs from changing and rebuilding the sources, as well as machine downtime. To reduce skilled labor requirements, the implanter's controls should be as automatic as possible. In addition, continuous or semicontinuous wafer feed, along with appropriate vacuum pumping mechanisms have to be employed. Also, care has to be taken in the mass analyses and the control of large current/small voltage ion-beams needed for solar cell fabrication, because space charge effects make those operations difficult. In some LSA process sequences, ribbon material is planned to be the substrate. Since rotation of elongated rectangular workpieces about their axis is impractical, other procedures to achieve uniform deposition have to be utilized in the future implanter, e.g., magnetic or mechanical beam scanning.

As mentioned previously, at present, PN junction formation using open tube diffusion is a small cost contributor to the solar cell module cost, constituting approximately 1%.[18] A replacement process for diffusions in future LSA process sequences would require lower costs, or yield higher performing

cells, or offer a simplified fabrication sequence. Implantation costs are expected to be lowered dramatically by increasing the ion implanter's throughput rate from about 2 m^2/h to nearly 200 m^2/h. To accomplish this, the total ion beam current, flux rate of ions impinging on the silicon, is expected to be increased from 4 mA to 100 mA. If multiple sources are used, then the ion beam current per source needs to be increased by a factor of 4 to 5. Increasing the beam current will, in general, increase the implanter's output rate in the same ratio. But, as shown on Figure III.3, the increase in the machine's cost per unit beam current decreases with beam current. In Figure III.3, the experienced machine cost per unit beam current is plotted as a function of the beam current together with an extrapolation to the future. The first four open circles reflect the costs of ion implantation machines that are in operation and the solid circles reflect projected data from the listed organizations.

In addition to larger ion sources, future implanters would have to be more reliable than current ones. The high capital cost of ion implanters necessitates their utilization rate to be as high as possible. Proposed future machines (Lockheed, RCA, Spire) have been projected to have utilization rates between 85-95% as opposed to today's . For Motorola's unanalyzed ion beam implanter, the uptime fraction is not as significant because of its relatively low cost. The Motorola machine is expected to cost $85,000 as opposed to at least $500,000 for any of the other three proposed machines which employ analyzing magnets. One reliability

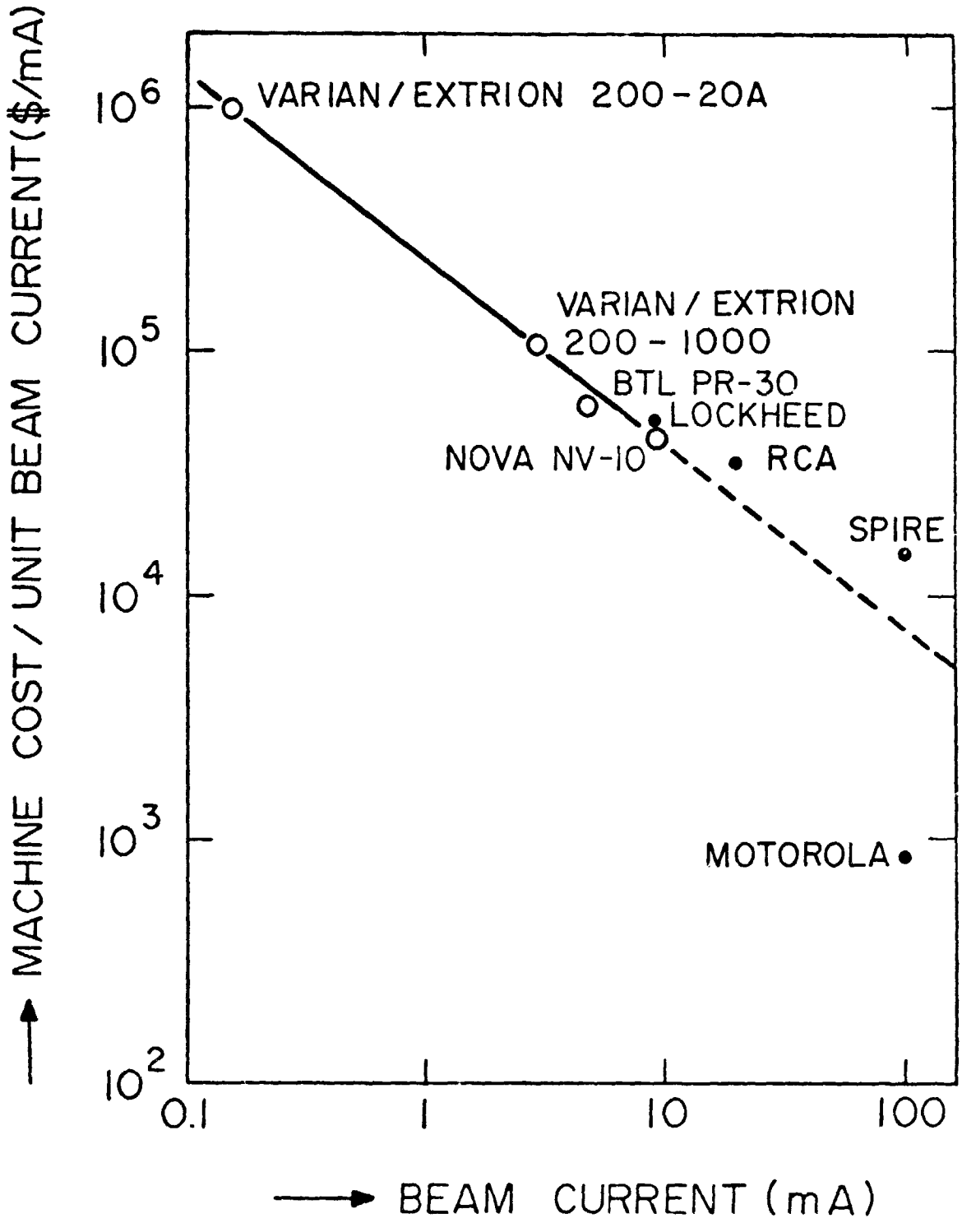
MACHINE COST / UNIT BEAM CURRENT ($/mA)
10^6
10^5
10^4
10^3
10^2
VARIAN / EXTRION 200-20A
VARIAN / EXTRION 200 - 1000
BTL PR-30
LOCKHEED
NOVA NV-10
RCA
SPIRE
MOTOROLA
0.1
1
10
100
BEAM CURRENT (mA)

FIGURE II.3

improvement is expected from increasing the source lifetime in terms of mAh's with beam current. However, although the source life expectancy decreases as beam current output increases, as shown in Figure III.2, the product of source current and lifetime increases with increasing output. Therefore more silicon can be processed between filament changes. In one proposal[7], multiple and spare sources are employed so that they could be replaced while the machine is operating. As listed on Table III-2, the source lifetime (mAh) is expected to increase in the future by a factor of ten.

Another projected improvement is the reduced dependence of the ion implanter's performance on operator skill. At present a skilled operator needs to monitor the operating ion implanter continuously to achieve optimum output rates. These skilled labor requirements are expected to be decreased, in future implanters, by simplifying the machine's operation,[6] by larger batch loads,[3,5] or by using microprocessors.[4] It is thus hoped that future implanters could be operated with unskilled labor, with skilled labor called upon only occasionally for mechanical and electrical servicing.

Since annealing is an integral part of the implantation process, studies are being conducted in the -LSA program on an optimum process.[19] Processes studied include thermal, electron pulse, and laser annealing with only thermal annealing yielding solar cells of comparable efficiency to those produced from diffusion. Thermal annealing costs, as mentioned previously are significant compared to those

TECHNOLOGY PROBLEMS TO BE RESOLVED FOR SUCCESSFUL LOW COST ION-IMPLANTATION

5-FOLD INCREASE OF BEAM CURRENT PER SOURCE (4 mA → 20 mA)

10-FOLD INCREASE OF SOURCE FILAMENT LIFE (25 mAh → 280 mAh)

REDUCED RELIANCE ON OPERATOR INFLUENCE FOR EFFICIENT MACHINE PERFORMANCE

REDUCED FREON LOSSES FROM COOLING SYSTEM (HIGH VOLTAGE.)

EASIER CLEANING OF SPURIOUS MATERIAL DEPOSITED IN SYSTEM. (DEPOSITION PROBABLY NOT AVOIDABLE.)

UNIFORM DEPOSITION W/O WORKPIECE ROTATION

REDUCED CAPITAL COST (CURRENT SINGLE SOURCE, 2 mA MACHINES CAPABLE OF 200 WAFERS/H COST ~$0.5 Mill.)

IMPROVED ANNEALING METHODS (PULSE ANNEALING?)

REDUCED ENERGY CONSUMPTION.

ALTERNATE TECHNOLOGIES:

COLD CATHODE, SOLID SOURCES (SIMPLER SYSTEM. BUT: FASTER SOURCE EROSION? MORE SPURIOUS DEPOSITION IN SYSTEM THAN FROM GASEOUS SOURCES?)

OMISSION OF ANALYZING MAGNET (CAPITAL COST AND ENERGY SAVINGS. BUT: IMPURITY PROFILE ACCEPTABLE? SPURIOUS IMPURITIES CONTROLLABLE?)

Table III-2

for future ion implantation processes. Also thermal annealing decreases the potential efficiency of ion implanted cells. The shallow implanted PN junction depth that can be obtained from implanting with low energy ions has the potential of yielding better performing cells than those from the diffusion process, because of greater UV-response. However, the thermal anneal cycle broadens the shallow implanted junctions depth, making it comparable to that obtained using gaseous diffusion.

For an effective use of the ion implantation process, an extended, automated, vacuum, production sequence has been proposed by Spire. For this sequence to be practical, the annealing process has to be performed in a short time interval. Since the conveyor belt, in the Spire sequence, moves at a rate of 30 cm/sec, a thermal annealing cycle of only 5 minutes would require an effective furnace length of 90 m. Electron or laser beam annealing would be compatible with a rapid production line, since they can be performed in fractions of seconds.[19,20] However, solar cells annealed with either of these two techniques show a decreased performance. A summary of some other technical problems that need to be solved for the successful implementation of ion implantation for future solar cell manufacturing processes is listed in Table III.2 These problems include uniform deposition of ribbon-shaped wafers, more effective coolant usage and convenient removal of deposited source material.

The importance of beam current size to implantation output is shown by the expression for the unit area ion implantation time:

$$t_p = k \frac{\left[1.602 \times 10^{-19} \text{ (a·sec/ion)}\right] \cdot \left[\text{ion flux (ions/cm}^2\text{)}\right]}{\text{Ion beam (amps)}} \text{ sec/cm}^2.$$

III-2.8

The proportionality constant, k, is ≤ 1 and depends on the degree of overscan and the beam utilization. Therefore, as a first approximation, the throughput rate of an ion implanter is proportional to its beam current. Because the implantation process is capital intensive, lowering the machine cost per unit beam current will lower the implantation cost in about the same ratio. As can be observed in Figure III.3 the machine costs normalized to their beam current are expected to decrease approximately proportionally with increased beam current. For future ion implanters, a large capital cost decrease per unit of output is anticipated by increasing the beam current without proportional increases in machine costs.

There are several approaches for increasing the ion beam current. One approach, proposed by Spire, is to increase the size and number of the hot cathode sources to 20 mA and 10, respectively.[7] The source current lifetime is increased by changing from a Freeman to a Chavet type filament. Higher currents are tolerable in the latter source, because the Chavet filament is looped and therefore is not as heavily degraded by the back ion bombardment. Although source lifetime does decrease with increasing currents, as shown in Figure III.2, this decrease is less than the increase in current. In another approach, a hollow cathode source, similar

to that used in ion beam thrusters, is proposed.[6] This source is expected to yield a current of 100 mA, but because of the non-collimated, large crossection nature of the beam it cannot be mass-analyzed. In an ion implanter proposed by RCA, two 10 mA ion beams are used simultaneously. One is used to implant the front of the wafer with phosphorus at a 1×10^{15} cm^{-2} dosage while the other implants boron with a dose of 5×10^{14} cm^{-2}.[3] The Lockheed proposal has ore 10 mA beam that can process about one 7.62-cm diameter wafer/second.[5] The wafers are loaded and unloaded to and from 4 side chambers which surround the central implant chamber.

In the proposed Spire machine, 7 of the 10 sources are operated simultaneously with six running at a current of 16 mA, and the seventh at 4 mA. The ion beam from each source passes through a collimator with a slit geometry of 2 x 75 mm to provide mass analysis. The larger six sources are broken into two sets with an analyzing magnet for each set. Three ion beams strike the moving silicon wafers at $+15^{o}$ to the normal and three at -15^{o}. The wafers are transported on 20x20 cm carriers on a belt moving at a rate of 30 cm/sec. The seventh and smaller ion beam is used for a final dose control. The three remaining sources are used as spares. As plotted in Figure III.2, it is expected, by Spire, that the average source lifetime can be increased to 24h, or approximately 400 mAh. This would mean, on average, a source replacement every 4 h with each replacement requiring 10-15 min. labor. A "dead" source is expected to be ready for replacement within 24 h. The implantation energy is designed to be 10 keV, dose uniformity to be $\pm$ 10%, and analysis to $\pm$ 0.5 AMU. In order not to

enhance the space charge effect of the large beams, electric fields after the extraction gap are avoided in the Spire machine design. The scanning deflector, shown in Fig. III.1, is operated magnetically.

The narrow width of the 16 mA ion beams makes them analyable since the radius of curvature of the ion beams caused by the magnetic field can be made larger than the beam's width. The radius of curvature is given by:

$$r = (m/e) \times v/B \qquad \text{III-2.9}$$

where (m/e) is the ion's mass to charge ratio, v is the ion velocity, and B is the magnetic field strength (in gauss). If a linear magnetic field is assumed, then the deflection angle is $\sin^{-1} [(e/m) \times (B/v) \ell]$, where ℓ is the length of the magnet. Therefore, the angle of deflection depends on the (e/m) ratio. A slit in the ion path placed preceding the beam selects the desired ion, as seen in the top drawing of Figure III.1.

A large, transient temperature increase ($\sim$800°C) can cause considerable stress in the silicon wafer, and make substrate movement and handling difficult. The energy flux density J, of a 10 keV ion beam at a density of 1×10^{15} ions/cm^2, is 1.602 j/cm^2. With the proposed output of the Spire implanter of 180 m^2/h, the implantation time is 0.002 sec/cm^2. The temperature rise of implanted wafers is given by,

$$\Delta T = J/C_p \rho (2D t_p)^{1/2} \quad {}^{o}C, \qquad \text{III-2.10}$$

where C_p is the specific heat of silicon (0.71 j/g°C)[21] at RT,

and ρ is the silicon density (2.34 g/cm^3). D is known as the heat diffusivity which is equal to $k/C_p\rho$, where k is the thermal conductivity of silicon (1.47 j/sec·cm ^oC).[22] The expression $\sqrt{2Dt_p}$ is the thermal diffusion length and cannot exceed the wafer's thickness. Equation III-2.10 is valid when the implanted junction depth is small compared to $\sqrt{2Dt_p}$ or the thickness of wafer. This condition is satisfied for NP solar cell NP junction formation. The junction depth is normally approximately 0.2 μm and the implantation time is sufficiently long to make the diffusion length several hundred microns. For implanting a 200 μm thick wafer, with the porposed Spire machine, the temperature increase over the environment is expected to be 48^oC.

In Motorola's proposal, shown in the bottom drawing of Figure III.1, a large ion current beam (100 mA) is obtained from a hollow-cathode source derived from ion thruster technology. Ion thrusters, using ionization of mercury, have very large beam currents (several amps), and lifetimes of thousands of hours. It is thought not to be difficult to modify the thruster to ionize phosphorus or other suitable dopants.[11] However, the ion thruster beam can not be mass-analyzed because of its circular cross-section and large diameter. The dispersion caused by a magnetic field would be less than the beam's diameter. In addition, the energy spread of ions emitted from a ion thruster type source hinders good magnetic separation, since the curvature radius of ions under the influence of a magnetic field is directly proportional to its velocity. The effect on solar cell efficiency of implanting

with an unanalyzed or a "roughly" analyzed beam is not yet known and investigations have just been initiated.[23] The proposed Motorola ion implanter is fairly simple in design; the wafers are transported (past the ion beam) by a belt through differentially pumped vacuum chambers. Dose uniformity might be a problem, because of the Gaussian distribution of the beam's intensity and an individual wafer might be exposed to only a selected portion of the ion beam. It takes less than 0.75 sec. to implant a 12-cm diameter wafer with a 2×10^{15} cm^{-2} dosage of phosphorus with a 100 mA beam. The low capital cost of this implanter, makes the Motorola proposed ion implanted process the lowest cost one studied in this report.

In the RCA and Lockheed proposed machines, hot cathode ion sources are employed. In the RCA-proposed machine,[3] both the PN and PP+ junctions are formed simultaneously by using two separate 10 mA beams. One beam is used for phosphorus and the other for boron. This machine can process approximately 100 cm^2/sec, and allowing time for beam scanning and beam loss at edges, the machine's throughput is 2000, 7.62-cm diameter wafers per hour. The wafers are transferred automatically from 500 wafer cartridges to 50 wafer cassettes from which they are then removed to a holder for implantation. The high capital cost of the RCA implanter relative to its output, makes the RCA process the most expensive of the future implantation process projections.

The Lockheed proposed machine uses a 10 mA beam, and can implant 3000 wafers/h (7.62-cm diameter).[5] The wafers,

which are batch-loaded, are held in 1200 ring-shaped trays or carousels (50 wafers/tray) that are stacked and distributed among 4 cylindrical vacuum chambers adjacent to the implantation chamber. During the implantation process, the trays are transferred to the central chamber where they are rotated such that each wafer is scanned on its underside by the ion beam. This is repeated 4 times for each tray to assure dose uniformity. The ion beam is kept constant at 7^{o} to the normal while the wafers are rotated. This eliminates the need for electrical or magnetic beam scanning. After all the wafers in the machine have been scanned, vacuum in the implantation system is broken and the wafer loading cylindrical chambers are replaced. It takes approximately 20 hours for the completion of one run: 2 hours for loading, 16 hours for processing, and 2 hours for unloading. The Lockheed process employs phosphorous pentaflouride (PF_5) as the source gas, instead of PH_3 or P. Phosphorous pentaflouride is very expensive and is a large cost contributor (about 16%) to the add-on process price.

6. Junction Formation Material, Labor, and Capital Requirements Cost Structures

The costs of present and future junction formation processes, broken up into their material, labor, capital, overhead, and return-on-equity components, are summarized in Table II.3. Also listed in Table III.3 is the throughput rate, in terms of number of wafers processed per hour and their diameter. The cost calculations are based on the SAMICS methodology[24]. The detail process parameters, including direct and indirect material, labor, and equipment and facility requirements are presented in Tables III-4A to III-4C for the diffusion processes, and in Tables III-5A to III-5C for the ion implantation processes. These data are given both in terms of unit area of cells processed and of net plant operating time. The hourly consumption rates were converted to unit area data by use of the "effective output rates" shown in line 1 of Tables III-4A and III-5A. The effective output rate is the produce of the operating machine's throughput rate and the usage fraction, (process "up-time" divided by plant operating time). The plant operating hours were taken to be 8280 h per year. For calculation of the material costs, the unit prices shown in Table III.6 were used. The labor costs were obtained by employing a labor rate of $3.894/h for the semiconductor assembler (SAMICS B3096D) and of $5.29 for the electronics technician (SAMICS B3704D). The total labor costs include an indirect labor charge of 25%, and a

Table III-3

Technical and Economic Comparison of Present and Proposed

Junctio.. Formation Processes

Add-on Cost Components ($/m^2)

ORGANIZATION	Varian-Extrion 200-1000 WF (Spire) (1978)	Spectrolab PH_3 diffusion (1978)	Motorola PH_3 diffusion (1986)	Motorola 5-step diffusion process (1986)	RCA 2-side ion implantation w/annealing (1986)	Lockheed PF_5 Implantation (1986)	Motorola Activation annealing (1986)	Motorola Unanalyzed beam implanter (1986)	Spire High thruput ion implanter (1986)
Throughput/rate [c.h^{-1}/dia.(cm)]	40/7.6-cm	129/7.6-cm	1000/12-cm	1000/12-cm	2000/7.6-cm	3,000/7.62-cm	2000/12-cm	4800/12-cm	18,000/10-cm
1. Direct Materials	0.01	0.02	0.29	2.26	0.25	0.86	--	0.03	0.07
2. Indirect Materials	0.75	0.19	0.20	0.25	0.69	0.68	0.03	0.07	0.02
3. Expendible tool	2.63	0.28	0.11	0.16	0.27		0.05	0.00	0.06
4. Electrical Energy	0.65	0.08	0.22	0.44	0.22	0.02	0.10	0.02	0.08
5. Total Materials (1.0526* (1.+2.+3.+4.))	4.26	0.59	0.86	3.27	1.51	1.63	0.19	0.13	0.24
6. Direct Labor	4.84	4.65	0.52	1.68	0.42	0.55	0.24	0.12	0.06
7. Maintenance Labor	1.36	--	0.08	0.37	0.14		--	0.02	0.02
8. Indirect Labor (0.25*(6.+ 7.))	1.55	1.17	0.15	0.51	0.14	0.14	0.06	0.03	0.02
9. Total Labor (1.3156 * (6.+ 7.))	8.19	6.12	0.78	2.72	0.73	0.73	0.32	0.18	0.1
10. Equipment	7.42	1.[illegible]	0.17	0.79	2.45	0.99	0.08	0.05	0.36
11. Facility	0.39	0.30	0.05	0.19	0.26	0.23	0.03	0.02	0.01
12. Capital (10.+ 11.)	7.81	1.45	0.22	0.98	2.71	1.22	0.10	0.07	0.37
13. Overhead	0.48	0.10	0.02	0.05	0.17	0.08	0.01	0.005	0.02
14. Return-on-equity	13.27	4.12	0.77	2.96	4.68	2.76	0.31	0.21	0.58
15. Add-on price of process	34.01	12.38	2.65	9.98	9.90	6.42	0.95	0.60	1.31
16. Yield (%)	99	99.9	99	--	--	99.2	99.4	99.8	99.9
17. Yielded add-on process price	34.36	12.39	2.68	9.98	9.90	6.47	0.95	0.60	1.31
18. Cost of silicon lost-in-process	3.51	0.35	0.42	1.78	0.84	0.32	0.25	0.08	0.04
19. Add-on price	37.86	12.74	3.10	11.76	10.74	6.79	1.20	0.68	1.35

Table III-4A

DIFFUSION PROCESS MATERIAL REQUIREMENTS

Organization	Spectrolab PH_3 diffusion (1978)	Motorola PH_3 diffusion (near-term)	RCA $POCl_3$ diffusion (near-term)	Motorola Activation Annealing
1. Effective output rate (m^2/h)	0.584	10.08	7.675	21.585
2. Direct material needs	257 mℓ/h of 500 ppm PH_3 in N_2 (440 mℓ/m^2)	3 ℓ/h of PH_3 (0.3 ℓ/m^2)	357 g/h of $POCl_3$ (46.5 g/m^2)	---
3. Nitrogen gas (ℓ/h) (ℓ/m^2)	60 103	---	2312 301	1440 66.7
4. Argon (ℓ/h) (ℓ/m^2)	---	398 39.5	---	---
5. Oxygen (ℓ/h) (ℓ/m^2)	minimal	---	56.1 7.3	---
6. Etching solution for cleaning quartzware (ℓ/h) (ℓ/m^2)	0.086 0.147	---	---	---
7. Quartzware ($/h) (type) ($/m^2)	095 (boats and tubes) 0.162	1.14 (boats and tubes) 0.11	0.65 (boats) 0.085	1.16 (boats and tubes) 0.054
8. Electricity (kW) (kWh/m^2)	1.4 2.4	70 6.94	34 4.43	70 3.24

Table III-4B

DIFFUSION PROCESS LABOR REQUIREMENTS

Organization	Spectrolab PH_3 diffusion (1978)	Motorola PH_3 diffusion (near-term)	RCA $POCl_3$ diffusion (near-term)	Motorola Activation Annealing
1. Semiconductor assembler (h/h)	0.5	1.0	0.35	1.0
($/m^2)*	6.14	0.69	0.32	0.32
2. Maintenance mechanic (h/h)	0	0.10	0.15	---
($/m^2)*		0.11	0.20	

*Includes fringe benefits, indirect labor, and overhead labor

Table III-4C

DIFFUSION PROCESS EQUIPMENT AND FACILITY REQUIREMENTS

Organization	Spectrolab PH_3 diffusion (1978)	Motorola PH_3 diffusion (near future)	RCA $POCl_3$ diffusion (near future)	Motorola Activation annealing (near future)
1. Type of furnace	One tube furnace w/temperature and gas flow controls	Thermco 8-tube furnace	Thermco SPARTAN furnace	Thermco 8-tube furnace
2. Auxilary equipment	Exhaust system & tube cleaning tower	Eight process controllers	furnace liners, paddles, heat coil and loaders	Eight process controllers
3. Total floor area (m^2)	16.3	25.55	25.55	25.55
4. Furnace cost	15,000	49,271	66,600	49,271
5. Other equipment cost ($)	10,000	16,000	39,600	16,000
6. Installation cost	2,500	---	---	---
7. Total capital cost	27,500	65,270	106,200	65,270
8. Gross output rate (m^2/run)	0.342	11.31	9.12	22.62
9. Operating availability (%)	99.8	90	85	96
10. Process yield (%)	99.9	99.0	99	99.4
11. Effective output rate	0.341	10.08	7.675	21.585
12. Cycle time (min)	35	60	60	60
13. Hourly throughput (m^2/h)	0.584	10.08	7.675	21.585

Table III-5A

Material Requirements for Ion Implantation

Organization	Varian-Extrion 200-1000F (Spire) (1978)	RCA 2-sided implantation (near-term)	Lockheed PF_5 implantation (near-term)	Motorola Unanalyzed beam implantation (long-range)	Spire High thruput (long-range)
1. Effective output rate (m^2/h)	1.083	7.675	12.9	43.34	179.36
2. Direct material needs	0.476 ℓ/h of 5% PH_3 in H_2 (0.44 ℓ/m^2)	$2.28/h ($0.29/m^2)	2.192 ℓ/h of 99% PF_5 (0.17 ℓ/m^2)	0.509 g/h of SeG phosphorus (0.012 g/m^2)	453 ℓ/h of 5% PH_3 in H_2 (2.53 ℓ/m^2)
3. Cooling water	0.48 kW 0.44 kWh/m^2	2400 ℓ/h 313 ℓ/m^2	7 kW 0.54 kWh/m^2	---	2.46 kW 0.014 kWh/m^2
4. Compressed air (ℓ/h) (ℓ/m^2)	---	---	168 13.0	---	---
5. Liquid nitrogen (ℓ/h) (ℓ/m^2)	2.69 2.48	9.25 1.20	3.75 0.29	0.625 0.014	---
6. Nitrogen gas (ℓ/h) (ℓ/m^2)	---	---	---	---	510 2.84
7. Argon (ℓ/h) (ℓ/m^2)	---	---	800 62	---	---
8. Spare parts ($/h) ($/m^2)	2.88 2.66	0.97 0.13	---	0.05 0.001	10.67 0.06
9. Electricity (kW) (kWh/m^2)	22.5 20.8	37 4.82	7 0.54	27 0.62	380 2.12

Table III-5B

Ion Implantation Process Labor Requirements

Organization	Varian-Extrion 200-1000f (Spire) (1978)	RCA 2-sided implantation (near-term)	Lockheed PF_5 implantation (near term)	Motorola Unanalyzed beam implantation (long range)	Spire High thruput implantation (long range)
1. Semiconductor assembler (h/h)	1.0	0.40	---	1.0	2.0
($/m^2)*	6.43	0.36		0.16	0.08
2. Maintenance mechanic (h/h)	0.10	0.10	---	0.10	0.2
($/m^2)*	0.94	0.13		0.02	0.01
3. Electronics technician (h/h)	0.10	---	1.0	---	0.2
($/m^2)*	0.87		0.73		0.01

* Includes fringe benefits, indirect labor and overhead labor.

Table III-5C

ION IMPLANTATION EQUIPMENT AND FACILITY REQUIREMENTS

Organization	Varian-Extrion 200-1000f (Spire) (1978)	RCA 2-sided implantation (near-term)	Lockheed PF_5 implantation (near term)	Motorola Unanalyzed beam implantation (long range)	Spire High thruput implantation (long range)
1. Source type	hot cathode (Freeman)	2 hot cathodes	hot cathode	hollow cathode	10 hot cathodes (Chavet)
2. Ion current (mA)	2-4	10/beam	10	100	100(total)
3. Scanning mechanism	electrical	electrical?	wafer rotation	wafer movement	linear substrate motion
4. Floor area (m^2)	19.51	79	139.355	37.2	93
5. Machine cost	315,000	700,000	500,000	85,000	2,500,000
6. Installation cost	---	---	---	---	30,000
7. Total capital cost	315,000	700,000	500,000	85,000	2,530,000
8. Gross Output rate (m^2/h)	1.368	9.12	13.68	54.29	141.3
9. Operating availability (%)	80	85	95	80	127*
10. Process yield (%)	99	99	99.2	99.8	99.9
11. Effective output rate (m^2/h)	1.083	7.675	12.9	43.34	179.36

* Refers to two machines operating to yield 1986 LSA-JPL factory output guidelines

5.26% addition for overhead expenses, both according to SAMICS. The equipment and facility costs were similarly calculated consistent with the SAMICS methodology.[24]

The cost of the wafers, which are reflected in the lost-in-process cost (Table III.3, line 18) are taken from our previous studies of slicing processes[17], and the 1986 silicon and sheet value goals listed in JPL-LSA's price allocation guidelines.[25] In addition to slicing, the cost of one-sided texture etching is included in the current and future wafer prices. The etching is performed by applying etch stop in the form of wax on one surface, texture etching with 30% NaOH at 90°C, and removing the wax with plasma etching. The etching step costs have been derived from information published by Motorola,[26] and add up to approximately $\$3.09/m^2$. The calculated prepared wafer prices are $\$350.98/m^2$ and $\$41.21/m^2$ for 1978 and 1986, respectively. The specific process for the current wafer price is slicing 10.16-cm diameter wafers with a HAMCO ID saw.

The first two columns of Table III.3 refer to current implantation and diffusion techniques, while the other columns detail the costs of proposed processes. Two multi-step sequences for producing front and BSF cells are also shown on Table III.3. The 5-step Motorola diffusion process, which is detailed in Table III.7, consists of protecting the front surface by spinning-on-silica, diffusion of the BSF using

Table III-6

Material Prices Used for Calculating Costs

Item	Unit Price ($)	Source
Direct needs		
500 ppm of PH_3 in N_2	42.86/m^3	Spectrolab
PH_3 gas	0.991/ℓ	Motorola
$POCl_3$	0.0204/g	SAMICS E1504D
5% PH_3 in H_2	0.029/ℓ	SAMICS E1472D
PF_5	0.0051/ml	Matheson
SeG-phosphorus	2.76/g	Alfa Products (Ventron)
Indirect Material		
Liquid nitrogen	0.202/ℓ	SAMICS C1080D
Nitrogen gas	0.0004/ℓ	Obtained from LN_2
Argon	0.005/ℓ	SAMICS E1112D
Oxygen gas	0.00018/ℓ	SAMICS E1448D
Compressed air	--	SAMICS C2032D
Cooling water	0.566/kWh	SAMICS C1128D
	1.996/m^2	SAMICS C1016B
Electricity	0.0319/kWh	SAMICS C1032B

BCl_3, a spin-on silica protection of the back surface, phosphine diffusion, and stripping of silica from both surfaces with a 4:1 NH_4OH:HF solution. The result is an N^+PP^+ wafer with no silica coating, ready for metallization or AR-coating. The other multi-step process consists of RCA's double-sided ion implantation followed by thermal annealing. The RCA 2-step process yields wafers equivalent to Motorola's 5-step wet chemical sequence.

The cost components for activation annealing are shown in Table III.3 because it is presently a necessary step after ion implantation to achieve state-of-the-art performing cells. Annealing costs are significant compared to those derived using the high throughput implanters proposed by Motorola and Spire.

The major cost components from Table III.3 are graphically represented on Figure III.4. In addition, Figure III.4 includes the cost of RCA's proposed gaseous diffusion using $POCl_3$. This diffusion process takes approximately one hour and has an output rate of 2,000 7.62-cm diameter wafers per hour.

The prices for the proposed PH_3 and $POCl_3$ diffusion processes are \$3.01/m^2 and \$3.86/m^2, respectively. These two processes should be available for near term production sequences; no major technical problems need to be solved for their applicability. The cost decreases for the diffusion processes are about a factor of four lower from current ones, and for the most part, depend upon throughput increases. The higher output rate for Motorola's diffusion process, as compared to Spectrolab's,

Table III-7

Yielded Add-on Cost Components for Motorola's 5-Step Wet Chemical Front Junction and BSF Sequence ($/m^2)

Process Step	Step Yield (%)	Cumulative Yield (%)	Materials	Labor	Capital	Return-on Equity	Lost Si (1986)	Subtotal
1. Spin-on silica (front surface)	99.0	95.9	1.06	0.50	0.28	0.72	0.43	2.99
2. BSF diffusion with BCl_3	99.0	96.8	0.33	0.81	0.24	0.69	0.43	2.50
3. Spin-on silica (back surface)	99.0	97.8	1.04	0.49	0.28	0.71	0.42	2.94
4. Phosphine diffusion for front junction	99.0	98.8	0.79	0.79	0.24	0.78	0.42	3.02
5. Stripping of silica with 4:1 NH_4OH:HF solution	99.8	99.8	0.06	0.15	0.01	0.05	0.08	0.35
Totals			3.28	2.74	1.05	2.95	1.78	11.80

JUNCTION FORMATION ADD-ON PRICES

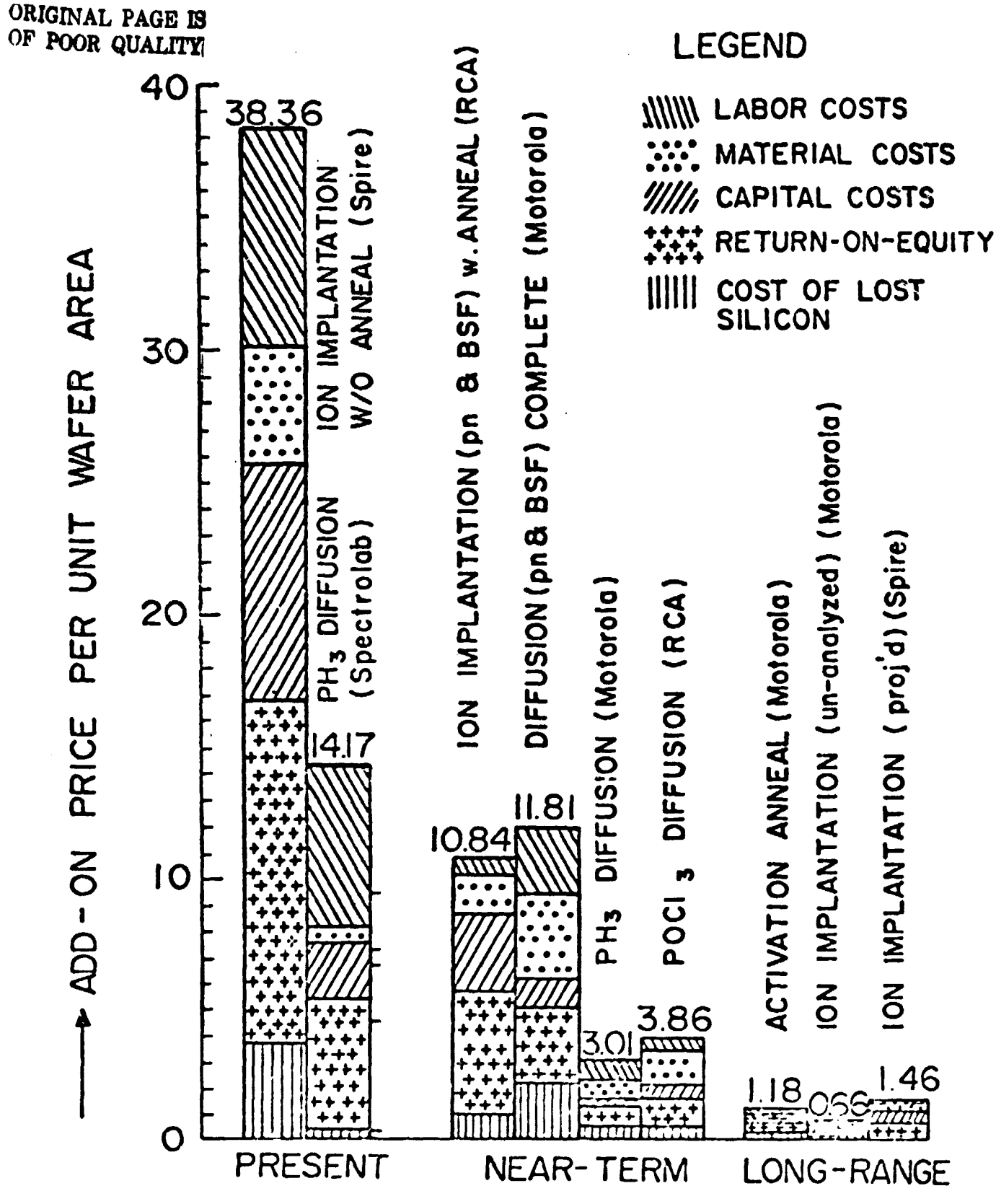

FIGURE III-4

is based on processing larger wafers (12-cm) at the same rate as smaller ones (7.62-cm). The larger area (2.48x) of the 12-cm diameter wafers accounts for the higher throughput rates of Motorola's process. RCA proposes to automatically transfer wafers from cassettes to furnace boats, and load/unload the boats from the furnace, to increase output rates. The loading and transferring machines add to the capital cost of the RCA process, but increase output sufficiently to lower unit area costs.

The RCA 2-sided implantation process, which is included on Figure III.4 with annealing, and the Lockheed implantation proposal, could be ready for near-term production (1982-1984). Both these machines have 10 mA ion beams. The RCA implanter actually has two 10 mA beams but only one is used for the front junction formation. This beam size is only twice as large as some machines in operation and a 10 mA machine, the NV-10, by Nova Associates, should be introduced into the marketplace shortly.

The processing costs from employing the high current (100 mA) machines by Motorola and Spire are the lowest ones listed on Table III.3 for junction formation. However, a longer time than for the other options discussed above will be needed before these machines are suitable for production use, because of larger extrapolations of ion currents and throughput rates. In addition, the Morotola 100 mA proposal has reductions

in labor, and capital costs because of its greatly simplified operation. It employs an unanalyzed beam from a hollow cathode source, thus eliminating the need for any acceleration, magnetic, and scanning capabilities. The hollow cathode source originally designed for space propulsion use in ion thrusters, should give the high currents and lifetimes necessary for a low-cost, high throughput operation, needed in solar cell manufacturing. But, the effects on cell performance by implanting with an unanalyzed beam are unknown, although investigations have recently been initiated.[23] Spire expects their implanter to have a 100-fold increase in output rate over current machines. This is to accomplished, for the most part, by increasing the beam current to 100 mA, by having a continuously pumped, belt system, feed mechanism, and by increases in machine reliability by extensive use of microprocessors and redundant beam sources.

7. Conclusions

In order for the front junction formation processes involving diffusion and ion implantation to fit into future (1986) low-cost solar cell fabrication sequences their costs will have to decrease by factors of approximately four and ten, respectively. At present, the phosphorus diffusion process cost is $\$12.74/m^2$ while the ion implantation of phosphorus costs $\$37.86/m^2$. It is anticipated that the future cost contribution for front junction formation would be less than $\$3.20/m^2$.

The costs in the long term ion implantation projections by themselves seem significantly lower than those of the diffusion processes, but adding the cost of the necessary activation annealing makes the costs comparable. For combined front and BSF sequences, the cost difference between a wet-chemical process (the 5-step Motorola sequence) and an equivalent multi-step process employing ion implantation, is about $\$1/m^2$. The closeness of these two projections makes it difficult to judge which would be economically advantageous in 1986. From our calculations, it would appear that ion implantation and diffusion could be competitive.

Future junction formation processes will have to fit well into high volume process sequences. Even though currently, gaseous diffusion is an inexpensive step in manufacturing solar cells, its costs have to be reduced

even more to fit into the future LSA framework. Cost reductions depend upon larger throughput rates to be achieved by processing larger diameter wafers, and by automatic wafer transfer. Wafer transferring could be accomplished using specifically designed machines, which would increase the capital cost of gaseous diffusion. Another cost reduction for diffusion is related to quartzware (boats and tube liners) cleaning using mild chemical etching. The cleaning is necessary to minimize wafer contamination and is currently a significant cost contributor to the diffusion process. The required cleaning frequency and alternative cleaning procedures should be investigated.

Ion implantation has recently been introduced into production activities, and its state-of-the-art performance is rapidly changing. During the last decade, ion beam current (and consequently the throughput rate) has increased by a factor of 1,000 - from a few microamps to a soon to be introduced 10 mA. For low-cost solar cell junction formation, the implanter's beam current would have to increase by an additional order of magnitude and its cost reduced by approximately a factor of 20. The feasibility of achieving these goals cannot, at this time, be assured. But certainly, activity in this area should be continued.

If ion implantation's cost reductions could be accomplished through larger throughput rates and greater reliability, and if a compatible annealing process could be perfected, then ion implantation would be a strong candidate for junction formation in future LSA process sequences.

The cost reductions required for gaseous diffusion to meet

the LSA future price goals are not as dramatic as those needed for ion implantation, and are not as dependent on technical development. However, studies should be continued in automatic wafer handling and in quartzware cleaning methods, because these are potential add-on price reduction areas for diffusion.

5. References

1. R. Oliver and E.L. Ralph, Spectrolab Corporation (Slymar, CA), private communication (4/79).

2. R.A. Pryor, L.A. Grenon and M.G. Coleman, Motorola Corporation (Phoenix, AZ), Report DOE/JPL-954363-78/8, 133-4, 172 (1/78).

3. R.V. D'Aiello, RCA Laboratories (Princeton, NJ), Report DOE/JPL-954352-77/4, 55-57, 82 (12/77).

4. J. Minnucci and A. Kirkpatrick, Spire Corporation (Bedford, MA), Report DOE/JPL 954786-78/05, 3, 22-23 (7/78).

5. Lockheed Missles and Space Company (Sunnyvale, CA), Report ERDA/JPL-954898-78/3, 22-27 (7/78) and Report DOE/JPL-954898-4, Appendix D (10/78).

6. M.G. Coleman et al., Motorola Corporation (Phoenix, AZ), Report DOE/JPL-954847-78/2, 105 (3/78).

7. J. Minnucci and A. Kirkpatrick, Spire Corporation (Bedford, MA), Report DOE/JPL-954786-78/1, 20-25 (1/78).

8. A. Kirkpatrick and J. Minnucci, presented at the 9th LSA-JPL Project Integration Meeting (Pasedena, CA) (4/78).

9. J. Minnucci and A. Kirkpatrick, Spire Corporation (Bedford, MA), Report DOE/JPL-954786-78/04, 5-7 (4/78).

10. J. Minnucci and A. Kirkpatrick, ibed ., 28 (4/78).

11. D. Fitzgerald, JPL, private communication (12/78).

12. B. Wyduta and F. Lee, RCA (Somerville, NJ), private communication (11/78).

13. J.G. McCallum, G.I. Robertson, A.F. Rodde, B. Weissman and N. Williams, J. Vac. Sci. Technol. 15 (3), 1067 (1978).

14. N. Williams, J. Vac. Sci. Technol. 15 (3), 1076 (1978).

15. B. Weissman, Western Electric Company, Engineering Research Center (Princeton, NJ), private communication (4/79).

16. G. Swanson, Nova Associates (Beverly, MA), private communication (5/79).

17. H. Goldman and M. Wolf, University of Pennsylvania (Philadelphia, PA), Report DOE/JPL-954796-78/4 (11/78).

18. D. Bickler, presented at the 12th LSA-JPL Project Integration Meeting, Pasadena, CA (4/79).

19. E.F. Kennedy et al. in Laser Solid Interactions and Laser Processing, 1978, American Institute of Physics Proceedings No. 50, NY (1979), 470-474.

20. C.W. White, J. Narayan and R.T. Young, Science, 204 (4392), 461 (5/79).

21. H.R. Shanks, et al., Phys. Rev. 130, 1743 (1963).

22. C.J. Glassbrenner and G.A. Slack, Phys. Rev. 134, A1058 (1964).

23. D. Fitzgerald, presented at the 12th LSA-JPL Project Integration Meeting, Pasadena, CA (4/79).

24. R.W. Aster and R.G. Chamberlain, JPL-LSA Project Report 5101-33 (9/77).

25. W. Callaghan, presented at the 9th LSA-JPL Project Integration Meeting, Pasadena, CA (4/78).

26. R.A. Pryor, L.A. Grenon and M.G. Coleman, Motorola, Inc. (Phoenix, AZ), Report DOE/JPL 954363-78/8 (1/78), and Report DOE/JPL 954847-78/2 (3/78)

IV. Methodology for Energy-Cost Effectiveness Evaluation of Subsystem Design and Manufacturing Process Options

1. Introduction

One of the important attributes of a photovoltaic solar energy conversion system is its economic viability. The evaluation of this attribute is regularly performed in decision making about the use of such a system in a particular application, as well as in comparing the merits of one particular system design or solar cell production process against another. The key aspect in such an evaluation is the comparison of the cost of electrical energy produced by the photovoltaic system with the cost of competitively available electrical energy.

The unit cost c_{En} of the electrical energy delivered from the photovoltaic system can be expressed, following ref. (1), as:

$$c_{En} = \frac{C_{op} + \gamma_{cap} C_{cap}}{E_{Ld}} \; ; \; [\$ \; kWh^{-1}] \qquad (IV.1)$$

where C_{op} are the annual operating costs [$\$ \; y^{-1}$], C_{cap} is the capital spent in acquiring the system [$] and γ_{cap} is the equivalent annual cost of capital [y^{-1}]. This equivalent annual cost of capital may, outside of the usual components of interest, taxes, depreciation, etc., include such considerations as desired profit, present or discounted value of life cycle costs, inflation adjustments, etc. As the "fuel" in a solar energy utilization system is "free", the operating costs are essentially reduced to the maintenance costs, at least for the smaller distributed systems. And since it is generally assumed, in the absence of information to the contrary, that the systems will be designed and built for high reliability and thus require little maintenance, the maintenance costs are usually neglected in comparison to the costs of the capital. E_{Ld} is the electrical energy usefully delivered during a year from the photovoltaic system to the load.

Thus:

$$c_{En} \approx \gamma_{cap} \frac{c_{cap}}{E_{Ld}} = \gamma_{cap} \cdot \Gamma \; ; \; [\$ \; kWh^{-1}] \qquad (IV.2)$$

$$\Delta c_{En} = \frac{c_{cap}}{E_{Ld}} \cdot \Delta \gamma cap$$

As γ_{cap} is a constant for a particular company at a given time, but will differ from company to company, the system dependent energy cost determinator is really the quantity:

$$\Gamma = \frac{C_{cap}}{E_{Ld}} \; ; [\$ \; kWh^{-1} \; y] \qquad (IV.3)$$

which is the ratio of the required investment to the energy delivered per year. The evaluation and optimization of this quantity is therefore of primary interest.

2. The Energy Delivered to the Load

The energy E_{Ld} delivered during the year to the load is clearly related to, although different from, the energy E_o delivered by the photovoltaic array itself to the remainder of the system. For a photovoltaic array of total exposed area $A_{Ar}[m^2]$, E_o is given by:

$$E_o = A_{Ar} \int_0^{8760h} H(t) \; \eta_{Ar}(H(t), T(t)) \; \phi(t) \; dt; \; [kWh \cdot y^{-1}] \qquad (IV.4)$$

where η_{Ar} (H(t), T(t)) is the effective array efficiency in the time interval dt around time t, with η_{Ar} being dependent on the temperature T(t) of the array and on the irradiance H(t) [kW m^{-2}] during that time interval, as well as on the varying spectral distribution and the angle of incidence of the light. $\phi(t)$ is a factor of magnitude between zero and one, which describes whether, or how much, energy can be delivered by an array for transfer to the load or to storage, depending on the existence of load and on the status of the storage system during the respective time interval. Eq. (IV.4), being a definite integral, can be expressed as:

$$E_o = A_{Ar} H_{pk} \eta_{Ar,\,std} f_{Ld} \cdot 8760; [kWh \cdot y^{-1}] \qquad (IV.5)$$

following the custom of referring the output to "nameplate rating", or peak power output capability, which is, for the solar array, expressed by the product of the expected peak irradiance H_{pk} and the array efficiency $\eta_{Ar,\,std}$ measured under standardized conditions (including the peak irradiance H_{pk}). The connection to eq. (IV.4) is made via the "load factor" f_{Ld} which is the ratio of the output actually delivered during the year to the "nameplate rating." f_{Ld} is usually determined from the results of a system simulation computer run for a one-year period, which includes the solar energy availability statistics - normally weather bureau data for a selected year - and the expected load statistics. Ideal would be a simulation run over the system life to determine an f_{Ld} value which represents the average over the system life. However, forward looking solar energy availability data do not exist, and even forward looking load statistics will be of doubtful validity. A compromise could be a backward looking simulation over a period equal in duration to the system life, using real data. The limited gain in confidence, however, generally does not justify the additional expense. A one-year run is usually felt necessary to properly include the seasonal changes and the short term meteorological variations.

The total number of hours in the year (8760 h), multiplied by the load factor f_{Ld} represent an "equivalent time" t_{eq} during which the array could have operated at peak power capability to produce the same amount of energy as actually delivered. It is additionally useful to define the quantity p_{pk}, the peak power output capability per unit area of the array, which is simply:

$$p_{pk} = H_{pk} \cdot \eta_{Ar,std}; [kW\ m^{-2}] \qquad (IV.6)$$

The energy $E_{Ld,dir}$ delivered from the array directly to the load will generally be less than E_o, being reduced by the power conditioning subsystem efficiency η_{PC}, and by the fraction f_{St} of the annual array output which is, in the average, transferred into the storage subsystem :.

$$E_{Ld,\ dir} = E_o\ (1 - f_{St}) \cdot \eta_{PC};\ [kWh \cdot y^{-1}], \qquad (IV.7)$$

In addition, the energy $E_{Ld,St}$ is delivered from the storage subsystem, to the load:

$$E_{Ld,St} = E_o f_{St}\ \eta_{St}\ \eta_{PC};\ [kWh \cdot y^{-1}] \qquad (IV.8)$$

where η_{St} is the efficiency of the storage subsystem.
In the relationship of eq. (IV.7), the assumption is made that all power conditioning occurs after storage. Otherwise, the efficiency η_{PC} would have to be broken into several terms.

Summing eq. (IV.7) and (IV.8) yields then the total energy E_{Ld} delivered to the load:

$$E_{Ld} = E_o\ [1 - f_{St}\ (1 - \eta_{St})]\ \eta_{PC};\ [kWh \cdot y^{-1}] \qquad (IV.9)$$

The expression in the brackets, which is a function of the load curve relative to the solar energy availability curve, as well as of system design, incl. type and capacity of the storage device, could be represented by a "storage transfer factor" τ_{St}, so that eq. (IV.9) can be written as:

$$E_{Ld} = E_o \cdot \tau_{St} \cdot \eta_{PC};[kWh\ y^{-1}] \qquad (IV.9a)$$

It has to be noted that the load factor f_{Ld}, included in E_o, is also dependent on the same variables as τ_{St}, and generally increases with increasing f_{St} and η_{St}.

The system power delivery capability P_{sy} which is usually limited by the power conditioning subsystem and/or the storage subsystem capacities, can be related through the factor f_{Po} to the array peak power capability:

$$P_{Sy} = A_{Ar} p_{pk} \cdot \tau_{St} \cdot \eta_{Pc} \cdot f_{Po}; \quad [kW] \tag{IV.10}$$

The factor f_{Po} may be smaller or greater than unity.

The storage subsystem capacity can illustratively be expressed by the "equivalent storage time" t_{St} which is the time interval for which the storage device, when originally fully charged, could provide energy at the peak system power delivery rate, until discharged to a predetermined minimum charge state:

$$E_{st} = P_{sy} \cdot t_{St}; \quad [kWh] \tag{IV.11}$$

3. Evaluation of the Energy-Cost Effectiveness of Competing Subsystem Options

The entire photovoltaic solar energy conversion system is composed of a network of subsystems, basically connected in series according to the energy flow, as indicated in Fig. IV.1. The individual subsystems may be defined in any way which facilitates the system analysis or the cost determination. Thus, a foundation for the solar array may be considered a subsystem, as a circuit breaker for system protection, or a battery for energy storage may be. Clearly, the entire system cost is the sum of all the individual subsystem costs C_i:

$$C_{cap} = \sum_{i=1}^{N} C_i; [\$] \tag{IV.12}$$

Generalized Photovoltaic Power System

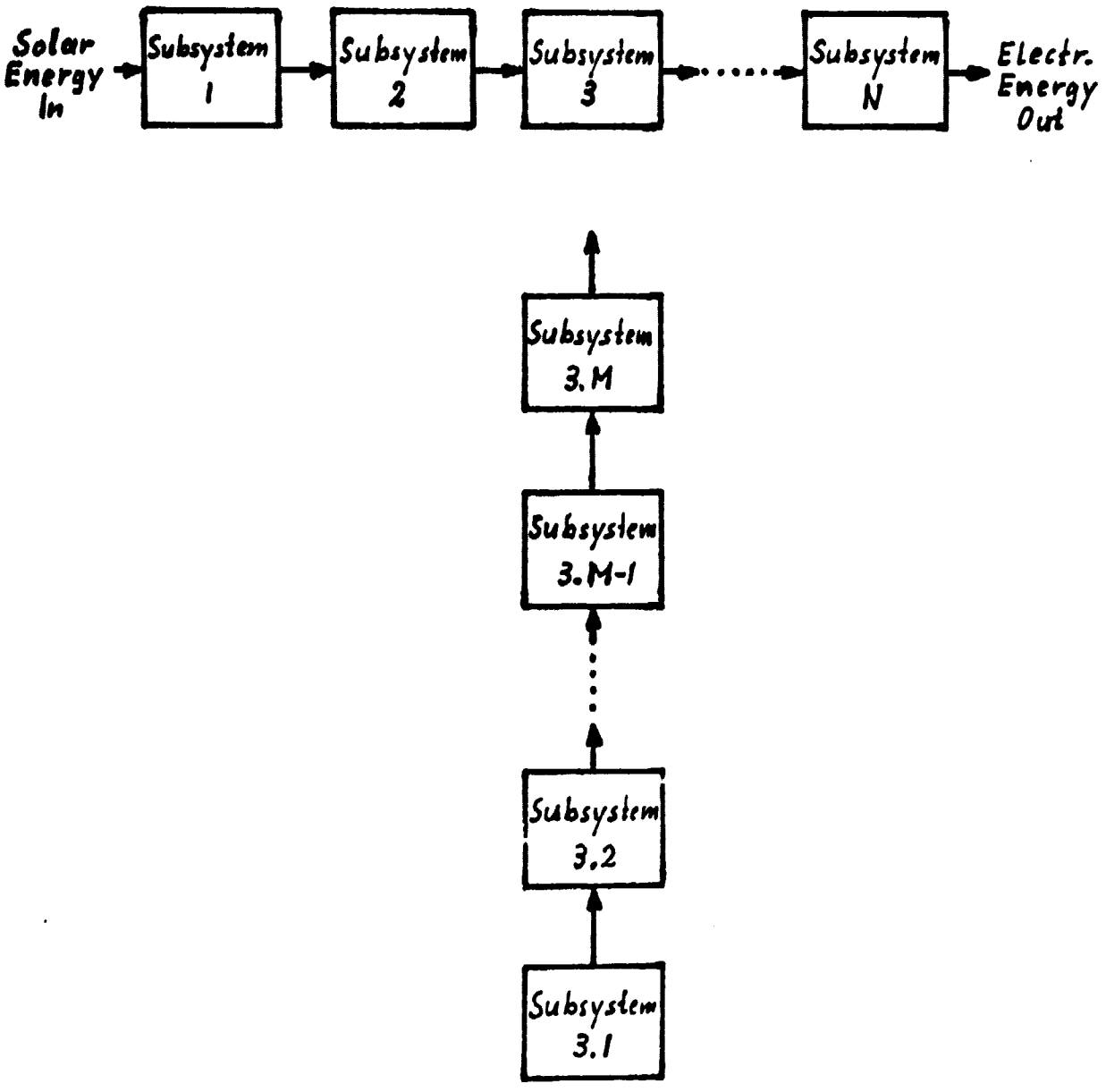

Fig. IV.1

and the system performance is a function of the performance of all the subsystems. Frequently, some subsystems are not directly in the line of energy flow, as indicated in Fig. IV.1 by subsystems 3.1 to 3.M. For an evaluation as discussed here, it is best to combine these into a "subsystem group" which, as a whole, is in the line of energy flow. The cost of the subsystem group is then the sum of the costs of the subsystems within the group. The evaluation of the cost effectiveness of an individual subsystem of the group can be performed by expansion of the methodology outlined here.

In general, both cost and performance of a subsystem are the result of an engineering design trade-off in which the performance characteristics of available devices and their commercial prices are considered, as well as the subsystem complexity and assembly cost. It is the purpose of this section to outline a methodology for assessing the cost effectiveness of such trade-offs from the viewpoint of the cost of the energy produced by the system.

Since the entire system (Fig. IV.1) can be viewed as a series connection of subsystems i or groups of subsystems, its efficiency can be expressed as the product of the efficiencies η_i' of the individual subsystems or groups of subsystems:

$$\eta_{syst} = \eta_{Ar,std} \cdot \tau_{St} \cdot \eta_{PC} \cdot f_{Ld} = \prod_{i=1}^{N} \eta'_i ; \qquad \text{(IV.13)}$$

or

$$\eta_{syst} = f'_{Ld} \prod_{i=1}^{N} \eta_i ; \qquad \text{(IV.13a)}$$

Representation (IV.13) is a generalization to the subsystem level of the expression contained in eq.IV.9a where the η'_i include all the contributions contained in the efficiencies $\eta_{Ar,std}$, η_{PC}, and in the quasi-efficiencies f_{St} and f_{Ld}. In the second version (eq. IV.13a), the η_i factors contain all the direct efficiency-like influences of each of the subsystems, while all indirect, or second-order influences are relegated to the "reduced load factor" f'_{Ld}. The application and practicality of this approach will be recognized later in this paper.

These subsystem efficiencies have an impact on the dimensioning of the individual subsystems, and consequently on their costs, since the system has to be designed to satisfy a given load by supplying a certain E_{Ld}. Thus, subsystems placed nearer the beginning of the series connected subsystem chain have to be dimensioned relatively larger to account for the losses of subsequent subsystems. This principle is recognizable in eq. IV.9a where the array output E_o is larger by the inverse of the product $f_{PC} \cdot f_{St}$ than the energy E_{Ld} which is delivered to the load.

The division into subsystems can be practically pursued to the smallest, separately identifiable, functional units with their individual efficiencies. This shall be illustrated by example of the photovoltaic array, with its array efficiency $\eta_{Ar, std,}$ which is frequently considered as composed of "subarrays" which are made up of "modules". The module contains a group of solar cells (a subsystem) which have an average efficiency $\eta_{Ce, std}$. In series/parallel connecting these cells of slightly differing characteristics into a "matrix" (a subsystem), a small loss in potential power output is incurred, expressed in the "matrixing efficiency" η_{Ma}. The interconnect wiring in this matrix is another separately identifiable subsystem with its

Joule losses, which are accounted for in the "wiring efficiency" η_{Wi}. The encapsulation forms two functional subsystems. The first is the window, including adhesive or pottant, with its optical transmission losses, leading to the encapsulation efficiency η_{En}. The second performance influencing attribute of the encapsulation is the heat transfer to the environment which determines the operating temperature of the array which controls the instantaneous operating efficiency of the module. This effect produces an "average annual cooling effectiveness factor" f_{Co}, a quasi-efficiency which usually is included in the load factor f_{Ld}. At the subarray (subscript SA) and the array (subscript Ar) levels, matrixing and wiring losses are again incurred, so that the cell energy output will have to be:

$$E_{Ce} = \frac{E_o}{\eta_{Ma}\,\eta_{Wi}\,\eta_{En} \cdot \eta_{Ma,SA}\,\eta_{Wi,SA} \cdot \eta_{Ma,Ar}\,\eta_{Wi,Ar}}\ ;\ [kWhy^{-1}] \qquad \text{(IV.14a)}$$

The installation of the subarrays forms another subsystem which influences system performance twofold: through the subarray orientation, which may include one-or-two-dimensional tracking, and through the cooling effectiveness. Both of these attributes form quasi-efficiency factors which are part of the load factor f_{Ld}.

Since the orientation/tracking effect is a direct influence which can, under exclusion of variable atmospheric effects, be analytically evaluated, it can be beneficial to eliminate this performance factor from the (reduced) load factor and attach it as an efficiency factor to the installation (or tracking) subsystem.

Formally applying these principles by combining eq.IV.5, IV.9a and IV.13, yields an expression for the energy delivered to the load, E_{Ld}, in terms of the subsystem efficiencies and quasi-efficiencies η_i':

$$E_{Id} = H_{pk} \cdot A_{Ar} \cdot 8760 \prod_{i=1}^{N} \eta_i' \ [kWhy^{-1}] \qquad \text{(IV.15)}$$

Introducing this expression together with eq. IV.12 into eq. IV.3 gives the energy cost determinator Γ in terms of subsystem cost and performance data, and constants, only:

$$\Gamma = \frac{1}{H_{pk} \cdot A_{Ar} \cdot 8760} \cdot \frac{\sum_{i=1}^{N} C_i}{\prod_{i=1}^{N} \eta_i'} \ ; \ [\$ \ kWh^{-1}y] \qquad \text{(IV.16)}$$

Following the approach used by Redfield in his "cost/Watt optimization" (2), the parameters of a single subsystem or subsystem group k of interest can be isolated in eq. IV.16:

$$\Gamma = \frac{1}{H_{pk} \cdot A_{Ar} \cdot 8760} \cdot \frac{\sum_{i=1}^{k-1} C_i + C_k + \sum_{i=k+1}^{N} C_i}{\prod_{i=1}^{k-1} \eta_i' \cdot \eta_k' \cdot \prod_{i=k+1}^{N} \eta_i'} \ ;$$

$$[\$ \ kWh^{-1}y] \qquad \text{(IV.17)}$$

or:

$$\Gamma = \frac{1}{H_{pk} \cdot A_{Ar} \cdot 8760} \cdot \frac{\sum_{i \neq k} C_i}{\prod_{i \neq k} \eta_i'} \cdot \left(\frac{1 + \frac{C_k}{\sum_{i \neq k} C_i}}{\eta_k'} \right) ; \ [\$ \ kWh^{-1}y] \qquad \text{(IV.17a)}$$

The expressions $\sum_{i \neq k}$ and $\prod_{i \neq k}$ stand for the sum or product, respectively, over all values of i from 1 to N, except for the value k. This form of Γ permits the evaluation of various design options for the same subsystem, or group of subsystems, with differing costs and efficiencies, with respect to their influence on the cost of the energy produced. Such an evaluation is particularly simple, if only C_k and η_k are variables of the design options. Then, a first order Taylor expansion yields:

$$\Delta\Gamma = B \cdot \left\{ \frac{\Delta C_k}{\eta'_k \sum_{i \neq k} C_i} - \frac{\left(1 + \frac{C_k}{\sum_{i \neq k} C_i}\right) \Delta\eta_k}{\eta_k'^2} \right\} \quad [\$kWh^{-1}y] \qquad (IV.18)$$

where ΔC_k and $\Delta\eta'_k$ are - positive or negative - differences against the base case in subsystem cost and efficiency, respectively, which result from the change in design of subsystem k. The constant B in eq. IV.18 is the product of the first two of the three terms on the right hand side of eq. IV.17a. A negative $\Delta\Gamma$ indicates a reduction in energy cost, and consequently a design improvement. It is readily apparent from eq. IV.18 that cost reductions and efficiency decreases counteract each other.

The condition imposed for the derivation of eq. IV.18, that only C_k and η'_k are variables of the design options, is in apparent conflict with several statements made in the preceding discussion. Thus, the load factor can be affected by changes in the system efficiency, particularly by changes in the storage transfer factor τ_{st}. To make the evaluations tractable, it is practical to proceed iteratively by considering the reduced load factor f'_{Ld} as temporarily constant and re-evaluating it only after several changes in the efficiencies. This procedure illuminates the need for the definition of a "reduced load factor"

f'_{Ld} according to eq. IV.13a which contains only second order effects of the efficiencies and quasi-efficiencies. The iteration is frequently speeded by reinforcing properties of the second order effects. For instance, efficiency improvements tend, at constant E_{Ld}, to result in increased load factors.

The condition for the validity of eq. IV.18 further requires that C_k and η_k are independent of the designs of the other subsystems, and particularly that the design choice of subsystem k does not influence costs and efficiencies of the remaining subsystems. This condition can, in principle, always be fulfilled by judicious choice of the designation "subsystem k", so that interdependent parts of the system are included in the same subsystem.

A change in the efficiency of one subsystem affects, however, the system as a whole. While the resulting change in output energy E_{Ld} is appropriately accounted for in Γ, one or more of the subsystems subsequent to the changed subsystem in the chain may now be over- or underdimensioned, and the load may no longer be supplied as desired. This problem requires considering the system of concern in somewhat more detail.

The majority of the functional subsystems of a photovoltaic solar energy conversion system are basically modular and thus essentially without economics of scale, at least within the range of concern in an individual design tradeoff study. The costs of these subsystems can therefore be expressed as a unit cost times a quantity factor. Such quantity factors are the array area A_{Ar}, the power handling capacity P of some subsystems, and, for some energy storage related subsystems, the energy capacity E. Generalizing the usage in ref (1) and (2), the system cost can then be expressed as:

$$C_{cap} = \sum_k A_k \, c_{A,k} + \sum_\ell P_\ell \, c_{P,\ell} + \sum_m E_m \, c_{E,m} + \sum_n C_{F,n}; \ [\$] \qquad \text{(IV.19)}$$

The area-based unit costs $C_{A,k}$ apply to the array related subsystems, including its installation and land costs. The power-based unit costs $c_{P,\ell}$ are connected with the power conditioning and other power handling equipment, although a part of the costs of the energy storage subsystems can also be proportional to power, for instance through the charge or discharge rates. The energy-based unit costs $c_{E,m}$ are concentrated in the storage subsystem. The remaining costs, including the system-status sensors and the control logic, represent the "fixed" costs, $C_{F,n}$.

Using this expression IV.19 for the capital costs in the energy cost determinator eq. IV.16, and simultaneously extracting the iteratively constant reduced load factor f'_{Ld}, from the efficiency product $\prod_i \eta_i$, yields the form:

$$\Gamma = \frac{1}{H_{pk} \cdot 8760 \cdot f'_{Ld}} \cdot \frac{\sum_{i=1}^{N} \left\{ \frac{A_i}{A_{Ar}} c_{A,i} + \frac{P_i}{A_{Ar}} c_{P,i} + \frac{E_i}{A_{Ar}} c_{E,i} + \frac{1}{A_{Ar}} C_{F,i} \right\}}{\prod_{i=1}^{N} \eta_i} ;$$

$$[\$\ kWh^{-1}y] \quad \text{(IV.20)}$$

It will be observed that, in general, for every index i in the sum, only one of the unit cost factors $c_{A,i}$, $c_{P,i}$, $c_{E,i}$, or $C_{F,i}$ will be unequal to zero. An exception to this rule is known to exist in certain advanced storage batteries whose price is based on a combination of energy and power rating. Also, power conditioning subsystem groups may contain fixed cost subsystems, such as control elements.

In considering the quantity factors A_i, P_i, and E_i, several possible simplifications are immediately noticeable. First, all area based unit costs are commonly related either to the array area or to the solar cell area. The

latter is connected to the array area through the packing factor $f_{Pg} < 1$:

$$A_{Ce} = f_{Pg} \cdot A_{Ar} \; ; \quad [m^2] \tag{IV.21}$$

Second, eq. IV.11 relates E_i to P_{Sy} through the equivalent storage time, and thus permits combined treatment of the second and third terms of eq. IV.20. Third, the dimensioning of each subsystem i of power dependent cost in the chain is determined by the system output specifications and the efficiencies of the subsystems subsequent to i in the direction of energy flow, so that:

$$P_i = \frac{P_{Sy}}{\prod_{\ell = i+1}^{N} \eta_\ell} \; ; \quad [kW] \tag{IV.22}$$

This permits expressing eq. IV.20, under use of eq. IV.6, IV.10, IV.11, IV.13a and IV.21, and under application of the subscript Ce to the cell area based costs, Ar to the array area based costs, as:

$$\Gamma = \sum_{i=1}^{N} \left\{ \frac{1}{H_{pk} \cdot 8760 \cdot f'_{Ld}} \; \frac{f_{Pg} \cdot c_{Ce,i} + c_{Ar,i}}{\prod_{\ell=1}^{N} \eta_\ell} \right.$$

$$\left. + \frac{f_{Po}}{8760 \cdot f'_{Ld}} \; \frac{c_{P,i} \; (1 + t_{St,i})}{\prod_{\ell = i+1}^{N} \eta_\ell} + \frac{i}{f_{Ld}} \; c_{F,i} \right\} ;$$

$$[\$ \; kWh^{-1} y] \tag{IV.23}$$

where $t_{St,i}$ is zero or t_{St}, depending on the existence of an energy based cost contribution in subsystem i. The fixed costs, shown in the third term in the brackets of eq. IV.23, contribute to the energy costs independently of the subsystem's or the system's performance. They are also the only ones ex-

hibiting any direct economics of scale.

The first term in the bracket of eq. IV.23 can be evaluated for the impact of design options for an individual subsystem k in complete analogy to eq. IV.17 to IV.18. The second term, however, requires a slightly different treatment:

$$\sum_{i=1}^{N} \left(\frac{c_{P,i}}{\prod_{\ell=i+1}^{N} \eta_\ell} \right) = \sum_{i=1}^{k-1} \left(\frac{c_{P,i}}{\prod_{\ell=i+1}^{N} \eta_\ell} \right) + \frac{c_{P,k}}{\prod_{\ell=k+1}^{N} \eta_\ell} + \sum_{i=k+1}^{N} \left(\frac{c_{P,i}}{\prod_{\ell=i+1}^{N} \eta_\ell} \right) \qquad \text{(IV.24)}$$

Consequently, first order Taylor expansion of eq. IV.23 yields the total cost-effectiveness criterion $\Delta\Gamma_k$ for a design change of subsystem k:

$$\Delta\Gamma_k = \Gamma_{A,i\neq k} \left[\frac{\Delta(f_{Pg} \cdot c_{Ce,k}) + \Delta c_{Ar,k})}{C_{A,\ i\neq k}} - \frac{\Delta\eta_k}{\eta_k} \left(1 + \frac{f_{Pg} c_{Ce,k} + c_{Ar,k}}{C_{A,\ i\neq k}} \right) \right]$$

$$+ \Gamma_{P,\ i<k} \left[\frac{\Delta[c_{P,k}\ (1 + t_{St,i})]}{C_{P,\ i<k} \cdot \prod_{\ell=k+1}^{N} \eta_\ell} - \frac{\Delta\eta_k}{\eta_k} \right]$$

$$+ \Gamma_{F,\ i\neq k} \frac{\Delta C_{F,k}}{C_{F,\ i\neq k}} \quad ; \quad [\$\ kWh^{-1}\ y] \qquad \text{(IV.25)}$$

where:

$$\Gamma_{A,\ i\neq k} = \frac{1}{H_{pk} \cdot 8760 \cdot f'_{Ld} \prod_{\ell=1}^{N} \eta_\ell} \sum_{i=1}^{N} (f_{Pg}\, c_{Ce,i} + c_{Ar,i}) \ ; \quad \text{but } i\neq k$$

$$[\$\ kWh^{-1}\ y] \qquad \text{(IV.26a)}$$

$$\Gamma_{P,\ i<k} = \frac{f_{Po}}{8760 \cdot f'_{Ld}} \sum_{i=1}^{k-1} \frac{c_{P,i}\ (1 + t_{St,i})}{\prod_{\ell=i+1}^{N} \eta_\ell} \quad ; \ [\$\ kWh^{-1}y] \qquad \text{(IV.26b)}$$

and:

$$\Gamma_{F,i\neq k} = \frac{1}{E_{Ld}} \sum_{\substack{i=1 \\ \text{but } i\neq k}}^{N} C_{F,i} \quad ; \quad [\$\ kWh^{-1}\ y] \qquad \text{(IV.26c)}$$

are the respective "investment per (unit energy per year)" ratios for all subsystems, except subsystem k, with area based unit costs, combined; for all subsystems preceding subsystem k in the chain, with power or energy based unit costs, combined; and for all subsystems, except subsystem k, with fixed subsystem costs, combined. Correspondingly defined are the total subsystem investments:

$$C_{A,\ i\neq k} = \sum_{\substack{i=1 \\ \text{but } i\neq k}}^{N} (f_{Pg} \cdot c_{Ce,i} + c_{Ar,i})_i \quad [\$] \qquad \text{(IV.27a)}$$

$$C_{P,\ i<k} = \sum_{i=1}^{k-1} \frac{c_{P,i}\ (1 + t_{St,i})}{\prod_{\ell=i+1}^{N} \eta_\ell} \quad ; \quad [\$] \qquad \text{(IV.27b)}$$

and

$$C_{F,\ i\neq k} = \sum_{\substack{i=1 \\ \text{but } i\neq k}}^{N} C_{F,i} \quad ; \qquad [\$] \qquad \text{(IV.27c)}$$

which represent the combined normalized costs of all subsystems, except subsystem k, with area based unit costs; of all subsystems preceeding subsystem k in the chain, with power or energy based unit costs; and of all subsystems, except subsystem k, with fixed subsystem costs; respectively. Examples of the application of eq. IV.25 are shown in the section entitled: "Examples of Application of the Methodology."

It is interesting to note that the three terms in the "cost effectiveness criterion" $\Delta\Gamma_k$ contain the "investment per (energy per year)" ratios for the remainder of the system, multiplied by the difference between two terms which are based on the relative cost change and the relative efficiency change, respectively. It is to be noted, however, that the relative cost change is based on the cost of the remainder of the system, while the relative efficiency change is based on the efficiency of the subsystem under evaluation. The expression "remainder of the system" refers here to the subsystems with equally based unit costs, and, in the case of power or energy based unit costs, only to the subsystems preceding in the chain the subsystem being evaluated. For the "fixed cost subsystems", there is no efficiency influence.

It may also be noted that the cost-effectiveness criterion (eq. IV.25) contains the terms

$$\Delta\Gamma_k = -\frac{\Delta\eta_k}{\eta_k}\left(\Gamma_{A,\, i\neq k} + \Gamma_{P,\, i<k}\right) + \ldots \quad [\$\ \mathrm{kWh}^{-1}\mathrm{y}]$$

where the relative efficiency change of subsystem k can refer to a subsystem of power based unit cost, but influence the cost-effectiveness through the subsystems of area based cost structure, or vice versa. The latter, inverse case is, however, not likely to occur as a subsystem of power based unit cost is rarely followed by a unit area cost based subsystem in the photovoltaic power system chain.

$$E_{Id} = H_{pk} \cdot A_{Ar} \cdot 8760 \prod_{i=1}^{N} \eta_i' \ [kWhy^{-1}] \qquad \text{(IV.15)}$$

Introducing this expression together with eq. IV.12 into eq. IV.3 gives the energy cost determinator Γ in terms of subsystem cost and performance data, and constants, only:

$$\Gamma = \frac{1}{H_{pk} \cdot A_{Ar} \cdot 8760} \cdot \frac{\sum_{i=1}^{N} C_i}{\prod_{i=1}^{N} \eta_i'} \ ; \ [\$ \ kWh^{-1}y] \qquad \text{(IV.16)}$$

Following the approach used by Redfield in his "cost/Watt optimization" (2), the parameters of a single subsystem or subsystem group k of interest can be isolated in eq. IV.16:

$$\Gamma = \frac{1}{H_{pk} \cdot A_{Ar} \cdot 8760} \cdot \frac{\sum_{i=1}^{k-1} C_i + C_k + \sum_{i=k+1}^{N} C_i}{\prod_{i=1}^{k-1} \eta_i' \cdot \eta_k' \cdot \prod_{i=k+1}^{N} \eta_i'} \ ;$$

$$[\$ \ kWh^{-1}y] \qquad \text{(IV.17)}$$

or:

$$\Gamma = \frac{1}{H_{pk} \cdot A_{Ar} \cdot 8760} \cdot \frac{\sum_{i \neq k} C_i}{\prod_{i \neq k} \eta_i'} \cdot \left(\frac{1 + \frac{C_k}{\sum_{i \neq k} C_i}}{\eta_k'} \right) ; \ [\$ \ kWh^{-1}y] \qquad \text{(IV.17a)}$$

The expressions $\sum_{i \neq k}$ and $\prod_{i \neq k}$ stand for the sum or product, respectively, over all values of i from 1 to N, except for the value k. This form of Γ permits the evaluation of various design options for the same subsystem, or group of subsystems, with differing costs and efficiencies, with respect to their influence on the cost of the energy produced. Such an evaluation is particularly simple, if only C_k and η_k are variables of the design options. Then, a first order Taylor expansion yields:

$$\Delta\Gamma = B \cdot \left\{ \frac{\Delta C_k}{\eta'_k \sum_{i \neq k} C_i} - \frac{\left(1 + \frac{C_k}{\sum_{i \neq k} C_i}\right) \Delta\eta_k}{\eta_k'^2} \right\} \quad [\$kWh^{-1}y] \qquad (IV.18)$$

where ΔC_k and $\Delta\eta'_k$ are - positive or negative - differences against the base case in subsystem cost and efficiency, respectively, which result from the change in design of subsystem k. The constant B in eq. IV.18 is the product of the first two of the three terms on the right hand side of eq. IV.17a. A negative $\Delta\Gamma$ indicates a reduction in energy cost, and consequently a design improvement. It is readily apparent from eq. IV.18 that cost reductions and efficiency decreases counteract each other.

The condition imposed for the derivation of eq. IV.18, that only C_k and η'_k are variables of the design options, is in apparent conflict with several statements made in the preceding discussion. Thus, the load factor can be affected by changes in the system efficiency, particularly by changes in the storage transfer factor τ_{st}. To make the evaluations tractable, it is practical to proceed iteratively by considering the reduced load factor f'_{Ld} as temporarily constant and re-evaluating it only after several changes in the efficiencies. This procedure illuminates the need for the definition of a "reduced load factor"

f'_{Ld} according to eq. IV.13a which contains only second order effects of the efficiencies and quasi-efficiencies. The iteration is frequently speeded by reinforcing properties of the second order effects. For instance, efficiency improvements tend, at constant E_{Ld}, to result in increased load factors.

The condition for the validity of eq. IV.18 further requires that C_k and η_k are independent of the designs of the other subsystems, and particularly that the design choice of subsystem k does not influence costs and efficiencies of the remaining subsystems. This condition can, in principle, always be fulfilled by judicious choice of the designation "subsystem k", so that interdependent parts of the system are included in the same subsystem.

A change in the efficiency of one subsystem affects, however, the system as a whole. While the resulting change in output energy E_{Ld} is appropriately accounted for in Γ, one or more of the subsystems subsequent to the changed subsystem in the chain may now be over- or underdimensioned, and the load may no longer be supplied as desired. This problem requires considering the system of concern in somewhat more detail.

The majority of the functional subsystems of a photovoltaic solar energy conversion system are basically modular and thus essentially without economics of scale, at least within the range of concern in an individual design tradeoff study. The costs of these subsystems can therefore be expressed as a unit cost times a quantity factor. Such quantity factors are the array area A_{Ar}, the power handling capacity P of some subsystems, and, for some energy storage related subsystems, the energy capacity E. Generalizing the usage in ref (1) and (2), the system cost can then be expressed as:

$$C_{cap} = \sum_k A_k \, c_{A,k} + \sum_\ell P_\ell \, c_{P,\ell} + \sum_m E_m \, c_{E,m} + \sum_n C_{F,n}; \ [\$] \qquad \text{(IV.19)}$$

The area-based unit costs $C_{A,k}$ apply to the array related subsystems, including its installation and land costs. The power-based unit costs $c_{P,\ell}$ are connected with the power conditioning and other power handling equipment, although a part of the costs of the energy storage subsystems can also be proportional to power, for instance through the charge or discharge rates. The energy-based unit costs $c_{E,m}$ are concentrated in the storage subsystem. The remaining costs, including the system-status sensors and the control logic, represent the "fixed" costs, $C_{F,n}$.

Using this expression IV.19 for the capital costs in the energy cost determinator eq. IV.16, and simultaneously extracting the iteratively constant reduced load factor f'_{Ld}, from the efficiency product $\prod_i \eta_i$, yields the form:

$$\Gamma = \frac{1}{H_{pk} \cdot 8760 \cdot f'_{Ld}} \cdot \frac{\sum_{i=1}^{N} \left\{ \frac{A_i}{A_{Ar}} c_{A,i} + \frac{P_i}{A_{Ar}} c_{P,i} + \frac{E_i}{A_{Ar}} c_{E,i} + \frac{1}{A_{Ar}} C_{F,i} \right\}}{\prod_{i=1}^{N} \eta_i} ;$$

$$[\$\ kWh^{-1}y] \quad \text{(IV.20)}$$

It will be observed that, in general, for every index i in the sum, only one of the unit cost factors $c_{A,i}$, $c_{P,i}$, $c_{E,i}$, or $C_{F,i}$ will be unequal to zero. An exception to this rule is known to exist in certain advanced storage batteries whose price is based on a combination of energy and power rating. Also, power conditioning subsystem groups may contain fixed cost subsystems, such as control elements.

In considering the quantity factors A_i, P_i, and E_i, several possible simplifications are immediately noticeable. First, all area based unit costs are commonly related either to the array area or to the solar cell area. The

latter is connected to the array area through the packing factor $f_{Pg} < 1$:

$$A_{Ce} = f_{Pg} \cdot A_{Ar} \; ; \quad [m^2] \tag{IV.21}$$

Second, eq. IV.11 relates E_i to P_{Sy} through the equivalent storage time, and thus permits combined treatment of the second and third terms of eq. IV.20. Third, the dimensioning of each subsystem i of power dependent cost in the chain is determined by the system output specifications and the efficiencies of the subsystems subsequent to i in the direction of energy flow, so that:

$$P_i = \frac{P_{Sy}}{\prod_{\ell = i+1}^{N} \eta_\ell} \; ; \quad [kW] \tag{IV.22}$$

This permits expressing eq. IV.20, under use of eq. IV.6, IV.10, IV.11, IV.13a and IV.21, and under application of the subscript Ce to the cell area based costs, Ar to the array area based costs, as:

$$\Gamma = \sum_{i=1}^{N} \left\{ \frac{1}{H_{pk} \cdot 8760 \cdot f'_{Ld}} \; \frac{f_{Pg} \cdot c_{Ce,i} + c_{Ar,i}}{\prod_{\ell=1}^{N} \eta_\ell} \right.$$

$$\left. + \frac{f_{Po}}{8760 \cdot f'_{Ld}} \; \frac{c_{P,i} \; (1 + t_{St,i})}{\prod_{\ell = i+1}^{N} \eta_\ell} + \frac{i}{f'_{Ld}} \; c_{F,i} \right\} ;$$

$$[\$ \; kWh^{-1}y] \tag{IV.23}$$

where $t_{St,i}$ is zero or t_{St}, depending on the existence of an energy based cost contribution in subsystem i. The fixed costs, shown in the third term in the brackets of eq. IV.23, contribute to the energy costs independently of the subsystem's or the system's performance. They are also the only ones ex-

hibiting any direct economics of scale.

The first term in the bracket of eq. IV.23 can be evaluated for the impact of design options for an individual subsystem k in complete analogy to eq. IV.17 to IV.18. The second term, however, requires a slightly different treatment:

$$\sum_{i=1}^{N} \left(\frac{c_{P,i}}{\prod_{\ell=i+1}^{N} \eta_\ell} \right) = \sum_{i=1}^{k-1} \left(\frac{c_{P,i}}{\prod_{\ell=i+1}^{N} \eta_\ell} \right) + \frac{c_{P,k}}{\prod_{\ell=k+1}^{N} \eta_\ell} + \sum_{i=k+1}^{N} \left(\frac{c_{P,i}}{\prod_{\ell=i+1}^{N} \eta_\ell} \right) \qquad \text{(IV.24)}$$

Consequently, first order Taylor expansion of eq. IV.23 yields the total cost-effectiveness criterion $\Delta\Gamma_k$ for a design change of subsystem k:

$$\Delta\Gamma_k = \Gamma_{A,i\neq k} \left[\frac{\Delta(f_{Pg} \cdot c_{Ce,k}) + \Delta c_{Ar,k})}{C_{A,\ i\neq k}} - \frac{\Delta\eta_k}{\eta_k} \left(1 + \frac{f_{Pg} c_{Ce,k} + c_{Ar,k}}{C_{A,\ i\neq k}} \right) \right]$$

$$+ \Gamma_{P,\ i<k} \left[\frac{\Delta[c_{P,k}\ (1 + t_{St,i})]}{C_{P,\ i<k} \cdot \prod_{\ell=k+1}^{N} \eta_\ell} - \frac{\Delta\eta_k}{\eta_k} \right]$$

$$+ \Gamma_{F,\ i\neq k} \frac{\Delta C_{F,k}}{C_{F,\ i\neq k}} \quad ; \quad [\$\ kWh^{-1}\ y] \qquad \text{(IV.25)}$$

where:

$$\Gamma_{A,\ i\neq k} = \frac{1}{H_{pk} \cdot 8760 \cdot f'_{Ld} \prod_{\ell=1}^{N} \eta_\ell} \sum_{i=1}^{N} (f_{Pg}\, c_{Ce,i} + c_{Ar,i}) \quad ;$$

$$\text{but } i\neq k$$

$$[\$\ kWh^{-1}\ y] \qquad \text{(IV.26a)}$$

$$\Gamma_{P,\ i<k} = \frac{f_{Po}}{8760 \cdot f'_{Ld}} \sum_{i=1}^{k-1} \frac{c_{P,i}\ (1 + t_{St,i})}{\prod_{\ell=i+1}^{N} \eta_\ell} \quad ; \ [\$\ kWh^{-1} y] \qquad \text{(IV.26b)}$$

and:

$$\Gamma_{F,i\neq k} = \frac{1}{E_{Ld}} \sum_{\substack{i=1 \\ \text{but } i\neq k}}^{N} C_{F,i} \quad ; \quad [\$\ kWh^{-1}\ y] \qquad \text{(IV.26c)}$$

are the respective "investment per (unit energy per year)" ratios for all subsystems, except subsystem k, with area based unit costs, combined; for all subsystems preceding subsystem k in the chain, with power or energy based unit costs, combined; and for all subsystems, except subsystem k, with fixed subsystem costs, combined. Correspondingly defined are the total subsystem investments:

$$C_{A,\ i\neq k} = \sum_{\substack{i=1 \\ \text{but } i\neq k}}^{N} (f_{Pg} \cdot c_{Ce,i} + c_{Ar,i})_i \quad [\$] \qquad \text{(IV.27a)}$$

$$C_{P,\ i<k} = \sum_{i=1}^{k-1} \frac{c_{P,i}\ (1 + t_{St,i})}{\prod_{\ell=i+1}^{N} \eta_\ell} \quad ; \quad [\$] \qquad \text{(IV.27b)}$$

and

$$C_{F,\ i\neq k} = \sum_{\substack{i=1 \\ \text{but } i\neq k}}^{N} C_{F,i} \quad ; \quad [\$] \qquad \text{(IV.27c)}$$

which represent the combined normalized costs of all subsystems, except subsystem k, with area based unit costs; of all subsystems preceeding subsystem k in the chain, with power or energy based unit costs; and of all subsystems, except subsystem k, with fixed subsystem costs; respectively. Examples of the application of eq. IV.25 are shown in the section entitled: "Examples of Application of the Methodology."

It is interesting to note that the three terms in the "cost effectiveness criterion" $\Delta\Gamma_k$ contain the "investment per (energy per year)" ratios for the remainder of the system, multiplied by the difference between two terms which are based on the relative cost change and the relative efficiency change, respectively. It is to be noted, however, that the relative cost change is based on the cost of the remainder of the system, while the relative efficiency change is based on the efficiency of the subsystem under evaluation. The expression "remainder of the system" refers here to the subsystems with equally based unit costs, and, in the case of power or energy based unit costs, only to the subsystems preceding in the chain the subsystem being evaluated. For the "fixed cost subsystems", there is no efficiency influence.

It may also be noted that the cost-effectiveness criterion (eq. IV.25) contains the terms

$$\Delta\Gamma_k = -\frac{\Delta\eta_k}{\eta_k}\left(\Gamma_{A,\ i\neq k} + \Gamma_{P,\ i<k}\right) + \ldots \quad [\$\ kWh^{-1}y]$$

where the relative efficiency change of subsystem k can refer to a subsystem of power based unit cost, but influence the cost-effectiveness through the subsystems of area based cost structure, or vice versa. The latter, inverse case is, however, not likely to occur as a subsystem of power based unit cost is rarely followed by a unit area cost based subsystem in the photovoltaic power system chain.

The "cost effectiveness criterion" $\Delta\Gamma_k$ permits the evaluation of various subsystem design options both with respect to their benefit (or harm) in comparison to a baseline design, through the sign of $\Delta\Gamma_k$, and with respect to the relative merits of the different options, through the magnitude of $\Delta\Gamma_k$. "Optimizations", that is a search for $\Delta\Gamma_k = 0$ as discussed in ref. (2), will, with very few exceptions, not be possible, since the relationships between cost and performance are usually not available in functional form and, moreover, seem always to be limited by the contemporary, and often rapidly changing status of technology. "Relative evaluations", as discussed here, applied to specific subsystem design options, are, however, readily performed.

The method is easy to apply, since for the subsystem to be evaluated, only the cost and performance differences against a baseline design have to be known, and since the other needed inputs involve only a few summary data on the remainder of the system. While it may be, in some cases, difficult to obtain exact data for the remainder of the system, intelligent estimates will frequently suffice. When such estimates are used for the cost of the remainder of the system, error estimates should be made, as mis-estimation of the cost could shift the relative impact of the competing terms involving the subsystem cost - and efficiency - changes.

4. Evaluation of Cost-Effectiveness of Manufacturing Process Options

While many of the subsystems in a photovoltaic solar energy system are assembled of standard components by common methods, the solar cells, their assembly into arrays, and at a later time perhaps also the energy storage device, are specially manufactured items which represent a significant part of the total system cost. Since producing these devices with their highest possible performance at the lowest price is the fundamental condition for

The "cost effectiveness criterion" $\Delta\Gamma_k$ permits the evaluation of various subsystem design options both with respect to their benefit (or harm) in comparison to a baseline design, through the sign of $\Delta\Gamma_k$, and with respect to the relative merits of the different options, through the magnitude of $\Delta\Gamma_k$. "Optimizations", that is a search for $\Delta\Gamma_k = 0$ as discussed in ref. (2), will, with very few exceptions, not be possible, since the relationships between cost and performance are usually not available in functional form and, moreover, seem always to be limited by the contemporary, and often rapidly changing status of technology. "Relative evaluations", as discussed here, applied to specific subsystem design options, are, however, readily performed.

The method is easy to apply, since for the subsystem to be evaluated, only the cost and performance differences against a baseline design have to be known, and since the other needed inputs involve only a few summary data on the remainder of the system. While it may be, in some cases, difficult to obtain exact data for the remainder of the system, intelligent estimates will frequently suffice. When such estimates are used for the cost of the remainder of the system, error estimates should be made, as mis-estimation of the cost could shift the relative impact of the competing terms involving the subsystem cost - and efficiency - changes.

4. Evaluation of Cost-Effectiveness of Manufacturing Process Options

While many of the subsystems in a photovoltaic solar energy system are assembled of standard components by common methods, the solar cells, their assembly into arrays, and at a later time perhaps also the energy storage device, are specially manufactured items which represent a significant part of the total system cost. Since producing these devices with their highest possible performance at the lowest price is the fundamental condition for

success in large scale introduction of photovoltaic solar energy systems, comparative evaluations of the various available options for each step of the manufacturing process sequence need to be performed. A methodology very similar to that outlined for evaluation of the subsystem design options can be applied for this purpose.

Evaluation methodologies for the solar cell and the module manufacturing processes are of greatest current interest. Both of these "subsystems" have an area based unit cost structure, and can therefore be treated by the same approach. The quantity to be reduced as far as possible is the "investment per (unit energy per year)" Γ (eq. IV.23) which can be expressed as the sum of various sub-gammas for the different subsystems:

$$\Gamma = \sum_{i=1}^{N} (\Gamma_{A,i} + \Gamma_{P,i} + \Gamma_{F,i}); \quad [\$\ kWh^{-1}y] \tag{IV.28}$$

where that for the subsystems of area based unit costs has the form:

$$\Gamma_{A,i} = \frac{1}{H_{pk} \cdot 8760 \cdot f'_{Ld}} \cdot \frac{(f_{Pg}\, c_{Ce,i} + c_{Ar,i})}{\prod_{\ell=1}^{N} \eta_\ell}; \quad [\$\ kWh^{-1}\ y] \tag{IV.29}$$

As the solar cells and the modules are among the first subsystems in the chain, and are not preceded by power based subsystems, only the $\Gamma_{A,i}$ terms need to be considered for an evaluation of the manufacturing processes for one of these two subsystems. Thus, for the solar cells as subsystem k, it is:

$$\Gamma_A = (\Gamma_{A,\ i\neq k} \cdot \eta_k)\, \frac{1}{\eta_k} + \frac{f_{Pg}}{H_{pk} \cdot 8760 \cdot f'_{Ld} \cdot \prod_{\substack{\ell=1 \\ \text{but } \ell\neq k}}^{N} \eta_\ell} \cdot \frac{c_{Ce,k}}{\eta_k};$$

$$[\$\ kWh^{-1}\ y] \tag{IV.30}$$

using eq. IV.26a for simplification. The product in the parenthesis of the first term is independent of subsystem k.

The fabrication process sequence for subsystem k, the solar cells, shall be composed of P process steps, with the individual step p costing $c_{Ce,k,p}$ on the basis of unit area of good work-in-process (partly processed solar cells) leaving the process station. The subsystem cost $c_{Ce,k}$, however, is based on the area of the finished, good cells leaving the end of the solar cell production line. Since each process step is afflicted with a certain yield y_p, the amount of solar cell area to be processed through step p has to be increased above the finished cell area to make up for the yield losses of the subsequent process steps. Consequently, the unit cell area cost of the subsystem k can be expressed as:

$$c_{Ce,k} = \sum_{p=1}^{P} \frac{c_{Ce,k,p}}{\prod_{\ell=p+1}^{P} y_\ell} \quad ; \quad [\$\ m^{-2}] \qquad \text{(IV.31)}$$

For solar cells, it has been long-standing practice[3] to calculate an idealized, theoretical "limit efficiency" $\eta_{k,Lim}$ and to gauge the success in design and fabrication of the "real" solar cells by determining the various "loss factors" ϕ which describe the degree of approach to ideality for the identified, efficiency influencing parameters. In variation of this practice, Redfield (2) assigned a loss factor to each of the process steps to facilitate his "cost/Watt" evaluation. Adapting this practice, the efficiency of the subsystem k can be expressed as a limit efficiency times a product of loss factors.

$$\eta_k = \eta_{k,Lim} \prod_{p=1}^{P} \phi_{k,p} \quad ; \qquad \text{(IV.32)}$$

Each of the loss factors $\phi_{k,p}$ is attributed to a step in the serial sequence of process steps, and it expresses, by being normally less than unity, the degree to which the individual process step causes the subsystem performance to deviate from ideality. Different competing process options can usually be expected to cause different degrees of deviation from ideality. While for solar cells, a limit efficiency near 0.25 is usually discussed, for the module or panel assembly, a limit efficiency of unity will be practical to assume.

Making use of eq. IV.27a, IV.29, IV.31, and IV.32 permits expressing eq. IV.30 in a form more conducive to derivation of the cost-effectiveness criterion:

$$\Gamma_A = \frac{(\Gamma_{A,i\neq k} \cdot \eta_k)}{\eta_{k,\lim} \prod_{p=1}^{P} \phi_{k,p}} \quad \frac{1}{\phi_{k,n}} \left\{ 1 + \frac{f_{Pg}}{C_{\Lambda,i\neq k}} \left[\sum_{p=n+1}^{P} \left(\frac{c_{Ce,k,p}}{\prod_{\ell=p+1}^{P} y_\ell} \right) \right. \right.$$

but $p \neq n$

ORIGINAL PAGE IS OF POOR QUALITY

$$\left. \left. + \frac{c_{Ce,k,n}}{\prod_{\ell=n+1}^{P} y_\ell} + \frac{1}{y_n} \sum_{p=1}^{n-1} \left(\frac{c_{Ce,k,p}}{\prod_{\ell=p+1}^{P} y_\ell} \right) \right] \right\}; [\$\ kWh^{-1}\ y] \qquad \text{(IV.33)}$$

but $p \neq n$

In this form, the three characteristic attributes $\phi_{k,n}$, Y_n, and $c_{Ce,k,n}$ of process step n which is the step to be evaluated, have been isolated. Applying again a first order Taylor expansion to the investment per (energy per year) ratio, this time based on eq. IV.28 and IV.33, yields the cost effectiveness criterion $\Delta\Gamma$ for the individual solar cell manufacturing process step n :

$$\Delta\Gamma_{\kappa,n} = \Gamma_{\Lambda,i\neq k} \left\{ \frac{f_{Pg} \cdot \Delta c_{Ce,k,n}}{C_{\Lambda,i\neq k} \cdot \prod_{\ell=n+1}^{P} y_\ell} - \frac{\Delta y_n}{y_n} \frac{f_{Pg}\, c_{Ce,k,VPn}}{C_{\Lambda,i\neq k} \cdot \prod_{\ell=n+1}^{P} y_\ell} \right.$$

$$\left. - \frac{\Delta \phi_{k,n}}{\phi_{k,n}} \left[1 + \frac{f_{Pg}\, c_{Ce,k}}{C_{\Lambda,\ i\neq k}} \right] \right\}; [SkWh^{-1}y] \qquad \text{(IV.34)}$$

where $C_{A,\ i\neq k}$ and $C_{A,\ i\neq k}$ are used as before (eq. IV.21a and IV.27a), and where:

$$c_{Ce,k,WPn} = \sum_{p=1}^{n-1} \frac{c_{Ce,k,p}}{\prod_{\ell=p+1}^{n} y_\ell} \quad ; \ [\$\ m^{-2}] \qquad \text{(IV.35)}$$

expresses the fully yielded cost of the work-in-process required as input for step n in order to fabricate a unit area of output work-in-process from this step. The factor $\prod_{\ell=n+1}^{p} y_\ell$ is the product of the yields of the process steps subsequent to step n. The inverse of this product gives the area of work-in-process to be processed through step n in order to obtain a unit area of finished product (subsystem k). The application of eq.IV.34 is demonstrated on hand of an example in the next section.

Similar to the subsystem cost-effectiveness criterion $\Delta\Gamma_k$, the manufacturing process cost-effectiveness criterion $\Delta\Gamma_{k,n}$ is the product of a variable factor and the "investment per (energy per year)" ratio for the remainder of the system, in this case, however, limited to the part of the system which is based on unit area costs. The variable factor contains three terms. The first describes the influence of the difference in cost $\Delta c_{Ce,k,n}$ of the subject process options against the baseline case, or against another option, taken relative to the total cost of all other subsystems of unit area based cost. The impact of this relative cost difference is magnified by the inverse of the product of the yields of all process steps which follow the step under evaluation (n) in the process sequence up to the finished subsystem k. The second term describes the impact of the relative change in the yield of process step n which would be incurred by switching to the option being evaluated. This relative yield change is multiplied by the cost of the input work-in-process to step n, divided by the total cost of all other subsystems of unit area based costs. Again, the impact of this term is increased through the yields of all subsequent process steps. The third term finally is principally

the relative solar cell efficiency change resulting from introduction of the subject process option. The impact of this relative efficiency change is raised above unity by the ratio of the cost (per unit area) of the subsystem considered to the sum of the unit area costs of all other subsystems of area based cost structure.

Examination of eq. IV.34 shows that the knowledge of the "investment per (energy per year)" ratio for the remainder of the system is not needed for comparative evaluation of different process options, as this ratio is a constant factor in the cost-effectiveness criterion. This leaves only four data required as constant inputs for the evaluation: the cost of the input work-in-process; the cost of the finished subsystem; the total cost of the remaining subsystems of area based costs; and the product of the yields of the subsequent process steps. The variable inputs are the relative changes in the three key attributes of the option for the process step to be evaluated: cost, yield, and efficiency contribution. Since exact data for the four constant inputs may be difficult to obtain, intelligent estimates will sometimes be substituted. This procedure appears, at first look, appropriate as these quantities form constant multipliers. However, this approach has to be applied with caution since significant mis-estimation could shift the relative impacts of the cost, yield, and efficiency terms. This caution will be necessary in the common cases, where the cost of the finished subsystem under evaluation is small compared to the total cost of the remaining subsystems of area based cost, so that the multiplier on the relative efficiency change would not be large compared to unity.

It is clear, that the method outlined here for the solar cell manufacturing process, and expressed in eq. IV.34, applies equally well to the array assembly processes, except for the omission of the packing factor f_{pg} in that case, and the replacement of the subscript Ce by subscript Ar.

5. Examples of Applications of the Methodology

Two examples will demonstrate the application of eq. IV.25 in evaluation of different design options for subsystem k.

The subsystem under consideration shall be the solar cell. The base case is a cell with a conversion efficiency of 17.5% on the basis of the solar cell area. The following relevant data for the base case are known:

Table IV.1

	Item	Symbol	Data	Units	Basic
1.	Solar cell price	$c_{Ce,k}$	61.38	$\$/m^2$	cell area
2.	Packing factor	f_{Pg}	0.90	--	--
	Solar cell price	$c_{A,k}$	55.24	$\$/m^2$	module area
3.	Module assembly add-on price	$c_{A,k+1}$	23.50	$\$/m^2$	module area
4.	Foundation, array assembly, installation, etc, add-on price	$c_{A,k+2}$	50.00	$\$/m^2$	module area
5.	Total area based costs	C_A	128.74	$\$/m^2$	module area
6.	Total area based costs except for subsystem k	$C_{A,i\neq k}$	73.50	$\$/m^2$	module area
7.	Module efficiency		15.75	%	module area

Problem 1.

A process is anticipated by which the efficiency of the solar cells could be raised to 20%. How much more could the solar cells cost to provide an at least equally cost-effective system?

Answer:

a) Since the subsystem of concern is of area based costs only, the second and third terms of eq. IV.25 are zero.

b) The subsystem k contains only cell-area based costs, designated by subscript Ce, and no array-area based costs, designated by subscripts Ar. Thus:

$$\Delta c_{Ar,k} = 0$$

$$c_{Ar,k} = 0$$

c) Since the packing factor f_{Pg} does not change with the change of cell efficiency:

$$\Delta(f_{Pg} \cdot c_{Ce,k}) = f_{Pg} \cdot \Delta c_{Ce,k}.$$

In this case, also, it is immaterial either module efficiences or cell efficiencies are used, as they are related through a constant proportionality factor.

d) Wanted is knowledge of $\Delta c_{Ce,k}$ for

$$\frac{\Delta \Gamma_k}{\Gamma_{A,i \neq k}} \leq 0.$$

Transforming eq. IV.25, after applying points a) to c) above; yields then:

$$\Delta c_{Ce,k} \leq \frac{\Delta \eta_k}{\eta_k} \left(\frac{c_{A,i \neq k}}{f_{Pg}} + c_{Ce,k} \right) . \qquad \text{(IV.36)}$$

e) The efficiency difference $\Delta\eta_k$ going from the base case to the new subsystem option is 2.5%. All other numbers entering into the relationship given in point d) relate to the base case. Thus:

$$\Delta c_{Ce,k} \leq \frac{+0.025}{0.175} \left(\frac{73.50}{0.9} + 61.38\right)$$

$$\leq + \underline{\underline{20.44\ \$/m^2 \text{ cell area.}}}$$

A 14% cell efficiency increase thus justifies a 33% cell cost increase for equal energy cost effectiveness, and any lower cost increase yields a more cost-effective system.

The maximum price is thus:

Base price:	61.38 $\$/m^2$ cell area
Maximum increase +	$\underline{20.44\ \$/m^2}$ cell area
	81.82 $\$/m^2$ cell area
Apply $f_{Pg} = 0.90$:	73.64 $\$/m^2$ module area
Module add-on cost:	$\underline{23.50\ \$/m^2}$ module area
Module cost	97.14 $\$/m^2$ module area

At 180 W_{pk}/m^2 output, this corresponds to 0.54 $\$/W_{pk}$.

Problem 2

In lieu of Czochralski grown wafers assumed to be used in the base case given above, the use of ribbon silicon is anticipated, resulting in a reduced cell efficiency of 14%, but an increased packing factor of 0.92. How much lower would the cell cost have to be to provide an at least equally cost effective system?

Answer:

a) Points a) and b) of answer 1 still apply.

b) As the packing factor changes,

$$\Delta(f_{Pg} \cdot c_{Ce,k}) = f_{Pg} \Delta c_{Ce,k} + c_{Ce,k} \cdot \Delta f_{Pg}$$

will have to be used.

c) Because of the change of packing factor, and since the energy cost determination is ultimately based on the array (or module) area related costs and efficiencies, the evaluation will have to use these latter efficiencies. For the base case, the module efficiency was 15.75%. For the option, it is 14·0.92 = 12.88%. Thus, $\Delta\eta_k = 2.87\%$.

d) Under consideration of points 2a) and 2b) above, and solving for

$$\frac{\Delta\Gamma_k}{\Gamma_{A,i\neq k}} \leq 0,$$

as in Answer 1, eq. (25) transforms into:

$$\Delta c_{Ce,k} \leq \frac{\Delta\eta_k}{\eta_k}\left(\frac{C_{A,i\neq k}}{f_{Pg}} + c_{Ce,k}\right) - \frac{\Delta f_{Pg}}{f_{Pg}} c_{Ce,k} ; \qquad \text{(IV.37)}$$

e) The difference in packing factor is +0.02, compared to the base case. Outside of the efficiency difference, only data from the base case are needed:

$$\Delta c_{Ce,k} \leq \frac{-0.0287}{0.1288}\left(\frac{13.50}{0.9} + 61.38\right) - \frac{0.02}{0.9} \cdot 61.38$$

$\Delta c_{Ce,k} \leq -26.07 - 1.36 = -27.43$ \$/m^2 cell area

The maximum cell price for equal cost effectiveness is thus:

61.38 \$/m^2 cell area

-27.43 \$/m^2 cell area

33.95 \$/m^2 cell area

and the corresponding module price:

Cells: 33.95 \$/m^2 · 0.92 = 31.23 \$/m^2 module area

Module add-on cost +23.50 \$/m^2 module area

54.73 \$/m^2 module area

At 128.8 W_{pk}/m^2 output, this corresponds to \$0.425/W_{pk} for the module.

Checks to Problems 1 and 2:

Try 100 kW_{pk} system:

Base case:

Area needed: 10^5 W_{pk} : 157.5 W_{pk}/m^2 = 632.9 m^2

Module price: 0.50 \$/W_{pk} → 50,000 \$

Installation etc.: 50 \$/m^2 → 31,645 \$

Total 81,645 \$

Option 1:

Module efficiency: 18%

Area needed: 10^5 W_{pk} : 180 W_{pk}/m^2 = 555.6 m^2

Module price 0.54 \$/W_{pk} → 54,000 \$

Installtion cost etc. 50 \$/m^2 → 27,780 \$

81,780 \$

Option 2:

Module efficiency	12.88%	
Area needed:	10^5 W_{pk} : 128.8 W_{pk}/m^2 =	776.4 m^2
Module price:	0.425 $/$W_{pk}$	42,500 $
Installation cost etc.	$50/$m^2$	38,820 $
		81,320 $

Problem 3

A process sequence for solar cell fabrication has been proposed by Motorola for 1986, which includes two diffusions for pn-junction and BSF layer formation. Starting with a texture-etched, cleaned wafer, a total of 5 process steps (spin-on silica front; BCl_3 diffusion; spin-on silica back, PH_3 diffusion; strip oxide both surfaces) is needed to produce a clean wafer ready for the next process step (AR coating).

RCA has proposed a completely different process sequence for cell fabrication for 1986 which includes ion implantation for both pn-junction and BSF layer formation. The conditions of the wafer before and after the 2-step process (ion-implantation, activation anneal) are equivalent to those before and after the 5-step Motorola diffusion process, except for possible differences in efficiency resulting from the two processes. Since the Motorola overall process sequence seems to be the less costly one, it will be used as the base case. Thus, in lieu of the diffusion process, ion implantation could be inserted into the base case process sequence.

Question:

One would like to know the relative cost effectiveness of the 2 competing process options for pn-junction and BSF layer formation.

Answer:

The costs and yields for the 2 process options are known, as well as the costs and yields for all the other solar cell manufacturing process steps in the base case. The cost data from the 2 companies have been normalized to the same economic base through application of the SAMICS standardized cost structure. No information is, however, available on the efficiency contributions of the 2 options. The evaluation will therefore be carried out by determining the efficiency difference which would make the 2 options equally cost-effective. Equation IV.34 is therefore to be solved for $\frac{\Delta\phi_{k,n}}{\phi_{k,n}}$ for the case $\frac{\Delta\Gamma_{k,n}}{\Gamma_{k,n}} = 0$, yielding:

$$\frac{\Delta\phi_{k,n}}{\phi_{k,n}} = \left[\Delta c_{Ce,k,n} - \frac{\Delta y_n}{y_n} c_{Ce,k,Wpn}\right] \frac{f_{Pg}}{(C_{A,i\neq k} + f_{P_g} c_{Ce,k}) \prod_{\ell=n+1}^{P} y_\ell} \qquad \text{(IV.38)}$$

The information displayed in Table IV.2 is available for the base process:

Table IV.2

	Process Step	1 Step Price* $/m^2	2 Step Yield %	3 Cumul. Sub-process %	4 Yielded Step Price† $/m^2	5 Sub-process Price† $/m^2	6 Following Sub-process Yield %	7 Yielded Subprocess Price◊ $/m^2	8 Total Process Price $/m^2
1.	Input polycrystal Si	(10 $/kg)	NA	(0.505m^2/kg)	19.41	19.81			
2.	Sheet generation	18	(0.513m^2/kg)	98.4	18.29				
3.	Apply etch stop back	1.24	99.4	99.0	1.25				
4.	Texture etch front	0.66	99.2	99.8	0.66				
5.	Remove etch stop back	1.58	99.8	100	1.58	41.59	86.7	47.97	
6.	Spin-on silica front	2.28	99.0	96.8	2.36		95.8		
7.	Diffuse BCl_3 back	1.94	99.0	97.8	1.98				
8.	Spin-on silica back	2.28	99.0	98.8	2.31				
9.	Diffuse PH_3 front	2.49	99.0	99.8	2.49				
10.	Strip both surfaces	0.26	99.8	100	0.26	9.40	90.5	10.39	
11.	AR coat Si_3N_4	0.93	99.2	91.3	1.02		90.5		
12.	Apply patterened resist front	1.24	99.4	91.8	1.35				
13.	Pattern front, strip back	0.26	99.8	92.0	0.28				
14.	Metallization	7.05	97.2	94.6	7.45				
15.	Solder coat	3.63	99.8	94.8	3.83				
16.	Electrical test	1.66	94.8	100	1.66	15.59		15.59	73.95
	Alternate Option:								
6a.	Ion implantation 2 sides	8.22	99.0	99.0	8.30				
7a.	Activation anneal	1.56	99.0	100	1.56	9.86	98.0	NA	NA

* Based on the unit area of work-in process leaving the respective process step.
† Based on the unit area of work-in-process leaving group of process steps, or sub-process.
◊ Based on the unit area of finished product.

Table IV.2 contains all the information needed for solving eq. IV.38, which is summarized in Table IV.3.

Table IV.3

	From Table II Column	Line	Base Case	Option
$c_{Ce,k,n}$	5	10	9.40	---
	5	7a	--	9.86
$\Delta c_{Ce,k,n}$	--	--	--	+0.46
y_n	6	6	0.958	---
	6	6a	--	0.980
Δ_{yn}	--	--	--	+0.022
$c_{Ce,k}$	8	--	73.95	---
$c_{Ce,k,WPn}$	5 (divided by yield shown in column 6, Line 6)	5	43.41	---
$\prod_{\ell=n+1}^{P} y_\ell$	6	10	0.905	---
$C_{A,i\neq k}$	from Probl. 1		73.50	---
f_{Pg}	from Probl. 1		0.90	---

Thus:

$$\frac{\Delta\phi_{k,n}}{\phi_{k,n}} = \left[0.46 - \frac{0.022}{0.958} \cdot 43.41\right] \cdot \frac{0.9}{(73.5 + 0.9 \cdot 73.95) \cdot 0.905}$$

$$= -0.0038$$

Result:

The RCA ion implantation process option thus could have an efficiency contribution 0.4% lower than that of the Motorola diffusion option, to achieve equal cost effectiveness in energy generation. The ion implantation process would thus, at equal efficiency contributions, be very slightly more cost-effective than the diffusion option, but the difference is so small that the two options really ought to be considered as equivalent.

It may also be noted that experimental results obtained at various laboratories indicate that the expectation of equal efficiency contributions from the two process options considered is justified. Thus, the result of economic equivalence of the two particular options analyzed is realistic, as far as the projections to 1986 for the various cost contributions and yields can be considered realistic.

Check:

Since the efficiency contributions are considered equal for the two competing processes, the check can be performed on the cost and yield basis alone.

Table IV.4

	Base Case	Option	Units
Input work in process on unit area basis	41.59	41.59	$\$/m^2$
Yield in process step	95.8	98.0	%
Needed input work-in-process for unit output work-in-process	1.044	1.02	m^2/m^2
Cost of input work-in-process	43.41	42.44	$\$/m^2$
Cost of process step per unit output work-in-process	9.44	9.86	$\$/m^2$
Cost of output work-in-process	52.85	52.30	$\$/m^2$

The option output work-in-process is thus 1% less costly. With its 0.4% lower permitted efficiency contribution, it becomes equivalent at the system level. At exact efficiency equality, it would be the (slightly) preferable process.

6. Conclusions

A quantitative comparative evaluation is frequently needed of the different design options for a particular subsystem in a photovoltaic solar energy conversion system, or of the different options for a process step in the manufacturing process sequence for such a subsystem. Such an evaluation has to be functional, which means, based on the cost of the electrical energy produced by such a system.

It is seen that such evaluations can be rather easily performed on the basis of knowledge of the quantitative differences of the key attributes of the particular option under consideration for a subsystem or a process step against the attributes of a baseline case or of a different option. The key attributes are cost and efficiency for the subsystem, assuming reliability and service life to be comparable, and cost, yield, and efficiency contribution for the process step. The other needed inputs are relatively few and of a rather fundamental nature, such as the investment needed for the whole system per unit of energy delivered annually; the total cost of the system exclusive of the subsystem being evaluated; or the cost of the input work-in-process to the particular process step being evaluated. In many instances, adequate evaluations can be performed by substituting estimated values for real data of these quantities.

It is also noteworthy that, particularly for the manufacturing process step evaluation, an analysis on the "cost per peak Watt" basis will often be adequate as a first order approximation, since the load factor which is the principal variable in the conversion to the "cost per kWh delivered" basis, is affected by the evaluation variables only through second order influences.

REFERENCES

1. Wolf, M., "The Near-Term Prospectives for Photovoltaic Solar Energy Conversion", Acta Electronica 20, 2, pp. 205-215, (1977).

2. Redfield, D., "Procedure for Minimizing the Cost per Watt of Photovoltaic Systems", RCA Review 38, pp. 463-499, Dec. 1977.

3. Wolf, M. "A New Look at Silicon Solar Cell Performance; Record 8th IEEE Photovoltaic Spec. Conf., IEEE Cat. No. 70 C 32 ED, pp. 360-371, Aug. 1970.
   Wolf, M., "Outlook for Si Photovoltaic Devices for Terrestrial Solar-Energy Utilization", J. Vac. Sci. Technol. 12, pp. 984-999, Sept/Oct. 1975.

V. Energy Analysis

1. Introduction

Energy consumption and corresponding payback times were reviewed for the current production process and for processes which may be used on manufacturing lines in 1982 and 1986. For a proper assessment of the payback times, the entire manufacturing process sequence from the mining of the ore, in this case quartzite, and its reduction to Si, up to the completion of the system, fully installed and ready for operation, should be analyzed. So far, we have only accumulated energy data up through module manufacture. Even for this part of the process sequence, we have so far performed only detailed energy analyses for those processes for which we have completed thourough technology and cost studies. These processes include the SiO_2 reduction in the arc furnace, Cz crystal pulling, slicing, junction formation, and the energy content of encapsulation materials. For the remaining parts of the process sequence, we have inserted data from other studies, such as Iles' 1974 compilation of the solar cell plant energy consumption[1], and Bickler's design data for a \$2/W(pk) and a \$0.50/W(pk)[3] Strawman process.

These energy consumption studies are summarized into two quantities of interest for energy source systems: 1. the total energy consumed in creating the energy source, and 2. the relation of this "invested" energy to the useful energy output of the system which, for solar energy utilization systems, is often called the "payback time". While the former is a reasonably well defined quantity, which depends primarily on the methods used for creating the energy source, the payback time depends also on the use of the system and is thus less uniquely defined.

2. Energy Payback Times

To calculate payback times for photovoltaic systems, the annual energy output of a unit module area must be known. This power output, for photovoltaic systems, is dependent upon the encapsulated cell efficiency, the module packing factor, the solar insolation, the efficiency of the power conditioning and storage subsystems, and the mismatch of the energy availability and demand statistics. This list of dependencies makes it clear that the output of the module will vary according to climate at the locality of installation, and to the individual load to be satisfied. The factors of influence on the useful system output, outside of the cell efficiency, are combined into the "capacity factor". As a reasonably representative, not too optimistic value for this capacity factor, the number 0.11 has been used, in consequence of the results of several system studies.[4] The capacity factor is essentially independent of the solar cell or module manufacturing process. Consequently, the energy payback time is only partly a function of the energy consumption for the solar module fabrication process, since the other system parameters strongly influence its absolute magnitude. In the calculations of energy payback times, encapsulated cell efficiencies η of 11.5% and 15% were employed for 1978 and 1982 and for 1986, respectively, assuming the use of EFG ribbons, of 12%. To obtain the energy payback times, the annual module output was calculated as $E = \eta \times 8766 \times 0.11 \times H_{pk}$, H_{pk} being the standardized peak solar irradiance, used as $1kW(pk)/m^2$. The factor 0.11 represents the "capacity factor".

Thus, annual energy outputs from a square meter of solar cells of 110.9, 144.6, and 115.7 $kWh/m^2.y$ are obtained for 1978, 1982, and 1986 respectively.

It is also to be observed that, since the energy recovery from solar cells is in the form of electrical energy, it is appropriate to convert those energy expenditures which occur in the form of heat of combustion, to equivalent electrical energy by applying the average efficiency of 0.30 experienced by the electric utilities in the conversion from heat of combustion of fuels to electric power delivered to the consumer[5].

3. Energy Consumption in Photovoltaic Solar Array Manufacturing Process Sequences

3.1 Data Sources.

The major sources of information for this energy analysis were data accumulated from LSA project reports and industry interviews. The energy consumed through materials, both direct and indirect materials, was obtained by converting the material consumption to energy units through multiplication with the material energy contents shown in Table V-1. Where specific information to the contrary was not available, the material energy values were assumed to be in the form of thermal energy. The equipment costs, were converted to energy units expressed on the basis of unit cell area of throughput, by assuming a lifetime of seven years, and an energy content of the equipment which corresponds in value to 2% of the equipment cost.[6] This energy cost has then been converted to a thermal energy using an energy price of $0.003/kWh(th)[7]. Finally, the general energy usage for operating the facility was derived from the machine floor area by using the annual SAMICS utility cost of $3.74/ft^2[8] and assuming that all of this "indirect" energy, since it is used primarily for lighting, air conditioning, and ventilating, in view of the high heat load in the building, is in the form of electricity at a cost of $0.0319/kWh[8]. The conversion factors for the equipment and facility energies thus become 0.9523 kWh(th)/$y and 1262 kWh/m^{2}y, respectively.

V. Energy Analysis

1. Introduction

Energy consumption and corresponding payback times were reviewed for the current production process and for processes which may be used on manufacturing lines in 1982 and 1986. For a proper assessment of the payback times, the entire manufacturing process sequence from the mining of the ore, in this case quartzite, and its reduction to Si, up to the completion of the system, fully installed and ready for operation, should be analyzed. So far, we have only accumulated energy data up through module manufacture. Even for this part of the process sequence, we have so far performed only detailed energy analyses for those processes for which we have completed thourough technology and cost studies. These processes include the SiO_2 reduction in the arc furnace, Cz crystal pulling, slicing, junction formation, and the energy content of encapsulation materials. For the remaining parts of the process sequence, we have inserted data from other studies, such as Iles' 1974 compilation of the solar cell plant energy consumption[1], and Bickler's design data for a \$2/W(pk) and a \$0.50/W(pk)[3] Strawman process.

These energy consumption studies are summarized into two quantities of interest for energy source systems: 1. the total energy consumed in creating the energy source, and 2. the relation of this "invested" energy to the useful energy output of the system which, for solar energy utilization systems, is often called the "payback time". While the former is a reasonably well defined quantity, which depends primarily on the methods used for creating the energy source, the payback time depends also on the use of the system and is thus less uniquely defined.

2. Energy Payback Times

To calculate payback times for photovoltaic systems, the annual energy output of a unit module area must be known. This power output, for photovoltaic systems, is dependent upon the encapsulated cell efficiency, the module packing factor, the solar insolation, the efficiency of the power conditioning and storage subsystems, and the mismatch of the energy availability and demand statistics. This list of dependencies makes it clear that the output of the module will vary according to climate at the locality of installation, and to the individual load to be satisfied. The factors of influence on the useful system output, outside of the cell efficiency, are combined into the "capacity factor". As a reasonably representative, not too optimistic value for this capacity factor, the number 0.11 has been used, in consequence of the results of several system studies.[4] The capacity factor is essentially independent of the solar cell or module manufacturing process. Consequently, the energy payback time is only partly a function of the energy consumption for the solar module fabrication process, since the other system parameters strongly influence its absolute magnitude. In the calculations of energy payback times, encapsulated cell efficiencies η of 11.5% and 15% were employed for 1978 and 1982 and for 1986, respectively, assuming the use of EFG ribbons, of 12%. To obtain the energy payback times, the annual module output was calculated as $E = \eta \times 8766 \times 0.11 \times H_{pk}$, H_{pk} being the standardized peak solar irradiance, used as $1kW(pk)/m^2$. The factor 0.11 represents the "capacity factor".

Thus, annual energy outputs from a square meter of solar cells of 110.9, 144.6, and 115.7 $kWh/m^2.y$ are obtained for 1978, 1982, and 1986 respectively.

It is also to be observed that, since the energy recovery from solar cells is in the form of electrical energy, it is appropriate to convert those energy expenditures which occur in the form of heat of combustion, to equivalent electrical energy by applying the average efficiency of 0.30 experienced by the electric utilities in the conversion from heat of combustion of fuels to electric power delivered to the consumer[5].

3. Energy Consumption in Photovoltaic Solar Array Manufacturing Process Sequences

3.1 Data Sources.

The major sources of information for this energy analysis were data accumulated from LSA project reports and industry interviews. The energy consumed through materials, both direct and indirect materials, was obtained by converting the material consumption to energy units through multiplication with the material energy contents shown in Table V-1. Where specific information to the contrary was not available, the material energy values were assumed to be in the form of thermal energy. The equipment costs, were converted to energy units expressed on the basis of unit cell area of throughput, by assuming a lifetime of seven years, and an energy content of the equipment which corresponds in value to 2% of the equipment cost.[6] This energy cost has then been converted to a thermal energy using an energy price of $0.003/kWh(th)[7]. Finally, the general energy usage for operating the facility was derived from the machine floor area by using the annual SAMICS utility cost of $3.74/ft^2[8] and assuming that all of this "indirect" energy, since it is used primarily for lighting, air conditioning, and ventilating, in view of the high heat load in the building, is in the form of electricity at a cost of $0.0319/kWh[8]. The conversion factors for the equipment and facility energies thus become 0.9523 kWh(th)/$y and 1262 kWh/m^{2}y, respectively.

Table V-1

Energy Contents of Selected Materials

Material	Original Units	Convenient Units (Thermal kWh's)	Reference
1. Acetic acid	3.28 lb of hi-press. steam plus 0.07 kWh(eℓ)/lb	3.18 kWh/g	1
2. Aluminum (Al)	520×10^6 kWh(th)/ton	0.17 kWh/g	2
3. Ammonia gas (NH_3)	8.05×10^3 Btu/lb	0.00534 kWh/g	3
4. Ammonium Hydroxide 30% (NH_4OH)	-	1.32 kWh/ℓ	4
5. Argon gas	1,100 Btu/lb	1.27×10^{-3} kWh/ℓ	5
6. Butyl acetate	4.32 lb of low-press. steam plus 0.082 kWh(eℓ)/lb	3.21 kWh/g	6
7. Copper (Cu)	16.2×10^6 Btu/ton	5.23 kWh/g	7
8. Energy for exhausting waste fumes without scrubbing.	0.46 kW/1000 ft^3/min	2.56×10^{-2} kWh/ 1000 ft^3	8
9. Freon-14 gas (CF_4)	-	2×10^{-3} kWh/ℓ	9
10. Hydrogen gas	43,300 Btu/lb	2.51×10^{-3} kWh/ℓ	5
11. HF (48%)	7,000 Btu/lb	5.22 kWh/ℓ	5
12. Nitrogen (liquid)	1,330 Btu/lb	0.69 KWh/ℓ	5
13. Nitrogen (gas from liquid)	-	1.44×10^{-3} kWh/ℓ	10
14. Nitric Acid (HNO_3, 67%)	14,500 Btu/lb	13.12 kWh/ℓ	5
15. Oxygen gas (O_2)	830 Btu/lb	7.66 kWh/ℓ	5
16. Phosphorus (solid)	23,790 Btu/lb	1.54×10^{-2} kWh/g	5
17. Phosphine gas (PH_3)	-	0.18 kWh/ℓ	11
18. Phosphorous oxychloride ($POC\ell_3$)	-	0.14 kWh/g	12
19. Plating resist	8,000 Btu/lb	5.20 kWh/ℓ	13
20. Silver	1260×10^6 Btu/ton	0.406 kWh/g	8
21. Sodium Hydroxide (NaOH)	by-product	0	5
22. Toluene	0.05 lb of low-press. steam plus 0.025 kWh(eℓ)/lb	0.0349 kWh/mℓ	14
23. Vacuum pump oil	3,000 kWh(th)/ barrel	18.87 kWh/ℓ	15
24. Wax	2,000 kWh/barrel	1.3×10^{-2} kWh/g	16

References for Table V-1

1. Assumed to be the same as that of acetone, which was taken from "Battelle Columbus Laboratories, Draft Target and Support Document for Developing a Maximum Energy Efficient Improvement Target for SIC 28", Federal Energy Administration, Washington, DC (1976).

2. J.T. Reding and B.P. Shepherd, "Energy Consumption, Report EPA-G50/2-75-032b", US Environmental Protection Agency, Washington, DC (4/75).

3. Federal Energy Administration, "Project Independence Blueprint," Vol. 3, Federal Energy Administration, Washington, DC (1974).

4. Calculated from the energy content for NH_3 and using a density of 0.824 g/mℓ for the NH_4OH solution.

5. Battelle Columbus Laboratories,"Draft Target and Support Document for Developing a Maximum Energy Efficient Improvement Target for SIC 28", Federal Energy Administration, Washington, DC (1976).

6. Assumed to be the same as that of butyl alcohol, as given in Ref.5.

7. H.W. Lownie, et al (Battelle Columbus Laboratories), "Draft Target Report on Development and Establishment of Energy Efficiency Improvement Targets for Primary Metal Industries," Federal Energy Administration, Washington, DC (9/76).

8. M.G. Coleman, et al., Motorola Final Report, DOE/JPL-954847-78/4, 183(11/78).

9. Estimated as approximately 50% more than the average energy content of commercial gases, as given in Ref. 5.

10. Calculated from the energy content for LN_2 assuming 480 ℓ of gas can be obtained from 1ℓ of LN_2.

11. Estimated as twice the energy content for P(s) plus $3/2H_2(g)$.

12. Estimated as twice the energy content of P(s), plus $\frac{1}{2}O_2(g)$, plus $\frac{3}{2}Cl_2(g)$. The energy content of Cl_2 was taken from ref. 5.

13. Assumed to be the same as that of wood rosin, as given in Ref. 5.

14. Taken as that of benzene, as given in ref. 5.

15. Taken as approximately twice the energy content of middle oil distillates.

16. From M. Sittig, Practical Techniques for Saving Energy in the Chemical Petroleum and Metals Industries, Noyes Data Corporation, Park Ridge, NJ (1977), and using a density of 0.97 g/ml for the wax.

V. Energy Analysis

1. Introduction

Energy consumption and corresponding payback times were reviewed for the current production process and for processes which may be used on manufacturing lines in 1982 and 1986. For a proper assessment of the payback times, the entire manufacturing process sequence from the mining of the ore, in this case quartzite, and its reduction to Si, up to the completion of the system, fully installed and ready for operation, should be analyzed. So far, we have only accumulated energy data up through module manufacture. Even for this part of the process sequence, we have so far performed only detailed energy analyses for those processes for which we have completed thourough technology and cost studies. These processes include the SiO_2 reduction in the arc furnace, Cz crystal pulling, slicing, junction formation, and the energy content of encapsulation materials. For the remaining parts of the process sequence, we have inserted data from other studies, such as Iles' 1974 compilation of the solar cell plant energy consumption[1], and Bickler's design data for a \$2/W(pk) and a \$0.50/W(pk)[3] Strawman process.

These energy consumption studies are summarized into two quantities of interest for energy source systems: 1. the total energy consumed in creating the energy source, and 2. the relation of this "invested" energy to the useful energy output of the system which, for solar energy utilization systems, is often called the "payback time". While the former is a reasonably well defined quantity, which depends primarily on the methods used for creating the energy source, the payback time depends also on the use of the system and is thus less uniquely defined.

2. Energy Payback Times

To calculate payback times for photovoltaic systems, the annual energy output of a unit module area must be known. This power output, for photovoltaic systems, is dependent upon the encapsulated cell efficiency, the module packing factor, the solar insolation, the efficiency of the power conditioning and storage subsystems, and the mismatch of the energy availability and demand statistics. This list of dependencies makes it clear that the output of the module will vary according to climate at the locality of installation, and to the individual load to be satisfied. The factors of influence on the useful system output, outside of the cell efficiency, are combined into the "capacity factor". As a reasonably representative, not too optimistic value for this capacity factor, the number 0.11 has been used, in consequence of the results of several system studies.[4] The capacity factor is essentially independent of the solar cell or module manufacturing process. Consequently, the energy payback time is only partly a function of the energy consumption for the solar module fabrication process, since the other system parameters strongly influence its absolute magnitude. In the calculations of energy payback times, encapsulated cell efficiencies η of 11.5% and 15% were employed for 1978 and 1982 and for 1986, respectively, assuming the use of EFG ribbons, of 12%. To obtain the energy payback times, the annual module output was calculated as $E = \eta \times 8766 \times 0.11 \times H_{pk}$, H_{pk} being the standardized peak solar irradiance, used as $1kW(pk)/m^2$. The factor 0.11 represents the "capacity factor".

Thus, annual energy outputs from a square meter of solar cells of 110.9, 144.6, and 115.7 $kWh/m^2.y$ are obtained for 1978, 1982, and 1986 respectively.

It is also to be observed that, since the energy recovery from solar cells is in the form of electrical energy, it is appropriate to convert those energy expenditures which occur in the form of heat of combustion, to equivalent electrical energy by applying the average efficiency of 0.30 experienced by the electric utilities in the conversion from heat of combustion of fuels to electric power delivered to the consumer[5].

3. Energy Consumption in Photovoltaic Solar Array Manufacturing Process Sequences

3.1 Data Sources.

The major sources of information for this energy analysis were data accumulated from LSA project reports and industry interviews. The energy consumed through materials, both direct and indirect materials, was obtained by converting the material consumption to energy units through multiplication with the material energy contents shown in Table V-1. Where specific information to the contrary was not available, the material energy values were assumed to be in the form of thermal energy. The equipment costs, were converted to energy units expressed on the basis of unit cell area of throughput, by assuming a lifetime of seven years, and an energy content of the equipment which corresponds in value to 2% of the equipment cost.[6] This energy cost has then been converted to a thermal energy using an energy price of $0.003/kWh(th)[7]. Finally, the general energy usage for operating the facility was derived from the machine floor area by using the annual SAMICS utility cost of $3.74/ft^2[8] and assuming that all of this "indirect" energy, since it is used primarily for lighting, air conditioning, and ventilating, in view of the high heat load in the building, is in the form of electricity at a cost of $0.0319/kWh[8]. The conversion factors for the equipment and facility energies thus become 0.9523 kWh(th)/$y and 1262 kWh/m^{2}y, respectively.

Table V-1

Energy Contents of Selected Materials

Material	Original Units	Convenient Units (Thermal kWh's)	Reference
1. Acetic acid	3.28 lb of hi-press. steam plus 0.07 kWh(eℓ)/lb	3.18 kWh/g	1
2. Aluminum (Al)	520×10^6 kWh(th)/ton	0.17 kWh/g	2
3. Ammonia gas (NH_3)	8.05×10^3 Btu/lb	0.00534 kWh/g	3
4. Ammonium Hydroxide 30% (NH_4OH)	-	1.32 kWh/ℓ	4
5. Argon gas	1,100 Btu/lb	1.27×10^{-3} kWh/ℓ	5
6. Butyl acetate	4.32 lb of low-press. steam plus 0.082 kWh(eℓ)/lb	3.21 kWh/g	6
7. Copper (Cu)	16.2×10^6 Btu/ton	5.23 kWh/g	7
8. Energy for exhausting waste fumes without scrubbing.	0.46 kW/1000 ft^3/min	2.56×10^{-2} kWh/ 1000 ft^3	8
9. Freon-14 gas (CF_4)	-	2×10^{-3} kWh/ℓ	9
10. Hydrogen gas	43,300 Btu/lb	2.51×10^{-3} kWh/ℓ	5
11. HF (48%)	7,000 Btu/lb	5.22 kWh/ℓ	5
12. Nitrogen (liquid)	1,330 Btu/lb	0.69 KWh/ℓ	5
13. Nitrogen (gas from liquid)	-	1.44×10^{-3} kWh/ℓ	10
14. Nitric Acid (HNO_3, 67%)	14,500 Btu/lb	13.12 kWh/ℓ	5
15. Oxygen gas (O_2)	830 Btu/lb	7.66 kWh/ℓ	5
16. Phosphorus (solid)	23,790 Btu/lb	1.54×10^{-2} kWh/g	5
17. Phosphine gas (PH_3)	-	0.18 kWh/ℓ	11
18. Phosphorous oxychloride ($POCl_3$)	-	0.14 kWh/g	12
19. Plating resist	8,000 Btu/lb	5.20 kWh/ℓ	13
20. Silver	1260×10^6 Btu/ton	0.406 kWh/g	8
21. Sodium Hydroxide (NaOH)	by-product	0	5
22. Toluene	0.05 lb of low-press. steam plus 0.025 kWh(eℓ)/lb	0.0349 kWh/mℓ	14
23. Vacuum pump oil	3,000 kWh(th)/ barrel	18.87 kWh/ℓ	15
24. Wax	2,000 kWh/barrel	1.3×10^{-2} kWh/g	16

References for Table V-1

1. Assumed to be the same as that of acetone, which was taken from "Battelle Columbus Laboratories, Draft Target and Support Document for Developing a Maximum Energy Efficient Improvement Target for SIC 28", Federal Energy Administration, Washington, DC (1976).

2. J.T. Reding and B.P. Shepherd, "Energy Consumption, Report EPA-G50/2-75-032b", US Environmental Protection Agency, Washington, DC (4/75).

3. Federal Energy Administration, "Project Independence Blueprint," Vol. 3, Federal Energy Administration, Washington, DC (1974).

4. Calculated from the energy content for NH_3 and using a density of 0.824 g/mℓ for the NH_4OH solution.

5. Battelle Columbus Laboratories,"Draft Target and Support Document for Developing a Maximum Energy Efficient Improvement Target for SIC 28", Federal Energy Administration, Washington, DC (1976).

6. Assumed to be the same as that of butyl alcohol, as given in Ref.5.

7. H.W. Lownie, et al (Battelle Columbus Laboratories), "Draft Target Report on Development and Establishment of Energy Efficiency Improvement Targets for Primary Metal Industries," Federal Energy Administration, Washington, DC (9/76).

8. M.G. Coleman, et al., Motorola Final Report, DOE/JPL-954847-78/4, 183(11/78).

9. Estimated as approximately 50% more than the average energy content of commercial gases, as given in Ref. 5.

10. Calculated from the energy content for LN_2 assuming 480 ℓ of gas can be obtained from 1ℓ of LN_2.

11. Estimated as twice the energy content for P(s) plus $3/2H_2(g)$.

12. Estimated as twice the energy content of P(s), plus $\frac{1}{2}O_2(g)$, plus $\frac{3}{2}Cl_2(g)$. The energy content of Cl_2 was taken from ref. 5.

13. Assumed to be the same as that of wood rosin, as given in Ref. 5.

14. Taken as that of benzene, as given in ref. 5.

15. Taken as approximately twice the energy content of middle oil distillates.

16. From M. Sittig, Practical Techniques for Saving Energy in the Chemical Petroleum and Metals Industries, Noyes Data Corporation, Park Ridge, NJ (1977), and using a density of 0.97 g/ml for the wax.

3.2 Energy Consumption in Si reduction and purification.

This process group starts with the reduction of SiO_2 in an arc furnace. This is a quite efficient and cost-effective process which is not very likely to be replaced by another approach. In contrast, the following step of Si purification is very inefficient and likely to be replaced by one of several alternate methods under development. Furthest advanced among these is the SiH_4 purification process being prepared for pilot line operations by Union Carbide Corp. It can be expected to be a production process by 1986.

a) Theoretical Material Balance for the Arc Furnace Process.

The chemical reaction of this process is:

	SiO_2	+ 2C	→ Si +	2 CO
Atomic Weights:	28 + 2(16)	+ 2(12)	→ 28 +	2(12 + 16)
	60	+ 24	→ 28 +	56
Masses, normalized to 1 kg Si out:	2.14 kg	+ 0.86 kg	→ 1 kg +	2 kg

According to Dow-Corning [9], the industrially experienced and actual conversion efficiency of SiO_2 to Si is 80%.
The required input is thus: 2.68 kg SiO_2 for 1 kg Si out
(Dow-Corning shows 2.71 kg SiO_2).

It is assumed that half of the lost SiO_2 input, or 0.27 kg, is used in the reaction:

	SiO_2	+ C	→ SiO	+ CO
Atomic Weights:	60	+ 12	→ 44	+ 28
	0.27 kg	+ 0.05 kg	→ 0.2 kg	+ 0.12 kg

where the SiO is lost at the top of the furnace.
Thus, the total theoretical carbon input would be 0.91 kg C per 1 kg MG-Si output.

2. Energy Payback Times

To calculate payback times for photovoltaic systems, the annual energy output of a unit module area must be known. This power output, for photovoltaic systems, is dependent upon the encapsulated cell efficiency, the module packing factor, the solar insolation, the efficiency of the power conditioning and storage subsystems, and the mismatch of the energy availability and demand statistics. This list of dependencies makes it clear that the output of the module will vary according to climate at the locality of installation, and to the individual load to be satisfied. The factors of influence on the useful system output, outside of the cell efficiency, are combined into the "capacity factor". As a reasonably representative, not too optimistic value for this capacity factor, the number 0.11 has been used, in consequence of the results of several system studies.[4] The capacity factor is essentially independent of the solar cell or module manufacturing process. Consequently, the energy payback time is only partly a function of the energy consumption for the solar module fabrication process, since the other system parameters strongly influence its absolute magnitude. In the calculations of energy payback times, encapsulated cell efficiencies η of 11.5% and 15% were employed for 1978 and 1982 and for 1986, respectively, assuming the use of EFG ribbons, of 12%. To obtain the energy payback times, the annual module output was calculated as $E = \eta \times 8766 \times 0.11 \times H_{pk}$, H_{pk} being the standardized peak solar irradiance, used as $1kW(pk)/m^2$. The factor 0.11 represents the "capacity factor".

Thus, annual energy outputs from a square meter of solar cells of 110.9, 144.6, and 115.7 $kWh/m^2.y$ are obtained for 1978, 1982, and 1986 respectively.

It is also to be observed that, since the energy recovery from solar cells is in the form of electrical energy, it is appropriate to convert those energy expenditures which occur in the form of heat of combustion, to equivalent electrical energy by applying the average efficiency of 0.30 experienced by the electric utilities in the conversion from heat of combustion of fuels to electric power delivered to the consumer[5].

3. Energy Consumption in Photovoltaic Solar Array Manufacturing Process Sequences

3.1 Data Sources.

The major sources of information for this energy analysis were data accumulated from LSA project reports and industry interviews. The energy consumed through materials, both direct and indirect materials, was obtained by converting the material consumption to energy units through multiplication with the material energy contents shown in Table V-1. Where specific information to the contrary was not available, the material energy values were assumed to be in the form of thermal energy. The equipment costs, were converted to energy units expressed on the basis of unit cell area of throughput, by assuming a lifetime of seven years, and an energy content of the equipment which corresponds in value to 2% of the equipment cost.[6] This energy cost has then been converted to a thermal energy using an energy price of $0.003/kWh(th)[7]. Finally, the general energy usage for operating the facility was derived from the machine floor area by using the annual SAMICS utility cost of $3.74/ft^2[8] and assuming that all of this "indirect" energy, since it is used primarily for lighting, air conditioning, and ventilating, in view of the high heat load in the building, is in the form of electricity at a cost of $0.0319/kWh[8]. The conversion factors for the equipment and facility energies thus become 0.9523 kWh(th)/$y and 1262 kWh/m^{2}y, respectively.

Table V-1

Energy Contents of Selected Materials

Material	Original Units	Convenient Units (Thermal kWh's)	Reference
1. Acetic acid	3.28 lb of hi-press. steam plus 0.07 kWh(eℓ)/lb	3.18 kWh/g	1
2. Aluminum (Al)	520×10^6 kWh(th)/ton	0.17 kWh/g	2
3. Ammonia gas (NH_3)	8.05×10^3 Btu/lb	0.00534 kWh/g	3
4. Ammonium Hydroxide 30% (NH_4OH)	-	1.32 kWh/ℓ	4
5. Argon gas	1,100 Btu/lb	1.27×10^{-3} kWh/ℓ	5
6. Butyl acetate	4.32 lb of low-press. steam plus 0.082 kWh(eℓ)/lb	3.21 kWh/g	6
7. Copper (Cu)	16.2×10^6 Btu/ton	5.23 kWh/g	7
8. Energy for exhausting waste fumes without scrubbing.	0.46 kW/1000 ft^3/min	2.56×10^{-2} kWh/ 1000 ft^3	8
9. Freon-14 gas (CF_4)	-	2×10^{-3} kWh/ℓ	9
10. Hydrogen gas	43,300 Btu/lb	2.51×10^{-3} kWh/ℓ	5
11. HF (48%)	7,000 Btu/lb	5.22 kWh/ℓ	5
12. Nitrogen (liquid)	1,330 Btu/lb	0.69 KWh/ℓ	5
13. Nitrogen (gas from liquid)	-	1.44×10^{-3} kWh/ℓ	10
14. Nitric Acid (HNO_3, 67%)	14,500 Btu/lb	13.12 kWh/ℓ	5
15. Oxygen gas (O_2)	830 Btu/lb	7.66 kWh/ℓ	5
16. Phosphorus (solid)	23,790 Btu/lb	1.54×10^{-2} kWh/g	5
17. Phosphine gas (PH_3)	-	0.18 kWh/ℓ	11
18. Phosphorous oxychloride ($POCl_3$)	-	0.14 kWh/g	12
19. Plating resist	8,000 Btu/lb	5.20 kWh/ℓ	13
20. Silver	1260×10^6 Btu/ton	0.406 kWh/g	8
21. Sodium Hydroxide (NaOH)	by-product	0	5
22. Toluene	0.05 lb of low-press. steam plus 0.025 kWh(eℓ)/lb	0.0349 kWh/mℓ	14
23. Vacuum pump oil	3,000 kWh(th)/ barrel	18.87 kWh/ℓ	15
24. Wax	2,000 kWh/barrel	1.3×10^{-2} kWh/g	16

References for Table V-1

1. Assumed to be the same as that of acetone, which was taken from "Battelle Columbus Laboratories, Draft Target and Support Document for Developing a Maximum Energy Efficient Improvement Target for SIC 28", Federal Energy Administration, Washington, DC (1976).

2. J.T. Reding and B.P. Shepherd, "Energy Consumption, Report EPA-G50/2-75-032b", US Environmental Protection Agency, Washington, DC (4/75).

3. Federal Energy Administration, "Project Independence Blueprint," Vol. 3, Federal Energy Administration, Washington, DC (1974).

4. Calculated from the energy content for NH_3 and using a density of 0.824 g/mℓ for the NH_4OH solution.

5. Battelle Columbus Laboratories,"Draft Target and Support Document for Developing a Maximum Energy Efficient Improvement Target for SIC 28", Federal Energy Administration, Washington, DC (1976).

6. Assumed to be the same as that of butyl alcohol, as given in Ref.5.

7. H.W. Lownie, et al (Battelle Columbus Laboratories), "Draft Target Report on Development and Establishment of Energy Efficiency Improvement Targets for Primary Metal Industries," Federal Energy Administration, Washington, DC (9/76).

8. M.G. Coleman, et al., Motorola Final Report, DOE/JPL-954847-78/4, 183(11/78).

9. Estimated as approximately 50% more than the average energy content of commercial gases, as given in Ref. 5.

10. Calculated from the energy content for LN_2 assuming 480 ℓ of gas can be obtained from 1ℓ of LN_2.

11. Estimated as twice the energy content for P(s) plus $3/2H_2(g)$.

12. Estimated as twice the energy content of P(s), plus $\frac{1}{2}O_2(g)$, plus $\frac{3}{2}Cl_2(g)$. The energy content of Cl_2 was taken from ref. 5.

13. Assumed to be the same as that of wood rosin, as given in Ref. 5.

14. Taken as that of benzene, as given in ref. 5.

2. Energy Payback Times

To calculate payback times for photovoltaic systems, the annual energy output of a unit module area must be known. This power output, for photovoltaic systems, is dependent upon the encapsulated cell efficiency, the module packing factor, the solar insolation, the efficiency of the power conditioning and storage subsystems, and the mismatch of the energy availability and demand statistics. This list of dependencies makes it clear that the output of the module will vary according to climate at the locality of installation, and to the individual load to be satisfied. The factors of influence on the useful system output, outside of the cell efficiency, are combined into the "capacity factor". As a reasonably representative, not too optimistic value for this capacity factor, the number 0.11 has been used, in consequence of the results of several system studies.[4] The capacity factor is essentially independent of the solar cell or module manufacturing process. Consequently, the energy payback time is only partly a function of the energy consumption for the solar module fabrication process, since the other system parameters strongly influence its absolute magnitude. In the calculations of energy payback times, encapsulated cell efficiencies η of 11.5% and 15% were employed for 1978 and 1982 and for 1986, respectively, assuming the use of EFG ribbons, of 12%. To obtain the energy payback times, the annual module output was calculated as $E = \eta \times 8766 \times 0.11 \times H_{pk}$, H_{pk} being the standardized peak solar irradiance, used as $1 kW(pk)/m^2$. The factor 0.11 represents the "capacity factor".

Thus, annual energy outputs from a square meter of solar cells of 110.9, 144.6, and 115.7 $kWh/m^2.y$ are obtained for 1978, 1982, and 1986 respectively.

It is also to be observed that, since the energy recovery from solar cells is in the form of electrical energy, it is appropriate to convert those energy expenditures which occur in the form of heat of combustion, to equivalent electrical energy by applying the average efficiency of 0.30 experienced by the electric utilities in the conversion from heat of combustion of fuels to electric power delivered to the consumer[5].

3. Energy Consumption in Photovoltaic Solar Array Manufacturing Process Sequences

3.1 Data Sources.

The major sources of information for this energy analysis were data accumulated from LSA project reports and industry interviews. The energy consumed through materials, both direct and indirect materials, was obtained by converting the material consumption to energy units through multiplication with the material energy contents shown in Table V-1. Where specific information to the contrary was not available, the material energy values were assumed to be in the form of thermal energy. The equipment costs, were converted to energy units expressed on the basis of unit cell area of throughput, by assuming a lifetime of seven years, and an energy content of the equipment which corresponds in value to 2% of the equipment cost.[6] This energy cost has then been converted to a thermal energy using an energy price of $0.003/kWh(th)[7]. Finally, the general energy usage for operating the facility was derived from the machine floor area by using the annual SAMICS utility cost of $3.74/ft^2[8] and assuming that all of this "indirect" energy, since it is used primarily for lighting, air conditioning, and ventilating, in view of the high heat load in the building, is in the form of electricity at a cost of $0.0319/kWh[8]. The conversion factors for the equipment and facility energies thus become 0.9523 kWh(th)/$y and 1262 kWh/m^{2}y, respectively.

Table V-1

Energy Contents of Selected Materials

Material	Original Units	Convenient Units (Thermal kWh's)	Reference
1. Acetic acid	3.28 lb of hi-press. steam plus 0.07 kWh(eℓ)/lb	3.18 kWh/g	1
2. Aluminum (Aℓ)	520x10^6 kWh(th)/ton	0.17 kWh/g	2
3. Ammonia gas (NH_3)	8.05x10^3 Btu/lb	0.00534 kWh/g	3
4. Ammonium Hydroxide 30% (NH_4OH)	-	1.32 kWh/ℓ	4
5. Argon gas	1,100 Btu/lb	1.27x10^{-3} kWh/ℓ	5
6. Butyl acetate	4.32 lb of low-press. steam plus 0.082 kWh(eℓ)/lb	3.21 kWh/g	6
7. Copper (Cu)	16.2x10^6 Btu/ton	5.23 kWh/g	7
8. Energy for exhausting waste fumes without scrubbing.	0.46 kW/1000 ft^3/min	2.56x10^{-2} kWh/ 1000 ft^3	8
9. Freon-14 gas (CF_4)	-	2x10^{-3} kWh/ℓ	9
10. Hydrogen gas	43,300 Btu/lb	2.51x10^{-3} kWh/ℓ	5
11. HF (48%)	7,000 Btu/lb	5.22 kWh/ℓ	5
12. Nitrogen (liquid)	1,330 Btu/lb	0.69 KWh/ℓ	5
13. Nitrogen (gas from liquid)	-	1.44x10^{-3} kWh/ℓ	10
14. Nitric Acid (HNO_3, 67%)	14,500 Btu/lb	13.12 kWh/ℓ	5
15. Oxygen gas (O_2)	830 Btu/lb	7.66 kWh/ℓ	5
16. Phosphorus (solid)	23,790 Btu/lb	1.54x10^{-2} kWh/g	5
17. Phosphine gas (PH_3)	-	0.18 kWh/ℓ	11
18. Phosphorous oxychloride ($POC\ell_3$)	-	0.14 kWh/g	12
19. Plating resist	8,000 Btu/lb	5.20 kWh/ℓ	13
20. Silver	1260x10^6 Btu/ton	0.406 kWh/g	8
21. Sodium Hydroxide (NaOH)	by-product	0	5
22. Toluene	0.05 lb of low-press. steam plus 0.025 kWh(eℓ)/lb	0.0349 kWh/mℓ	14
23. Vacuum pump oil	3,000 kWh(th)/ barrel	18.87 kWh/ℓ	15
24. Wax	2,000 kWh/barrel	1.3x10^{-2} kWh/g	16

References for Table V-1

1. Assumed to be the same as that of acetone, which was taken from "Battelle Columbus Laboratories, Draft Target and Support Document for Developing a Maximum Energy Efficient Improvement Target for SIC 28", Federal Energy Administration, Washington, DC (1976).

2. J.T. Reding and B.P. Shepherd, "Energy Consumption, Report EPA-G50/2-75-032b", US Environmental Protection Agency, Washington, DC (4/75).

3. Federal Energy Administration, "Project Independence Blueprint," Vol. 3, Federal Energy Administration, Washington, DC (1974).

4. Calculated from the energy content for NH_3 and using a density of 0.824 g/mℓ for the NH_4OH solution.

5. Battelle Columbus Laboratories,"Draft Target and Support Document for Developing a Maximum Energy Efficient Improvement Target for SIC 28", Federal Energy Administration, Washington, DC (1976).

6. Assumed to be the same as that of butyl alcohol, as given in Ref.5.

7. H.W. Lownie, et al (Battelle Columbus Laboratories), "Draft Target Report on Development and Establishment of Energy Efficiency Improvement Targets for Primary Metal Industries," Federal Energy Administration, Washington, DC (9/76).

8. M.G. Coleman, et al., Motorola Final Report, DOE/JPL-954847-78/4, 183(11/78).

9. Estimated as approximately 50% more than the average energy content of commercial gases, as given in Ref. 5.

10. Calculated from the energy content for LN_2 assuming 480 ℓ of gas can be obtained from 1ℓ of LN_2.

11. Estimated as twice the energy content for P(s) plus $3/2H_2(g)$.

12. Estimated as twice the energy content of P(s), plus $\frac{1}{2}O_2(g)$, plus $\frac{3}{2}Cl_2(g)$. The energy content of Cl_2 was taken from ref. 5.

13. Assumed to be the same as that of wood rosin, as given in Ref. 5.

14. Taken as that of benzene, as given in ref. 5.

15. Taken as approximately twice the energy content of middle oil distillates.

16. From M. Sittig, Practical Techniques for Saving Energy in the Chemical Petroleum and Metals Industries, Noyes Data Corporation, Park Ridge, NJ (1977), and using a density of 0.97 g/ml for the wax.

3.2 Energy Consumption in Si reduction and purification.

This process group starts with the reduction of SiO_2 in an arc furnace. This is a quite efficient and cost-effective process which is not very likely to be replaced by another approach. In contrast, the following step of Si purification is very inefficient and likely to be replaced by one of several alternate methods under development. Furthest advanced among these is the SiH_4 purification process being prepared for pilot line operations by Union Carbide Corp. It can be expected to be a production process by 1986.

a) Theoretical Material Balance for the Arc Furnace Process.

The chemical reaction of this process is:

	SiO_2	+ 2C	→ Si	+ 2 CO
Atomic Weights:	28 + 2(16)	+ 2(12)	→ 28	+ 2(12 + 16)
	60	+ 24	→ 28	+ 56
Masses, normalized to 1 kg Si out:	2.14 kg	+ 0.86 kg	→ 1 kg	+ 2 kg

According to Dow-Corning [9], the industrially experienced and actual conversion efficiency of SiO_2 to Si is 80%.
The required input is thus: 2.68 kg SiO_2 for 1 kg Si out
(Dow-Corning shows 2.71 kg SiO_2).

It is assumed that half of the lost SiO_2 input, or 0.27 kg, is used in the reaction:

	SiO_2	+ C	→ SiO	+ CO
Atomic Weights:	60	+ 12	→ 44	+ 28
	0.27 kg	+ 0.05 kg	→ 0.2 kg	+ 0.12 kg

where the SiO is lost at the top of the furnace.
Thus, the total theoretical carbon input would be 0.91 kg C per 1 kg MG-Si output.

2. Energy Payback Times

To calculate payback times for photovoltaic systems, the annual energy output of a unit module area must be known. This power output, for photovoltaic systems, is dependent upon the encapsulated cell efficiency, the module packing factor, the solar insolation, the efficiency of the power conditioning and storage subsystems, and the mismatch of the energy availability and demand statistics. This list of dependencies makes it clear that the output of the module will vary according to climate at the locality of installation, and to the individual load to be satisfied. The factors of influence on the useful system output, outside of the cell efficiency, are combined into the "capacity factor". As a reasonably representative, not too optimistic value for this capacity factor, the number 0.11 has been used, in consequence of the results of several system studies.[4] The capacity factor is essentially independent of the solar cell or module manufacturing process. Consequently, the energy payback time is only partly a function of the energy consumption for the solar module fabrication process, since the other system parameters strongly influence its absolute magnitude. In the calculations of energy payback times, encapsulated cell efficiencies η of 11.5% and 15% were employed for 1978 and 1982 and for 1986, respectively, assuming the use of EFG ribbons, of 12%. To obtain the energy payback times, the annual module output was calculated as $E = \eta \times 8766 \times 0.11 \times H_{pk}$, H_{pk} being the standardized peak solar irradiance, used as $1 kW(pk)/m^2$. The factor 0.11 represents the "capacity factor".

Thus, annual energy outputs from a square meter of solar cells of 110.9, 144.6, and 115.7 $kWh/m^2.y$ are obtained for 1978, 1982, and 1986 respectively.

It is also to be observed that, since the energy recovery from solar cells is in the form of electrical energy, it is appropriate to convert those energy expenditures which occur in the form of heat of combustion, to equivalent electrical energy by applying the average efficiency of 0.30 experienced by the electric utilities in the conversion from heat of combustion of fuels to electric power delivered to the consumer[5].

3. Energy Consumption in Photovoltaic Solar Array Manufacturing Process Sequences

3.1 Data Sources.

The major sources of information for this energy analysis were data accumulated from LSA project reports and industry interviews. The energy consumed through materials, both direct and indirect materials, was obtained by converting the material consumption to energy units through multiplication with the material energy contents shown in Table V-1. Where specific information to the contrary was not available, the material energy values were assumed to be in the form of thermal energy. The equipment costs, were converted to energy units expressed on the basis of unit cell area of throughput, by assuming a lifetime of seven years, and an energy content of the equipment which corresponds in value to 2% of the equipment cost.[6] This energy cost has then been converted to a thermal energy using an energy price of $0.003/kWh(th)[7]. Finally, the general energy usage for operating the facility was derived from the machine floor area by using the annual SAMICS utility cost of $3.74/ft^2[8] and assuming that all of this "indirect" energy, since it is used primarily for lighting, air conditioning, and ventilating, in view of the high heat load in the building, is in the form of electricity at a cost of $0.0319/kWh[8]. The conversion factors for the equipment and facility energies thus become 0.9523 kWh(th)/$y and 1262 kWh/m^{2}y, respectively.

Table V-1

Energy Contents of Selected Materials

Material	Original Units	Convenient Units (Thermal kWh's)	Reference
1. Acetic acid	3.28 lb of hi-press. steam plus 0.07 kWh(eℓ)/lb	3.18 kWh/g	1
2. Aluminum (Aℓ)	520x10^6 kWh(th)/ton	0.17 kWh/g	2
3. Ammonia gas (NH_3)	8.05x10^3 Btu/lb	0.00534 kWh/g	3
4. Ammonium Hydroxide 30% (NH_4OH)	-	1.32 kWh/ℓ	4
5. Argon gas	1,100 Btu/lb	1.27x10^{-3} kWh/ℓ	5
6. Butyl acetate	4.32 lb of low-press. steam plus 0.082 kWh(eℓ)/lb	3.21 kWh/g	6
7. Copper (Cu)	16.2x10^6 Btu/ton	5.23 kWh/g	7
8. Energy for exhausting waste fumes without scrubbing.	0.46 kW/1000 ft^3/min	2.56x10^{-2} kWh/ 1000 ft^3	8
9. Freon-14 gas (CF_4)	-	2x10^{-3} kWh/ℓ	9
10. Hydrogen gas	43,300 Btu/lb	2.51x10^{-3} kWh/ℓ	5
11. HF (48%)	7,000 Btu/lb	5.22 kWh/ℓ	5
12. Nitrogen (liquid)	1,330 Btu/lb	0.69 KWh/ℓ	5
13. Nitrogen (gas from liquid)	-	1.44x10^{-3} kWh/ℓ	10
14. Nitric Acid (HNO_3, 67%)	14,500 Btu/lb	13.12 kWh/ℓ	5
15. Oxygen gas (O_2)	830 Btu/lb	7.66 kWh/ℓ	5
16. Phosphorus (solid)	23,790 Btu/lb	1.54x10^{-2} kWh/g	5
17. Phosphine gas (PH_3)	-	0.18 kWh/ℓ	11
18. Phosphorous oxychloride ($POC\ell_3$)	-	0.14 kWh/g	12
19. Plating resist	8,000 Btu/lb	5.20 kWh/ℓ	13
20. Silver	1260x10^6 Btu/ton	0.406 kWh/g	8
21. Sodium Hydroxide (NaOH)	by-product	0	5
22. Toluene	0.05 lb of low-press. steam plus 0.025 kWh(eℓ)/lb	0.0349 kWh/mℓ	14
23. Vacuum pump oil	3,000 kWh(th)/ barrel	18.87 kWh/ℓ	15
24. Wax	2,000 kWh/barrel	1.3x10^{-2} kWh/g	16

References for Table V-1

1. Assumed to be the same as that of acetone, which was taken from "Battelle Columbus Laboratories, Draft Target and Support Document for Developing a Maximum Energy Efficient Improvement Target for SIC 28", Federal Energy Administration, Washington, DC (1976).

2. J.T. Reding and B.P. Shepherd, "Energy Consumption, Report EPA-G50/2-75-032b", US Environmental Protection Agency, Washington, DC (4/75).

3. Federal Energy Administration, "Project Independence Blueprint," Vol. 3, Federal Energy Administration, Washington, DC (1974).

4. Calculated from the energy content for NH_3 and using a density of 0.824 g/mℓ for the NH_4OH solution.

5. Battelle Columbus Laboratories,"Draft Target and Support Document for Developing a Maximum Energy Efficient Improvement Target for SIC 28", Federal Energy Administration, Washington, DC (1976).

6. Assumed to be the same as that of butyl alcohol, as given in Ref.5.

7. H.W. Lownie, et al (Battelle Columbus Laboratories), "Draft Target Report on Development and Establishment of Energy Efficiency Improvement Targets for Primary Metal Industries," Federal Energy Administration, Washington, DC (9/76).

8. M.G. Coleman, et al., Motorola Final Report, DOE/JPL-954847-78/4, 183(11/78).

9. Estimated as approximately 50% more than the average energy content of commercial gases, as given in Ref. 5.

10. Calculated from the energy content for LN_2 assuming 480 ℓ of gas can be obtained from 1ℓ of LN_2.

11. Estimated as twice the energy content for P(s) plus $3/2H_2(g)$.

12. Estimated as twice the energy content of P(s), plus $\frac{1}{2}O_2(g)$, plus $\frac{3}{2}Cl_2(g)$. The energy content of Cl_2 was taken from ref. 5.

13. Assumed to be the same as that of wood rosin, as given in Ref. 5.

14. Taken as that of benzene, as given in ref. 5.

15. Taken as approximately twice the energy content of middle oil distillates.

16. From M. Sittig, Practical Techniques for Saving Energy in the Chemical Petroleum and Metals Industries, Noyes Data Corporation, Park Ridge, NJ (1977), and using a density of 0.97 g/ml for the wax.

3.2 Energy Consumption in Si reduction and purification.

This process group starts with the reduction of SiO_2 in an arc furnace. This is a quite efficient and cost-effective process which is not very likely to be replaced by another approach. In contrast, the following step of Si purification is very inefficient and likely to be replaced by one of several alternate methods under development. Furthest advanced among these is the SiH_4 purification process being prepared for pilot line operations by Union Carbide Corp. It can be expected to be a production process by 1986.

a) Theoretical Material Balance for the Arc Furnace Process.

The chemical reaction of this process is:

	SiO_2	+ 2C	→ Si +	2 CO
Atomic Weights:	28 + 2(16)	+ 2(12)	→ 28 +	2(12 + 16)
	60	+ 24	→ 28 +	56
Masses, normalized to 1 kg Si out:	2.14 kg	+ 0.86 kg	→ 1 kg +	2 kg

According to Dow-Corning [9], the industrially experienced and actual conversion efficiency of SiO_2 to Si is 80%. The required input is thus: 2.68 kg SiO_2 for 1 kg Si out (Dow-Corning shows 2.71 kg SiO_2).

It is assumed that half of the lost SiO_2 input, or 0.27 kg, is used in the reaction:

	SiO_2	+ C	→ SiO	+ CO
Atomic Weights:	60	+ 12	→ 44	+ 28
	0.27 kg	+ 0.05 kg	→ 0.2 kg	+ 0.12 kg

where the SiO is lost at the top of the furnace.
Thus, the total theoretical carbon input would be 0.91 kg C per 1 kg MG-Si output.

2. Energy Payback Times

To calculate payback times for photovoltaic systems, the annual energy output of a unit module area must be known. This power output, for photovoltaic systems, is dependent upon the encapsulated cell efficiency, the module packing factor, the solar insolation, the efficiency of the power conditioning and storage subsystems, and the mismatch of the energy availability and demand statistics. This list of dependencies makes it clear that the output of the module will vary according to climate at the locality of installation, and to the individual load to be satisfied. The factors of influence on the useful system output, outside of the cell efficiency, are combined into the "capacity factor". As a reasonably representative, not too optimistic value for this capacity factor, the number 0.11 has been used, in consequence of the results of several system studies.[4] The capacity factor is essentially independent of the solar cell or module manufacturing process. Consequently, the energy payback time is only partly a function of the energy consumption for the solar module fabrication process, since the other system parameters strongly influence its absolute magnitude. In the calculations of energy payback times, encapsulated cell efficiencies η of 11.5% and 15% were employed for 1978 and 1982 and for 1986, respectively, assuming the use of EFG ribbons, of 12%. To obtain the energy payback times, the annual module output was calculated as $E = \eta \times 8766 \times 0.11 \times H_{pk}$, H_{pk} being the standardized peak solar irradiance, used as $1kW(pk)/m^2$. The factor 0.11 represents the "capacity factor".

2. Energy Payback Times

To calculate payback times for photovoltaic systems, the annual energy output of a unit module area must be known. This power output, for photovoltaic systems, is dependent upon the encapsulated cell efficiency, the module packing factor, the solar insolation, the efficiency of the power conditioning and storage subsystems, and the mismatch of the energy availability and demand statistics. This list of dependencies makes it clear that the output of the module will vary according to climate at the locality of installation, and to the individual load to be satisfied. The factors of influence on the useful system output, outside of the cell efficiency, are combined into the "capacity factor". As a reasonably representative, not too optimistic value for this capacity factor, the number 0.11 has been used, in consequence of the results of several system studies.[4] The capacity factor is essentially independent of the solar cell or module manufacturing process. Consequently, the energy payback time is only partly a function of the energy consumption for the solar module fabrication process, since the other system parameters strongly influence its absolute magnitude. In the calculations of energy payback times, encapsulated cell efficiencies η of 11.5% and 15% were employed for 1978 and 1982 and for 1986, respectively, assuming the use of EFG ribbons, of 12%. To obtain the energy payback times, the annual module output was calculated as $E = \eta \times 8766 \times 0.11 \times H_{pk}$, H_{pk} being the standardized peak solar irradiance, used as $1kW(pk)/m^2$. The factor 0.11 represents the "capacity factor".

Thus, annual energy outputs from a square meter of solar cells of 110.9, 144.6, and 115.7 $kWh/m^2.y$ are obtained for 1978, 1982, and 1986 respectively.

It is also to be observed that, since the energy recovery from solar cells is in the form of electrical energy, it is appropriate to convert those energy expenditures which occur in the form of heat of combustion, to equivalent electrical energy by applying the average efficiency of 0.30 experienced by the electric utilities in the conversion from heat of combustion of fuels to electric power delivered to the consumer[5].

3. Energy Consumption in Photovoltaic Solar Array Manufacturing Process Sequences

3.1 Data Sources.

The major sources of information for this energy analysis were data accumulated from LSA project reports and industry interviews. The energy consumed through materials, both direct and indirect materials, was obtained by converting the material consumption to energy units through multiplication with the material energy contents shown in Table V-1. Where specific information to the contrary was not available, the material energy values were assumed to be in the form of thermal energy. The equipment costs, were converted to energy units expressed on the basis of unit cell area of throughput, by assuming a lifetime of seven years, and an energy content of the equipment which corresponds in value to 2% of the equipment cost.[6] This energy cost has then been converted to a thermal energy using an energy price of $0.003/kWh(th)[7]. Finally, the general energy usage for operating the facility was derived from the machine floor area by using the annual SAMICS utility cost of $3.74/ft^2[8] and assuming that all of this "indirect" energy, since it is used primarily for lighting, air conditioning, and ventilating, in view of the high heat load in the building, is in the form of electricity at a cost of $0.0319/kWh[8]. The conversion factors for the equipment and facility energies thus become 0.9523 kWh(th)/$y and 1262 kWh/m^{2}y, respectively.

15. Taken as approximately twice the energy content of middle oil distillates.

16. From M. Sittig, Practical Techniques for Saving Energy in the Chemical Petroleum and Metals Industries, Noyes Data Corporation, Park Ridge, NJ (1977), and using a density of 0.97 g/ml for the wax.

3.2 Energy Consumption in Si reduction and purification.

This process group starts with the reduction of SiO_2 in an arc furnace. This is a quite efficient and cost-effective process which is not very likely to be replaced by another approach. In contrast, the following step of Si purification is very inefficient and likely to be replaced by one of several alternate methods under development. Furthest advanced among these is the SiH_4 purification process being prepared for pilot line operations by Union Carbide Corp. It can be expected to be a production process by 1986.

a) Theoretical Material Balance for the Arc Furnace Process.

The chemical reaction of this process is:

	SiO_2	+ 2C	→ Si +	2 CO
Atomic Weights:	28 + 2(16)	+ 2(12)	→ 28 +	2(12 + 16)
	60	+ 24	→ 28 +	56
Masses, normalized to 1 kg Si out:	2.14 kg	+ 0.86 kg	→ 1 kg +	2 kg

According to Dow-Corning [9], the industrially experienced and actual conversion efficiency of SiO_2 to Si is 80%. The required input is thus: 2.68 kg SiO_2 for 1 kg Si out (Dow-Corning shows 2.71 kg SiO_2).

It is assumed that half of the lost SiO_2 input, or 0.27 kg, is used in the reaction:

	SiO_2	+ C	→ SiO	+ CO
Atomic Weights:	60	+ 12	→ 44	+ 28
	0.27 kg	+ 0.05 kg	→ 0.2 kg	+ 0.12 kg

where the SiO is lost at the top of the furnace.
Thus, the total theoretical carbon input would be 0.91 kg C per 1 kg MG-Si output.

2. Energy Payback Times

To calculate payback times for photovoltaic systems, the annual energy output of a unit module area must be known. This power output, for photovoltaic systems, is dependent upon the encapsulated cell efficiency, the module packing factor, the solar insolation, the efficiency of the power conditioning and storage subsystems, and the mismatch of the energy availability and demand statistics. This list of dependencies makes it clear that the output of the module will vary according to climate at the locality of installation, and to the individual load to be satisfied. The factors of influence on the useful system output, outside of the cell efficiency, are combined into the "capacity factor". As a reasonably representative, not too optimistic value for this capacity factor, the number 0.11 has been used, in consequence of the results of several system studies.[4] The capacity factor is essentially independent of the solar cell or module manufacturing process. Consequently, the energy payback time is only partly a function of the energy consumption for the solar module fabrication process, since the other system parameters strongly influence its absolute magnitude. In the calculations of energy payback times, encapsulated cell efficiencies η of 11.5% and 15% were employed for 1978 and 1982 and for 1986, respectively, assuming the use of EFG ribbons, of 12%. To obtain the energy payback times, the annual module output was calculated as $E = \eta \times 8766 \times 0.11 \times H_{pk}$, H_{pk} being the standardized peak solar irradiance, used as $1kW(pk)/m^2$. The factor 0.11 represents the "capacity factor".

2. Energy Payback Times

To calculate payback times for photovoltaic systems, the annual energy output of a unit module area must be known. This power output, for photovoltaic systems, is dependent upon the encapsulated cell efficiency, the module packing factor, the solar insolation, the efficiency of the power conditioning and storage subsystems, and the mismatch of the energy availability and demand statistics. This list of dependencies makes it clear that the output of the module will vary according to climate at the locality of installation, and to the individual load to be satisfied. The factors of influence on the useful system output, outside of the cell efficiency, are combined into the "capacity factor". As a reasonably representative, not too optimistic value for this capacity factor, the number 0.11 has been used, in consequence of the results of several system studies.[4] The capacity factor is essentially independent of the solar cell or module manufacturing process. Consequently, the energy payback time is only partly a function of the energy consumption for the solar module fabrication process, since the other system parameters strongly influence its absolute magnitude. In the calculations of energy payback times, encapsulated cell efficiencies η of 11.5% and 15% were employed for 1978 and 1982 and for 1986, respectively, assuming the use of EFG ribbons, of 12%. To obtain the energy payback times, the annual module output was calculated as $E = \eta \times 8766 \times 0.11 \times H_{pk}$, H_{pk} being the standardized peak solar irradiance, used as $1kW(pk)/m^2$. The factor 0.11 represents the "capacity factor".

Thus, annual energy outputs from a square meter of solar cells of 110.9, 144.6, and 115.7 $kWh/m^2.y$ are obtained for 1978, 1982, and 1986 respectively.

It is also to be observed that, since the energy recovery from solar cells is in the form of electrical energy, it is appropriate to convert those energy expenditures which occur in the form of heat of combustion, to equivalent electrical energy by applying the average efficiency of 0.30 experienced by the electric utilities in the conversion from heat of combustion of fuels to electric power delivered to the consumer[5].

3. Energy Consumption in Photovoltaic Solar Array Manufacturing Process Sequences

3.1 Data Sources.

The major sources of information for this energy analysis were data accumulated from LSA project reports and industry interviews. The energy consumed through materials, both direct and indirect materials, was obtained by converting the material consumption to energy units through multiplication with the material energy contents shown in Table V-1. Where specific information to the contrary was not available, the material energy values were assumed to be in the form of thermal energy. The equipment costs, were converted to energy units expressed on the basis of unit cell area of throughput, by assuming a lifetime of seven years, and an energy content of the equipment which corresponds in value to 2% of the equipment cost.[6] This energy cost has then been converted to a thermal energy using an energy price of $0.003/kWh(th)[7]. Finally, the general energy usage for operating the facility was derived from the machine floor area by using the annual SAMICS utility cost of $3.74/ft^2[8] and assuming that all of this "indirect" energy, since it is used primarily for lighting, air conditioning, and ventilating, in view of the high heat load in the building, is in the form of electricity at a cost of $0.0319/kWh[8]. The conversion factors for the equipment and facility energies thus become 0.9523 kWh(th)/$y and 1262 kWh/m^{2}y, respectively.

Table V-1

Energy Contents of Selected Materials

Material	Original Units	Convenient Units (Thermal kWh's)	Reference
1. Acetic acid	3.28 lb of hi-press. steam plus 0.07 kWh(eℓ)/lb	3.18 kWh/g	1
2. Aluminum (Aℓ)	520×10^6 kWh(th)/ton	0.17 kWh/g	2
3. Ammonia gas (NH_3)	8.05×10^3 Btu/lb	0.00534 kWh/g	3
4. Ammonium Hydroxide 30% (NH_4OH)	-	1.32 kWh/ℓ	4
5. Argon gas	1,100 Btu/lb	1.27×10^{-3} kWh/ℓ	5
6. Butyl acetate	4.32 lb of low-press. steam plus 0.082 kWh(eℓ)/lb	3.21 kWh/g	6
7. Copper (Cu)	16.2×10^6 Btu/ton	5.23 kWh/g	7
8. Energy for exhausting waste fumes without scrubbing.	0.46 kW/1000 ft^3/min	2.56×10^{-2} kWh/ 1000 ft^3	8
9. Freon-14 gas (CF_4)	-	2×10^{-3} kWh/ℓ	9
10. Hydrogen gas	43,300 Btu/lb	2.51×10^{-3} kWh/ℓ	5
11. HF (48%)	7,000 Btu/lb	5.22 kWh/ℓ	5
12. Nitrogen (liquid)	1,330 Btu/lb	0.69 KWh/ℓ	5
13. Nitrogen (gas from liquid)	-	1.44×10^{-3} kWh/ℓ	10
14. Nitric Acid (HNO_3, 67%)	14,500 Btu/lb	13.12 kWh/ℓ	5
15. Oxygen gas (O_2)	830 Btu/lb	7.66 kWh/ℓ	5
16. Phosphorus (solid)	23,790 Btu/lb	1.54×10^{-2} kWh/g	5
17. Phosphine gas (PH_3)	-	0.18 kWh/ℓ	11
18. Phosphorous oxychloride ($POC\ell_3$)	-	0.14 kWh/g	12
19. Plating resist	8,000 Btu/lb	5.20 kWh/ℓ	13
20. Silver	1260×10^6 Btu/ton	0.406 kWh/g	8
21. Sodium Hydroxide (NaOH)	by-product	0	5
22. Toluene	0.05 lb of low-press. steam plus 0.025 kWh(eℓ)/lb	0.0349 kWh/mℓ	14
23. Vacuum pump oil	3,000 kWh(th)/ barrel	18.87 kWh/ℓ	15
24. Wax	2,000 kWh/barrel	1.3×10^{-2} kWh/g	16

Table V-1

Energy Contents of Selected Materials

Material	Original Units	Convenient Units (Thermal kWh's)	Reference
1. Acetic acid	3.28 lb of hi-press. steam plus 0.07 kWh(eℓ)/lb	3.18 kWh/g	1
2. Aluminum (Aℓ)	520×10^6 kWh(th)/ton	0.17 kWh/g	2
3. Ammonia gas (NH_3)	8.05×10^3 Btu/lb	0.00534 kWh/g	3
4. Ammonium Hydroxide 30% (NH_4OH)	-	1.32 kWh/ℓ	4
5. Argon gas	1,100 Btu/lb	1.27×10^{-3} kWh/ℓ	5
6. Butyl acetate	4.32 lb of low-press. steam plus 0.082 kWh(eℓ)/lb	3.21 kWh/g	6
7. Copper (Cu)	16.2×10^6 Btu/ton	5.23 kWh/g	7
8. Energy for exhausting waste fumes without scrubbing.	0.46 kW/1000 ft^3/min	2.56×10^{-2} kWh/ 1000 ft^3	8
9. Freon-14 gas (CF_4)	-	2×10^{-3} kWh/ℓ	9
10. Hydrogen gas	43,300 Btu/lb	2.51×10^{-3} kWh/ℓ	5
11. HF (48%)	7,000 Btu/lb	5.22 kWh/ℓ	5
12. Nitrogen (liquid)	1,330 Btu/lb	0.69 KWh/ℓ	5
13. Nitrogen (gas from liquid)	-	1.44×10^{-3} kWh/ℓ	10
14. Nitric Acid (HNO_3, 67%)	14,500 Btu/lb	13.12 kWh/ℓ	5
15. Oxygen gas (O_2)	830 Btu/lb	7.66 kWh/ℓ	5
16. Phosphorus (solid)	23,790 Btu/lb	1.54×10^{-2} kWh/g	5
17. Phosphine gas (PH_3)	-	0.18 kWh/ℓ	11
18. Phosphorous oxychloride ($POC\ell_3$)	-	0.14 kWh/g	12
19. Plating resist	8,000 Btu/lb	5.20 kWh/ℓ	13
20. Silver	1260×10^6 Btu/ton	0.406 kWh/g	8
21. Sodium Hydroxide (NaOH)	by-product	0	5
22. Toluene	0.05 lb of low-press. steam plus 0.025 kWh(eℓ)/lb	0.0349 kWh/mℓ	14
23. Vacuum pump oil	3,000 kWh(th)/ barrel	18.87 kWh/ℓ	15
24. Wax	2,000 kWh/barrel	1.3×10^{-2} kWh/g	16

References for Table V-1

1. Assumed to be the same as that of acetone, which was taken from "Battelle Columbus Laboratories, Draft Target and Support Document for Developing a Maximum Energy Efficient Improvement Target for SIC 28", Federal Energy Administration, Washington, DC (1976).

2. J.T. Reding and B.P. Shepherd, "Energy Consumption, Report EPA-G50/2-75-032b", US Environmental Protection Agency, Washington, DC (4/75).

3. Federal Energy Administration, "Project Independence Blueprint," Vol. 3, Federal Energy Administration, Washington, DC (1974).

4. Calculated from the energy content for NH_3 and using a density of 0.824 g/mℓ for the NH_4OH solution.

5. Battelle Columbus Laboratories,"Draft Target and Support Document for Developing a Maximum Energy Efficient Improvement Target for SIC 28", Federal Energy Administration, Washington, DC (1976).

6. Assumed to be the same as that of butyl alcohol, as given in Ref. 5.

7. H.W. Lownie, et al (Battelle Columbus Laboratories), "Draft Target Report on Development and Establishment of Energy Efficiency Improvement Targets for Primary Metal Industries," Federal Energy Administration, Washington, DC (9/76).

8. M.G. Coleman, et al., Motorola Final Report, DOE/JPL-954847-78/4, 183(11/78).

9. Estimated as approximately 50% more than the average energy content of commercial gases, as given in Ref. 5.

10. Calculated from the energy content for LN_2 assuming 480 ℓ of gas can be obtained from 1ℓ of LN_2.

11. Estimated as twice the energy content for P(s) plus $3/2H_2(g)$.

12. Estimated as twice the energy content of P(s), plus $\frac{1}{2}O_2(g)$, plus $\frac{3}{2}Cl_2(g)$. The energy content of Cl_2 was taken from ref. 5.

13. Assumed to be the same as that of wood rosin, as given in Ref. 5.

14. Taken as that of benzene, as given in ref. 5.

15. Taken as approximately twice the energy content of middle oil distillates.

16. From M. Sittig, Practical Techniques for Saving Energy in the Chemical Petroleum and Metals Industries, Noyes Data Corporation, Park Ridge, NJ (1977), and using a density of 0.97 g/ml for the wax.

3.2 Energy Consumption in Si reduction and purification.

This process group starts with the reduction of SiO_2 in an arc furnace. This is a quite efficient and cost-effective process which is not very likely to be replaced by another approach. In contrast, the following step of Si purification is very inefficient and likely to be replaced by one of several alternate methods under development. Furthest advanced among these is the SiH_4 purification process being prepared for pilot line operations by Union Carbide Corp. It can be expected to be a production process by 1986.

a) Theoretical Material Balance for the Arc Furnace Process.

The chemical reaction of this process is:

	SiO_2	+ 2C	→ Si +	2 CO
Atomic Weights:	28 + 2(16)	+ 2(12)	→ 28 +	2(12 + 16)
	60	+ 24	→ 28 +	56
Masses, normalized to 1 kg Si out:	2.14 kg	+ 0.86 kg	→ 1 kg +	2 kg

According to Dow-Corning [9], the industrially experienced and actual conversion efficiency of SiO_2 to Si is 80%. The required input is thus: 2.68 kg SiO_2 for 1 kg Si out (Dow-Corning shows 2.71 kg SiO_2).

It is assumed that half of the lost SiO_2 input, or 0.27 kg, is used in the reaction:

	SiO_2	+ C	→ SiO	+ CO
Atomic Weights:	60	+ 12	→ 44	+ 28
	0.27 kg	+ 0.05 kg	→ 0.2 kg	+ 0.12 kg

where the SiO is lost at the top of the furnace.
Thus, the total theoretical carbon input would be 0.91 kg C per 1 kg MG-Si output.

2. Energy Payback Times

To calculate payback times for photovoltaic systems, the annual energy output of a unit module area must be known. This power output, for photovoltaic systems, is dependent upon the encapsulated cell efficiency, the module packing factor, the solar insolation, the efficiency of the power conditioning and storage subsystems, and the mismatch of the energy availability and demand statistics. This list of dependencies makes it clear that the output of the module will vary according to climate at the locality of installation, and to the individual load to be satisfied. The factors of influence on the useful system output, outside of the cell efficiency, are combined into the "capacity factor". As a reasonably representative, not too optimistic value for this capacity factor, the number 0.11 has been used, in consequence of the results of several system studies.[4] The capacity factor is essentially independent of the solar cell or module manufacturing process. Consequently, the energy payback time is only partly a function of the energy consumption for the solar module fabrication process, since the other system parameters strongly influence its absolute magnitude. In the calculations of energy payback times, encapsulated cell efficiencies η of 11.5% and 15% were employed for 1978 and 1982 and for 1986, respectively, assuming the use of EFG ribbons, of 12%. To obtain the energy payback times, the annual module output was calculated as $E = \eta \times 8766 \times 0.11 \times H_{pk}$, H_{pk} being the standardized peak solar irradiance, used as $1kW(pk)/m^2$. The factor 0.11 represents the "capacity factor".

Thus, annual energy outputs from a square meter of solar cells of 110.9, 144.6, and 115.7 $kWh/m^2.y$ are obtained for 1978, 1982, and 1986 respectively.

It is also to be observed that, since the energy recovery from solar cells is in the form of electrical energy, it is appropriate to convert those energy expenditures which occur in the form of heat of combustion, to equivalent electrical energy by applying the average efficiency of 0.30 experienced by the electric utilities in the conversion from heat of combustion of fuels to electric power delivered to the consumer[5].

3. Energy Consumption in Photovoltaic Solar Array Manufacturing Process Sequences

3.1 Data Sources.

The major sources of information for this energy analysis were data accumulated from LSA project reports and industry interviews. The energy consumed through materials, both direct and indirect materials, was obtained by converting the material consumption to energy units through multiplication with the material energy contents shown in Table V-1. Where specific information to the contrary was not available, the material energy values were assumed to be in the form of thermal energy. The equipment costs, were converted to energy units expressed on the basis of unit cell area of throughput, by assuming a lifetime of seven years, and an energy content of the equipment which corresponds in value to 2% of the equipment cost.[6] This energy cost has then been converted to a thermal energy using an energy price of $0.003/kWh(th)[7]. Finally, the general energy usage for operating the facility was derived from the machine floor area by using the annual SAMICS utility cost of $3.74/ft^2[8] and assuming that all of this "indirect" energy, since it is used primarily for lighting, air conditioning, and ventilating, in view of the high heat load in the building, is in the form of electricity at a cost of $0.0319/kWh[8]. The conversion factors for the equipment and facility energies thus become 0.9523 kWh(th)/$y and 1262 kWh/m^{2}y, respectively.

Table V-1

Energy Contents of Selected Materials

Material	Original Units	Convenient Units (Thermal kWh's)	Reference
1. Acetic acid	3.28 lb of hi-press. steam plus 0.07 kWh(eℓ)/lb	3.18 kWh/g	1
2. Aluminum (Aℓ)	520×10^6 kWh(th)/ton	0.17 kWh/g	2
3. Ammonia gas (NH_3)	8.05×10^3 Btu/lb	0.00534 kWh/g	3
4. Ammonium Hydroxide 30% (NH_4OH)	-	1.32 kWh/ℓ	4
5. Argon gas	1,100 Btu/lb	1.27×10^{-3} kWh/ℓ	5
6. Butyl acetate	4.32 lb of low-press. steam plus 0.082 kWh(eℓ)/lb	3.21 kWh/g	6
7. Copper (Cu)	16.2×10^6 Btu/ton	5.23 kWh/g	7
8. Energy for exhausting waste fumes without scrubbing.	0.46 kW/1000 ft^3/min	2.56×10^{-2} kWh/ 1000 ft^3	8
9. Freon-14 gas (CF_4)	-	2×10^{-3} kWh/ℓ	9
10. Hydrogen gas	43,300 Btu/lb	2.51×10^{-3} kWh/ℓ	5
11. HF (48%)	7,000 Btu/lb	5.22 kWh/ℓ	5
12. Nitrogen (liquid)	1,330 Btu/lb	0.69 KWh/ℓ	5
13. Nitrogen (gas from liquid)	-	1.44×10^{-3} kWh/ℓ	10
14. Nitric Acid (HNO_3, 67%)	14,500 Btu/lb	13.12 kWh/ℓ	5
15. Oxygen gas (O_2)	830 Btu/lb	7.66 kWh/ℓ	5
16. Phosphorus (solid)	23,790 Btu/lb	1.54×10^{-2} kWh/g	5
17. Phosphine gas (PH_3)	-	0.18 kWh/ℓ	11
18. Phosphorous oxychloride ($POC\ell_3$)	-	0.14 kWh/g	12
19. Plating resist	8,000 Btu/lb	5.20 kWh/ℓ	13
20. Silver	1260×10^6 Btu/ton	0.406 kWh/g	8
21. Sodium Hydroxide (NaOH)	by-product	0	5
22. Toluene	0.05 lb of low-press. steam plus 0.025 kWh(eℓ)/lb	0.0349 kWh/mℓ	14
23. Vacuum pump oil	3,000 kWh(th)/ barrel	18.87 kWh/ℓ	15
24. Wax	2,000 kWh/barrel	1.3×10^{-2} kWh/g	16

2. Energy Payback Times

To calculate payback times for photovoltaic systems, the annual energy output of a unit module area must be known. This power output, for photovoltaic systems, is dependent upon the encapsulated cell efficiency, the module packing factor, the solar insolation, the efficiency of the power conditioning and storage subsystems, and the mismatch of the energy availability and demand statistics. This list of dependencies makes it clear that the output of the module will vary according to climate at the locality of installation, and to the individual load to be satisfied. The factors of influence on the useful system output, outside of the cell efficiency, are combined into the "capacity factor". As a reasonably representative, not too optimistic value for this capacity factor, the number 0.11 has been used, in consequence of the results of several system studies.[4] The capacity factor is essentially independent of the solar cell or module manufacturing process. Consequently, the energy payback time is only partly a function of the energy consumption for the solar module fabrication process, since the other system parameters strongly influence its absolute magnitude. In the calculations of energy payback times, encapsulated cell efficiencies η of 11.5% and 15% were employed for 1978 and 1982 and for 1986, respectively, assuming the use of EFG ribbons, of 12%. To obtain the energy payback times, the annual module output was calculated as $E = \eta \times 8766 \times 0.11 \times H_{pk}$, H_{pk} being the standardized peak solar irradiance, used as $1kW(pk)/m^2$. The factor 0.11 represents the "capacity factor".

Thus, annual energy outputs from a square meter of solar cells of 110.9, 144.6, and 115.7 $kWh/m^2.y$ are obtained for 1978, 1982, and 1986 respectively.

It is also to be observed that, since the energy recovery from solar cells is in the form of electrical energy, it is appropriate to convert those energy expenditures which occur in the form of heat of combustion, to equivalent electrical energy by applying the average efficiency of 0.30 experienced by the electric utilities in the conversion from heat of combustion of fuels to electric power delivered to the consumer[5].

3. Energy Consumption in Photovoltaic Solar Array Manufacturing Process Sequences

3.1 Data Sources.

The major sources of information for this energy analysis were data accumulated from LSA project reports and industry interviews. The energy consumed through materials, both direct and indirect materials, was obtained by converting the material consumption to energy units through multiplication with the material energy contents shown in Table V-1. Where specific information to the contrary was not available, the material energy values were assumed to be in the form of thermal energy. The equipment costs, were converted to energy units expressed on the basis of unit cell area of throughput, by assuming a lifetime of seven years, and an energy content of the equipment which corresponds in value to 2% of the equipment cost.[6] This energy cost has then been converted to a thermal energy using an energy price of $0.003/kWh(th)[7]. Finally, the general energy usage for operating the facility was derived from the machine floor area by using the annual SAMICS utility cost of $3.74/ft^2[8] and assuming that all of this "indirect" energy, since it is used primarily for lighting, air conditioning, and ventilating, in view of the high heat load in the building, is in the form of electricity at a cost of $0.0319/kWh[8]. The conversion factors for the equipment and facility energies thus become 0.9523 kWh(th)/$y and 1262 kWh/m^{2}y, respectively.

Table V-1

Energy Contents of Selected Materials

Material	Original Units	Convenient Units (Thermal kWh's)	Reference
1. Acetic acid	3.28 lb of hi-press. steam plus 0.07 kWh(eℓ)/lb	3.18 kWh/g	1
2. Aluminum (Aℓ)	520×10^6 kWh(th)/ton	0.17 kWh/g	2
3. Ammonia gas (NH_3)	8.05×10^3 Btu/lb	0.00534 kWh/g	3
4. Ammonium Hydroxide 30% (NH_4OH)	-	1.32 kWh/ℓ	4
5. Argon gas	1,100 Btu/lb	1.27×10^{-3} kWh/ℓ	5
6. Butyl acetate	4.32 lb of low-press. steam plus 0.082 kWh(eℓ)/lb	3.21 kWh/g	6
7. Copper (Cu)	16.2×10^6 Btu/ton	5.23 kWh/g	7
8. Energy for exhausting waste fumes without scrubbing.	0.46 kW/1000 ft^3/min	2.56×10^{-2} kWh/ 1000 ft^3	8
9. Freon-14 gas (CF_4)	-	2×10^{-3} kWh/ℓ	9
10. Hydrogen gas	43,300 Btu/lb	2.51×10^{-3} kWh/ℓ	5
11. HF (48%)	7,000 Btu/lb	5.22 kWh/ℓ	5
12. Nitrogen (liquid)	1,330 Btu/lb	0.69 KWh/ℓ	5
13. Nitrogen (gas from liquid)	-	1.44×10^{-3} kWh/ℓ	10
14. Nitric Acid (HNO_3, 67%)	14,500 Btu/lb	13.12 kWh/ℓ	5
15. Oxygen gas (O_2)	830 Btu/lb	7.66 kWh/ℓ	5
16. Phosphorus (solid)	23,790 Btu/lb	1.54×10^{-2} kWh/g	5
17. Phosphine gas (PH_3)	-	0.18 kWh/ℓ	11
18. Phosphorous oxychloride ($POC\ell_3$)	-	0.14 kWh/g	12
19. Plating resist	8,000 Btu/lb	5.20 kWh/ℓ	13
20. Silver	1260×10^6 Btu/ton	0.406 kWh/g	8
21. Sodium Hydroxide (NaOH)	by-product	0	5
22. Toluene	0.05 lb of low-press. steam plus 0.025 kWh(eℓ)/lb	0.0349 kWh/mℓ	14
23. Vacuum pump oil	3,000 kWh(th)/ barrel	18.87 kWh/ℓ	15
24. Wax	2,000 kWh/barrel	1.3×10^{-2} kWh/g	16

References for Table V-1

1. Assumed to be the same as that of acetone, which was taken from "Battelle Columbus Laboratories, Draft Target and Support Document for Developing a Maximum Energy Efficient Improvement Target for SIC 28", Federal Energy Administration, Washington, DC (1976).

2. J.T. Reding and B.P. Shepherd, "Energy Consumption, Report EPA-G50/2-75-032b", US Environmental Protection Agency, Washington, DC (4/75).

3. Federal Energy Administration, "Project Independence Blueprint," Vol. 3, Federal Energy Administration, Washington, DC (1974).

4. Calculated from the energy content for NH_3 and using a density of 0.824 g/mℓ for the NH_4OH solution.

5. Battelle Columbus Laboratories,"Draft Target and Support Document for Developing a Maximum Energy Efficient Improvement Target for SIC 28", Federal Energy Administration, Washington, DC (1976).

6. Assumed to be the same as that of butyl alcohol, as given in Ref. 5.

7. H.W. Lownie, et al (Battelle Columbus Laboratories), "Draft Target Report on Development and Establishment of Energy Efficiency Improvement Targets for Primary Metal Industries," Federal Energy Administration, Washington, DC (9/76).

8. M.G. Coleman, et al., Motorola Final Report, DOE/JPL-954847-78/4, 183(11/78).

9. Estimated as approximately 50% more than the average energy content of commercial gases, as given in Ref. 5.

10. Calculated from the energy content for LN_2 assuming 480 ℓ of gas can be obtained from 1ℓ of LN_2.

11. Estimated as twice the energy content for P(s) plus $3/2H_2(g)$.

12. Estimated as twice the energy content of P(s), plus $\frac{1}{2}O_2(g)$, plus $\frac{3}{2}Cl_2(g)$. The energy content of Cl_2 was taken from ref. 5.

13. Assumed to be the same as that of wood rosin, as given in Ref. 5.

14. Taken as that of benzene, as given in ref. 5.

15. Taken as approximately twice the energy content of middle oil distillates.

16. From M. Sittig, Practical Techniques for Saving Energy in the Chemical Petroleum and Metals Industries, Noyes Data Corporation, Park Ridge, NJ (1977), and using a density of 0.97 g/ml for the wax.

3.2 Energy Consumption in Si reduction and purification.

This process group starts with the reduction of SiO_2 in an arc furnace. This is a quite efficient and cost-effective process which is not very likely to be replaced by another approach. In contrast, the following step of Si purification is very inefficient and likely to be replaced by one of several alternate methods under development. Furthest advanced among these is the SiH_4 purification process being prepared for pilot line operations by Union Carbide Corp. It can be expected to be a production process by 1986.

a) Theoretical Material Balance for the Arc Furnace Process.

The chemical reaction of this process is:

	SiO_2	+ 2C	→ Si +	2 CO
Atomic Weights:	28 + 2(16)	+ 2(12)	→ 28 +	2(12 + 16)
	60	+ 24	→ 28 +	56
Masses, normalized to 1 kg Si out:	2.14 kg	+ 0.86 kg	→ 1 kg +	2 kg

According to Dow-Corning [9], the industrially experienced and actual conversion efficiency of SiO_2 to Si is 80%. The required input is thus: 2.68 kg SiO_2 for 1 kg Si out (Dow-Corning shows 2.71 kg SiO_2).

It is assumed that half of the lost SiO_2 input, or 0.27 kg, is used in the reaction:

	SiO_2	+ C	→ SiO	+ CO
Atomic Weights:	60	+ 12	→ 44	+ 28
	0.27 kg	+ 0.05 kg	→ 0.2 kg	+ 0.12 kg

where the SiO is lost at the top of the furnace.
Thus, the total theoretical carbon input would be 0.91 kg C per 1 kg MG-Si output.

2. Energy Payback Times

To calculate payback times for photovoltaic systems, the annual energy output of a unit module area must be known. This power output, for photovoltaic systems, is dependent upon the encapsulated cell efficiency, the module packing factor, the solar insolation, the efficiency of the power conditioning and storage subsystems, and the mismatch of the energy availability and demand statistics. This list of dependencies makes it clear that the output of the module will vary according to climate at the locality of installation, and to the individual load to be satisfied. The factors of influence on the useful system output, outside of the cell efficiency, are combined into the "capacity factor". As a reasonably representative, not too optimistic value for this capacity factor, the number 0.11 has been used, in consequence of the results of several system studies.[4] The capacity factor is essentially independent of the solar cell or module manufacturing process. Consequently, the energy payback time is only partly a function of the energy consumption for the solar module fabrication process, since the other system parameters strongly influence its absolute magnitude. In the calculations of energy payback times, encapsulated cell efficiencies η of 11.5% and 15% were employed for 1978 and 1982 and for 1986, respectively, assuming the use of EFG ribbons, of 12%. To obtain the energy payback times, the annual module output was calculated as $E = \eta \times 8766 \times 0.11 \times H_{pk}$, H_{pk} being the standardized peak solar irradiance, used as $1kW(pk)/m^2$. The factor 0.11 represents the "capacity factor".

Thus, annual energy outputs from a square meter of solar cells of 110.9, 144.6, and 115.7 $kWh/m^2.y$ are obtained for 1978, 1982, and 1986 respectively.

It is also to be observed that, since the energy recovery from solar cells is in the form of electrical energy, it is appropriate to convert those energy expenditures which occur in the form of heat of combustion, to equivalent electrical energy by applying the average efficiency of 0.30 experienced by the electric utilities in the conversion from heat of combustion of fuels to electric power delivered to the consumer[5].

3. Energy Consumption in Photovoltaic Solar Array Manufacturing Process Sequences

3.1 Data Sources.

The major sources of information for this energy analysis were data accumulated from LSA project reports and industry interviews. The energy consumed through materials, both direct and indirect materials, was obtained by converting the material consumption to energy units through multiplication with the material energy contents shown in Table V-1. Where specific information to the contrary was not available, the material energy values were assumed to be in the form of thermal energy. The equipment costs, were converted to energy units expressed on the basis of unit cell area of throughput, by assuming a lifetime of seven years, and an energy content of the equipment which corresponds in value to 2% of the equipment cost.[6] This energy cost has then been converted to a thermal energy using an energy price of $0.003/kWh(th)[7]. Finally, the general energy usage for operating the facility was derived from the machine floor area by using the annual SAMICS utility cost of $3.74/ft^2[8] and assuming that all of this "indirect" energy, since it is used primarily for lighting, air conditioning, and ventilating, in view of the high heat load in the building, is in the form of electricity at a cost of $0.0319/kWh[8]. The conversion factors for the equipment and facility energies thus become 0.9523 kWh(th)/$y and 1262 kWh/m^{2}y, respectively.

Table V-1

Energy Contents of Selected Materials

Material	Original Units	Convenient Units (Thermal kWh's)	Reference
1. Acetic acid	3.28 lb of hi-press. steam plus 0.07 kWh(eℓ)/lb	3.18 kWh/g	1
2. Aluminum (Aℓ)	520×10^6 kWh(th)/ton	0.17 kWh/g	2
3. Ammonia gas (NH_3)	8.05×10^3 Btu/lb	0.00534 kWh/g	3
4. Ammonium Hydroxide 30% (NH_4OH)	-	1.32 kWh/ℓ	4
5. Argon gas	1,100 Btu/lb	1.27×10^{-3} kWh/ℓ	5
6. Butyl acetate	4.32 lb of low-press. steam plus 0.082 kWh(eℓ)/lb	3.21 kWh/g	6
7. Copper (Cu)	16.2×10^6 Btu/ton	5.23 kWh/g	7
8. Energy for exhausting waste fumes without scrubbing.	0.46 kW/1000 ft^3/min	2.56×10^{-2} kWh/ 1000 ft^3	8
9. Freon-14 gas (CF_4)	-	2×10^{-3} kWh/ℓ	9
10. Hydrogen gas	43,300 Btu/lb	2.51×10^{-3} kWh/ℓ	5
11. HF (48%)	7,000 Btu/lb	5.22 kWh/ℓ	5
12. Nitrogen (liquid)	1,330 Btu/lb	0.69 KWh/ℓ	5
13. Nitrogen (gas from liquid)	-	1.44×10^{-3} kWh/ℓ	10
14. Nitric Acid (HNO_3, 67%)	14,500 Btu/lb	13.12 kWh/ℓ	5
15. Oxygen gas (O_2)	830 Btu/lb	7.66 kWh/ℓ	5
16. Phosphorus (solid)	23,790 Btu/lb	1.54×10^{-2} kWh/g	5
17. Phosphine gas (PH_3)	-	0.18 kWh/ℓ	11
18. Phosphorous oxychloride ($POC\ell_3$)	-	0.14 kWh/g	12
19. Plating resist	8,000 Btu/lb	5.20 kWh/ℓ	13
20. Silver	1260×10^6 Btu/ton	0.406 kWh/g	8
21. Sodium Hydroxide (NaOH)	by-product	0	5
22. Toluene	0.05 lb of low-press. steam plus 0.025 kWh(eℓ)/lb	0.0349 kWh/mℓ	14
23. Vacuum pump oil	3,000 kWh(th)/ barrel	18.87 kWh/ℓ	15
24. Wax	2,000 kWh/barrel	1.3×10^{-2} kWh/g	16

References for Table V-1

1. Assumed to be the same as that of acetone, which was taken from "Battelle Columbus Laboratories, Draft Target and Support Document for Developing a Maximum Energy Efficient Improvement Target for SIC 28", Federal Energy Administration, Washington, DC (1976).

2. J.T. Reding and B.P. Shepherd, "Energy Consumption, Report EPA-G50/2-75-032b", US Environmental Protection Agency, Washington, DC (4/75).

3. Federal Energy Administration, "Project Independence Blueprint," Vol. 3, Federal Energy Administration, Washington, DC (1974).

4. Calculated from the energy content for NH_3 and using a density of 0.824 g/mℓ for the NH_4OH solution.

5. Battelle Columbus Laboratories,"Draft Target and Support Document for Developing a Maximum Energy Efficient Improvement Target for SIC 28", Federal Energy Administration, Washington, DC (1976).

6. Assumed to be the same as that of butyl alcohol, as given in Ref. 5.

7. H.W. Lownie, et al (Battelle Columbus Laboratories), "Draft Target Report on Development and Establishment of Energy Efficiency Improvement Targets for Primary Metal Industries," Federal Energy Administration, Washington, DC (9/76).

8. M.G. Coleman, et al., Motorola Final Report, DOE/JPL-954847-78/4, 183(11/78).

9. Estimated as approximately 50% more than the average energy content of commercial gases, as given in Ref. 5.

10. Calculated from the energy content for LN_2 assuming 480 ℓ of gas can be obtained from 1ℓ of LN_2.

11. Estimated as twice the energy content for P(s) plus $3/2H_2(g)$.

12. Estimated as twice the energy content of P(s), plus $\frac{1}{2}O_2(g)$, plus $\frac{3}{2}Cl_2(g)$. The energy content of Cl_2 was taken from ref. 5.

13. Assumed to be the same as that of wood rosin, as given in Ref. 5.

14. Taken as that of benzene, as given in ref. 5.

References for Table V-1

1. Assumed to be the same as that of acetone, which was taken from "Battelle Columbus Laboratories, Draft Target and Support Document for Developing a Maximum Energy Efficient Improvement Target for SIC 28", Federal Energy Administration, Washington, DC (1976).

2. J.T. Reding and B.P. Shepherd, "Energy Consumption, Report EPA-G50/2-75-032b", US Environmental Protection Agency, Washington, DC (4/75).

3. Federal Energy Administration, "Project Independence Blueprint," Vol. 3, Federal Energy Administration, Washington, DC (1974).

4. Calculated from the energy content for NH_3 and using a density of 0.824 g/mℓ for the NH_4OH solution.

5. Battelle Columbus Laboratories,"Draft Target and Support Document for Developing a Maximum Energy Efficient Improvement Target for SIC 28", Federal Energy Administration, Washington, DC (1976).

6. Assumed to be the same as that of butyl alcohol, as given in Ref. 5.

7. H.W. Lownie, et al (Battelle Columbus Laboratories), "Draft Target Report on Development and Establishment of Energy Efficiency Improvement Targets for Primary Metal Industries," Federal Energy Administration, Washington, DC (9/76).

8. M.G. Coleman, et al., Motorola Final Report, DOE/JPL-954847-78/4, 183(11/78).

9. Estimated as approximately 50% more than the average energy content of commercial gases, as given in Ref. 5.

10. Calculated from the energy content for LN_2 assuming 480 ℓ of gas can be obtained from 1ℓ of LN_2.

11. Estimated as twice the energy content for P(s) plus $3/2H_2(g)$.

12. Estimated as twice the energy content of P(s), plus $\frac{1}{2}O_2(g)$, plus $\frac{3}{2}Cl_2(g)$. The energy content of Cl_2 was taken from ref. 5.

13. Assumed to be the same as that of wood rosin, as given in Ref. 5.

14. Taken as that of benzene, as given in ref. 5.

15. Taken as approximately twice the energy content of middle oil distillates.

16. From M. Sittig, Practical Techniques for Saving Energy in the Chemical Petroleum and Metals Industries, Noyes Data Corporation, Park Ridge, NJ (1977), and using a density of 0.97 g/ml for the wax.

3.2 Energy Consumption in Si reduction and purification.

This process group starts with the reduction of SiO_2 in an arc furnace. This is a quite efficient and cost-effective process which is not very likely to be replaced by another approach. In contrast, the following step of Si purification is very inefficient and likely to be replaced by one of several alternate methods under development. Furthest advanced among these is the SiH_4 purification process being prepared for pilot line operations by Union Carbide Corp. It can be expected to be a production process by 1986.

a) Theoretical Material Balance for the Arc Furnace Process.

The chemical reaction of this process is:

	SiO_2	+ 2C	→ Si +	2 CO
Atomic Weights:	28 + 2(16)	+ 2(12)	→ 28 +	2(12 + 16)
	60	+ 24	→ 28 +	56
Masses, normalized to 1 kg Si out:	2.14 kg	+ 0.86 kg	→ 1 kg +	2 kg

According to Dow-Corning [9], the industrially experienced and actual conversion efficiency of SiO_2 to Si is 80%. The required input is thus: 2.68 kg SiO_2 for 1 kg Si out (Dow-Corning shows 2.71 kg SiO_2).

It is assumed that half of the lost SiO_2 input, or 0.27 kg, is used in the reaction:

	SiO_2	+ C	→ SiO	+ CO
Atomic Weights:	60	+ 12	→ 44	+ 28
	0.27 kg	+ 0.05 kg	→ 0.2 kg	+ 0.12 kg

where the SiO is lost at the top of the furnace.
Thus, the total theoretical carbon input would be 0.91 kg C per 1 kg MG-Si output.

3.2 Energy Consumption in Si reduction and purification.

This process group starts with the reduction of SiO_2 in an arc furnace. This is a quite efficient and cost-effective process which is not very likely to be replaced by another approach. In contrast, the following step of Si purification is very inefficient and likely to be replaced by one of several alternate methods under development. Furthest advanced among these is the SiH_4 purification process being prepared for pilot line operations by Union Carbide Corp. It can be expected to be a production process by 1986.

a) Theoretical Material Balance for the Arc Furnace Process.

The chemical reaction of this process is:

	SiO_2	+ 2C	→ Si +	2 CO
Atomic Weights:	28 + 2(16)	+ 2(12)	→ 28 +	2(12 + 16)
	60	+ 24	→ 28 +	56
Masses, normalized to 1 kg Si out:	2.14 kg	+ 0.86 kg	→ 1 kg +	2 kg

According to Dow-Corning [9], the industrially experienced and actual conversion efficiency of SiO_2 to Si is 80%. The required input is thus: 2.68 kg SiO_2 for 1 kg Si out (Dow-Corning shows 2.71 kg SiO_2).

It is assumed that half of the lost SiO_2 input, or 0.27 kg, is used in the reaction:

	SiO_2	+ C	→ SiO	+ CO
Atomic Weights:	60	+ 12	→ 44	+ 28
	0.27 kg	+ 0.05 kg	→ 0.2 kg	+ 0.12 kg

where the SiO is lost at the top of the furnace.
Thus, the total theoretical carbon input would be 0.91 kg C per 1 kg MG-Si output.

b) Theoretical Energy Balance.

The energy required from the electric arc for the reduction of SiO_2 to Si would firstly be expected to equal the heat of formation of SiO_2 at the reduction temperature ($-\Delta H^0_{f2000}$=210kcal/mol), or 8.7 kWh for 1 kg of Si formed. However, the carbon charged into the furnace also participates in the reaction, and, in its oxidation to CO, supplies approximately 25% of the required energy. Thus, the theoretical minimum energy required from the electric arc would be 6.6 kWh/kg Si.

In addition, energy is required to heat the furnace charge to reaction temperature, an energy which is not recovered. Heating the SiO_2 charge (2.7 kg) to the reaction temperature will require approximately 1.2 kWh, plus 0.1 kWh, for a total minimum theoretical energy requirement of 10.8 kWh/Si, outside of the heat loss of the furnace.

c) Experienced Material/Energy Balances.

Table II compares the experienced material and energy balances with the theoretical one. Experience data have been taken from ref. 9 which lists "data from a major manufacturer of MG-Si", ref. 10 which cites data from a not widely distributed Battelle report, and ref. 11 which gives data on an experimental arc furnace run at Elkem. Several observations have resulted from the study of these data:

i. The quality of the date does not justify better than 2-digit precision.

ii. Mining and transportation energy expenditures for quartz and coal are quite variable, depending on source, method, location of user, etc., but are in all cases so small as to be negligible. (It is good that the referenced authors, as well as these investigators, have checked the data, so that this statement can be made with confidence.)

Table V-2

Material/Energy Balance Data for the Arc-Furnace Process (per kg Si out)

	Theoretical				Dow-Corning Industrial Data				Dow-Corning Elkem Exper't.				Interlake Production Run				Solarex Battelle Data			
	kWh (el)	kg	kWh (th)	F.C. kg	kWh (el)	kg	kWh (th)	F.C. kg	kWh (el)	kg	kWh (th)	F.C. kg	kWh (el)	kg	kWh (th)	F.C. kg	kWh (el)	kg	kWh (th)	F.C. kg
Electrical Energy	8.6				13				44.1				13.5				15.4			
Quartzite		2.14	-	-		2.71	-	-		2.43	-	-		2.77	-	-		3.26	-	-
Wood Chips (4.75 kWh/kg) (25% F.C.)						2.77	13.2	0.69		1.46	6.9	0.37		2.48 (40% H_2O)	8.2	0.15 (6%)		1.77	8.4	0.44
Met. Coal (8.9 kWh/kg) (70% F.C.)						0.84	7.5	0.59		0.51	4.5	0.36		1.05	9.5	0.67		0.66	5.9	0.46
Pet. Coke (8.0 kWh/kg) (87.7% F.C.)						0.44	3.5	0.39		0.28	2.2	0.24		0.28	2.4	0.22		0.83	6.6	0.73
Electrode (9.1 kWh/kg) (99% F.C.)						0.1	0.9	0.1		0.50	4.6	0.50		0.09	0.8	0.09		0.17	1.5	0.17
Totals	8.6	-	2.2	0.86	13	-	25	1.8	44.1	-	18	1.5	13.5	-	20.9	1.13	15.4	-	22	1.8

iii. Energy expenditures for plant operation (lighting, ventilation, crane operation, etc.) and energy content of equipment have evidently not yet been analyzed. We added 1 kWh (el) per kg MG-Si produced as an estimate for these energy expenditures (Tables V-4A, 4B, - 4C, each Line 1 (p.p. V-15, V-16, V-17).

iv. The electrical energy consumption in the industrial processes seems only about a factor of 2 higher than theoretically required.

v. The use of "fixed carbon" (F.C.) is also approximately a factor of 2 higher than theoretically required.

vi. The use of thermal energy is an order of magnitude larger than theoretical. The following reasons prevail:

1. The oxidation of carbon goes only to CO, with only about 1/3 of the heat of combustion of C to CO_2 utilized.
2. The carbon sources used contain also combustible volatile components of high heat of combustion (hydrocarbons) which are not utilized.

vii. Both ref.'s 9 and 10 add a considerable energy expenditure for the coking process. The petro coke is, however, a byproduct of gasoline refining, obtained by coking the heavy residues from the distillation process. This coking process provides a higher yield of gasoline. It seems, therefore, that the energy expenditure for the coking process should be attributed to the gasoline production and not to the "coke".

viii. For the conversion from heat of combustion to electrical energy, the factor 0.33 has been used, corresponding the average efficiency of electric power generation in thermal plants. In this, the transmission/distribution losses have been omitted since large power users, such as arc furnace operators, are usually located close to generating plants.

ix. The data given in ref. (9) and Table 13 of ref. (11) do not seem to agree with the standard specifications (12) for "low volatile coal" shown in ref. (9).

x. The energy content of "wood chips" used in ref. (9) is approximately a factor of 2 lower than that of ref. (10) and (13), with credance given to the latter. The energy content of the volatile component of the woodchips on the unit mass basis, was originally assumed to equal that of metallurgical coal. However, comparing the total heat of combustion for wood thus obtained with that given in standard tables, after adjustment for moisture content, showed that the energy content of the volatiles of wood, as the only unknown, had to be lower by approximately a factor of 2 than that of the volatiles of coal. There probably is better information on this subject available in the literature, but it was not deemed beneficial to the project to expend more effort on this subject, particularly since this energy does not participate in the reaction, but exits via the

off-gas. Thus, both input and output of the energy balance are reduced by an equal amount.

xi. Ref. (9) lists the conversion efficiency of SiO_2 to Si as 80%, but ref. (10) uses only 66%. Nevertheless, ref. (10) arrives at approximately the same total energy consumption.

xii. The July 1977 Dow-Corning quarterly report [14] contains very useful detailed data on this subject, which have been augmented by additional information obtained directly from Interlake.[15]

The final energy balance, which was capable of accounting for 90% of the input energy (Table V-3), contains the interesting finding that nearly half of the energy input to the process leaves the furnace as chemical energy in the off-gas. About 60% of this energy is contained in volatile gases, in good part originating from the wood chips. The other 40% is contained in the carbon monoxide which results from the fixed carbon used to reduce the SiO_2. This off-gas is not utilized at present, but is mostly burned off at the top of the furnace. A utilization of this off-gas could reduce the net energy consumption of the process to approximately one half its current value, and such an improvement has been assumed accomplished for the energy balance projections to 1982 and

Table V-3

Energy Balance
Arcfurnace Reduction of SiO_2 to Si(MG)

Energy Input (per kg Si output)

Material	Mass kg	Component	Mass %	Mass kg	Energy Content Chem kWh	Energy Content Elect'l kWh
Quartzite	2.77	SiO_2	100	2.77	-	-
Woodchips	2.48	H_2O	40	0.98	-	-
		Fixed C	6	0.15	1.4	-
		Volatiles	54	1.34	E 6.8	-
		Ash	0	0.01	-	-
Petro Coke	0.28	H_2O	6	0.01	-	-
		Fixed C	79	0.22	2.0	-
		Volatiles	15	0.04	0.4	-
		Ash	0	0.01	-	-
Met. Coal (Imperial)	0.53	H_2O	4	0.02	-	-
		Fixed C	64	0.34	3.1	-
		Volatiles	30	0.16	1.7	-
		Ash	2	0.01	-	-
(Sewell)	0.52	H_2O	3	0.02	-	-
		Fixed C	63	0.33	3.0	-
		Volatiles	31	0.16	1.7	-
		Ash	3	0.01	-	-
Electrode	0.09	Fixed C	98	0.09	0.8	-
		Ash	2	0	-	-
Totals (Carbon Containing)	3.90	H_2O	26	1.03	-	-
		Fixed C	29	1.13	10.3	-
		Volatiles	44	1.70	10.6	-
		Ash	1	0.04	-	-
Electrical Energy	-	-	-	-	-	13.5

Energy Output (per kg Si output)

Material	Mass kg	Component	Mass %	Mass kg	Energy Content Chem kWh	Energy Content Thermal kWh
Metal at 1500°C	1			1	8.7	0.8
Off-gas at 290°C	5.08	H_2O	20	1.03	-	0.98
		Volatiles	34	1.70	10.6 (like input)	0.66
		CO	16	2.35	6.6	0.18
Fume and Multiclone at 290°C	0.61	Ash	6	0.04	-	0
		SiO	32	0.20	1.1	0.01
		SiO_2	44	0.27	-	0.02
		C	18	0.11	1.0	0.05
Furnace Heat Loss		Radiation		-	-	0.22-0.36
		Conduction/ Convection		-	-	0.07
Subtotals					28.0	3.13
Total Output						31.1
Input						34.4
Unaccounted						3.3

E = estimated

beyond.

For the purification of silicon by the standard $SiHCl_3$ process and the generation of the "Polylog", published data [16] and corroboration [17] were used. The energy consumption data computed on this basis are shown in Table V-4A, lines 2, 3, and 4 for the $SiHCl_3$ generation, the $SiHCl_3$ distillation, and the $SiHCl_3$ reduction to purified silicon, respectively, and correspondingly in Table V-4B.

As an alternate purification process, which can be expected to have replaced the $SiHCl_3$ purification process by 1986, the projected energy consumption data for the SiH_4 process under development at Union Carbide Corp. [18] are detailed in lines 2 and 3 of Table V-4C.

Table V-4A

PROCESS ENERGY CONSUMPTION IN THE CURRENT (1978) MANUFACTURING SEQUENCE FOR SILICON WAFERS.

		Yield or Conversion Rate	Direct Material Energy		Indirect Material Energy		Direct Energy		Equipment and Facility Energy		Total Energy Content of Material in Process		Ref.
			Th	El	Th	El	Th	El	Th	El	Th	El	
1.	SiO_2 reduction (kWh/kg)	2.77 kg SiO_2/ kg MG-Si	-	-	20.9	-	-	13.5	-	1.0	20.9	14.5	(1)
2.	$SiHCl_3$ generation (kWh/kg)	1.67 kg MG-Si/ kg Si in $SiHCl_3$	34.9	24.2	3.6	2.25	-	0.8	-	0.1	38.5	27.4	(2,3)
3.	$SiHCl_3$ distillation (kWh/kg)	1.0 kg $SiHCl_3$/ kg $SiHCl_3$	38.5	27.4	-	-	40.0	-	-	-	78.5	27.4	(2,3)
4.	$SiHCl_3$ reduction to SG-Si (kWh/kg)	2.67 kg Si in $SiHCl_3$/ kg SG-Si	210	73	27	0.3	200	400	-	-	437	473	(2,3)
5.	Cz crystal growth (kWh/kg)	1.13 kg SG-Si/ kg cyl Si	493	535	-	50.6	-	95	-	2	493	682	(4)
6.	Grinding and Slicing (kWh/m^2)	Area conversion 0.552 m^2/kg cyl Si	894	1236	49	-	-	10.2	-	2	945	1253	(4)
											↳	284	
7.	Electrical Energy Equivalent (kWh/m^2)	Conversion 0.3kWh(el) per kWh(th)									Total:	1537	
8.	Energy Content of Material Lost in Process (kWh (el)/m^2)	dto.										1314	

(1) See Table V-2, columns "Interlake Production Run," and p. V-10, item iii, both of this report.

(2) L.P. Hunt, Proc. 12th IEEE Photovoltaic Spec. Conf., IEEE Cat. No. 76CH1144-9 ED, pp. 347-52 (10/76).

(3) C.S. Fang, et al., Lamar Univ. Report ERDA/JPL 954 343-77/3, pp. 15-46 (9/77).

(4) M. Wolf, H. Goldman and A. Lawson, 13th IEEE Photovoltaic Spec. Conference., Cat. No. 76CH 1271-3, pp. 271-80 (6/78), and this report.

TABLE V-4B

PROJECTION FOR 1982 OF PROCESS ENERGIES IN THE MANUFACTURING SEQUENCE FOR SILICON WAFERS

		Yield or Conversion Rate	Direct Material Energy		Indirect Material Energy		Direct Energy		Equipment and Facility Energy		Total Energy		Ref.
			Th	El	Th	El	Th	El	Th	El	Th	El	
1.	SiO_2 reduction (kWh/kg)	2.77 kg SiO_2/ kg MG-Si	-	-	10.3	-	-	13.5	-	1.0	10.3	14.5	(1)
2.	$SiHCl_3$ generation (kWh/kg)	1.67 kg MG-Si kg Si in $SiHO_3$	17.2	24.2	3.6	2.25	-	0.8	-	0.1	20.8	27.35	(2,3)
3.	$SiHCl_3$ distillation (kWh/kg)	1.0 kg $SiHCl_3$/ kg $SiHCl_3$	20.8	27.3	-	-	40.8	-	-	-	61.6	27.3	(2,3)
4.	$SiHCl_3$ reduction to SG-Si (kWh/kg)	2.67 kg Si in $SiHCl_3$/ kg SG-Si	164.7	72.8	27.4	0.3	200	400	-	-	391.6	473.1	(2,3)
5.	Cz crystal growth (kWh/kg)	1.13 kg SG-Si/ kg cyl Si	442.5	534.7	-	11	-	52.5	-	1	442.5	599.1	(4)
6.	Grinding and Slicing (kWh/m^2)	Area conversion 0.846 m^2/kg cyl Si	523.0	708.2	21	0.2	-	5.1	-	1	541.9	717.5	(4)
7.	Electrical Energy Equivalent										↳	162.6	
8.	Energy Content of Material Lost in Process										Total:	880, 725.0	

1. Same as for 1978 analysis, but off-gases are recycled
2. L.P. Hunt, Proc. 12th IEEE Photovoltaic Spec. Conf., IEEE Cat. No. 76CH1142-9, ED, pp.347-52 (10/76).
3. C.S. Fang, et al., Lamar Univ. Report ERDA/JPL 954343-77/3, pp. 15-46 (9/77).
4. M. Wolf and H. Goldman, University of Pennsylvania, unpublished JPL Quarterly Reports ,and ref. (4) of Table IV A

Table V-4C

PROJECTION FOR 1986 OF PROCESS ENERGIES IN THE MANUFACTURING SEQUENCE

FOR SILICON RIBBON (USING THE SILANE PURIFICATION AND THE MOBIL TYCO EFG PROCESS)

		Yield or Conversion Rate	Direct Material Energy		Indirect Material Energy		Direct Energy		Equipment and Facility Energy		Total Energy		Ref.
			Th	El	Th	El	Th	El	Th	El	Th	El	
1.	SiO_2 reduction (kWh/kg)	2.77 kg SiO_2/ kg MG-Si	-	-	10.3	-	-	13.5	-	1.0	10.3	14.5	(1)
2.	Silane (SiH_4) production (kWh/kg)	90%	11.4	16.1	-	12.45	207.25	10.53	-	-	218.7	39.1	(2,3)
3.	Chemical vapor deposition of silane (kWh/m^2)	Area conversion 2.575 m^2/kg at 90% yield	84.9	15.2	-	-	-	14 (e)	-	-	84.9	29.2	
4.	Ribbon growth (kWh/m^2)	95%	89.4	30.8	-	-	-	107	-	-	89.4	137.8	(4)
5.	Electrical Energy Equiv. (kWh/m^2)										↳	26.8	
											Total:	165	
6.	Energy Content of Material Lost in Process kWh(el)/m^2											20.6	

(e) Estimated

1. As in Table IV B
2. W.C. Breneman, et al., Union Carbide Corp. (Sisterville, West Va.), Report DOE/JPL-954334-78/5 (12/77)
3. C.S. Fang, et al., Lamar University (Beaumont, TX) Report ERDA/JPL 954343-78/1, pp. 11-80 (3/78).
4. F.V. Wald, Mobil-Tyco Corporation (Waltham, MA), Contract No. DOE/JPL 954355

3.3 Energy Consumption in Sheet Generation

The current process group for sheet generation contains Czochralski crystal pulling followed by wafer slicing either by ID diamond blade sawing, multiblade or multi-wire slurry sawing.

The Czochralski process can be expected to be improved both with respect to cost and energy consumption. Competing are the heat exchanger method (HEM) of single crystal growth, and semicrystal casting. All of these processes, however, require sawing, with very substantial kerf losses. Consequently, the energy balance of the sawing processes is dominated by the energy content of the silicon material lost in the kerf. The primary possibility for energy savings lies therefore in the replacement of the bulk crystal growing methods, with subsequent sawing, by one of the ribbon growing methods under development. In the projections, improved Czochralski crystal growing and sawing methods are used for 1982, and a ribbon growing method for 1986.

a) Czochralski crystal growth and slicing.

The analysis of the Czochralski crystal pulling process, was based on a review of an earlier analysis[19] and the addition of newer data from Texas Instruments[20] and Dow Corning[21]. The projections contain primarily three improvements of energy impact: a reduction of the crucible usage, an increase in the furnace productivity, and additional technology advances which include better furnace design for reduced energy consumption.

The projected crucible usage reduction is based on the assumption that crucibles can be used for the equivalent

of 10 individual crystal pulls, either with re-seeding or (quasi-) continuous pulling, rather than the currently practiced usage for one crystal only.

The second projected reduction of energy consumption is connected with a projected furnace productivity increase. Approximately half of this productivity increase is expected to result from an increase in crystal diameter from the presently common, nominally 75 mm (3") diameter to nominally 100 mm (4") by 1982 and to 150 mm (6") by 1986. The other half of the productivity increase, however, is expected to come from a higher linear pull rate, thus more closely approximating the thermodynamically computed theoretical maximum pull rate. This prediction of a linear pull rate increase is more risky as two currently not adequately explored effects are involved. The first concerns crystal perfection which may decrease with increasing pulling speed and may possibly prevent attainment of the expected pull rates. The second unknown is based on an analysis by Rea [22] who found that the radiative energy transfer from the melt surface and the heater environment to the grown crystal prevents any close approach to the limit growth rates computed in the earlier thermodynamic analyses[23]. This spurious radiative heat transfer could, in principle, be reduced by introduction of appropriate heat shields. To what degree this can be achieved in practice, without interfering with other aspects of the crystal growing process, needs to be explored.

Some of the possible reduction in energy consumption is not just related to the productivity increase

through a reduction of the time for unit mass crystal growth, during which heat losses occur at a constant rate, but is directly connected with the dependence of the heat losses on the system geometry. The estimates are based on the - only conditionally valid - assumption that the heat losses in unit time are directly related to the crystal geometry change, and thus would increase proportionately to the crystal radius. The increased mass pull rate, which results from the radius increase, however, leads to a reduction of the energy losses inversely proportional to the radius. Finally, the required decrease of the linear pull rate results in a reduction of the energy losses inversely proportional to the square root of the crystal radius.

Twice as large a reduction in energy consumption than by the geometry change is, however, expected to result from technology improvements, consisting in the use of better heat shielding and insulation in future furnace designs. Another technology advance has been assumed in the substantial decrease in usage of replacement parts for the crystal pulling furnace, which reflects itself in reduced energy content of the replacement parts used per unit mass of crystal pulled.

Prior to slicing, the ingots are brought to constant diameter in a grinding process, which, by current production experience, costs 8% of the mass of the crystals grown. With the use of larger diameter crystals, projected for 1982, this grinding loss has been assumed to be reduced to 6%.

A similar analysis has been carried out for the slicing process, both as currently practiced and with projected technology improvements. Data on the current production processes include the multi-blade slurry sawing process [24] and the inside diameter diamond blade sawing process [25,26]. Also, ex-

perimental and projected data on advanced slicing methods were examined for the multi-blade slurry saw [27,28], for the ID diamond blade saw[29], and for the Yasunaga and Crystal Systems multiwire slurry sawing processes. [30,31] The slurry and the blade packs used in the multi-blade process constitute a substantial indirect materials consumption with significant energy content, as do the diamond saw blades in the ID sawing process.

The slicing technology improvements projected for the 1982 production lines as far as they concern the energy balance, are the results of current experimental runs. For the multi-blade saw, the primary advancement will be a 25% blade thickness reduction, in combination with a 37.5% wafer thickness decrease, to 250 μm wafer thickness and 200 μm kerf, while maintaining the present practical wafer yield of 95%. This results in a 50% increase in the mass to area conversion, to 0.9 m^2 per kg silicon crystal. A similar reduction in wafer thickness is anticipated in the ID sawing process, but without reduction of the kerf. The slurry multi-wire saw, which also could be on the 1982 production lines, can yield wafers with similar thickenss and kerf as the multi-blade slurry saw.

For the 1986 projections, energy consumption data given for the EFG ribbon growing process [32], but not yet reviewed by us, were used.

In consequence of the discussed process improvements, the energy content of the wafers or ribbons of silicon is expected to fall from the 1978 value of 1537 kWh(el)/m^2 to 880 kWh(el)/m^2 in 1982 and 165 kWh(el)/m^2 in 1986 (Tables V-4A to C, pp. V-15 to V-17).

3.4 Energy Consumption in the Solar Cell and Module Fabrication Process Sequence

The energy analysis of the solar cell fabrication process sequence is, in some respects, simpler than that for the sequence up through sheet generation, and more complicated in others. It is simpler, because one is dealing only with areas of silicon wafers or ribbons, no longer converting from one material form to another, or from mass units to area units. It is more complicated, however, because there exist many more process options and potential sequences.

In any such sequence, the accumulation of yields from the individual process steps is as important for the energy consumption as it is for the costs. In fact, for the entire process from SiO_2 to finished cells, the energy content of the silicon lost in the various conversions and due to yields of the process steps far exceeds the energy going in direct line into the finished product.

Consequently, the total energy expended for producing a unit of work-in-process (or finished product) leaving a given process step n is described by $E_{n-1}/\lambda_n + \Delta E_n$, where E_{n-1} is the total energy expended for producing a unit of work-in-process entering the respective step, ΔE_n is the total energy needed to process a unit of work-in-process through the step, and λ_n is the yield of the process step. The total energy $E_{T,N}$ expended in a process sequence up to step N (inclusive) is then:

$$E_{T,N} = \frac{E_o + \sum_{n=1}^{N} \Delta E_n \prod_{k=1}^{n} \lambda_k}{\prod_{k=1}^{N} \lambda_k} \qquad (V-1)$$

where E_o is the energy content of a unit of work-in-process or direct material (e.g. wafer or ribbon) entering into step 1 of the sequence. $E_{T,N}$ is, for instance, the energy shown in the right hand columns headed "Total Energy" in Tables V-4 A to C and V-8A to C, or "Subtotal" and "Total" in Table V-6. These total energies cannot be summed, but can be used for entry as E_{n-1} to another step or sub-sequence. Thus, the data in the left-hand columns headed "Direct Material Energy" or "Input Material" in Table V-6, and in Tables V-4A to C and V-8A to C, represent the values of E_{n-1}/λ_n.

The total energy "content" of the input work-in-process required to produce a unit of good output from step n is $\frac{E_{n-1}}{\lambda_n}$, so that the energy content $E_{L,n}$ of the material lost in the step n is given by:

$$E_{L,n} = \left(\frac{1}{\lambda_n} - 1 \right) E_{n-1} \qquad (V-2)$$

This quantity includes the energy content of all material lost in the preceding steps. The energy given by eq. (V-2) is an important ingredient of the "add-on-energy" $E_{A,n}$ for a unit of good work-in-process leaving process step n:

$$E_{A,n} = E_{L,n} + \Delta E_n ; \qquad (V-3)$$

Data generated by use of eq. (V-3) are included, e.g., in the right-hand column headed, "Total Add-On Energy" of Table V-5, while the left-hand column headed "Energy Content of Lost Silicon" includes data obtained by use of eq. (V-2),

with:

$$E_{n-1} = E_{n-2} + E_{A,n-1} \qquad \text{(V-4)}$$

Neither the add-on energies, nor the energy values for material lost in a process step, can be summed directly to obtain the total energy expenditures in a process sequence up to step N inclusively, because of the yields of the process steps subsequent to a given step n. Thus, for a unit area of product to leave step N, the total energy content $E_{L,N,n}$ of the material lost in step n is:

$$E_{L,N,n} = \frac{E_{L,n}}{\prod_{k=n+1}^{N} \lambda_k} \qquad \text{(V-5)}$$

and the total add-on energy for the sequence from step 1 to step N, inclusive is given by:

$$E_{A,T} = \sum_{n=1}^{N} \frac{E_{L,n} + \Delta E_n}{\prod_{k=n+1}^{N+1} \lambda_k} ; \qquad \text{(V-6)}$$

with $\lambda_{N+1}=1$.

Eq. (V-5) has been applied to obtain the "Totals" for the "Energy of Lost Silicon" in Table (V-7), and an equivalent relationship for the other energy component totals. The farthest right-hand column of Table (V-7) represents data resulting from application of eq. (V-6). The energy content of the total material lost is then simply:

$$E_{L,T} = E_{A,T} - \sum_{n=1}^{N} \Delta E_n \quad . \qquad \text{(V-7)}$$

The quantities $E_{L,n}$ and $E_{A,n}$, and correspondingly $E_{L,N,n}$ and $E_{A,T}$, include in the energy content that of all material lost in processing the good, remaining work-in-process. They are therefore not suitable for the determination of the total energy content of the material lost in a sequence of process steps, or of the "total net energy content" of the good work-in-process leaving such a sequence. This total net energy content does not include the energy content of the lost material. Thus its computation has to be based on the net energy contents of the input work-in-process, including consideration of the yields of the subsequent process steps. In analogy to eq. (V-2), the net energy lost in step n for a unit of good work-in-process leaving this step is:

$$E_{L,n,n} = \left(\frac{1}{\lambda_n} - 1 \right) E_{n,n-1} \qquad \text{(V-8)}$$

where:

$$E_{n,n-1} = E_o + \sum_{k=1}^{n-1} \Delta E_k \qquad \text{(V-9)}$$

is the net energy content of the input work-in-process. Similarly, the total net energy lost in step n for a unit of good work-in-process to leave a process sequence after step N is given by:

$$E_{L,n,N,n} = \frac{E_{L,n,n}}{\prod_{k=n+1}^{N} \lambda_k} \qquad \text{(V-10)}$$

and the total lost energy in all process steps by:

$$E_{L,n,T} = \sum_{n=1}^{N} \frac{E_{L,n,n}}{\prod_{k=n+1}^{N+1} \lambda_k} \quad ; \qquad \text{(V-11)}$$

with $\lambda_{N+1} = 1$.

Corresponding to eq. (V-9), the total net energy content of the good work-in-process, or finished product, leaving step N is:

$$E_{n,T} = E_o + \sum_{k=1}^{N} \Delta E_k \quad ; \qquad \text{(V-12)}$$

This total is represented in the farthest right hand column labeled "Total" in Tables V-9A to C, while the entries in the columns labeled "Energy content in lost Si" of those tables represent data according to eq. (V-10), and the totals of those columns correspond to eq. (V-11) as well as eq. (V-7).

In the solar cell processing sequence, we have accumulated the energy consumption data for the texture etching and the junction formation processes, and we have examined the direct material content of the encapsulation materials. The metallization and antireflection coating processes are presently being analyzed, and their energy data will be presented in a later report. In addition to these detailed analyses, we have accumulated the energy data for the 1982 \$2.00/W(pk) and the 1986 \$0.50/W(pk) JPL Strawman process sequences. From our detail analyses for the individual

processes and the available data for the remainder of the sequence, such as the Strawman data, we have synthesized overall process sequence energy consumption and payback time data.

a. Energy Consumption of Junction Formation Processes

The energy consumption of the various present and projected junction formation processes was studied in detail in connection with the analysis of their cost-effectiveness. In the evaluations, SAMICS overhead energy standards were used throughout, except for the 1974 and 1977 experience data shown in Table V-5, lines 1 and 2.

The wagers or ribbons resulting from the Cz/slicing (1978 and 1982), or EFG ribbon (1986) processes were tentatively assumed to be jubjected to the same texture etching process, with the same yield, independent of the junction formation processes used or the time frame. This unified wafer preparation consists of a 3-step process sub-sequence [33], which includes the application of an etch-stop (wax) to the back surface of the cell, texturing of the front surface by a hot NaOH etch, and removal of the etch-stop (Table V-6). The wafers resulting from this process sub-sequence are assumed to form the input material for the various junction formation processes.

The add-on energies for the junction formation processes are summarized in Table V-5. These processes have been grouped into present (Table V-5, lines 2 - 3), near term (Table

Table V-5

PROCESS ENERGIES FOR JUNCTION FORMATION PROCESSES (kWh/m^2)

Process	Yield (%)	Energy Content of Lost Silicon (th)	(el)	Mat. Energy (th)	Direct Energy (el)	Equip. Energy (th)	Facil. Energy (el)	Total Add-On Energy (th)	(el)	Equiv. El.Eng'y (el)	Payback Time (d)
1. Diffusion (Iles, 1974)	NA	NA	NA	NA	30	NA	32	—	62	62	NA
2. Diffusion (Solarex, 1977)	NA	NA	NA	(a)	19.38	(a)	12.21	-		32.00	NA
3. PH_3 Diffusion (Spectrolab, 1978)	99.9	0.97	1.28	0.81	2.39	4.48	2.15	6.26	5.82	7.70	25
4. P Ion Implantation (Varian-Extrion, 1978)	99	9.68	12.79	1.75	20.78	33.44	2.74	44.87	36.31	49.77	164
5. $POCl_3$ diffusion (JPL Strawman, 1982)	99.8	1.11	1.46	0.445	1.97	1.3	0.42	2.86	3.85	4.71	13
6. PH_3 Diffusion (Motorola, 1986)	99	0.94	1.41	0.098	6.69	0.74	0.39	1.78	8.49	9.04	24
7. 5-step PH and BSF Diffusion Sequence (Motorola, 1986)[a]	96.8	4.23	6.39	0.23	14.35	3.58	1.05	7.37	21.79	24.00	65
8. PF_5 Ion Implantation Lockheed, 1986)	99.2	0.77	1.14	0.30	0.54	4.46	1.65	5.53	3.39	4.99	14
9. 2-side Ion Implantation w/Annealing (RCA, 1986)	98.4	1.52	2.27	0.92	7.92	10.82	1.75	13.26	11.94	15.91	43
10. High Thruput P Implantation (Spire, 1986)	99.9	0.095	0.14	0.021	2.18	1.42	0.07	1.54	2.31	2.79	8
11. Unanalyzed P Beam Implantation (Motorola, 1986)	99.8	0.19	0.28	0.01	0.62	0.23	0.13	0.43	1.03	1.16	3
12. Ion Implantation PH_3 (JPL Strawman, 1 .86)	99.8	0.18	0.28	0.0	1.07	1.64	0.31	0.82	1.66	2.21	6
13. Activation Annealing (Motorola, 1986)	99.4	0.57	0.85	0.09	3.1	0.34	0.18	1.00	4.13	4.43	12

(a) = included in Facility Energy
NA = not available

[a] See Table V-6 for detail

Conversion Factor:
0.3 kWh (el) = 1 kWh (th)

Energies of Starting Material

	th	el
1978	965	1279
1982	554	733
1986	92.4	142

Table V-6

Energy Components of Surface Preparation Processes Preceding Junction Formation (in kWh/m²)

1978

Process	Yield	Input Material (th)	Input Material (el)	Ind. Mat. (th)	Processing (el)	Equip. (th)	Facility (el)	Subtotal (th)	Subtotal (el)	Total (el)
1. Wolaren 1977 data		NA	NA	(a)	2.83	(a)	5.72	-		
2. Input Work-in-Process: C_s wafers (Table V-4A, Line 6)						-		945	1253	
3. Application of etch stop on back	0.99	954.55	1265.56	0.05	0.5	0.55	0.11	955.25	1266.27	
4. Texturing front surface	0.992	962.95	1276.48	-	0.08	0.15	0.068	963.12	1276.62	
5. Removal of etch-stop on back	0.998	965.05	1279.19	0.001	0.11	0.26	0.065	965.31	1279.36	1567

1982

Process	Yield	Input Material (th)	Input Material (el)	Ind. Mat. (th)	Processing (el)	Equip. (th)	Facility (el)	Subtotal (th)	Subtotal (el)	Total (el)
1. Input Work-in-Process: Cs wafers (Table V-4B, Line 6)								541.9	717.5	
2. Application of etch stop on back	0.99	547.37	724.75	0.05	0.5	0.65	0.11	548.07	725.35	
3. Texturing front surface	0.992	552.19	731.21	--	0.08	0.15	0.068	552.64	731.36	
4. Removal of etch-stop on back	0.998	553.75	732.82	0.001	0.11	0.26	0.065	554.01	733.00	899

1986

Process	Yield	Input Material (th)	Input Material (el)	Ind. Mat. (th)	Processing (el)	Equip. (th)	Facility (el)	Subtotal (th)	Subtotal (el)	Total (el)
1. Input Work-in-Process: EFG Ribbons (Table V-4C, Line 4)				-		-	-	89.4	137.8	
2. Application of etch stop on back	0.99	90.30	139.19	0.05	0.5	0.65	0.11	91.0	139.8	
3. Texturing front surface	0.992	91.73	140.73	-	0.08	0.15	0.068	91.88	140.88	
4. Removal of etch-stop on back	0.998	92.07	141.36	0.001	0.11	0.26	0.065	92.36	141.55	169

Data for Application of Etch Stop, Texturizing, and Removal of Etch Stop were derived from Motorola (ref. (36)).

(a) Included in facility energy
(NA) Not Applicable

V-5, line 4) and long range projected junction formation processes (Table V-5, lines 5-13). For comparison purposes, the 1974 data [1] for the direct energy consumed in a diffusion process have been included in Table V-5, line 1. Since the data of this reference include indirect energy consumption only for the entire plant, including wafer generation, cell processing, and environmental testing which is probably more connected with the space power cells produced predominantly in 1974, the indirect energy consumption was, for the purposes of this report, allocated to the various process areas in proportion to their direct energy consumption.

The 1978 Spectrolab phosphine diffusion process (Table V-5, line 3), for which detailed experience data had been made available[34], shows approximately an order of magnitude lower total equivalent electrical energy consumption than Iles' numbers. This energy consumption is, in many respects, comparable to that for the $POCl_3$ diffusion process contained in the JPL 1982 Strawman process (Table V-5, line 5)[35]. It is noteworthy that the "equipment energy," derived from the equipment price as outlined on p. V-4 of this report, is the item of highest energy consumption in the Spectrolab process (Table V-5, line 3).

Motorola's diffusion process data [36], also for phosphine diffusion, are used as a projection to 1986, with the much lower energy content, per m^2, of the silicon ribbon expected to be used then. This difference expresses itself in the energy consumption for lost silicon. Essentially counterbalancing this change, however, is Motorola's assumption of

a lower yield. Another significant difference is in the material energy consumption, which is based on Spectrolab's substantial use of acids for quartzware cleaning, an item which is not included in Motorola's data.

Also included in Table V-5, line 7, is a 5-step process sub-sequence (Motorola) for the formation of both the pn junction and the BSF layer. This 5-step process includes the phosphine diffusion step just discussed. Its five process steps and their energy consumption are detailed in Table V-7.

Besides diffusion, ion implantation is presently used for junction formation. But in its present practice[37], ion implantation is much more energy intensive than the diffusion process (Table V-5, line 4). The process energy of ion implantation is, however, projected to decrease significantly through improvements in equipment design. These designs stress higher projected throughput rates relative to material usage, and capital equipment and facility requirements. In contrast, for the diffusion process, the add-on energy is not expected to change substantially since significant future increases in furnace efficiency are not anticipated.

It is also necessary to consider associated processes in the sequence, and the yields in such sequences. Thus, the ion implantation process should never be considered without adding the needed annealing step (Table V-5, line 13). Consequently, the 5-step pn junction and BSF layer diffusion process and the 2-sided ion implantation process with annealing (Table V-5, lines 2 and 9, respectively)

Table V-7

Add-On Process Energies for Motorola's Five-Step Diffusion Process
(in kWh/m^2)

Process	Yield (%)	Energy Content of Lost Si (th)	Energy Content of Lost Si (el)	Mat. Energy (th)	Direct Energy (el)	Equip. Energy (th)	Facility Energy (el)	Total Add-On Energy (th)	Total Add-On Energy (el)	Elec. Equiv. of Total Add-On Energy (el)	Cumulative yield $\prod_{k=n+1}^{5} \lambda_k$	Add-On Energy Needed to Produce 1 m^2 of Mat'l. Leaving Step 5 (el)
1. Spin-on silica on front surface	99%	0.96	1.427	-	0.61	1.01	0.12	1.969	2.157	2.748	0.968	2.838
2. Back p^+ (boron) diffusion w/BCl_3	99%	0.979	1.449	0.087	6.25	0.745	0.39	1.811	8.089	8.632	0.978	8.825
3. Protection of back surface with spin-on silica	99%	0.9972	1.531	-	0.61	1.01	0.12	2.007	2.261	2.863	0.988	2.898
4. Phosphorous (PH_3) diffusion	99%	1.0175	1.554	0.077	6.69	0.74	0.39	1.8345	8.5335	9.184	0.998	9.202
5. Stripping of both surfaces w/4:1 NH_4:HF	99.8	0.2055	0.3255	0.067	0.012	0.011	0.014	0.2835	0.3515	0.437	-	0.437
TOTALS	96.8	4.227	6.388	0.233	14.354	3.580	1.049	8.037	21.79		0.968	24.2

constitute comparable processes. Differing yields, or assumptions of yields, can have significant influence on the energy consumption. Thus, the lower overall yield (96.4%) of the 5-step Motorola sequence compared to that of the competing ion implantation process (98.4%) accounts for nearly 50% of the difference seen in the energy consumption of the 2 processes. This difference is in favor of the ion implantation for this particular example. Because of the importance of high yields for achieving processes with low energy consumption, most of the 1936 solar module fabrication sequence has been projected to be composed of individual processes of very high yields. Modifying the projected Motorola PH_3 diffusion process to be consistent with Spectrolab's experience of 99.9% yield and, in addition, a 17.5% "capacity factor" for the furnace energy consumption, would reduce its payback time from 24 to 9 days, and that of the 5-step sequence to 33 days. This would then be slightly less than the energy payback time of the competing 2-sided ion implantation process with annealing.

The data of Table V-5 are illustrated in Figure V-1. It shows the projected ion implantation processes to require less add-on process energies than the projected diffusion processes. However, after adding the process energy for activation annealing to that of the implantation process leads to comparable energy expenditures and payback times for the future ion implantation processes and the diffusion processes.

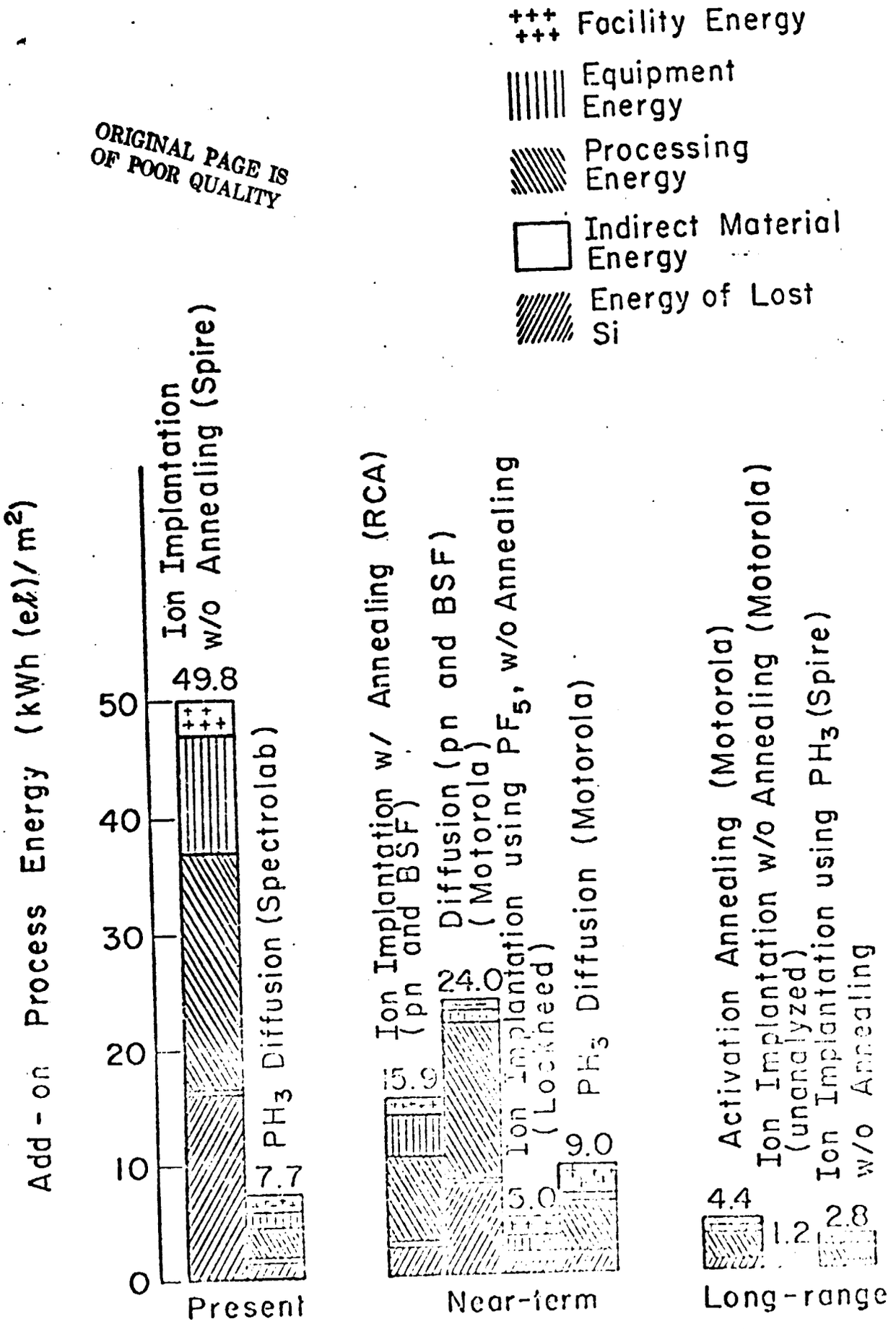

Figure 1: Junction Formation Process Add-On Energies

It may also be noted that the energy payback times for the projected diffusion processes are more "firm" than those for ion implantation, since the latter are based on equipment which has not yet been built. In contrast, the projected diffusion processes represent relatively small extrapolations from current production equipment and practices, primarily modifying throughputs to meet the LSA-JPL output goals.

b. Module assembly (encapsulation)

The major energy contributions in the module assembly step seem to come from the energy content of the encapsulation materials. Consequently, time has not yet been spent on determining the direct energy consumption in the encapsulation process (interconnect attachment, matrix connection, encapsulation material layup, potting material curing, junction box assembly), and the facility energy consumption for the respective part of the plant.

For the 1978 module assembly process, the encapsulation materials chosen were two 3 mm (1/8" thick) glass plates, along with a 1 mm thick layer of potting material. The cell packing density of 80% requires 1.25 m^2 of encapsulation material for each square meter of cell area. Cell yield in this area was tentatively taken as 100%. With a glass energy content of 46.1 kWh/m^2 [38], and a potting material energy content of about 12 kWh/kg, both assumed to be predominantly thermal energy, the energy content of the encapsulation materials alone is about 130 $kWh(th)/m^2$ of cell area. For the present

process, Iles[1] gave no energy consumption data for the encapsulation sequence, but Solarex presented data [39] which are tentatively used in Table V-8A.

For 1982, an 85% packing factor has been used for the solar cells in the module, reducing the encapsulation area to 1.18 m^2/m^2 of cells, and the energy content of the encapsulation materials to 120 kWh(th)/m^2 of cells. At the same time, the energy consumption data from the JPL \$2/W(pk) Strawman process have been used for the direct energy use and for the facility energy.[35]

For 1986, the packing factor has been assumed to be further improved to 95%, and the back glass layer replaced with a 0.25 mm thick Mylar film, or another material of similar energy content. Use of the improved packing factor alone without back glass replacement, results in an encapsulation material energy content of 107 kWh(th)/m^2 of cells, while use of the Mylar film backing leads to 62 kWh/m^2 of cells. In addition, the relatively small direct and indirect energy consumption data of the 1982 Strawman process for the encapsulation process group have also been used for 1986.

c. Full solar module process sequences.

Using the energy content of the input work-in-process to the solar module fabrication process sequence which was summarized in Tables V-4A to C for the current silicon wafers as well as projected wafers (1982) and ribbons (1986), the

TABLE V-8A

CURRENT PROCESS ENERGIES IN THE MANUFACTURING SEQUENCE FOR SILICON SOLAR CELL MODULES ALONG WITH THE TOTAL PAYBACK TIME

		Yield or Conversion Rate	Direct Material Energy (th)	Direct Material Energy (el)	Indirect Material Energy (th)	Indirect Material Energy (el)	Direct Energy (th)	Direct Energy (el)	Equipment and Facility Energy (th)	Equipment and Facility Energy (el)	Total Energy (th)	Total Energy (el)	Ref.
1.	Wafer input	-	-	-	-	-	-		-		945	1253	
2.	Cell processing (kWh/m^2)	80% yield to good cells	1181.3	1566.3	-	76	-	52	8	50	1181.3	1752.3	(1)
3.	Encapsulation (kWh/m^2)	80% packing factor ($1.25\ m^2$ for $1\ m^2$ of cells)	1181.3	1752.3	130*	-	-	11.1	-	21.0	1311.3	1784.4	(1)
4.	Total equivalent electrical energy consumed (kWh/m^2)	Energy conversion 0.3 kWh(el)/ kWh(th)									→	395	
											Total:	2178	
5.	Payback Time (y)	Recovery rate (110.9 $kWh/m^2 \cdot y$)										19.5	

* Refers to the energy content of the encapsulation material.

(1) J. Lindmayer, et al., Solarex Corp. (Rockville, MD), Report ERDA/JPL 954606-77/1, pp. 48-50 (4/77), and this report.

energy content of the completed modules was estimated or projected, based on available data. It turned out that the differences in these data for current processes are so large that they cannot be significantly improved by introducing the data resulting from our texturizing and junction formation process analysis into these other sequences.

A first analysis of the electrical power requirements of a solar cell production plant had been performed by Iles[1]. Iles estimated the contemporary (1974) solar cell fabrication plant energy consumption from the installed equipment power ratings, and extrapolated the plant's productive capacity by assuming that a five times larger solar cell area could be handled annually in the same plant, with approximately the same energy consumption, by going from the then-prevalent 2x2 cm space power cells to 2" diameter cells. Deducting Iles' direct energy consumption values for crystal growing and slicing leaves a direct electrical energy consumption of 120 kWh/m^2 of cell area produced. Allocating the indirect energy consumption in proportion to the direct energy, leads to 125 kWh/m^2 of cell area for the solar cell process plant, These data contain, e.g., a direct energy consumption for diffusion which is an order of magnitude larger than Spectrolab's experience data (see Table V- 5 , lines 1 and 2). On the other hand, Iles' data do not contain the energy content of the indirect materials consumed, nor that of the equipment installed (see Table V-8A).

The Solarex data[39] amount to about half the energy consumption found by Iles, but include the energy contents of the indirect materials consumed and the equipment. Comparing these data with those resulting from the analysis of texturizing and junction formation shows the Solarex energy consumption to be much higher than that given by Motorola for the texturizing process group, and by Spectrolab for diffusion. In contrast, the indirect energy consumption of Solarex (plant lighting etc.) amounts to only 1.7 kWh/m^2 of cells processed and is much lower than any other data given for this item. We consequently increased this consumption to 50kWh/m^2 of cells, or nearly 100% of the direct energy consumption, about in line with the other available data. One reason for this change is also the apparent omission by Solarex of the indirect energy consumption for the common areas, offices, etc.

In the encapsulation area, we used the energy content of the direct materials from section V-3.4b of this report, amounting to 130 kWh/m^2 of cells, for 2 sheets of glass and potting material. This number omits the energy content of the interconnectors, a junction box, or a frame possibly applied. Considering these facts, as well as a possibly lower packing factor for Solarex, Solarex's value of 205 kWh/m^2 of cells for this item appears quite compatible. For the direct and the indirect energy consumption in this process step, the Solarex data have been used as the only ones so far available. It may also be noted that 100% cell yield has been assumed for this

encapsulation process group, which may be slightly optimistic.

The consequence of these entries is a total energy consumption of 2179 kWh equivalent electrical energy consumed in the production of 1 m^2 of encapsulated cell area. At 80% cell yield from wafers to finished modules, it turns out that 1920 kWh, or 88% of the total module energy content, was already contained in the wafers entering the solar cell processing line. Of the 259 kWh added in the solar cell/module process line, over one quarter is attributable to module assembly and encapsulation.

For the 1982 projections, the summary numbers given for the JPL-Task IV Strawman process [35] have been reviewed. These data include a 93% overall cell processing yield, and an 85% module packing factor. The energy data for the diffusion step in this Strawman process sequence agree quite well with those of the current Spectrolab diffusion process, except for the equipment and facility energy values, which are considerably lower in the Strawman process because of higher assumed throughput rates. This comparison on one significant process step gives a degree of credibility to the remainder of the data. Again, we used our energy content data for the double glass encapsulation. As Table V-8B shows, the energy content of the completed module has been reduced to about half of that of the 1978 module, but the energy content of the input wafers now constitutes 93% of the module energy content. Also, module assembly and encapsulation now consumes 59% of the cell and module process energy. These shifts are

TABLE V-8 B

PROJECTION FOR 1982 of PROCESS ENERGIES IN THE MANUFACTURING SEQUENCE FROM SILICON Cz WAFERS TO SOLAR MODULES

		Yield or Conversion Rate	Direct Material Energy (th)	Direct Material Energy (el)	Indirect Material Energy (th)	Indirect Material Energy (el)	Direct Energy (th)	Direct Energy (el)	Equip't. Energy (th)	Facility Energy (el)	Total Energy Content (th)	Total Energy Content (el)	Ref.
1.	Wafer input	--	--	--	--	--	--	--	--	--	541.9	713.5	
2.	Cell processing (kWh/m^2)	93% yield to good cells	582.7	771.5	48.7	-	-	9.0	9.9	4.0	641.3	784.5	(1)
3.	Encapsulation (kWh/m^2)	1.18 m^2 for 1 m^2 of cells	643.6	781.3	121*		-	3.4	2.6	2.9	764.9	790.8	(1)
4.	Total equivalent electrical energy consumed (kWh/m^2)	Energy conversion 0.3 kWh(el)/ kWh(th)									→	229.5	
											Total:	1020	
5.	Payback Time (y)	Recovery rate 144.6kWh/(m^2.y)										7.05	

*Refers to the energy content of the encapsulation material.

1. D. Bickler, Jet Propulsion Laboratory (Pasadena, CA), Interoffice Memo 341-77-D-968 (10/77), and this section.

due primarily to the considerable reduction in energy consumption on the solar cell process line, and are reinforced by the yield improvement on this line from 80% to 90%.

The projections to 1986 were similarly based on the JPL "Candidate Process" data[3], which lead to a $0.50/W(pk) encapsulated module price. The input material is assumed to be silane purified, EFG grown ribbon, according to Table V-4C. Use of the "Candidate Process" leads to a total energy consumption of 206 kWh/m^2 of equivalent electrical energy (Table V-8C), of which 172 kWh/m^2, or 84%, is represented in the input ribbon material. Also, 57% of the solar cell and module process energy is added in module assembly, predominantly in the energy content of the encapsulation material.

Tables V-9A to C present additional data to augment those of Tables V-8A to C. They give the mass flow of silicon to the unit of finished encapsulated cell area, the net energy content per unit mass of the work-in-process at the key process stages, as well as the energy content of the silicon lost in the major process groups, and the net process energy of the material appearing in the good finished product, as contributed by these process groups. Again, these data are provided for the contemporary processes and for the projections to 1982 and 1986.

TABLE V-8c

PROJECTION FOR 1986 OF PROCESS ENERGIES IN THE MANUFACTURING SEQUENCE FROM SILICON EFG RIBBON TO MODULES.

		Yield or Conversion Rate	Direct Material Energy (th)	Direct Material Energy (el)	Indirect Material Energy (th)	Indirect Material Energy (el)	Direct Energy (th)	Direct Energy (el)	Equipment and Facility Energy (th)	Equipment and Facility Energy (el)	Total Energy (th)	Total Energy (el)	Ref.
1.	Ribbon input	-	-	-	-	-	-	-	-	-	89.4	137.9	
2.	Cell processing (kWh/m^2)	95%	94.1	145.0	8.1	-	-	7.5	5.65	1.65	107.9	154.1	(1)
3.	Encapsulation	95% packing factor	107.9	154.1	62*	-	-	0.14	0.82	0.1	170.7	154.3	(1)
											↳	51.2	
4.	Total equivalent electrical energy (kWh/m^2)	0.3 kWh (el)/ kWh (th)									Total:	206	
5.	Payback time (y)	115.7 $kWh/m^2.y$										1.8	

* Refers to the energy content of the encapsulation material.

(1) R.W. Aster, Jet Propulsion Laboratory (Pasadena, CA), LSA Doc. No. 5101-96 (12/78).

TABLE V-9A

ENERGY AND MASS REQUIRED TO PRODUCE $1m^2$ of SILICON SOLAR CELLS[a]

IN AN ARRAY, AS ESTIMATED FOR 1978 BY THE UNIVERSITY OF PENNSYLVANIA

	Process Step	Mass of Si Processed (kg)	Mass of Si lost in Process (kg)	Net energy content of work-in-process (kWh(el)/kg)	Energy content in lost Si (kWh(el))	Energy of Si in finished array for a unit process step (kWh(el))
1.	SiO_2 reduction	-	-	-	-	14.5
2.	$SiHCl_3$ generation and distillation (1.67 kg/kg)	11.41	4.58	20.8	95.3	11.4
3.	$SiHCl_3$ reduction to SG-Si (2.67 kg/kg)	6.83	4.27	37.0	158.1	327.9
4.	Cz crystal pulling (1.13 kg/kg)	2.56	0.30	505.4	151.6	103.3
5.	Grinding and slicing (0.552 m^2/kg)	2.26	1.39	653.0	907.7	26.9
6.	Cell Processing (80% yield)	0.875 (1.25 m^2)	0.175	691.4	121.0	180.4
7.	Encapsulation (1.0 m^2 of cells)	0.7 (1.0 m^2)	0			71.1
	Totals		10.715		1433.7	735.5
	Total Energy Content:				2170 kWh(el)/m^2-Si cells	

(a) Cells are 300 μm thick and the packing factor is 80%.

C-3

TABLE V-9B

ENERGY AND MASS REQUIRED TO PRODUCE $1m^2$ OF SILICON SOLAR CELLS[a]

IN AN ARRAY, AS PROJECTED FOR 1982 BY THE UNIVERSITY OF PENNSYLVANIA

	Process Step	Mass of Si Processed (kg)	Mass of Si lost in Process (kg)	Net energy content of work-in-process (kWh(el)/kg)	Energy content in lost Si (kWh(el))	Energy of Si in finished array for a unit process step (kWh(el))
1.	SiO_2 reduction	-	-	-	-	10.2
2.	$SiHCl_3$ generation and distillation (1.67 kg/kg)	6.38	2.55	17.6	44.9	9.6
3.	$SiHCl_3$ reduction to SG-Si (2.67 kg/kg)	3.83	2.39	34.1	81.5	272.9
4.	Cz crystal pulling (1.13 kg/kg)	1.44	0.165	502.6	83.0	37.0
5.	Grinding and slicing (0.846 m^2/kg)	1.27	0.645	567.1	365.6	7.3
6.	Cell processing (93% yield)	0.626 (1.07 m^2)	0.044	579.7	25.4	30.6
7.	Encapsulation (1.0 m^2 of cells)	0.583 (1.0 m^2)				43.4
	Totals		5.81		600.5	411.0
	Total Energy Content:				2012 kWh(el)/m^2-Si cells	

(a) Cells are 250 μm thick and the packing factor is 85%.

TABLE V-9C

ENERGY AND MASS REQUIRED TO PRODUCE 1m^2 OF SILICON SOLAR CELLS[a] IN AN ARRAY WITH THE SILANE PURIFICATION AND EFG PROCESSES, AS PROJECTED FOR 1986 BY THE UNIVERSITY OF PENNSYLVANIA

	Process Step	Mass of Si Processed (kg)	Mass of Si lost in Process (kg)	Net energy content of work-in-process (kWh(el)/kg)	Energy content in lost Si (kWh(el))	Energy of Si in finished array for a unit process step (kWh(el)
1.	SiO_2 reduction	-	-	-	-	4.1
2.	Silane (SiH_4) Production (90% conversion)	0.48	0.05	17.59	0.84	19.8
3.	Chemical Vapor Deposition of silane (2.575 m^2/kg)	0.43	0.17	102.7	17.7	14.0
4.	Ribbon to Ribbon Crystal Re-growth (95% yield)	0.258	0.013	162.8	2.1	107
5.	Cell Processing (95% yield)	0.245 (1.05 m^2)	0.012	622.1	7.6	13.2
6.	Encapsulation	0.233				19.1
	Totals		0.25		28.3	177.3
	Total Energy Content:				206 kWh(el)/m^2-Si cells	

(a) Cells are 100 μm thick and the packing factor is 95%.

4. Conclusions

The results of the energy consumption analysis are summarized in pictorial form in Fig. V-2. This figure clearly demonstrates three points:

a. most of the current high energy content is associated with the losses incurred in material conversion and in process yields.

b. the biggest reductions in the energy consumption will be connected with the introduction of new processes for silicon purification and sheet generation.

c. much of the reduction in cell processing energy comes from higher throughput rates; this effect is already observable now.

The numbers on energy consumption are to be considered as rough approximations, since the data for the current process practice show a large spread, and since the future data represent projections. But in toto, the energy payback times can be expected to decrease rapidly from their recent value near 20 years to below 10 years by 1982 and to less than 2 years by 1986. This last prediction is somewhat obvious since the modules are expected to be close to cost-effective by then as replacement supplies for energy generally available from other sources.

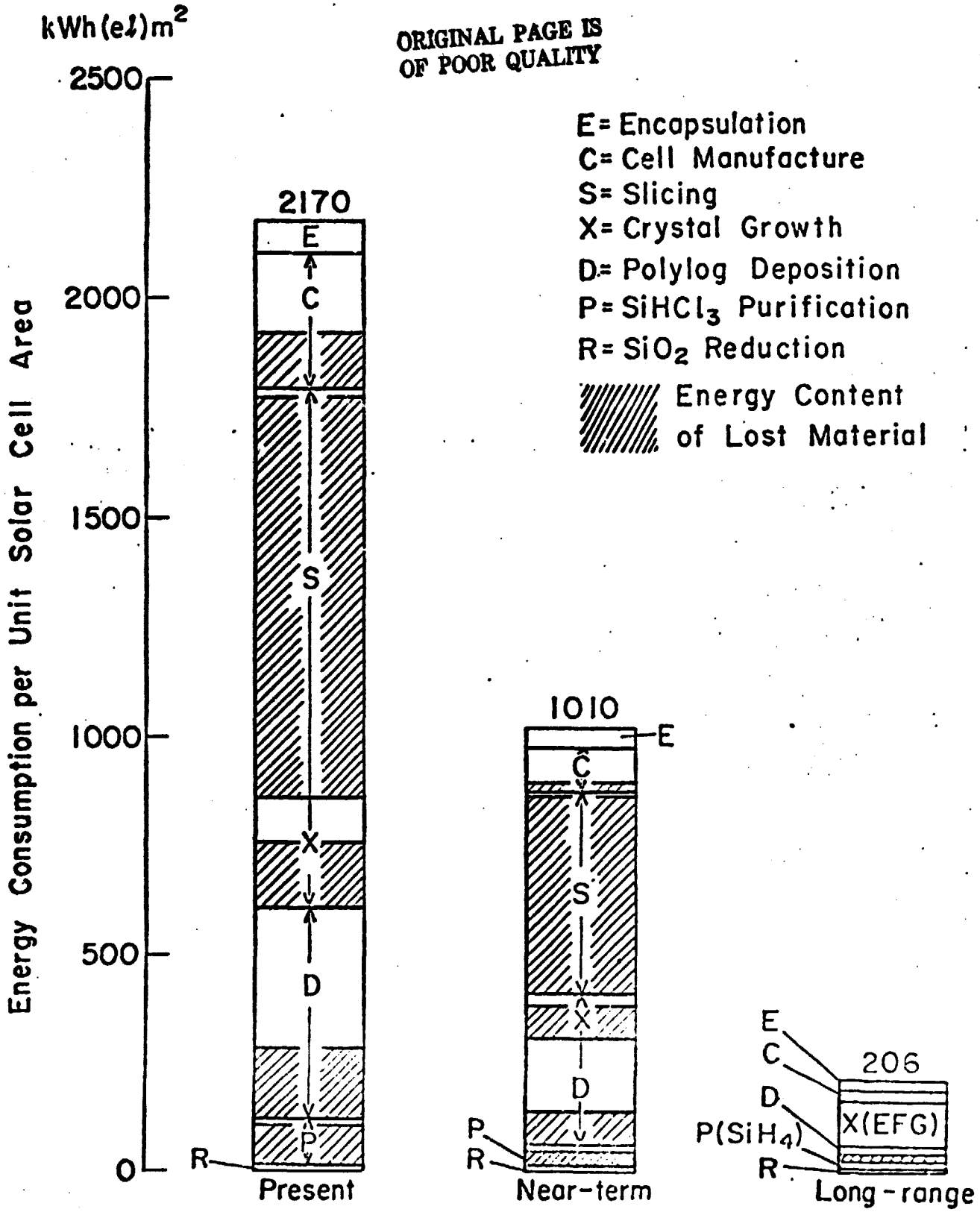

Figure 2: Processing Energy Components For Module Manufacturing

REFERENCES

1. P.A. Iles in "Proceedings of the Material Science Aspects of Thin Film Systems for Solar Energy Conversion," NSF Grant GI-43795, pp. 37-45 (5/74).

2. D.B. Bickler, presented at the 8th JPL-LSA Progress Intergration Meeting (12/77).

3. R.W. Aster, LSA-JPL Report 5101-94 (12/78).

4. M. Wolf, Energy Conversion, 16, 79 (1976).

5. "Statistical Yearbook of the Electric Utility Industry for 1970," Edison Electric Institute, New York, NY.

6. National Economic Research Associates, "Energy Consumption and Gross National Product in the United States," NY, NY (1971).

7. US Department of the Interior, "Energy Perspectives 21," US Government Printing Office, Washington, DC (6/79), p. 89.

8. R.W. Aster and R.G. Chamberlain, "Interim Price Estimation Guidelines," JPL-LSA Project Report 5101-33, Pasedena, CA (9/77).

9. L.P. Hunt in "Proc. 12th IEEE Photovoltaic Spec. Conf.," IEEE Cat. No. 76H1142-9 Ed., pp. 78-79 (10/76).

10. J. Lindmayer, et al., Solarex Corp. (Rockville, MD), Report No. ERDA/JPL-954606-77/1, pp. 40-3 (4/77).

11. L.P. Hunt, et al., Dow Corning (Hemlock, Mich.) Report No. ERDA/JPL 954559-76/2, pp. 24-28 (1/77).

12. US Bureau of Mines, "Technology of Lignite Coals," US Bureau of Mines Inform. Circ. 796 (1950).

13. N.A. Lange, ed., Handbook of Chemistry" p. 1505, McGraw-Hill, NY (1961).

14. L.P. Hunt, et al., Dow Corning (Hemlock, Mich) Report ERDA/JPL 954559-77/2, pp. 13-27, (7/77).

15. A. Winkler, Interlake, Inc. Private communication.

16. L.P. Hunt in Proceedings 12th IEEE Photovoltaic Specialists Conference, IEEE Cat. No. 76411429 Ed., pp. 347-52 (10/76).

17. C.S. Fang, et al., Lamar University (Beaumont, TX), Report No. ERDA/JPL 954343-77/3, pp. 15-46 (9/77).

18. W.C. Breman, et al., Union Carbide Corp. (Sisterville, West Virginia), Report DOE/JPL 954334-78/5, pp. (12/77).

19. M. Wolf, et al., University of Pennsylvania (Phila., PA), Final Report ERDA/SE/EG(11-1)-2721/FR/76/1, 187-89 (1/76).

20. S.W. Rea and P.S. Gleim Texas Instruments (Dallas, TX), Final Report ERDA/JPL 954475-77/4, pp. 91-99 (4/77).

21. L.P. Hunt, et al., Dow Corning (Hemlock, Mich.), Report ERDA/JPL-954559-77/2, 32-45 (7/77).

22. S.N. Rea and P.S. Gleim, Texas Instruments (Dallas, TX), Report ERDA/JPL-954475-77/4, 12 (4/77)

23. T.F. Cizek, J. Appl. Phys., 47, p. 440 (1976).

24. R. Oliver, Spectrolab Inc. private communication.

25. H.I. Yoo, Optical Coating Laboratory Inc., (City of Industry, CA) Report DOE /JPL 954830-77/12, p. 38 (12/77).

26. C. McGinnis, HAMCO (Rochester, NY), private communication.

27. S.N. Rea and P.S. Gleim, Texas Instruments (Dallas, TX), Report ERDA/JPL 954374-77/2, p. 17 (9/77).

28. S.C. Holden and J.R. Fleming, Varian ASsociates (Lexington, MA), Report ERDA/JPL-954374-77/2, p. 22 (7/77).

29. P. Aharonyan, Silicon Technology Corp. (Oakland, NJ), private communications (8/78).

30. J. Lindmayer, et al., Solarex Corp. (Rockville, MD), Report ERDA/JPL 954606-77/2, pp. 11-19 (7-77). Also: C.P. Chen, JPL-LSA Project Report DOE/JPL-1012-75/7 (2/78).

31. F. Schmid and C.P. Khattack, Crystal Systems (Salem MA), Report ERDA/JPL 954373-77/3, pp. 78-79 (10/77).

32. F.V. Wald, Mobil-Tyco Corporation, (Waltnam, MA), Contract No. DOE /JPL 954355.

33. M.G. Coleman, et al., Motorola Corporation (Phoenix, AZ), Annual Report DOE/JPL-954847-78/4, (11/78).

34. R. Oliver, Spectrolab Corporation, (Slymar, CA), private communication (4/79).

35. D.E. Bickler, Jet Propulsion Laboratory (Pasadena, CA), JPL-LSA Interoffice Memo 341-77-D-968 (11/10/77).

36. R.A. Pryor, L.A. Grenon, and M.G. Coleman, Motorola Corporation (Phoenix, AZ), Report DOE/JPL-954363-78/8, pp. 133-4, 172 (1/78).

37. J. Munnicci and A. Kirkpatrick, Spire Corporation (Bedford, MA), Report DOE/JPL 954786-78/05, pp. 3, 20-23, (1/78).

38. R.W. Olson, PPG Industries, Inc. (Pittsburgh, PA), private communication (5/78).

39. J. Lindmeyer, et al., Solarex Corporation (Rockville, MD), Report ERDA/JPL-954606-77/1, 48-50 (4/77).

Chapter VI

Plans

In progress are the analyses of metallization processes and of antireflection coatings, which will be reported in the next quarterly reports. The effort will then shift to masking and material removal processes, back surface field layer formation processes, and the evaluation of ingot versus ribbon technologies.